Stimulation of Wound Healing and Vascularization with Calcium-Releasing Biomaterials

Claudia Navarro Requena

TESI DOCTORAL UPC / BARCELONA, 2017

Directora: Dra. Elisabeth Engel
Co-Directora: Dra. Soledad Pérez Amodio

Programa de Doctorat en Enginyeria Biomèdica
Departament de Ciència dels Materials i Enginyeria Metal·lúrgica

Tesi presenada per obtenir el títol de Doctora
per la Universitat Politècnica de Catalunya

A mis queridísimos padres y hermana

Curiosity is the essence of human existence. 'Who are we? Where are we? Where do we come from? Where are we going?'... I don't know. I don't have any answers to those questions. I don't know what's over there around the corner. But I want to find out..

Eugene Cernan

Acknowledgments

Finalment ha arribat, l'ocàs d'una etapa. Queda molt lluny el moment en que vaig tenir l'oportunitat de començar el doctorat però, alhora, el recordo perfectament. Han passat cinc anys ja i, acabada aquesta fase, és inevitable rememorar totes les experiències viscudes, totes les coses apreses, i tota la gent que ha fet possible, d'una manera o altra, fer d'aquesta etapa una de les millors de la meva vida, a pesar dels moments d'estrès i frustració.

Primer de tot vull agrair el suport rebut de les meves directores de tesis, l'Elisabeth i la Soledad, sense les quals aquest treball no hagués estat possible. Eli, agraeixo infinitament el teu recolzament i optimisme i haver fet possible moltes de les grans experiències viscudes durant la tesis, tal com l'estada, les classes a la universitat i l'assistència a diversos congresos internacionals. Sole, ¡tantísimas cosas que agradecerte! Conseguiste mostrarme la luz en momentos difíciles y tu ayuda y guía diaria en el laboratorio ha sido imprescindible. Muchísimas gracias también a Oscar por toda la ayuda prestada con los biomateriales, especialmente al inicio de mi proyecto.

Durant aquests anys de tesis he pogut compartir bons moments amb moltes de les persones que han passat o segueixen en el grup. Els doctorands veterans, com el Tiziano, Riccardo, Zaida, Arlyng, Xavi i Aitor, que van ser uns grans referents. O les noves generacions, Joan, Irene, Jesús, Gerard i Sergi, que no han estat només companys de poyata sinó també bons amics, i m'han ajudat a afrontar la feina sempre amb un somriure. També han marcat aquest camí altres estudiants, com l'aventurer Doug, l'alegre Pau, i el boig d'en Max. I també la Mireia, amb la que he forjat una valuosa amistat.

A l'IBEC, i en gran mesura gràcies al temps en que vaig participar al comitè d'estudiants, he pogut conèixer a altres persones meravelloses amb

les que he compartit molt més que feina. Cristina, Carlos, Anna, Marc, Ágata, Natalia, Montse, Gizem, Maider i Martí, moltíssimes gràcies per haver fet possible tants bons moments. Sou unes bellíssimes persones i em sento molt afortunada d'haver-vos conegut.

Mil gràcies per la Maria, per ajudar-me des de el principi amb el tema de les ferides, guiar-me amb els tantíssims productes que existeixen i ajudar-me a dissenyar i disseminar l'enquesta. Agraeixo també a la Belén i les noies de Core, Cristina, Laura, Jeni i Ramona, per aconseguir facilitar moltíssim la feina al laboratori.

La estancia de tres meses que realicé en el grupo de Andrés J. García, en Atlanta, fue una de las grandes experiencias vividas a lo largo de mi tesis. Andrés, no tengo palabras para expresar mi gratitud por toda la guía y atención prestada, y por dejarme formar parte de tu grupo durante ese tiempo. Cristina, qué gran suerte tuve de conocerte, muchísimas gracias por todo el apoyo. I would like to thank all the great people who helped me there, specially Dennis, Jessica, José, and Joachim. Also, thanks to Avery, Josh and Scott for welcoming to their home and making the experience of living with twenty-year-old army guys much more enjoyable than expected.

Fóra de l'àmbit científic, també he comptat amb grans suports. Moltes gràcies als amics del Masnou, Laia, Irene, Olivia, Marta, Nina i Sori, pels soparets i vermutillos. Als Primos, per haver compartit les penes i glòries viscudes, sempre amb bon humor, i fer de cada trobada un moment inoblidable. També a l'Edgar i l'Esther, per comptar amb el seu recolzament en tot moment. I a les noies ex-capoeristes i l'Àlex, per les sortides esbargidores.

Obviamente, agradezco el apoyo vital y constante recibido de mis padres, mi hermana Diana y mi abuela Ofelia. Muchísimas gracias por todos

los ánimos y paciencia, y por estar a mi lado siempre que lo necesito. Us ho dec tot!

Per últim, vull agrair-te Marçal el recolzament i ajuda incondicional que m'has donat durant tot aquest temps. Gràcies per la paciència infinita, el bon humor, els consells i les hores de teràpia. Gràcies per ajudar-me a creure en mi mateixa, a reptar-me contínuament i mostrar-me una manera diferent de veure les coses.

Abstract

Chronic skin wounds are a major socioeconomic burden in developed societies, affecting specially elder and diabetic people. It is estimated that 1 to 2% of the population will suffer a chronic wound in their lifetime and, as global population ages and adopts a sedentary lifestyle, the incidence of these wounds will continue its upward trend. Chronic injuries are characterized for presenting a complicated and diverse pathophysiology that make them resistant to current therapies. For this reason, novel therapeutic strategies based on the release of growth factors and the use of tissue engineered constructs are being investigated and show promising results. However, very few biologically based products reach the market, mainly due to regulatory, economic and stability constraints, amplifying the need for easily translational novel treatments.

Recently, inorganic biomaterials known as bioceramics have been acknowledged for their wound healing and vascularization capability, mainly due to their ion release. Based on this concept, the present thesis project was dedicated to investigate the potential application of novel bioceramics on wound healing and soft tissue regeneration. More specifically we focused on the role of the calcium ion and its release from newly designed bioceramics to stimulate wound healing and blood vessel formation in both *in vitro* and *in vivo* systems.

Although it is known that calcium affects all the phases of wound healing, the concentrations and release profile that can improve the healing process has not been described. For this reason, we evaluated the effect of different concentrations of extracellular calcium *in vitro* on dermal fibroblast, a crucial cell type in the skin and the healing process, and found stimulation of relevant biological responses at specific concentrations. In addition, we compared whether similar effects could be obtained with the

ion release of newly designed bioceramic particles containing equivalent calcium concentrations. Interestingly, while stimulating most of the effects, the ion release inhibited some responses triggered by calcium alone that are not desired in the context of chronic wound healing.

Then, we investigated the cellular mechanism mediating some of the responses stimulated by calcium, focusing on the implication of the calcium-sensing receptor (CaSR). Several agonists of the receptor stimulated similar effects than calcium, suggesting the relevance of the CaSR on fibroblasts behavior, and opening a window to the design of novel bioceramics that release CaSR-agonists.

In order to test the healing capability of the above mentioned bioceramic particles *in vivo*, they were incorporated in a mat of poly(lactic acid) (PLA) fibers. This novel dressing was applied on a model of chronic wounds *in vivo*, and compared with a mat of particle-free PLA and to a frequently used commercially available dressing. We found that the PLA-bioceramic mat accelerated wound closure and increased vasculature at the injured site at initial time-points. Thus, improved healing was achieved with the newly designed dressing.

Finally, a different composite material was synthesized combining bioceramic particles and human mesenchymal stromal cells (hMSC) in a degradable hydrogel, and its vasculogenic potential was evaluated in soft tissue. This material supported hMSC survival and stimulated the release of the angiogenic factor IGF-1 from these cells *in vitro*. In addition, when implanted in soft tissue of immunocompromised mice, the composite construct improved hMSC survival and generated a more mature vasculature at the site of implantation.

In conclusion, this thesis shows that calcium-releasing bioceramics can successfully contribute to the treatment of chronic wounds and soft tissue regeneration.

Contents

List of Figures

List of Tables

1 General introduction, motivation and outline of the thesis

The skin is our largest organ and provides multiple vital functions that allow maintenance of body homeostasis and protection from the environment (Fenner and Clark, 2016). When this organ is damaged, survival is at stake and, for this reason, the body has evolved mechanisms that try to repair the injury as fast as possible (Reinke and Sorg, 2012). In some situations, however, these natural mechanisms might not be sufficient to achieve wound closure. It is then that wounds can become chronic.

Chronic wounds, also known as hard-to-heal wounds or ulcers, are skin injuries with diverse etiologies that fail to heal over a period of 3 months (Werdin et al., 2009). The burden of chronic cutaneous wounds is immense both personally and financially. Moreover, as chronic wounds risk factors, such as advanced age, diabetes or obesity, increase in developed countries, the incidence rate of chronic wounds continues its upward trend to the point of being considered a silent epidemic (Sen et al., 2009).

Currently, different strategies exist to treat chronic wounds, always involving the use of dressings. Dressings are materials that cover the wound, providing not only a physical protection from the environment but also, de-

pending on their composition, they can improve the healing process (Jones, 2006). Despite the great variety of dressings available in the market, most of them are based on a major scientific breakthrough made in 60s: the conception that a controlled moist environment allows a better healing than a dry one (Winter, 1995). However, the particular pathophysiology of chronic wounds complicate their healing in such an extent that, generally, the humid environment is not sufficient to promote their cure.

The last two decades have seen the rise of biologically based products that can actively stimulate the healing process, such as growth factor therapy and tissue engineering constructs (Pang et al., 2017). Although these possess great healing potential, their translation into the clinic is hampered by regulatory, economic, and scalable impairments. Thus, novel, affordable, safe, off-the-shelf, efficient strategies are needed to stimulate an improved healing of chronic injuries.

Recently, bioceramics, which are biomaterials with a traditional application towards bone and teeth regeneration, have been acknowledged for their healing capability and potential to stimulate the generation of new blood vessels in soft tissues (Miguez-pacheco et al., 2015). Their stimulating properties are mainly explained by the effect that ions released by these materials exert on cell behavior.

Calcium, which is present in most bioceramic compositions, plays an important role in the skin and the healing process (Lansdown, 2002a). Indeed, extracellular calcium is not only essential as a clotting factor during hemostasis, the first step of the healing process, but it also participates in the other phases of the healing process and in the regulation of keratinocytes, one of the main cell types of the skin.

Based on the idea that calcium affects the healing process, we hypothesized that calcium-releasing bioceramics could be optimized to stimulate the healing of chronic wounds. Aiming to provide a prove of concept for

this idea, during the course of this thesis, we mainly explored the effect of calcium and calcium-releasing bioceramics on wound healing and soft tissue, focusing on dermal fibroblasts and on the formation of new blood vessels. Briefly, the main goals pursued were the following:

- Describe and compare the effect of extracellular calcium, either from calcium chloride or from calcium-releasing bioceramics, on dermal fibroblasts *in vitro*.
- Identify the concentration or range of concentrations that stimulate dermal fibroblasts towards an improved healing.
- Detect the implication of the calcium-sensing receptor (CaSR) in the mediation of some of the responses stimulated on dermal fibroblasts.
- Synthesize and characterize a novel dressing made with poly(lactic acid) (PLA) fibers and fast-degradable calcium-releasing bioceramic.
- Evaluate the healing efficacy of the newly designed dressing in an *in vivo* model of chronic wound.
- Design and synthesize a new composite for soft tissue regeneration, based on the combination of a functionalized hydrogel, slow-degradable calcium-releasing bioceramics, and human mesenchymal stromal cells (hMSC).
- Characterize the physical properties of this material.
- Evaluate the *in vitro* and *in vivo* response of this material, focusing on its capability to stimulate the formation of new blood vessels.

The development of these objectives is structured in the following chapters:

In **Chapter 2**, different topics relevant for this thesis are reviewed. These include the structure and function of the skin, the phases of the healing process and the role of calcium in healthy and injured skin. Then, we focus on the pathophysiology of chronic wounds and the treatment currently available for them, including tissue engineered constructs. In addition, we explain the existing evidence for the healing and vasculogenic capability of bioceramics. We conclude this introductory chapter exposing the main *in vitro* and *in vivo* models used to test new treatments for chronic wounds.

In **Chapter 3**, we evaluate the effect of a wide range of extracellular calcium concentrations, obtained via the dissolution of calcium chloride, over different responses carried out by dermal fibroblasts. These include cell growth, cell migration, extracellular matrix (ECM) remodeling, contractile capacity, and gene expression related to wound healing. Then, we synthesize calcium-phosphate bioceramic particles with fast calcium-release coded SG5, and compare whether the stimulating effects obtained with specific calcium concentrations are similar than with conditioned media produced by incubating SG5 with culture media.

In **Chapter 4** we detect the expression of the CaSR on dermal fibroblast and use different agonist and antagonist of the CaSR to study the implication of this receptor in the mediation of some of the biological responses stimulated by calcium in this cell type.

In **Chapter 5** we develop a new dressing consisting of a mat of PLA fibers containing SG5, and test its healing properties on an *in vivo* model of chronic wound. First we observe the composite microstructure and show its calcium release profile. After evaluating its non-toxicity *in vitro*, we perform an *in vivo* test applying the dressing on pressure ulcers generated on the back of obese diabetic mice. Finally, we analyze the speed of wound

closure, the skin structure, and the number of vessels in the injured area over time.

In **Chapter 6** we evaluate the vasculogenic potential of a new composite biomaterial composed of a cell-adhesive biodegradable hydrogel containing hMSC and slow calcium-releasing bioceramic microparticles. Firstly, we assess the vasculogenic potential of the microparticles alone. Then, we study whether the incorporation of the particles in the hydrogel alters the mechanical properties of the hydrogel, stimulates the release of vasculogenic factors by hMSC, and impacts cell survival and vascularization in an *in vivo* model.

Finally, **Chapter 7** exposes the conclusions reached through the experimental work developed in this thesis, and provides future perspectives for the continuation of this research.

The studies presented in this thesis were performed at the Biomaterials for Regenerative Therapies group of the Institute for Bioengineering of Catalonia (IBEC), under the supervision of Elisabeth Engel and Soledad Pérez Amodio. In addition, part of the experimental work explained in Chapter 6 was developed at the Georgia Institute of Technology (Atlanta, USA), in collaboration with Prof. Andrés J. García. The author would like to acknowledge the Spanish Ministry of Education, Culture and Sport (MECD) for providing financial support through the FPU program (Formación de Profesorado Universitario - University Lecturer Training, grant reference AP-2012-5310) and the FPU mobility grant.

2 Introduction and state of the art

2.1 Functions and anatomy of healthy skin

The skin is the largest organ of the human body. It constitutes the 16% of a person's body weight, about 4 kg, and has an average surface area of 1.8 m^2 (Fenner and Clark, 2016). The skin is a metabolically active organ with multiple vital functions that allow maintenance of body homeostasis and protection from the environment (Fenner and Clark, 2016). For example, it acts as a barrier to chemical and physical agents, prevents the loss of body fluids, and helps to regulate body temperature (Fenner and Clark, 2016). The skin also serves as a sensory organ and produces antimicrobial peptides that prevent infections (Nejati et al., 2013). In addition, the skin is responsible for the production or activation of several hormones, neuropeptides and cytokines that exert biological effects throughout the whole body, such as Vitamin D, melatonin and sex steroids (Nejati et al., 2013).

Anatomically, the skin consists of three layers, the epidermis, the dermis, and the hypodermis, that contain other structures called skin appendages (Fig. 2.1). The epidermis is the thin, stratified outer layer that constitutes the physical and chemical barrier between the interior body and the exterior environment. The dermis is a thicker deeper layer formed

of connective tissue that provides the structural support of the skin. Below the dermis there is the hypodermis or subcutaneous fatty tissue, which contains an important fat reservoir that maintains body temperature. Finally, skin appendages include hair, nails, sebaceous glands, and sweat glands, which are regarded as derivatives of the skin (McGrath et al., 2004). The following sections will describe in more detail these four components of the skin.

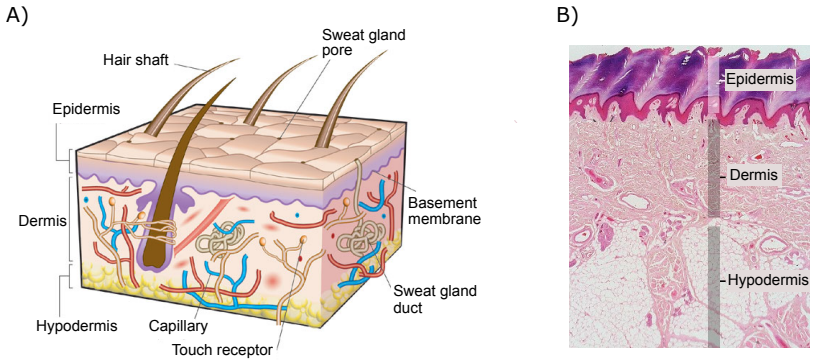

Figure 2.1: Cross-section of the skin showing its different components. A) Representation of the different skin layers and skin appendages (Dead Sea Source, 2016). B) Histological section of the skin stained with hematoxylin and eosin (H&E), which basically stain nuclei in blue and connective tissue in pink/red, and allow to distinguish the different layers of the skin. Adapted from Slomianka (2000).

2.1.1 Epidermis

The epidermis is the outer layer of the skin. It contains different cell populations, including keratinocytes, Langerhans cells, Merkel cells and melanocytes (Gilaberte et al., 2016). Keratinocytes are by far the most abundant population and are responsible for the stratified structure of the epidermis (Gilaberte et al., 2016). Indeed, the epidermis is substructured in strata that contain keratinocytes in different stages of differentiation. The

differentiation process occurs while keratinocytes progress from the inner to the external side of the epidermis. This is a dynamic process that allows the complete renewal of the epidermis every month (Gilaberte et al., 2016).

Independently of its thickness, which ranges from 0.05 mm in the eyelids to 1.5 mm on the palms and soles, the epidermis lacks of direct blood supply (Han, 2015). Consequently, it depends on the underlying dermis for nutrient supply and waste disposal via diffusion through the epidermal basement membrane (Han, 2015), which is a semipermeable thin tissue formed by extracellular matrix that separates the epidermis from the dermal connective tissue (Eady, 1988).

Epidermal layers

The epidermis is usually divided into four strata, each of which contains keratinocytes in different levels of differentiation: the stratum basale, the stratum spinosum, the stratum granulosum, and the stratum corneum (Fig. 2.2A). A fifth layer named stratum lucidum, found between the stratum corneum and stratum granulosum, is present only in the thick skin of palms and soles (Fig. 2.2B) (Fenner and Clark, 2016).

The stratum basale is the deepest layer, in direct contact with the basement membrane. It has the thickness of a single cell layer and it is the only layer of the epidermis in which cell mitosis occurs. It contains two populations of stem cells: the epidermal stem cells, with a long life span and very slow division rates, and the epidermal progenitor cells, with a shorter lifespan and rapid proliferative rate (Gilaberte et al., 2016). Keratinocytes, which are generated from the differentiation of this last cell population, leave the stratum basale to continue differentiation by ascending up the next stratum, the stratum spinosum. The stratum spinosum consist of several rows of more mature keratinocytes and contains a high concentration of keratin filaments and transmembrane structures called desmosomes that

tightly adhere adjacent cells to one another (Fenner and Clark, 2016). The next stratum, the stratum granulosum, is the last layer that contains living cells. At the interface between the stratum granulosum and the stratum corneum, the most external layer, keratinocytes undergo the last step of differentiation, becoming flat, hard, anucleated dead cells: the corneocytes. Both these cell and keratin are the main components of the startum corneum and play a vital role in generating the protective barrier against the environment (Fenner and Clark, 2016).

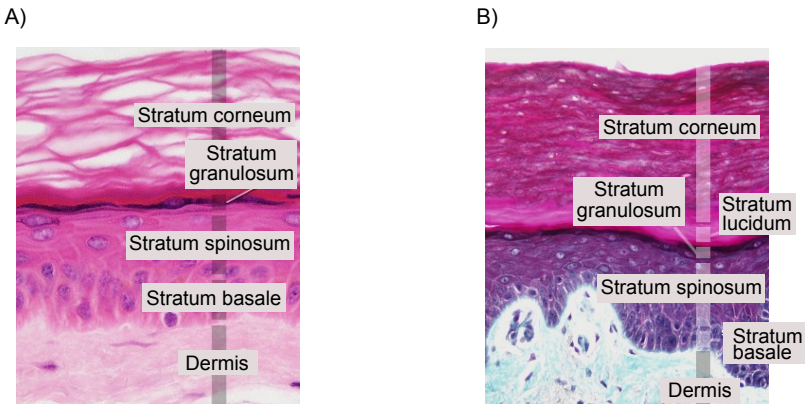

Figure 2.2: Epidermal layers. Staining of histological sections of A) thin and B) thick skin, showing the different epidermal layers. Adapted from Slomianka (2000).

Epidermal cells

Keratinocytes make up 80% of the total population of the epidermis (Gilaberte et al., 2016). These cells undergo differentiation while they transit through the different strata of the epidermis until becoming corneocytes in a process called keratinization. This process begins as soon as keratinocytes differentiate from the cells in the stratum basale. Once they reach the stratum spinosum, their cytoplasm expands and they begin to pro-

duce keratin. Intracellularly, keratin acts as intermediate filaments, forming part of the cytoskeleton and providing mechanical strength to the cell. In addition, they connect with desmosomes, which are specialized cadherin complexes located in the plasma membrane that bind epidermal cells together (Fenner and Clark, 2016). The formation of these adhesions provides the epidermis with a tension-resistant structure capable of supporting shear forces (Fenner and Clark, 2016). As keratinocytes ascend through the stratum granulosum, enzymes induce degradation of their nuclei and organelles, and keratin is agglomerated (Fenner and Clark, 2016). In the stratum corneum, cells appear flattened and dead. Nonetheless, cells are so tightly bonded to each other in this layer that water evaporation is prevented and the skin is kept hydrated (Lee and Jung, 2016). In addition, the disulfide bonds created in keratin provide strength to this layer but as intercellular desmosomal connections are lost, cells are shed from the skin (Fenner and Clark, 2016).

Other cell types present in the epidermis are melanocytes, Langerhans cells and Merkell cells. Melanocytes are found in the startum basale, but their dendrites reach keratinocytes in the stratum spinosum. Their primary function is to produce melanin, a pigment that absorbs UV radiation, protecting keratinocytes from its harmful effects (Fenner and Clark, 2016). Langerhans cells, scattered in the stratum spinosum, constitutes the first line of immunologic defense in the skin. They attack and engulf foreign materials and serve as antigen-presenting cells (Fenner and Clark, 2016). Finally, Merkell cells are found directly above the basement membrane, in the startum basale, and are specialized in the perception of light touch (Han, 2015).

2.1.2 Dermis

The dermis is the fibrous and elastic tissue located beneath the epidermis. Its thickness can range from 0.3 mm on the eyelid to 6.0 mm on the back, constituting a thicker layer than the epidermis (Han, 2015). The dermis is mainly composed of extracellular matrix (ECM), or connective tissue, produced by stromal cells known as fibroblasts (Gilaberte et al., 2016). Different structures can be found within the dermis, from blood vessels and nerves, which provide nutritional support and sensation, respectively, to lymph vessels, small quantities of striated muscle, and various appendages including sweat glands, hair follicles, and sebaceous glands (Fenner and Clark, 2016). In addition, different immune cells reside in or traffic through the dermis, such as dendritic cells and leukocytes (Lugović et al., 2001; Nestle and Nickoloff, 1995).

The connective tissue which composes the dermis is made of collagen, elastin, and proteoglycans (Gilaberte et al., 2016). Collagen fibers constitute 70% of this connective tissue, primarily type I (85% of the total collagen) and type III (15% of the total collagen) and provide strength and toughness. Elastic fibers, which constitute less than 1% of the weight of the dermis, maintain normal elasticity and flexibility while proteoglycans provide viscosity and hydration (Gilaberte et al., 2016).

The connective tissue undergoes a constant remodeling by calcium- and zinc-dependent proteolytic enzymes known as matrix metalloproteases (MMPs). These enzymes participate in multiple processes in the skin (Vu, 2000). Depending on their target, they are classified in three groups: collagenases, gelatinases, and stromelysins (Gilaberte et al., 2016). Collagenases (MMP-1, MMP-8, MMP-13, and MMP-18) cleave interstitial collagen, gelatinases (MMP-2 and MMP-9) degrade basement membrane collagens and denaturated structural collagens, and stromelysins (MMP-3, MMP-10, MMP-11, and MMP-19) degrade basement membrane col-

lagens and non-collagenous connective tissue macromolecules, including proteoglycans, laminin and fibronectin. MMPs are produced by multiple cell types, including keratinocytes, fibroblasts, neutrophils, and mast cells (Caley et al., 2015).

Dermal layers

The dermis is composed of two layers: the thin and superficial papillary dermis, and the thicker and deeper reticular dermis (Fig. 2.3).

The papillary dermis is a thin layer of loose connective tissue containing capillaries, elastic fibers, reticular fibers, and poorly organized collagen fibers, particularly of type III. This layer interdigitates with the epidermal basement membrane in areas called dermal papillae, producing a structure that resembles an egg carton (Fig. 2.3B). In thick skin, the papillary dermis is more complex, increasing resistance to shear stress of the basement membrane (Ovalle and Nahirney, 2007).

The reticular dermis is a thick layer of dense connective tissue containing larger blood vessels, closely interlaced elastic fibers, and well organized collagen fiber bundles of type III and I that run parallel to the skin surface (Gilaberte et al., 2016). It extends from the base of the papillary layer to the hypodermis (Fenner and Clark, 2016).

Fibroblasts

Fibroblasts are the most abundant cell population in the dermis and are responsible for the maintenance of the different components of the ECM, including collagen, elastin and proteoglycans (Wang et al., 2007). In addition, they secrete various growth factors -e.g., transforming growth factor-beta (TGF-β)-, cytokines -e.g., tumor necrosis factor-alpha (TNF-α)- and MMPs that have a direct effect on keratinocyte proliferation and differentiation, and formation of the ECM. All in all, fibroblasts play a central role

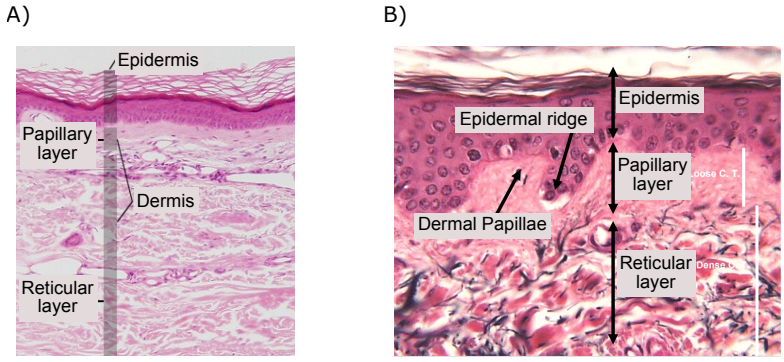

Figure 2.3: Dermal layers. Staining of histological sections showing A) the papillary and reticular layers of the dermis and B) the differences in structure of connective tissue of the dermis. It can be noticed the loose connective tissue in the reticular layer, the denser connective tissue of the papillary layer and the interdigitation of this layer into the epidermis with the dermal papillae. Adapted from Slomianka (2000).

in tissue remodeling and wound healing processes and are involved in the pathogenesis of connective tissue disorders (Wang et al., 2007).

2.1.3 Hypodermis

The hypodermis or subcutaneous tissue lies between the dermis and muscle and its thickness varies from person to person (Fenner and Clark, 2016). The hypodermis serves a variety of relevant functions to the skin and body. It provides insulation from the cold, serves as an energy reservoir, protects deep tissues from trauma and even acts as an endocrine organ by participating in the synthesis of estrone and leptin (Gilaberte et al., 2016; Fenner and Clark, 2016). The main component of the hypodermis are adipocytes, cells specialized in storing fat. These cells are organized into lobules that are separated by a fibrous connective tissue, known as septa, that contains

nerves, lympatic vessels and a rich microvascular network that provides oxygenation and nutrient exchange (Fenner and Clark, 2016).

2.1.4 Skin appendages

The appendages of the skin include hair follicles, nails, sebaceous glands, sweat glands, mammary glands, and ceruminous glands (Fig. 2.4) (Lee and Jung, 2016). Hair follicles are generated by basal cells in the basement membrane. They are made of keratinized dead cells and are distributed throughout the whole body, except for palms and soles. They contribute to maintain body temperature and to perceive touch sensation (Lee and Jung, 2016). Nails are also composed of keratinized, flattened, dead cells (Gilaberte et al., 2016). Sebaceous glands are found at the base of hair follicles, to which they secrete an oily substance known as sebum, that lubricates and waterproofs the skin and hair (Han, 2015). Sweat glands secrete sweat to the surface of the skin (Fenner and Clark, 2016), and mammary and ceruminous glands are modified sweat glands that produce milk and cerumen, respectively (Lee and Jung, 2016).

2.2 Wound healing

The skin is the first line of protection of our body against the dangers of the external environment. When this barrier is disrupted, whether through injury or disease, survival chances decrease. To restore the anatomic continuity and function of the skin, evolution has conferred the skin the ability to heal through dynamic and highly regulated processes that begin directly after wounding. Healing can occur through two different mechanisms: regeneration or repair (Reinke and Sorg, 2012). While regeneration achieves the complete recovery of the original tissue, repair results in the formation of a scar (Reinke and Sorg, 2012). Scars are of poorer quality than the orig-

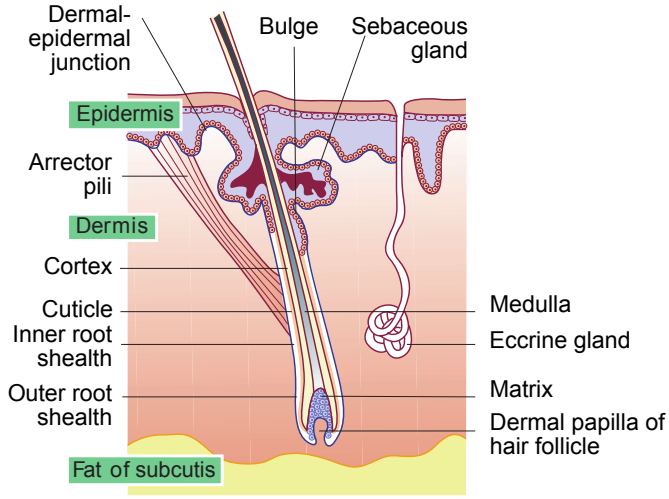

Figure 2.4: Skin appendages. Graphic illustration of the different appendages of the skin. Adapted from McGrath et al. (2010).

inal tissue, since they are weaker and lack the presence of skin appendages or specialized cells like melanocytes. Unfortunately, human skin regeneration only happens to early gestation fetuses and to mucosal surfaces (Sanon et al., 2016). In adults, the main mechanism by which skin heals is through repairing (Reinke and Sorg, 2012), and thus this is the process in which this thesis will focus.

Normal wound healing in adult individuals involve the interplay of multiple cell types, growth factors, cytokines, and a balanced pool of metal ions, such as calcium, zinc and magnesium (Lansdown et al., 1999; Sanon et al., 2016). The healing process, summarized in Fig. 2.5, progresses through four phases that overlap in time and space: hemostasis, inflammation, proliferation, and remodeling. Each of these stages will be explained in detail in the following sections.

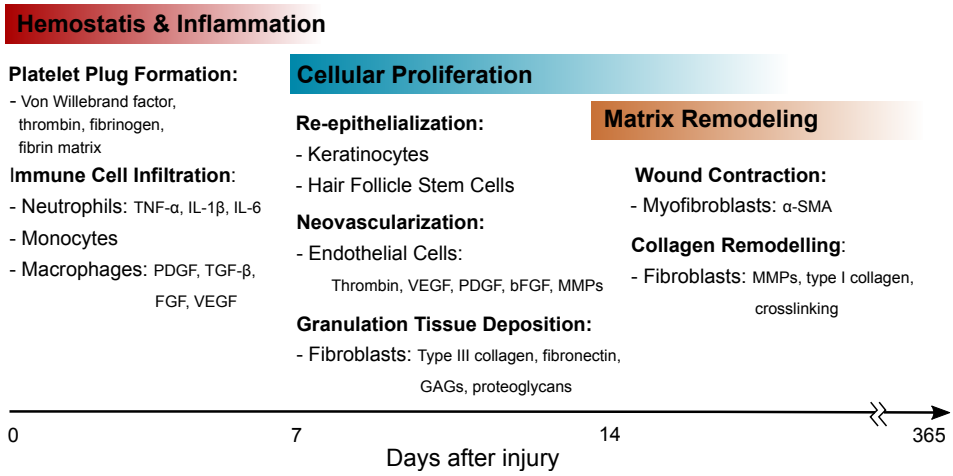

Figure 2.5: Wound healing process. Cellular and molecular players involved in each stage of the healing of wounds. Adapted from Sanon et al. (2016)

2.2.1 Hemostasis

Right after injury, bleeding occurs, flushing out bacteria and/or antigens from the wound (Boateng et al., 2008). The hemostatis phase, which take place during the first few hours after injury (Sanon et al., 2016), is the process by which the injury stops bleeding and results in the formation of a provisional matrix made of fibrin, and the initiation of the inflammatory phase (Sanon et al., 2016). The formation of the fibrin clot involves different steps. First, von Willebrand factor binds to the exposed tissue, allowing platelet aggregation and the formation of a platelet plug (Sanon et al., 2016). Then, platelets from this plug and other clotting factors released from the injured tissue activate the coagulation cascade that generates thrombin, which subsequently converts fibrinogen from the bloodstream into a fibrin matrix (Sanon et al., 2016). This provisional scaffold allows the migration of cells to the injured site and acts as a reservoir of growth factors (Sanon et al., 2016). In addition, factors released from platelets trigger vasoconstriction and act as chemotactic agents for recruit-

ing leukocytes to the site, thus beginning the inflammatory response (Goh et al., 2016).

2.2.2 Inflammation

Inflammation begins minutes after injury, when neutrophils reach the wound site (Sanon et al., 2016). Neutrophiles start cleaning the wound from foreign debris and bacteria, and release chemotactic agents that amplify the immune response, such as TNF-α, interleukin 1-beta (IL-1β), and interleukin 6 (IL-6) (Sanon et al., 2016). Monocytes are then recruited to the wound site and mature into macrophages. Macrophages continue the cleaning process and release essential factors for the progression of the healing process, such as transforming growth factor alpha (TGF-α), TGF-β, and insulin-like growth factor 1 (IGF-1) (Goh et al., 2016). By releasing these signaling factors, macrophages play a crucial role in the transition from the inflammation to the proliferation phase (Sanon et al., 2016).

2.2.3 Proliferation

The proliferative phase starts 24-48 hours after injury, when the first fibroblasts arrive at the site of injury attracted by the factors released by platelets and macrophages in the fibrin clot (Bainbridge, 2013). Once in the fibrin clot, fibroblasts proliferate and produce MMPs and ECM components such as collagen III, fibronectin and hyaluronic acid, transforming the clot into a new matrix of connective tissue (Trebaul et al., 2007). In addition, during this stage other important events take place, such as re-epithelialization, neovascularization, and formation of granulation tissue, explained in the following sections (Bainbridge, 2013).

Re-epithelialization

Re-epithelialization starts within hours after injury and is the process by which the new epidermis is created (Goh et al., 2016). Due to loss of contact inhibition and by the presence of growth factors released in the wound bed, keratinocytes and fibroblasts of the wound periphery are stimulated to proliferate and migrate into the newly formed ECM (Goh et al., 2016). Stem cells from the hair follicle bulge also contribute to epidermal restoration by differentiating into epidermal progenitor cells (Ito et al., 2005). Thanks to this process, the basement membrane and the different epidermal layers are reestablished but hair follicles and other skin appendages are not usually regenerated (Sanon et al., 2016).

Neovascularization

Neovascularization involves the growth of new capillaries in the injured site and, despite having a major role in the proliferation phase, it is actually initiated immediately after tissue injury (Kumar et al., 2015). This process allows to provide the newly created tissue with nutrients and gas exchange, and it is critical for a successful wound healing and maintenance of the tissue (Sanon et al., 2016). Interestingly, the density of blood vessels generated during the proliferative phase is higher than in uninjured skin (Johnson and Wilgus, 2014).

Neovascularization occurs through three different mechanisms: angiogenesis, vasculogenesis and arteriogenesis (Stavrou, 2008). Angiogenesis is the formation of new blood vessels through splitting or sprouting of pre-existing ones (Tahergorabi and Khazaei, 2012). Vasculogenesis is the *de novo* generation of vessels by homing and assembling of circulating endothelial progenitor cells (EPCs) produced in the bone marrow into capillaries in the tissue (Asahara, 1997; Takahashi et al., 1999; Crosby et al., 2000). Arteriogenesis is the process of structural enlargement and

remodeling of pre-existing small arterioles into larger vessels (Helisch and Schaper, 2003). Among these mechanisms, the one that mostly contributes to restore the blood supply in skin injuries is angiogenesis through sprouting, by which endothelial cells (ECs) from pre-existing capillaries get activated, proliferate, migrate and form new vessels (Johnson and Wilgus, 2014). This process is shown in Fig. 2.6 and is explained in detail in the next paragraph.

In healthy tissue, blood vessels are maintained in a quiescent state. In the inner surface, endothelial cells are tightly adhered to each other creating a barrier that allows the normal circulation of blood flow (Johnson and Wilgus, 2014). In addition, mature vessels are surrounded by a basement membrane composed mainly of collagen IV and laminin covered by mural cells (Maragoudakis, 2000). Mural cells, which include pericytes and smooth muscle cells, promote ECs survival and help maintain vessel stability (Maragoudakis, 2000). In the event of an injury, there is an increase of pro-angiogenic factors in the wound site that activates endothelial cells. These pro-angiogenic factors consist of blood components, such as thrombin and fibrinogen fragments, as well as several growth factors released by inflammatory cells, keratinocytes and fibroblasts in response to hypoxia and inflammation, including vascular endothelial growth factor (VEGF), platelet derived growth factor (PDGF), TGF-β, and angiopoietin-1 (Ang-1) (Stavrou, 2008). When these factors bind to ECs surface receptors, they begin loosing their cell-cell adhesion, and start to proliferate and migrate. In addition, they release proteolytic enzymes, mainly MMPs, which detach mural cells and degrade the vessel basement membrane, providing the route to generate a new sprout. A single endothelial cell at the leading edge of the sprout, known as tip cell, guides the growth of the new vessel towards and within the wound bed (Gerhardt et al., 2003). Subsequently, ECs adjacent to the tip cell become stalk cells, which proliferate

and migrate behind the tip cell, forming a tubular structure and resulting in the elongation of the sprouting vessel (Carmeliet and Jain, 2011). These sprouts must fuse with neighboring sprouts to become functional in a process called anastomosis, otherwise they will regress (Johnson and Wilgus, 2014). Once fusion occurs, blood flow is established, ECs become quiescent, a new basement membrane is formed, and vessels are stabilized with mural cells (Tahergorabi and Khazaei, 2012).

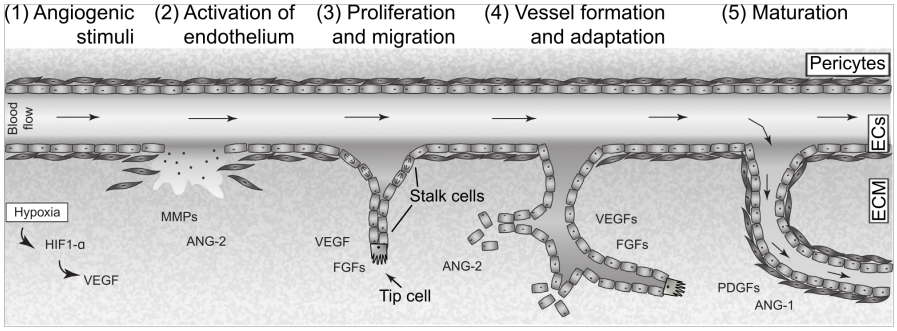

Figure 2.6: Cellular and molecular steps involved in the process of sprouting. Generation of new blood vessels via sprouting takes place through different steps, depicted here. In the event of tissue injury, local factors such as hypoxia up-regulate the release of pro-angiogenic growth factors. These activate ECs, stimulating their proliferation, migration and morphogenesis. The outgrowth of the sprout is led by the tip cell, and followed by the stalk cells. ECs form a tubular structure, that anastomose to other growing sprouts, allowing blood flow. Finally, vessels get stabilized when covered by pericytes. Abbreviations: ANG-1 and 2, angiopoietin 1 and 2; HIF1-α, hypoxia-inducible factor 1-alpha; PLGF, placental growth factor. The rest are defined in the abbreviations list. Adapted from Sanz-Nogués and O'Brien (2016).

Granulation tissue formation

About 4 days after injury, the connective tissue produced by fibroblasts progresses towards the formation of a rudimentary tissue called granulation tissue (Sanon et al., 2016). This tissue, made by loosely organized

collagen bundles and other ECM components, is invaded by a vascular network, fibroblasts, inflammatory cells, and lymphatic vessels (Sanon et al., 2016; Boateng et al., 2008). The high amount of blood vessels present in this tissue provides it with its characteristic red or deep pink color, which indicates the proper progression of the healing (Sanon et al., 2016).

2.2.4 Tissue remodeling and wound contraction

The final phase of the healing process consists in the contraction and remodeling of the granulation tissue and its reorganization into a mature scar (Sanon et al., 2016). This process begins about 2-3 weeks after injury and can lasts for more than two years (Reinke and Sorg, 2012; Allen-Hoffmann and Rooney, 2016). Mechanical tensions experienced by fibroblasts in the granulation tissue, together with factors such as PDGF and TGF-β, are known to trigger fibroblast differentiation into myofibroblast (Rodemann and Rennekampff, 2011). Myofibroblasts contain high amounts of alpha-smooth muscle actin (α-SMA), which are incorporated in intracellular stress fibers capable of generating tensile forces responsible for wound contraction (Sanon et al., 2016).

Simultaneously to wound contraction, tissue remodeling takes place. MMPs, tissue inhibitor of metalloproteinases (TIMPs), and fibroblasts allow the replacement of collagen III to collagen I, which has a much higher tensile strength, producing a more cross-linked matrix (Sanon et al., 2016). During this phase, there is also regression of the vascular network and cell population, returning to levels close to uninjured skin (Goh et al., 2016). Although restoration of skin continuity is achieved, the scar that this process generates has 30% less mechanical strength than the uninjured tissue (Sanon et al., 2016).

2.3 Types of wounds

Wounds can be classified according to multiple parameters. Nevertheless, the most important factors for their evaluation are etiology or causing agent of the wound, depth of the injury, and duration of the healing process (Percival, 2002).

The way in which skin injury occurs totally determines how the wound will heal (Percival, 2002). Following this criteria, wounds are classified as incised, shearing, crushing, burns, and contaminated (Percival, 2002).

Depending on the number of skin layers affected by the injury, wounds are referred to as superficial wounds, partial thickness wounds and full-thickness wounds. If only the epidermis is affected, the wound is termed superficial (Boateng et al., 2008). Injuries reaching both the epidermis and deeper dermal layers affecting blood vessels, sweat glands and hair follicles are referred to as partial thickness wounds (Boateng et al., 2008). Finally, when the injury also reaches the hypodermis or deeper tissues, then they are considered full-thickness wounds (Boateng et al., 2008).

Alternatively, if the classification criteria focuses on the duration of the healing process, wounds can be acute or chronic. When wounds are able to progress through the different stages of the healing process they are considered acute. On the other hand, if healing is not achieved beyond 3 months post-injury they are classified as chronic (Boateng et al., 2008; Percival, 2002). Chronic wounds are further described in Section 2.5 and, due to their socioeconomic impact, their challenging healing, and the lack of effective therapies, they are the focus of this thesis project.

2.4 Role of calcium in healthy skin and wound healing

Calcium is the fifth most abundant atom and the most common mineral ion in the human body (B.E.C.Nordin, 1988), and plays myriad relevant physiological roles. In bones and teeth, which contain 99% of body calcium, it mainly has a structural function in combination with inorganic phosphate (Bonjour, 2011). In the rest of the body, where calcium is distributed in cells, blood, and body fluids, it is implicated in many physiological processes due to its capacity to alter electrostatic fields and protein conformation (Clapham, 2007).

One of the most crucial functions of calcium is to act as a second messenger in signal transduction pathways (Koolman and Roehm, 2005; B.E.C.Nordin, 1988). Many extracellular stimuli -e.g. growth factors - initiate intracellular signaling cascades that lead to the opening of different calcium channels from the plasma membrane or from intracellular reservoirs, such as the endoplasmic reticulum, causing sudden spikes of calcium in the cell cytoplasma (Koolman and Roehm, 2005). This results in the occurrence of processes such as exocitosis, skeletal and cardiac muscle contraction, nerve excitation, and cell migration, proliferation and apoptosis (B.E.C.Nordin, 1988). The speed and effectiveness of these calcium-controlled processes is partly possible due to the 20,000-fold gradient present between the intracellular ($\approx$ 100 nm free) and extracellular ($\approx$ 2 mM) space, the maintenance of which requires much of cells' energy (Clapham, 2007).

Calcium also acts as a primary signal, since extracellular calcium can bind to transmembrane receptors activating intracellular cascades that modulate cell behavior (Breitwieser, 2008). More specifically, calcium has been described to bind to G-protein coupled receptors, which are

transmembrane receptors that initiate multiple intracellular signaling cascades upon binding of an extracellular ligand (Kobilka, 2007). The most widely studied G-protein coupled receptor activated by calcium is the calcium-sensing receptor (CaSR) (Hofer, 2005). Initially found in parathyroid glands playing an essential role in regulating calcium homeostasis, this receptor is also expressed by many other different cell types and exerts a variety of functions throughout the body (Vezzoli et al., 2017).

In the skin, extracellular calcium plays a vital role both in healthy skin maintenance and in the healing process. As this section will review, calcium is essential not only for keratinocyte differentiation in the healthy epidermis and as a cofactor in the coagulation cascade, but it is also implicated in every step of the healing process (Lansdown, 2002a).

2.4.1 Calcium effect in healthy skin

In intact skin, a clear calcium gradient exists in the epidermis which seems to regulate keratinocytes behavior while they progress to the outer layers of the epidermis (Elias et al., 2002; Kulesz-Martin et al., 1984). Calcium content is low in basal and spinous layers, in which keratinocytes proliferate, whereas calcium levels increase progressively towards the outer stratum granulosum as keratinocyte differentiation takes place, and decreases again in the stratum corneum (Menon et al., 1985). Interestingly, this behavior correlates with *in vitro* studies showing that keratinocytes in low calcium (0.1 mM or lower) media have increased motility and proliferation rate (Magee et al., 1987), while in higher concentrations they undergo the so-called *calcium switch*, which involves passing from a proliferative to a differentiation state (Kulesz-Martin et al., 1984).

The CaSR seems to play a critical role in calcium-mediated keratinocyte differentiation (Tu et al., 2004). Reducing the expression of

the CaSR in keratinocytes cultured *in vitro* impairs cell differentiation (Tu et al., 2001) and its absence in an *in vivo* model demonstrated perturbation in the calcium gradient of the epidermis and in barrier permeability (Tu et al., 2012).

On the other hand, such gradient of calcium has not been reported in the dermis, but extracellular calcium regulates several processes on fibroblasts that can impact the healing process, as it will be explained in the next section.

2.4.2 Calcium effect in the healing process

In vitro an *in vivo* studies suggest that calcium plays an important role in all the phases of wound healing, even though the best acknowledged of these is its implication in the clotting cascade (Lansdown, 2002a).

As explained in Section 2.2.1, hemostasis depends on the aggregation of blood platelets and the clot formation through the release of clotting factors. One of the factors released by platelets is calcium, which acts as a cofactor of several of the clotting factors (Palta et al., 2014). The relevance of calcium in the clotting cascade is illustrated by the fact that calcium chelants, such as ethylenediaminetetraacetic acid (EDTA), sodium citrate, and oxalate, are routinely added to extracted blood to avoid coagulation (Mikaelsson, 1991). In addition to playing this cofactor role, up to 88% of the calcium released by platelets accumulates in the cytosol and triggers a change in platelet shape that facilitates their aggregation in the bleeding area (Koolman and Roehm, 2005).

Extracellular calcium could also play a role in the inflammatory phase of the healing process, since it has been described to function as a chemokinetic substance of monocytes to the wounded area (Olszak et al., 2000) and as an activating agent for neutrophils (Lansdown et al., 1999).

In addition, it is also important in the proliferative phase. In an *in vivo* study with guinea pigs, the application of calcium chloride to the wound was found to help granulation tissue development (Mizumoto, 1987). *In vitro* studies have shown that calcium stimulates proliferation (Dulbecco and Elkington, 1975; Kulesz-Martin et al., 1984; Bhagavathula et al., 2009; Jenkins et al., 2011; Zhang et al., 2014), collagen synthesis (Kulesz-Martin et al., 1984; Rokosova and Bentley, 1986), changes in cell morphology (Dulbecco and Elkington, 1975), migration (Zhang et al., 2014), MMPs expression (Bhagavathula et al., 2009; Jenkins et al., 2011; Zhang et al., 2014) and TIMP expression (Bhagavathula et al., 2009; Jenkins et al., 2011; Zhang et al., 2014), although calcium stimulating concentrations for wound healing have not been deeply explored. The CaSR seems to be implicated in the mediation of many of these processes (Bhagavathula et al., 2009; Jenkins et al., 2011; Zhang et al., 2014). In addition, calcium might stimulate neovascularization, since it promotes mobilization, differentiation and tube formation of EPCs (Aguirre et al., 2010).

Knowledge of the role of calcium during the remodeling phase is fragmentary, but it has been suggested to affect myofibroblast contraction (Follonier Castella et al., 2010) and regulate the apoptosis undergone by cells in this last phase of the healing process (Hennings et al., 1980).

Considering the essential role of dermal fibroblasts in the healing process, the impact of extracellular calcium in the behavior of this cell type, and the lack of studies exploring the optimal stimulating concentrations, Chapter 3 is devoted to find the concentration of extracellular calcium that stimulate a maximum level of different responses carried out by dermal fibroblasts. In addition, in Chapter 4 we gain insight into the implication of the CaSR in mediating some of the responses.

2.4.3 Changes in calcium concentration during healing

Despite the knowledge of the implication of extracellular calcium in so many processes during wound healing, technical difficulties hamper the measurement of concentrations of calcium at every stage. The attempts reported in the literature to measure the evolution of calcium concentrations during the healing process provide conflicting information and studies in human wounds are lacking. In one study that quantified calcium levels from full-thickness skin wound biopsies in rats by atomic absorption spectroscopy, a high increase was detected during the first 5 days after wounding, and normal levels were reached by day 7 (Lansdown et al., 1999). In contrast, another study that measured the calcium composition from porcine and rat wound fluids collected through different methods found that calcium levels decreased in early stages of the healing process (Grzesiak and Pierschbacher, 1995). Thus, new or optimized techniques are needed in order to achieve a precise quantification of the extracellular levels of calcium in the healing process.

2.5 Chronic wounds

Chronic wounds, also called hard-to-heal or difficult-to-heal wounds/ulcers, are skin injuries that fail to heal over a period of 3 months (Werdin et al., 2009). They are considered a major health and economic burden for developed countries and cause a significant impact in the well-being of people suffering from them (Herber et al., 2007; Vileikyte, 2001). On top of that, the incidence of this silent epidemic is expected to increase in modern societies as risk factors associated with chronic wounds, such as advanced age, obesity, and diabetes, continue their upward trend (Günter and Machens, 2012).

Many different underlying causes can trigger the chronicity of wounds. Taking these into account, the Wound Healing Society classifies chronic wounds into four categories: pressure ulcers, diabetic ulcers, venous ulcers, and arterial insufficiency ulcers (The Wound Healing Society, 2006). Despite their different causative etiologies, these wounds present some common traits that impair their healing, such as a prolonged inflammatory phase, increased levels of proteases and poorly vascularized tissue. All this prevents the wound from forming granulation tissue and achieving re-epithelialization (Werdin et al., 2009; Nunan et al., 2014; Allen-Hoffmann and Rooney, 2016). This section will review the social and economic impact of chronic wounds, their general patophysiology, the main characteristics of the different types of chronic wounds, and the treatments currently available.

2.5.1 Social and economic impact

It is suggested that 1 to 2% of the population in developed countries will experience a chronic wound during their lifetime, although reliable estimates in the total prevalence and incidence of chronic wounds worldwide are lacking (Järbrink et al., 2016; Gottrup, 2004). Patients with chronic wounds suffer from pain, odor, loss of mobility, distress, depression, and diminished self-image that increase their social isolation (Herber et al., 2007; Vileikyte, 2001). In addition, complications of these wounds may result in limb amputation, leading to disability, or even death (Herber et al., 2007; Vileikyte, 2001). In the USA alone, chronic wounds are estimated to affect 6.5 million people and to cost more than US $25 billion each year to the healthcare system (Vileikyte, 2001). In Spain, the cost represents around 5% of the total annual healthcare expenditure (Soldevilla Agreda et al., 2007). Due to the expected increase in the incidence and prevalence of chronic wounds, and the enormous economic impact that they have on

the healthcare system worldwide, the design of novel strategies to treat these wounds is imperative.

2.5.2 Pathophysiology

A combination of different factors, both local and systemic, can turn a wound into chronic and determines what type of chronic wound develops. Some of the most important local factors that trigger chroncity include infection, tissue maceration, presence of foreign bodies, hypoxia, vascular insufficiency, and mechanical trauma -e.g. pressure- (Guo and DiPietro, 2010; Medina et al., 2005). From a systemic point of view, the most important factors affecting chronic wounds are advanced age, diseases such as diabetes mellitus and renal disease, nutritional deficiencies, obesity, bad habits such as alcoholism or smoking, and consumption of glucocorticoid steroids or chemotherapeutic drugs (Guo and DiPietro, 2010; Medina et al., 2005).

However, regardless of the different underlying factors, all chronic wounds present some common traits. One of the main characteristics is that chronic wounds tend to stall in the inflammation phase of the healing and fail in generating granulation tissue and re-epithelialization. In fact, they present a continuous infiltration of inflammatory cells (Frykberg and Banks, 2015).

Abnormal upregulation of proteinases plays a key role in the development and maintenance of chronic wounds. When compared to acute wounds, the exudate of chronic wounds exhibits much higher levels of pro-inflammatory cytokies, proteinases and reactive oxygen species (ROS) and decreased growth factor activity (Harris et al., 1995; Mast and Schultz, 1996; Frykberg and Banks, 2015). Interestingly, chronic wounds show an imbalance between proteinases, such as MMPs, and their inhibitors (Ladwig et al., 2002), called TIMPs. This causes a decrease in growth factor

levels, receptors and excessive degradation of the ECM, which prevents the healing of the wound (Chen et al., 1992; Harding, 2002). Among the different MMPs active in the wound, MMP1, MMP2 and MMP9 are particularly predominant in chronic wounds (Wysocki et al., 1993; Medina et al., 2005).

Difficulties in generating granulation tissue arise not only from an excessive breakdown of the ECM but also from a decreased collagen deposition (Fleck and Simman, 2010). As mentioned in Section 2.2.3, dermal fibroblasts are the main responsibles for generating new connective tissue. However, in chronic wounds fibroblast present a senescent state, specially in patients of advanced age. This decreases fibroblast proliferation, migration and collagen production rate, and reduces their capability to respond to growth factors (Hasan et al., 1997; Ågren et al., 1999; Wall et al., 2008; Brem et al., 2007).

All together, the general state of a chronic wound can be defined as a prolonged inflammatory phase in which there is excessive breakdown of collagen and decreased synthesis of ECM. Nevertheless, as already mentioned, chronic wounds present different underlying etiologies. For this reason, the next sections will focus in the explanation of the differences among the main types of chronic wounds, including pressure ulcers, vascular -venous and arterial- ulcers, and diabteic food ulcers.

Pressure ulcers

Pressure ulcers, sometimes referred to as bedsores or decubitus ulcers, occur when a tissue is subjected to a constant external force (either shear, compression or both) leading to tissue ischemia, shortage of oxygen and nutrient supply, and eventually tissue necrosis (Bhattacharya and Mishra, 2015). Normally, pressure ulcers develop over a bony prominence, due to the compression and/or shear between the skeleton and soft tissue. These

types of wounds occur mostly to people with immobility, who are confined in beds or chairs for prolonged periods of time due to mental or physical health conditions (Bhattacharya and Mishra, 2015). Many of these patients are localized in hospitals, in which prevalence of pressure wounds is normally above 20% both in Europe and the USA (Sen et al., 2009).

Advanced age is one of the main risk factors for pressure ulcers. In fact, approximately two-thirds of pressure ulcers occur in people aged 60-80 (Leblebici et al., 2007). Skin of elderly people is more sensitive to pressure due to the increased fragility of their blood vessels and connective tissue, and due to loss of fat and muscle, which otherwise cushion the friction between bone and skin (Bhattacharya and Mishra, 2015). Other health conditions that affect blood supply, such as type-2 diabetes, can also make a person more vulnerable to pressure ulcers (Bhattacharya and Mishra, 2015).

Vascular ulcers

Vascular ulcers are caused due to abnormalities in blood circulation and include both venous and arterial ulcers.

Venous ulcers are the most common ulcers of the lower limb, affecting approximately 1% of the population and 3% of people over 80 years of age in westernized countries (Posnett et al., 2009). They occur to people with venous insufficiency, in which blood return is impaired (Sasanka, 2012), and are generally generated in the skin area that spans from the knee to the ankle, since this region is specially affected by venous insufficiency (Sasanka, 2012). Although tissue hypoxia and inflammation are always present in these type of wounds, the underlying mechanisms behind venous ulcers remain unknown (Liu et al., 2011). Different hypothesis have been devised, but neither of them has been properly demonstrated (Liu et al., 2011).

On the other hand, arterial ulcers occur in patients with arterial obstruction, which lead to tissue ischemia. The typical location of arterial ulcerations is the foot and toe region in the advanced arterial disease, and in the ankle in the worse stages (Pannier and Rabe, 2013). Different arterial pathologies can lead to arterial ulcers, but peripheral artery disease (PAD) is the most common (Spentzouris and Labropoulos, 2009). Some of the main factors contributing to PAD development include smoking, advanced age, diabetes mellitus, and hypertension (Bartholomew and Olin, 2006).

Diabetic food ulcers

Diabetic ulcers develop in one every four people diagnosed with diabetes mellitus and, if not treated properly, they may lead to limb amputation (Boulton et al., 2005). Due to the high prevalence of diabetes, approximately 5-10% of the global population (International Diabetes Federation, 2017), diabetic food ulcers are a common health problem in developed countries. Complications associated with the patophysiology of diabetes are the main causing factors of diabetic food ulcers and include neuropathy, vascularity and infection (Han, 2016).

The onset of diabetic food ulcers usually occurs due to the excessive pressure that patients' feet undergo. More than 80% of diabetic foot patients suffer from neuropathy, which causes degeneration of motor and sensory nerves (Blakytny and Jude, 2009; Han, 2016). As a consequence, their foot arches and, together with the loss of pain sensation, this deformity results in excessive friction of the foot against the footwear, opening the wound (Blakytny and Jude, 2009; Han, 2016).

Once the wound is opened, the state of the vascular system in diabetic patients takes a toll on their healing. Diabetic patients often suffer from atherosclerosis, which causes insufficient blood irrigation (Han, 2016). When this lack of blood supply affects the wound site, cellular

activity is limited due to the unmet need for oxygen and nutrients (Han, 2016). In addition, infection is a common complication in these type of wounds, as inflammatory cells are generally attenuated due to diabetes, facilitating bacterial growth (Han, 2016). Bacteria not only deprive cells in the wound from oxygen and nutrients but also release toxins that impair the healing process (Han, 2016).

2.5.3 Current therapies

Among the myriad strategies that are used for the treatment of chronic wounds, from negative pressure therapy to compression therapy, this section will focus mainly on dressings and other topically applied products.

Dressings are materials placed in direct contact with the wound and are always used to help in the healing of chronic wounds (Jones, 2006). Considering the high impact of this type of injuries in developed societies, it is not surprising the wide variety of products available for their treatment (Jones, 2006). As a matter of fact, the global market of wound dressings, valued in US$4.82 billion in 2016 (Visiongain-Ltd, 2017), represents an important segment of the medical and pharmaceutical market.

Dressings have evolved from simple materials that cover the wound, to advanced care systems that maintain the wound protected from the environment while providing an optimal moisture for the healing process (Boateng et al., 2008). More recently, products with bioactive properties have become available. These are able to actively stimulate the healing process generally through administration of growth factors or cells to the injury (Boateng et al., 2008). All these strategies are reviewed in this section.

Moist wound environment

In 1962, the British researcher George Winter made a discovery that revolutionized the conception of wound healing. In an *in vivo* study performed

on pigs he observed that wounds healed faster if kept moist through an accelerated re-epithelialization (Winter, 1995). This was contrary to the conventional conception that wounds should be allowed to dry out and form a scab to heal. Numerous studies followed, demonstrating other benefits promoted by wound occlusion and moisture, such as scar reduction, increased angiogenesis, and reduced pain in patients (Eaglstein, 2001).

Based on this idea, many dressings were designed during the 80's and 90's and still today represent the gold standard therapy for the treatment of chronic wounds (Singh et al., 2013). These include moist-retentive dressings like occlusive films, hydrogels, and hydrocolloids used in wounds with low to moderate exudate levels; and absorbent dressings like foams and alginates, used in heavily exuding wounds (Jones, 2006; Singh et al., 2013).

Debridement

Very often, chronic wounds develop dead tissue known as necrotic tissue, caused by local ischemia and the reduced phagocitic capacity of immune cells (Nunan et al., 2014). The presence of this devitalized tissue seems to be an important contributing factor to wound chronicity, because it supports bacterial growth and act as a physical barrier to healing (Singh et al., 2013). Indeed, removal of this tissue, achieved through debridement, is critical to accelerate the healing process of chronic wounds (Cardinal et al., 2009; Steed et al., 1996).

Debridement methods are classified as surgical, enzymatic, autolytic, mechanical, and biologic (Singh et al., 2013). Among these, the only method performed with the use of dressings is the autolytic debridement. Autolytic debridement is a process carried out by phagocytic cells and proteolytic enzymes present in the wound, by which necrotic tissue separates from healthy tissue (Singh et al., 2013). By using dressings that

promote a moist environment, such as transparent films, hydrogels, hydrocolloids, and alginates, debridement is accelerated because the moist environment promotes phagocytic cell migraton into the wound bed (Jones, 2006; Slachta, 2012; Singh et al., 2013).

Antimicrobials

Infection is present in many chronic wounds and can hamper their healing. Excessive bacterial burden impairs the healing process by reducing the oxygen and nutrients available and producing toxins that damage the tissue (Han, 2016). Most of the products with antimicrobial activity used nowadays are antiseptics that try to minimize the harm on healthy tissue while destroying pathogens. Some examples include silver, cadexomer iodine, polyhexamethyl biguanide, and honey (Vowden et al., 2011). Generally, these are administered by incorporating them in the dressings. However, since these products can damage or irritate healthy tissue, their use is only advised in cases of clear infection (Lansdown, 2002b).

Growth factor therapy

The abundance of many growth factors that have crucial roles in the healing process is decreased in chronic wounds (Lali et al., 2016). Based on this, exogenous administration of growth factors has been explored to improve wound healing and minimize scar. Several growth factors, such as granulocyte macrophage-colony stimulating factor, endothelial growth factor and fibroblast growth factor (FGF), are being evaluated in clinical trials with successful results (Lali et al., 2016).

However, safety concerns in the use of these type of products remain and hinder their approval by regulatory agencies. In 1999, the European Medicines Agency approved the first growth-factor based product for the treatment of chronic wounds, Regranex®, which contained recombinant

PDGF. Thirteen years later this product had to be withdrawn after concerns of increasing risk cancer were raised (European Medicines Agency, 2017; FDA, 2008) and, ever since, no more therapies of this kind have been authorized in Europe. All in all, the application of growth factors is promising but still not a clinical reality.

Skin grafts

Skin grafts consist in the transplantation of one or more layers of skin from the same patient (autograft), a human donor (allograft), or other species (xenograft). Despite being used in the clinic, they present many limitations. Autografts require the creation of a second wound in the patient, while allografts and xenografts might not be available and are associated with immune rejection and transmission of disease. Furthermore, clinical trials have not provided evidence of significant benefits with the use of this type of therapy in front of regular dressings (Warburg et al., 1994; Jankunas et al., 2007).

Skin substitutes

Nowadays, skin substitutes are regarded as the future for wound healing treatment, since they have the potential to not only repair but also regenerate the function of injured skin (Pang et al., 2017). Skin substitutes are artificial skin replacements made by materials of biological or synthetic origin, or a combination of both, and can contain living cells (International Consensus, 2010). Depending on their design and composition, and the type of wound treated, they can act as temporary wound covers or as permanent skin replacements of epidermis, dermis, or both skin layers. These products have emerged from the multidisciplinary field known as tissue engineering. Owing to the current relevance of tissue engineering in biomedical research and its potential in the generation of new therapies for healing

chronic wounds, the following section will provide a deeper insight into this field and into the products that are being developed and already used in the clinics.

2.5.4 Tissue Engineering for chronic wound healing

The emerge of regenerative medicine, and in particular the field of tissue engineering, is envisaged with the potential to offer definite solutions to tissue and organ defects. Tissue engineering is a multidisciplinary field that aims to regenerate tissues - or even organs - combining various aspects of medicine, materials science, engineering, and biology (International Consensus, 2010). Recently, it was defined as "the creation (or formation) of new tissue for the therapeutic reconstruction of the human body, by the deliberate and controlled stimulation of selected target cells through a systematic combination of molecular and mechanical signals" (Williams, 2009).

The classical tissue engineering paradigm consists in seeding cells, ideally from the own patient, on structures that can be made with different biomaterials and serve as temporary scaffolds (Dvir et al., 2011). Cells are then allowed to populate the scaffold *in vitro* and to reorganize themselves into functional tissue before being implanted into the patient. Mechanical signals and bioactive molecules such as growth factors can be introduced in the scaffold to guide the behavior of the cells seeded in it or present in the implantation site - e.g. differentiation towards a specific lineage-. A schematic representation of this process is shown in Fig. 2.7.

Although not always necessary for all the strategies, biomaterials are key elements in the field of tissue engineering. The meaning of the term *biomaterial* has evolved through time, with the advances of material science and health technology (Williams, 2009). Currently, the most accepted definition of biomaterials is the one decided by the American National In-

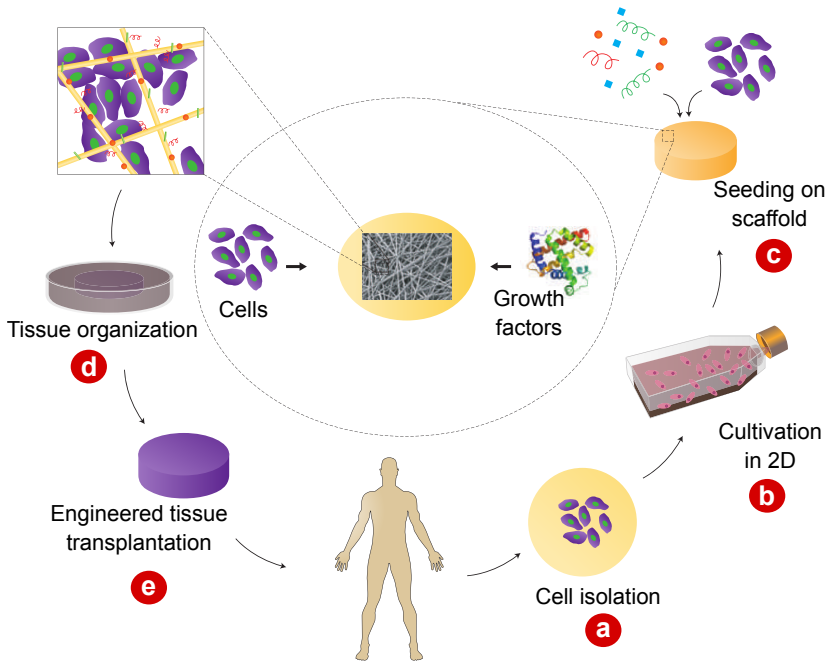

Figure 2.7: Tissue Engineering schematic representation. A typical strategy of TE involving the seeding of cells within porous biomaterial scaffolds. A) Cells are isolated from the patient B) and expanded *in vitro*. C) Cells are then seeded on the scaffolds and other molecules such as growth factors might be added. D) Cell constructs are then cultivated to allow organization into functional tissue. Bioreactors are normally used to allow penetration of nutrients and oxygen within the construct. E) When ready, the construct is transplanted on the defected site of the patient. Adapted from Dvir et al. (2011).

stitute of Health in 1982 that describes biomaterials as "any substance or combination of substances, other than drugs, synthetic or natural in origin, which can be used for any period of time, which augments or replaces partially or totally any tissue, organ or function of the body, in order to maintain or improve the quality of life of the individual". A successful biomaterial should possess a few important properties, such as being compatible with the body (biocompatible), non-toxic, non-immunogenic, non-

thrombogenic, non-carcinogenic, and inexpensive (Bergmann and Stumpf, 2013).

Due to its accessibility and relatively simple structure, the skin is the organ for which more tissue-engineered therapies have been developed, and increasing number of skin substitutes are being commercialized (Varkey et al., 2015). The following sections will review the history of skin substitutes, its different designs, and the products currently available.

Skin substitutes: from their origins to their current status

Skin tissue engineering started with the work of Rheinwald and Green with the cultivation and expansion of keratinocytes to generate epithelial grafts from small skin biopsies (Rheinwald and Green, 1975; Green et al., 1979). Curiously, this was a decade before the the term "tissue engineering" was coined by the Washington National Science Foundation bioengineering panel meeting in 1987 (Nerem, 1992). Since then, a wide variety of skin substitutes have been designed and approved for their clinical application (Varkey et al., 2015).

These artificial skin replacement products not only provide a rapid and safe coverage of the injury but also improve the healing rate compared to standard therapies (Brigido, 2006; Driver et al., 2015; Mostow et al., 2005; Marston et al., 2003; Harding et al., 2013). Moreover, they can act as permanent skin replacements of one or both skin layers.

Skin substitutes may contain cells or be acellular, and can be made by materials of biological or synthetic origin, or a combination of both (International Consensus, 2010). Depending on the presence or absence of cells in the construct, and what skin layer is being mimicked, skin substitutes are classified as acellular dermal equivalents and cellular skin substitutes, which include epidermal, dermal, and bilayered products (Metcalfe and Ferguson, 2007).

Acellular dermal equivalents

The majority of skin substitutes approved by the Food and Drug Administration (FDA) in the United States are acellular dermal equivalents, which are basically cell-free scaffolds with a structure mimicking the dermis. Materials used to make these products include single or combined ECM components, such as purified, animal-derived collagen or hyaluronic acid, or decellularized human cadaver skin or animal (porcine, equine or bovine) tissues - e.g. dermis, small intestine submucosa, pericardium, etc - (International Consensus, 2010).

When used on chronic wounds, these materials are not fully incorporated in the skin. Nevertheless, several clinical trials have shown that they improve healing with respect to standard therapies (Brigido, 2006; Driver et al., 2015; Mostow et al., 2005). Current acellular dermal equivalents approved by the FDA for the treatment of chronic wounds in the USA include CellerateRx®, Integra®, PriMatrix®, AlloDerm®, Graftjacket®, Oasis Wound Matrix®, and EpiFix® (Allen-Hoffmann and Rooney, 2016).

The mechanisms by which acellular matrices promote wound healing are not fully understood, and might depend on the structure and source of the dermal equivalent used. The degradation product of ECM from several sources has multiple biological properties, such as angiogenic, chemotactic, and antibacterial activity (Ko et al., 2005; Brennan et al., 2008; Li et al., 2004). In addition, some substrates reduce the excessive amount of proteases present in chronic wounds (Ulrich et al., 2011).

Overall, acellular dermal equivalents products are showing superior performance to other therapies, but concerns regarding the risk of transmission of disease and their elevated cost limit their application (Hughes et al., 2016).

Cellular skin substitutes

In addition to acellular dermal equivalents, tissue engineered skin substitutes containing autologous or allogenic living cells have also been produced. These products not only provide structural integrity and a barrier to infection, as other skin analogs, but their cell content actively stimulates the healing process by changing the wound microenvironment through the release of growth factors, cytokines and immflamatory mediators (Catalano et al., 2013; Allen-Hoffmann and Rooney, 2016).

Depending on the skin layer they aim to restore, these skin substitutes can be classified as epidermal, dermal and bilayered (Montfrans et al., 2014). Epidermal substitutes are usually created by expansion of patient-derived keratinocytes in the laboratory. Different products are being commercialized, such as Epicel ™, and they are indicated for treating extensive burns rather than chronic wounds. However, they are fragile, costly, slow to produce, and present a varied engraftment success (Sanon et al., 2016).

Cellular dermal substitutes that are being commercialized contain fibroblasts from either autologous or allogenic origin (Groeber et al., 2011). An example of a dermal skin substitute approved by the FDA is Dermagraft® (Organogenesis Inc.), which contains cryopreserved human foreskin fibroblasts within a bioabsorbable polyglactin mesh scaffold. This product functions by providing a dermal matrix that facilitates re-epithelialization by the patient's own keratinocytes. In addition, fibroblast present in the substitute stimulate the healing process by secreting ECM proteins, growth factors, and cytokines into the wound until they undergo normal apoptosis a few weeks post-implantation (Groeber et al., 2011). This product improved the healing of diabetic food ulcers and venous ulcers when compared to conventional therapies (Marston et al., 2003; Harding et al., 2013).

Bilayered skin substitutes are anatomically similar to intact human skin because they are composed of stratified human keratinocytes grown on dermal equivalents containing living human fibroblasts. Currently, only a few have been approved by the FDA and only Apligraf® (Novartis) is indicated to treat chronic skin wounds, as long as they are not infected. This product contains a stratified epidermis made with human neonatal keratinocytes and a dermal equivalent made with bovine type I collagen containing human neonatal fibroblasts (Organogenesis, 2010). It lacks the presence of other skin structures such as hair follicles, sweat glands or blood vessels and it does not provoke host immune rejection (Lovas, 2002). Clinical trials have demonstrated the accelerated healing capacity of Apligraf® even when compared to acellular dermal equivalents (Kirsner et al., 2015). However, it presents a higher risk of infection because the shelf life of this product, 10 days, is insufficient to complete sterility tests needed (Rep, 1998).

Future directions

Skin substitutes have already proven their efficacy in the treatment of chronic wounds. However, there is considerable room for improvement in their understanding, design and commercialization.

Despite the initial promising results, larger randomized clinical trials are needed to validate the efficacy of skin substitutes in front of other strategies in the treatment of chronic wounds. In addition, their clinical use is still limited due to economic and regulatory issues, so they must clearly prove to be cost-effective and safe in order to become a clinical standard. Thus, different steps of the manufacturing chain must be improved, such as the standardization of production processes, reduction in costs, and better control over the entire process (Catalano et al., 2013). The rise of new technologies such as 3D bioprinting might offer solutions

to these issues (Binder and Skardal, 2016). Another factor that limits their large-scale marketing is their short lifespan, so preservation and storage protocols must be optimized and standardized (Catalano et al., 2013).

Skin substitutes have the potential to completely restore the function of the skin. To reach this goal, many improvements should be implemented. Skin appendages such as swat glands and hair follicles could be introduced, as well as different cell types such as melanocytes (Furth, 2016). In addition, skin substitutes should stimulate angiogenesis in the implanted site to increase engraftment success (Furth, 2016). All in all, despite the still-needed improvements, tissue-engineered skin substitutes are a very promising strategy for treating chronic wounds.

2.6 Bioceramics for soft tissue regeneration

Bioceramics are inorganic biomaterials that contain calcium and other mineral ions. They are chemically similar to bone and have been widely investigated for bone and teeth regeneration purposes. Bioceramics are characterized for being bioactive, which means that they induce a specific biological activity (Hastings, 1989). Bioceramics' bioactivity has normally been attributed to their capability of binding to living tissues (Hench and Wilson, 1984). Recently, their bioactivity has also been related to the inorganic ions that they release as they degrade which, in the right concentration and rate, can stimulate antibacterial activity or biological processes such as angiogenesis (Hoppe et al., 2011). This has motivated to extend the application of bioceramics from hard tissue to soft tissue regeneration.

Depending on their structural characteristics, bioceramics are classified as bioactive ceramics, bioactive glasses, or bioactive glass-ceramics . Bioactive ceramics normally have a crystalline structure made with calcium-phosphate. Bioactive glasses have an amorphous

structure and they are composed of glass-forming oxide such as SiO_2 -e.g. bioglass 45S5-, B_2O_3 (borate glass), or P_2O_5 (phosphate glass). Finally, bioactive glass-ceramics consist of a two-phase mixture of crystals in a glass-matrix. In the three cases, the structural differences of these materials affect their degradability and their mechanical properties (Vallet-Regi, 2014).

Among the different bioceramics, bioactive glasses are the ones most extensively studied for application in soft tissue regeneration. One of the main advantages of bioactive glasses, specially the ones obtained through the process known as sol-gel method, is that their structural and chemical composition can be tailored at a molecular level by changing the starting material, temperature, or the way they are processed (Gorustovich et al., 2010). Thus, their degradation and bioactive properties can be adjusted to a specific tissue engineering application. Table 2.1 shows the atomic composition of some of the bioglasses that have been used for soft tissue regeneration.

Table 2.1: Examples of some bioglass compositions investigated in laboratories worldwide. Adapted from Miguez-pacheco et al. (2015).

Composition (wt%)	Na_2O	K_2O	MgO	CaO	SiO_2	P_2O5	B_2O_3	CaF_2
45S5	24.5	-	-	24.5	45.00	6.00	-	-
13-93	6.00	12.00	5.00	20.00	53.00	4.00	-	-
13-93B3	5.50	11.10	4.60	18.50	-	3.70	56.60	-
58S	-	-	-	32.60	58.20	9.20	-	-
S53P4	23.00	-	-	20.00	53.00	4.00	-	-
13-93	21.64	-	-	21.64	50.76	5.99	-	-
45S5F	24.50	-	-	12.25	45.00	6.00	-	12.25
S53P4	23.00	-	-	20.00	53.00	4.00	-	-
46S6	24.00	-	-	24.00	46.00	6.00	-	-

The formulation 45S5, also known by the commercial name Bioglass®, has been the most studied for soft tissue regeneration. This bioactive glass was designed by Hench et al. (1971) more than 40 years ago and

is considered the grandfather composition (Jones, 2013). Additionally, other glass-forming systems such as borate or phosphate glass have also shown bioactive properties (Rahaman, 2014). Many studies have demonstrated the biocompatibility of these materials with soft tissues and their beneficial repairing properties in wound healing, cardiac and laryngeal tissue, lung, nerve, gastrointestinal and urinary tract, and vascularization (Miguez-pacheco et al., 2015). In the following section, two of these new stimulatory applications of bioceramics will be reviewed: wound healing and angiogenesis.

2.6.1 Wound healing application

Several studies have reported improved healing when some compositions of bioceramics have been added on wounds of animal models (Kawai et al., 2011; Jebahi et al., 2013; Li et al., 2016), or even on human patients (Wray, 2011). The improvement of the healing rate has been often related to the increased vascularization observed at the wound site after bioceramic application (Li et al., 2016; Sen et al., 2002). In addition, some other studies have acknowledged other effects, such as increase of tissue strength (Gillette et al., 2001), hemostatic activity (Dai et al., 2009; Ostomel et al., 2006a), proliferation of fibroblasts (Li et al., 2016), and formation of connective tissue (Majeed and Naimi, 2012) and granulation tissue (Li et al., 2016).

As reviewed in Section 2.4, calcium is involved in many processes related to the healing process and could be playing an important role in the above mentioned studies. However, again, these studies generally fail in reporting the concentration of the different ions released from these materials and relating the biological effects observed with these ions. These information would considerably contribute to the design of bioceramics with optimal ion release for wound healing.

This thesis project is mainly devoted to gain insight into this matter. Chapter 3 explores what concentrations of calcium from calcium chloride and calcium released from a newly designed calcium-phosphate bioglass particles stimulate different biological responses carried out by dermal fibroblasts that can impact the healing process. In addition, Chapter 4 studies the implication of the calcium-sensing receptor in the mediation of some of these processes. Then, in Chapter 5 the above mentioned particles are introduced in a dressing and the effect on wound healing and angiogenesis is evaluated on an *in vivo* pressure ulcer model.

2.6.2 Angiogenic application

Neovascularization is essential in the process of wound healing (Section 2.2.3) but also for the successful implantation of tissue engineered scaffolds. The need for a proper vascularization lies on the fact that, when cells are further than 100-200 μm from capillaries, their survival is hindered due to limited diffusion of nutrients, oxygen and waste products (Jain et al., 2005). Tissue engineering strategies to achieve increased vascularization have consisted mainly in the introduction of growth factors - e.g. VEGF - and signaling molecules in scaffolds. However, translation into the clinics of protein therapy faces several challenges, including excessive costs of production, poor stability and short half-life of the protein, and difficulties in delivering safe and effective doses (Formiga et al., 2012). Therefore, new strategies are needed to achieve neovascularization of the tissue engineered constructs in the implanted site.

Bioceramics are regarded as a promising biological-free alternative to stimulate angiogenesis, based on the properties of the ions they release. *In vitro* studies have demonstrated that, when in contact with Bioglass® or its ionic dissolution, different cell types including fibroblasts and ECs are

stimulated to proliferate (Day et al., 2004; Day, 2005) and to release key angiogenic factors such VEGF or FGF-b (Day et al., 2004; Keshaw et al., 2005; Day, 2005; Leu and Leach, 2008). In addition, media previously incubated with these materials induces the creation of networks among ECs in the tube formation experimental model (Leu and Leach, 2008; Zeng et al., 2014).

When evaluated on *in vivo* models, such as the chorioallantoic membrane (CAM) of chick embryos or the subcutaneous implantation in rodent, Bioglass® or Bioglass®-containing composites have shown to be well tolerated by the tissue and to promote neovascularization (Gerhardt et al., 2011; Day et al., 2004). These studies also point out that an optimal dose of ionic release is needed to achieve bioactivity while avoiding toxicity, but did not explore which specific ionic products and concentrations stimulate cells. Neither did they investigate through what specific pathways the stimulation occurs.

Calcium could be partly implicated with the observed angiogenic stimulation. Extracellular calcium has been reported to stimulate migration, tube formation and activation of signaling pathways of endothelial progenitor cells (EPCs) (Aguirre et al., 2010). In addition, calcium-releasing bioceramics promote angiogenesis *in vitro* by increasing proliferation and tube formation of EPCs and human umbilical vein endothelial cells (HUVEC) (Chen et al., 2015; Aguirre et al., 2010) and stimulate blood vessel formation *in vivo* (Oliveira et al., 2016; Chen et al., 2015; Castaño et al., 2014; Vila et al., 2013).

Other ions that have shown to stimulate angiogenic responses have also been incorporated in the structure of bioceramics. Copper and cobalt, for instance, have been found to activate hypoxia inducible factor-1α, which enhances the transcription of several angiogenic genes, including VEGF (Feng et al., 2009; Tanaka et al., 2005). Indeed, bioglasses containing these

ions have showed improved angiogenic stimulation *in vitro* (Wu et al., 2012; Rath et al., 2014; Sen et al., 2002) and *in vivo* (Barralet et al., 2009; Lin et al., 2014). Thus, bioceramics seem to offer great possibilities as angiogenic-stimulating agents in tissue engineered scaffolds. Yet, a better understanding of the biological effects stimulated by the different ions *in vitro* and *in vivo*, as well as the range of optimal dose, is required.

In Chapter 6, we characterize the calcium release from novel glass-ceramic particles and test the vasculogenic capability of a composite material made with the combination of a functionalized synthetic hydrogel, the glass-ceramic particles, and human mesenchymal stromal cells.

2.7 Models to study wound healing therapies

Similarly to the preclinical analysis that any new drug must undergo in order to reach human patients, new treatments for wound healing also need to be subjected to several tests to ensure their safety, efficacy and efficiency. To achieve this, numerous *in vitro* and *in vivo* models have been developed that allow to test a treatment in the context of wound healing.

Chronic wounds respond differently to treatment than acute wounds, due to their different patophysiology (Demidova-Rice et al., 2012). For this reason, when choosing a model, it is important to take into account the specific aspects of the type of wound that aims to be treated.

In this section I will review some of the most common models that are employed to study therapies to treat chronic wounds, as some of them are used in the present thesis work. These include *in vitro* experiments that assess the response to a treatment of cells implicated in the healing process, mainly keratinocytes and fibroblasts, and the generation of different types of chronic wounds in animal models to test the efficacy of a dressing. Owing to the high relevance of vascularization in the healing process, and

because it is studied in this thesis, *in vitro* and *in vivo* angiogenic models are also described. For the sake of concision, models that focus on inflammation and antibacterial properties are not included in this review.

2.7.1 *In vitro* models

Cytotoxicity and proliferation

The first step needed for the development of drugs or medical devices consists in the assessment of its cytotoxic effect on cells *in vitro*. If the therapy wants to be translated into the clinics, this analysis should be carried out following the ISO 10993 (Standards, 2009) guidelines. This ISO specifies that, depending on the nature of the sample to be evaluated, the potential site of use, and the type of application of the medical devise, cytotoxicity can be studied by exposing the cells to the material either directly, indirectly, or to an extract of it. Then, cytotoxicity should be analyzed through different methods that allows to assess cell damage by morphological means (microscopic examination), measurement of cell death - e.g. live-dead assay, lactate dehydrogenase (LDH) release into the media -, measurement of cell growth - e.g. Brdu incroportaion into newly synthesized DNA, Picogreen binding into double-stranded DNA-, and quantification of cellular metabolic -activity - e.g. MTT, Alamar Blue^{TM} -. For a complete cytotoxic and proliferative analysis, two or more of these assays should be performed (Standards, 2009). When cell viability is reduced more than 30%, the material is considered cytotoxic. This ISO encourages the use of cell lines, but primary cell cultures can also be used if reproducibility is demonstrated. When testing wound healing therapies, dermal fibroblasts, keratinocytes and ECs are normally used.

Migration

Migration of the different cell types involved in the healing process, including dermal fibroblasts, keratinocytes and ECs, is crucial for the closure of the wound. Different *in vitro* models have been used to study migration of these cells, the most widely used ones being the scratch wound assay and the transfilter assay.

The scratch wound assay is a simple, quick (usually 8-24 h) and inexpensive method to quantify the ability of cells to cover the area affected by a wound (Sanz-Nogués and O'Brien, 2016). For this assay, cells that have formed a confluent monolayer on plate-wells are mechanically injured using a tip, needle, or cell scrapper. Then, the evolution of the wound area is quantified (Sanz-Nogués and O'Brien, 2016). Alternatively, cells can be injured thermally, electrically, and optically. To ensure that wound closure is due solely to migration, cell proliferation can be inhibited by culturing them in low serum conditions or treating them with mitomycin C (Eccles et al., 2009).

Transfilters, also known as modified Boyden chambers, allow the quantification of directional migration towards a stimulus. These assays comprise two chambers divided by a 8 μm pore polycarbonate filter usually coated with collagen, fibronectin or Matrigel, to mimic the *in vivo* environment (Tahergorabi and Khazaei, 2012). Cells are seeded on the upper chamber and culture medium with the angiogenic agent is placed in the lower chamber. After some time of incubation, normally from several hours up to 48h, cells that have crossed the filter are counted (Sanz-Nogués and O'Brien, 2016). The more chemotactic a substance is, the more cells cross the filter.

Proteolytic enzyme production

The detection of altered synthesis rates and/or activity of proteolytic enzymes such as MMPs is important when studying chronic wounds. A common technique used to measure these changes is the zymography assay. This semi-quantitative technique allows to detect the activity of proteolytic enzymes contained in a cell lysate or supernatant. Samples are loaded onto a polyacrylamide gel containing sodium dodecyl sulfate (SDS) to linearize the proteins, and a substrate for the enzyme, usually gelatin (Vandooren et al., 2013). Then, proteins are separated by molecular weight under an electric current and nonreducing conditions. Afterwards, the gel is placed in a renaturing buffer that partially refolds proteins to their active conformation followed by immersion in a developing buffer that allows the enzymes to degrade the substrate contained in the gel. Finally, after staining and washing the excess dye, clear bands in the gel appear showing the area that has been digested by the proteolytic enzymes (Hu and Beeton, 2010). Densitometric quantification of the band intensity is used to estimate the protease content of the sample (Hu and Beeton, 2010). Alternatively, other methods such as Enzyme-Linked ImmunoSorbent Assay (ELISA), Real Time polymerase chain reaction (RT-PCR) or Western Blot can be used to quantify the synthesis of proteolytic enzymes and their inhibitors.

ECM synthesis

Quantification of synthesis of ECM components such as collagen, fibronectin, elastin, laminin, and hyaluronic acid can be performed by different methods, including immunostaining, colorimetric methods (Tebu-bio, 2017), ELISA or RT-PCR.

Tube formation

The tube formation assay is a rapid (4-16 h) and quantitative model widely used to screen angiogenic stimulators and inhibitors (Sanz-Nogués and O'Brien, 2016). This assay models morphogenesis that ECs undergo in the late stages of the angiogenic process. Cells are seeded on a substrate, usually growth factor-reduced Matrigel, were they start to form capillary-like structures after a few hours of being exposed to angiogenic stimulus. Then, several random views area acquired and one or more features are quantified: total amount of networks per field, network length, number of sprouts or branches, and number of ring structures (Sanz-Nogués and O'Brien, 2016).

Fibroblast-populated collagen lattices

In recent years, awareness has been raised on the idea that both dimensionality and stiffness of the substrate affect cell responses (Engler et al., 2006; Reilly and Engler, 2010; Bott et al., 2010; Stamm et al., 2016). Although most cell-based assays have been performed in two-dimensional (2D) monolayer cells cultured on flat and rigid substrates, which allows the simplification and better control of the parameters of study, new models have been designed to expose cells into a more realistic context. These models aim to culture cells in a 3D environment with a stiffness similar to the original tissue to obtain a more realistic cell behavior.

Among the different cell types, fibroblasts are particularly sensitive to the matrix stiffness and the 3D environment (Grinnell, 2003; Rhee and Grinnell, 2007; Bott et al., 2010). To study the interaction of fibroblast with ECM in a 3D matrix, a simple model known as the fibroblast-populated collagen lattices (FPCLs) is used. Basically, FPCLs are collagen matrices casted on a petri dish with fibroblasts embedded in them.

Depending on the cell response that wants to be studied, two versions of the FPCL model are utilized: the free-floating (FF) or the attached-delayed-released (ADR). The FF-FPCL has been found to mimics better the granulation tissue while the ADR-FPCL seems to be a better model for scar formation (Carlson and Longaker, 2004). The FF-FPCL, introduced by Bell et al. (1979), is casted on Petri dishes, detached soon after manufacture and let to contract for about 2 days. In this model, cells are not subjected to mechanical tension and fibroblast contract the collagen through traction forces related to locomotion. On the other hand, the ADR-FPCL, firstly reported by Tomasek et al. (1992), is released 4 or 5 days after casting. During those days, fibroblasts develop tension and differentiate into myofibroblasts, expressing α-SMA. When the lattice is detached, they contract very rapidly: within 10 minutes most of the contraction is completed. In both cases, the contraction of the material is quantified by comparing the initial area of the lattice to the final time point.

3D skin models

The use of *in vitro* cellular systems that combine the dermal and epidermal layers, known as 3D skin models, is on the rise. Their increased utilization is explained by the nonexistence of animal models with the same structure as human skin, and the encouragement of a more ethical use of animal testing based on the 3R principles (replace, reduce and refine). Several models for dermatological testing are even already commercially available, such as EpiDermFT™, Phenion® FT Model, and StrataTest® (Stamm et al., 2016).

Despite the inherent limitations of these models, such as lack of blood supply, lymphatic clearance, innervation, and hormonal regulation, the complexity of 3D skin models can be tuned to mimic as much as possible diseased skin (Ruffner et al., 2016). For instance, when patient-derived

fibroblasts from diabetic food ulcers are incorporated, they present some of the aspects of chronic wounds (Maione et al., 2015).

Wounds can be created with many different methods, including mashers, scalpels, biopsy punches, dermatomes, liquid nitrogen, and lasers (Xie et al., 2010; Falanga et al., 2002). Then, soluble substances and different materials can be added on the wound to test their ability to accelerate the healing process (El Ghalbzouri et al., 2004; Xie et al., 2010; Marquardt et al., 2015).

Although ample room for improvement remains to better mimic the complexity of the skin and the features of specific types of wounds, in the future, these models are expected not only to provide fundamental new information of wound healing processes but also to facilitate preclinical optimization of dosage, duration of therapies, and treatment strategies prior to clinical trials (Xie et al., 2010).

2.7.2 *In vivo* models

Despite the advantages that 2D and 3D skin models offer, the complexity of the healing process *in vivo* cannot yet be fully recreated in a culture dish. Thus, animal models are still needed to elucidate the real response of a wound against a treatment.

Although many species have served as wound healing models, the vast majority of translational studies use rodent and swine (Ignacio et al., 2016). Rodents are usually the first choice as they are easier and more economical to house and maintain, and allow manipulation of genetic, dietary, and environmental variables (Wong et al., 2011). However, anatomical and wound healing differences exist between rodent and human. Rodents' loose skin is not attached to the subcutis and has a subcutaneous panniculus carnosus muscle that is believed to facilitate wound contraction and collagen formation (Dorsett-Martin and Wysocki, 2008). On the contrary,

human skin is tight and has no panniculus carnosus. Even though wound contraction occurs in both species during skin wound healing, it is considered the main mechanism by which rodent skin heals, while reepithelialization is the main mechanism for tight-skinned species (Dorsett-Martin and Wysocki, 2008).

On the other hand, pig skin is anatomically and functionally very similar to human, and it is also tight, which makes this animal a very useful model of wound healing (Nunan et al., 2014). However, the cost involved in the breeding and maintenance of pigs, together with their poor genetic tractability, limit the use of this model (Nunan et al., 2014).

Unfortunately, there is currently no ideal animal model of the chronic wound, which may explain the lack of success in the translation of novel therapies to human. Indeed, chronic wounds do not naturally occur in laboratory and domestic animals and the animals used fail to recreate the complexity of comorbidities associated with human chronic wounds (Mustoe et al., 2006; Liu et al., 2011). To overcome this limitation, wounds with delayed healing are created by subjecting the skin to lesions such as ischemia, pressure and reperfusion cycles, or by using diabetic, aged, or ovariectomized animals. This section will review the strategies used to create different types of chronic wounds, as well as a widely used animal model to study angiogenic stimulation, the chick CAM model.

The pressure ulcer model

To mimic pressure ulcers, ischemic-reperfusion models are used. Cycles that consist in interrupting and reestablishing blood supply to a specific area of the skin are performed, generally by pinching the skin with magnets and removing them after some hours (Fig. 2.8A-B) (Sundin et al., 2000; Peirce et al., 2000; Stadler et al., 2004; Wassermann et al., 2009). The local hypoxia generated damages the tissue, causing the release of in-

flammatory mediators and ROS, which in turn produce additional damage. The repetition of this process over a number of cycles generates an ulcerous wound. This model has been used on rats (Peirce et al., 2000), mice (Stadler et al., 2004; Wassermann et al., 2009), rabbits, and pigs (Sundin et al., 2000).

Chronic ischemic wounds

Ischemia modeling has been achieved by interrupting the blood supply of specific vessels to the tissue. In the rabbit ulcer model (Fig. 2.8D), an ischemic zone is generated by suturing off two or three arteries that supply the ear before making a wound down to the cartilage to create a full-thickness injury that has very little lateral vascular supply (Ahn and Mustoe, 1990). In mouse and rat, severe necrotic skin wounds can be generated within a week transecting the superior or inferior epigastric vessels. This method is known as the transverse rectus abdominal myocutaneous flap (Peirce et al., 2000). A less severe ischemic model used in rat, mouse and pig is the bipedal flap model (Fig. 2.8C), in which blood flow supplying excisional wounds is surgically prevented (Biswas et al., 2010; Roy et al., 2009; Chen et al., 1999).

Diabetic animal wound models

Some of the patophysiological factors associated with diabetic food ulcers can be mimicked using diabetic animals. One option is to use animal strains generated through genetic manipulation or by selective inbreeding, such as the Akita, NONcNZ010, and db/db mice (Ignacio et al., 2016). Alternatively, diabetes can be chemically induced by administration of toxins such as streptozotocin, which induce hyperglycemia by provoking pancreatic damage (Michaels et al., 2007).

The CAM model

The chick CAM is one of the most widely used models for testing the angiogenic potential of substances and materials. Used for more than 100 years, this inexpensive assay is an *in vivo* test that carry less ethical constraints than rodent experiments, since national legislations worldwide do not consider unhatched birds as living animals (Aleksandrowicz, 2015).

The CAM is an extraembryonic specialized respiratory tissue present in the development of avian species. It allows for gas exchange with the outer environment or, in other words, it functions as a lung during embryonic life (Romanoff, 1960). Between day 8 and 10 of embryo development, the central portion of the CAM is fully developed and responsive to pro- and antiangiogenic stimuli (Deryugina and Quigley, 2008). It is at this time when test substances are grafted on the CAM, and after 3 to 5 days the angiogenic response can be analyzed (Deryugina and Quigley, 2008). The model allows to evaluate the angiogenic response both qualitatively and quantitatively (Ribatti et al., 2006).

This assay can be carried out *in ovo* (Fig. 2.8E) or *ex ovo* (Fig. 2.8F). When performed *in ovo*, a window is carefully created on the eggshell and test substances are applied to the exposed area (Staton et al., 2004). Alternatively, the entire egg content can be transfered into a Petri dish on day 3 of development, so that the whole CAM membrane is exposed. This allows to test a major number of replicates and to visualize the progression of the angiogenic response (Deryugina and Quigley, 2008).

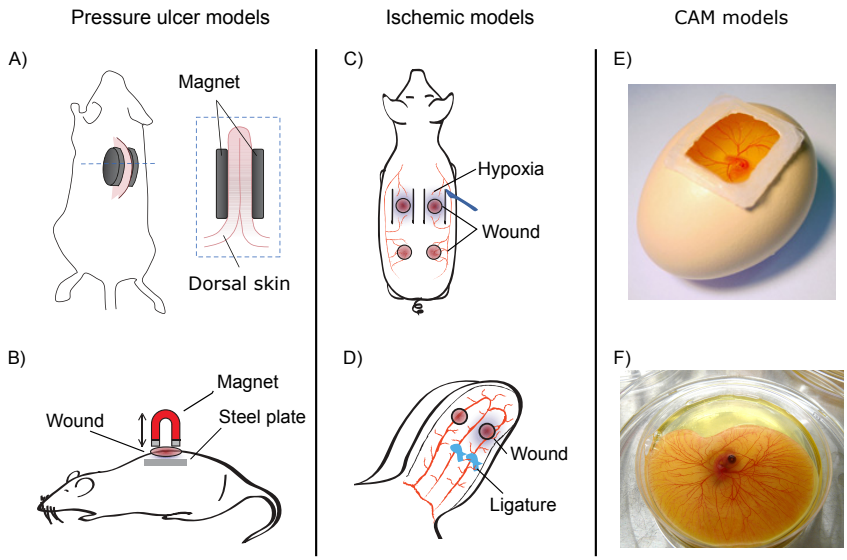

Figure 2.8: Animal models used for testing treatments for chronic wounds. A) Ischemia-reperfusion model in which cyclical pressure is applied with opposing magnets and interpositioned skin. B) Alternative method for ischemia-reperfusion model, in which a metal plate is implanted under the skin of a loose skinned animal and periodic compressions of the skin are applied using an external magnet. C) Pig flap ischemia model, in which surgical incision severs blood flow to specific regions of skin, creating hypoxic zones. D) Rabbit ear ischemia model, where ischemia to a full-thickness wound is generated by ligating the blood vessels that supply the wounded area. E) *In ovo* CAM model. F) *Ex ovo* CAM model. Adapted from Wong et al. (2011) and Nunan et al. (2014).

3 *Effects of extracellular calcium and calcium-phosphate bioglass on dermal fibroblast*

3.1 Introduction

Chronic wounds are a major threat world-wide, specially to developed countries, for the increased presence of risk factors such as an aged population, diabetes, and obesity. Section 2.5 explained in detail the socioeconomic impact of this common disease, its general patophysiology, the distinct features of each type of chronic wound, and the treatments that are currently used. Unfortunately, current therapies, which mainly involve the use of dressings with moisture controlled properties, commonly fail to heal many chronic wounds. Although research in protein therapies and skin substitutes is showing promising results, their translation to the clinic seems to be hampered by regulatory and economical constraints (European Medicines Agency, 2017; FDA, 2008; Frykberg and Banks, 2015). Thus, there is an urgent need to develop new, economic, effective therapies that reach the clinic faster.

In the last years, bioactive glasses have emerged as an alternative strategy to biological treatments for tissue regeneration and wound healing purposes owing their antibacterial, angiogenic and cell stimulating properties (Section 2.6). Indeed, recent studies have claimed accelerated wound healing when applying composite materials containing bioactive glasses on skin injuries (Xu et al., 2015a; Yu et al., 2016; Ma et al., 2014). The ion release produced while bioceramics degrade seems to be behind their stimulatory effects, as observed in *in vitro* studies in which cells are stimulated by media previusoly incubated with bioceramics (Day et al., 2004; Day, 2005; Li et al., 2016). However, little attention has been paid to the individual biological contribution of each of the ionic species. Calcium ion is released by most of the bioceramics and, due to its complex role in skin and the healing process, it could be involved in some of the stimulatory effects observed.

As reviewed in Section 2.4, calcium it is not only relevant acting as a crucial clotting factor at the initial stages of the healing process, but also plays an important role as an extracellular regulator and internal modulator of key cell types of the process including fibroblasts. Indeed, *in vitro* studies revealed that extracellular calcium affects proliferation, collagen synthesis and morphology of fibroblasts (Kulesz-Martin et al., 1984; Rokosova and Bentley, 1986; Dulbecco and Elkington, 1975; Wang et al., 2015). However, in most of the studies performed, the optimal stimulating concentrations have not been deeply explored. Considering the pivotal role of dermal fibroblast in the healing process as described in Section 2.2, from the late inflammatory phase until full re-epithelialization, it is relevant to achieve a better understanding of the effect of different calcium concentrations on the biological response of fibroblasts.

To date, the only calcium ion releasing dressings available in the market are alginates, but these are normally applied regarding their moisture

controlling properties. When alginates are placed on exuding wounds, an ion-exchange takes place between calcium ions in the dressing and sodium ions in serum or wound fluid (Thomas, 2000), releasing calcium into the wound bed. Although this effect has an acclaimed value in hemostasis and coagulation in the early lesion of acute injuries (Groves and Clawrence, 1986), the benefits and implications in subsequent stages of healing by the released calcium has attracted minimal attention.

Studies aiming to unravel the impact of calcium in wound healing performed in animal models by topical administration of $CaCl_2$ have shown conflicting results. One study showed how diary administration of 5 mM in guinea pig impaired wound healing (Sank et al., 1989), while another showed how $CaCl_2$ administration improved the formation of granulation tissue (Mizumoto, 1987). Considering the impact of calcium on the healing process and the relevance on the dose administrated, new systems with controlled calcium ion release could be designed to improve the wound outcome.

Such control could be achieved with bioactive glasses. High calcium-releasing bioactive glasses have generally been utilized for hemostatic purposes (Dai et al., 2009; Ostomel et al., 2006b), but not for stimulating other healing stages. For wound healing, most of the studies have used silica-based bioglasses with a relatively low calcium content and release (Xu et al., 2015a; Yu et al., 2016; Ma et al., 2014). Recently, novel bioactive glasses have been designed, named calcium-phosphate organically modified glasses (CaP ormoglasses), that allow a more tunable behavior of the ion release, thus improving their instructive capacity (Sachot et al., 2013; Castaño et al., 2014; Sachot et al., 2015). Indeed, composite materials based on the combination of a polymeric support (i.e. poly-lactic acid) and CaP ormoglass provided a controlled calcium release of biologically relevant concentrations able to elicit an angiogenic effect both *in vitro* and *in*

vivo (Oliveira et al., 2016). Therefore, with a better understanding of the necessary doses of extracellular calcium to improve the healing of wounds, CaP ormoglasses might be promising candidates to be used as off-the-shelf biological-free bioactive system on chronic wounds.

Based on the idea of exploring the potential use of calcium and CaP ormoglasses in the context of chronic wound healing, this study aimed to identify concentrations of extracellular calcium and calcium-releasing ormoglasses that stimulate biological responses of skin wound healing carried out by dermal fibroblasts *in vitro*. More specifically, sol-gel produced CaP ormoglasses coded SG5 were characterized and media conditioned with different concentrations of calcium from $CaCl_2$ (Ca-$CaCl_2$) or released by the bioactive glass (Ca-SG5) were tested on rat dermal fibroblasts to study cell growth, cell migration, extracellular matrix (ECM) remodeling, contractile capacity, and wound-healing related gene expression.

3.2 Materials and Methods

3.2.1 Calcium-phosphate particle preparation and size characterization

Ormoglass particles of oxide based composition $CaO{:}P_2O_5{:}Na_2O{:}TiO_2$ (44.5 : 44.5:6:5) were prepared by controlled hydrolysis sol-gel method at inert atmosphere as described previously (Lansdown, 2002a). The precursors used were prepared as follows. Calcium (Ca) and sodium (Na) 2-methoxyethoxides precursor solutions were prepared by refluxing metallic calcium (Sigma-Aldrich, 98%) and sodium (Panreac, 99%) respectively in anhydrous 2-methoxyethanol (Sigma-Aldrich, 99%) at 124 °C during 24 h. Phosphorus (P) ethoxide precursor solution was prepared by refluxing P_2O_5 (Sigma-Aldrich, 99,99%) in absolute ethanol (Panreac,

99,9%) at 78 °C during 24 h. Titanium (Ti) alkoxides precursor solution was prepared by diluting Ti-tetraisopropoxide (Alfa Aesar, 97%) in absolute ethanol. Then, Ti, Ca and Na precursors were added in a balloon with 1h of vigorous stirring, followed by the addition of previously distilled 1,4-dioxane until a 5% v/v concentration was reached. The last precursor solution, P alkoxides precursor, was added at a control rate of 2.5 mL/h at 4 °C with an infusion pump. Then a basic catalyzing aqueous solution with a molar relation 20:0.1:4 H_2O:NH_3:EtOH and a Ti:H_2O ratio of 1:60 was added at 1 mL/h and 4 °C. The solution was aged in a closed vial at 70 °C for 4 days under vigorous stirring. After aging, the produced particles were washed with ethanol and centrifuged five times for 5min at 1,000 g. Finally, the SG5 particles were grinded, dried at 90 °C and stored in a desiccator for further use.

The size of the particles was assessed by dynamic light scattering (DLS) on a Malvern Instruments Zetasizer Nano-ZS instrument. The solution used was absolute ethanol containing 1% Tween® 20 (Sigma) to avoid particle degradation and agglomeration. Before the measurement, the solution containing SG5 was homogenized in a bath sonicator and transferred into a quartz cuvette. SG5 morphology was observed with scanning electron microscope (SEM) ((Nova Nano SEM-230, FEI Company, USA) uncoated on a silicon plate.

3.2.2 Ion release from calcium-phosphate particles and pH change

Ion concentrations and pH changes of the dissolution product of SG5 were measured in two different aqueous solutions: complete culture media (CCM) made with calcium-free Dulbecco's Modified Eagle Medium (DMEM), and MilliQ water with 10 mM 4-(2-hydroxyethyl)-1-

piperazineethanesulfonic acid (HEPES) and 110 mM NaCl and pH adjusted to 7.6 (MQ).

Particle suspensions of 1.2 mg/mL were prepared and incubated at 5% (v/v) CO_2 and 37 °C. Prior to incubation, the lid of the containers with CCM was perforated with a needle to allow gas exchange. After 24 h incubation, suspensions were centrifuged for 10 min at 1,000 g. For the control condition utilized to measure total release of ions from the particles, instead of using the above mentioned aqueous solutions, particles were degraded with 5% HCl in the same proportion (wt/v) as for the release by incubating them at 37 °C in an automatic shaker (Thermomixer Comfort, Eppendorf). The supernatant of all solutions was diluted 1/10 in 1% in HNO_3 and the Ca, P, Na and Ti levels of each solution were measured by inductively coupled plasma optical emission spectrometry (ICP-OES) (PerkinElmer Optima 3200 RL) in triplicates.

Before assessing pH values of the conditioned media, samples were diluted adjusting calcium concentration to the levels used for *in vitro* experiments. Calcium concentration were quantified with the colorimetric method 0-cresolphtalein complexone (Sigma) (Cohen and Sideman, 1979), reading absorbance at 570 nm on the Infinite M200pro microplate reader (Tecan). Once dilutions were made, samples containing CCM were kept in perforated tubes while samples in the MQ solution were completely sealed. Then, samples were kept in the incubator for 30 min to allow stabilization of pH and temperature. Finally, pH was measured with a Laquatwin pH-meter (B-712, Horiba).

3.2.3 Cell isolation and culture

Primary cultures of rat dermal fibroblast were used for all the experiments. Skin biopsies from 2-4 weeks old Wistar rats were used to isolate dermal fibroblasts. Briefly, after separating the dermis from the epidermis, the

dermis was minced and incubated in collagenase/dispase (1.5 mg/mL/ 2.5 mg/mL, respectively) for 2 h at 37 °C. Next, the collagenase/dispase solution containing the dermis was filtered twice with a 100 μm cell strainer (Sigma-Aldrich) to obtain a single cell suspension. The isolated fibroblasts were expanded in CCM consisting of DMEM (Gibco) supplemented with 10% fetal bovine serum (FBS) (Sigma-Aldrich), L-glutamine (L-Glut, Invitrogen), 100 U/mL penicillin (P, Gibco) and 100 U/mL streptomycin (S, Gibco). A stock of cell passage 2 was kept in liquid nitrogen in 10% Dimethyl sulfoxide (DMSO) (Sigma-Aldrich) in FBS. All protocols concerning animal care were approved by the Committee on Ethics and Animal Experiments of the Scientific Park of Barcelona (Permit No. 0006S/13393/2011). When needed, cells were thawed from the frozen stock, grown at 37 °C in 5% (v/v) CO_2, and used within passage 4-6. Medium was changed every three days.

3.2.4 Media conditioning and cell treatment

Ca-$CaCl_2$ media was prepared by dissolving $CaCl_2$ (>96%, Sigma-Aldrich) in calcium-free DMEM, incubating overnight and filter sterilizing it with a 0.22 μm pore size filter. Ca-SG5 media was prepared as follows. A particle suspension of 0.6 mg/mL in calcium-free DMEM supplemented as regular medium was prepared and incubated for 24 h at 37 °C in 5% (v/v) CO_2. After incubation, the suspension was centrifuged for 10 min at 1,000 g and the supernatant was collected and sterile filtered with a 0.22 μm pore size filter.

Calcium released in the conditioned media was measured using the quantitative colorimetric method 0-cresolphtalein complexone (Sigma) as explained in Section 3.2.2. Dilutions were made to prepare specific concentrations needed for the assays. In all experiments, 24 h after seeding cells were rendered quiescent by an overnight incubation in low-serum

and 0.1 mM calcium medium. Afterwards, the different conditioned media were added to the cells.

3.2.5 Cell growth

Cell growth in conditioned media containing 10% FBS was studied by measuring metabolic activity and DNA quantification at day 1, 3 and 6. For metabolic activity determination, cells (2.5 x 10^3) were seeded in 48 well plates. At each time point, Alamar Blue™(Alamar Blue kit, Thermo Fisher Scientific) was added following manufacturer's instructions and fluorescence was read at Ex/Em wavelength of 530/590.

Increase of cell number overtime was assessed by DNA quantification with the Picogreen double-stranded DNA (dsDNA) Assay Kit (Invitrogen). Briefly, 1 x 10^4 cells/well were seeded in 24-well plates. At the above-mentioned time points, cells were lyzed in cold Tris-EDTA buffer (Sigma-Aldrich) by three freeze-thaw cycles and quantification of DNA was performed following manufacturer's instructions. Finally, fluorescence was read at Em/Ex 480/520. For both assays, fluorescence measurement was assessed on the Infinite M200pro (Tecan) microplate reader. Both Alamar Blue™ and Picogreen assays were repeated three times containing five and four replicates per condition respectively.

3.2.6 Total collagen

Collagen secreted in media by the cells cultured with the different conditioned media was measured using the Sircol Collagen Assay (Biocolor, UK), following the manufacturer's protocol. Cells (2.5 x 10^5) were seeded in T25 flasks in complete DMEM. After starvation, cells were treated with 3.5 mL/flask of conditioned media containing 2% FBS for 24 h. Subsequently, media from the flasks was transferred in low protein binding

microcentrifuge tubes and total collagen was measured following manufacturer's protocol. Absorbance signal was measured at 555 nm on the Infinite M200pro (Tecan) microplate reader and values were normalized to the protein content from the cell extract measured with the bicinchoninic acid (BCA) protein assay (Thermo Fisher Scientific). The experiment was repeated three times using four replicates per condition.

3.2.7 Scratch wound assay

To determine the effect on cell migration of the different conditioned media, a scratch-wounded fibroblast monolayer model was employed. Briefly, cells were seeded into 12-well tissue culture plates and cultured to confluence. Confluent dermal fibroblasts were scrape-wounded using a sterile p200 pipette tip by one perpendicular linear scratch. Wells were washed with Phosphate-Buffered Saline (PBS) to eliminate floating and dead cells and conditioned media (2% FBS) was added. Wound closure was monitored by collecting digitized images immediately after the scratch and 24 h afterwards. To ensure recording of the same wound area at every time point, a black line perpendicular to the scratch was painted under the bottom of the plate before cell seeding. Images of two sites per well were captured with an inverted microscope (Nikon TE200) with digital camera (Olympus DP72) using the 4x phase contrast objective lens. Reduction of wound areas was analyzed with Image J 1.48i software. Four replicates per condition were used and the experiment was repeated three times.

3.2.8 Gelatin zymography assay

The activities of matrix metalloprotease (MMP)2 and MMP9 of cell culture supernatants were measured by a gelatin zymogram protease assay. Cells (4×10^4) were seeded in 24-well plates. After starvation, conditioned me-

dia containing 2% FBS) was added and, after 24 h media, was collected and centrifuged at 10,000 g for 10 min at 4 °C. Aliquots of supernatants were mixed with non-reducing sample buffer 3x (0.3% sodium dodecyl sulfate (SDS); 15% 1M Tris-HCl pH 6.8, 30% glycerol and 0.075% bromophenol blue) and 30 µL were loaded on 8% SDS polyacrylamide gels containing 0.1% gelatin (Gelatin from porcine skin BioReagent, Type A, Sigma). Then, prepared samples were subjected to electrophoresis under a constant voltage of 125 mV for 90 min. A protein marker (Kaleidoscope™ Prestained SDS-PAGE Standards, Bio-Rad) was run in parallel for molecular weight identification. Following electrophoresis, gels were washed in 2% Triton X-100 (Sigma) for 30 min at room temperature to remove SDS. Gels were then incubated at 37°C for 18 h in 1x Development buffer (10x Zymogram Development Buffer, Bio-Rad) and stained with 0.5% Coomassie Blue R250 (Bio-Rad) in 50% methanol and 10% glacial acetic acid for 1 day. After destaining, gelatinolytic activities were identified as clear bands against the blue background. To quantify the amount of gelatinase production, gels were scanned on a densitograph (LAS4000 Imaging System) and intensities of the digitalized bands were measured with ImageJ software. All density values were normalized to the intensity of the 0.1 mM sample and to the protein level of the cell extract, which was measured with the BCA protein assay (Thermo Fisher Scientific). The whole process was repeated two times using triplicates per condition, which were run in separate gels.

3.2.9 VEGF ELISA

For quantification of the vascular endothelial growth factor (VEGF)-A released in the medium, the Rat VEGF DuoSet Enzyme-Linked ImmunoSorbent Assay (ELISA) (R&D Systems) was used. Cells (1.5 x 10^4) were seeded in 24 well-plates with complete DMEM. After overnight starvation,

cells were incubated with calcium/SG5-conditioned media containing 10% FBS for 24 h or 72 h. At the final time point, supernatants were collected, centrifuged at 1,500 rpm for 10 min to remove debris and kept at -80 °C until used in the ELISA. Cells were washed with PBS and Mammalian Protein Extraction Reagent (M-PER) (Thermo Fisher Scientific) was added to obtain the cell lysate, which was used to quantify total protein with the BCA protein assay (Thermo Fisher Scientific). This was used to normalize measured values of VEGF in the media of each condition. The experiment was repeated two times using four replicates per condition.

3.2.10 Fibroblast-populated collagen lattice

The attached-delayed-released (ADR)-fibroblast-populated collagen lattice (FPCL) model was used as previously described (Tomasek et al., 1992). Briefly, collagen lattices were polymerized in 6-well tissue-culture plates. Two hundred microliters of the mix of OptiCol^{TM} Rat Collagen Type I (Cell guidance systems) at a concentration of 1.2 mg/mL containing 2 x 10^4 rat dermal fibroblasts were carefully added in each well and allowed to gel for 1 h in a 5% (v/v) CO_2 humidified atmosphere at 37 °C. Then, 2.7 mL of the different conditioned media was added. Gels were cultured for 5 days, at which time digital images were taken of each gel using a Leica MZ16 F stereomicroscope. Then, gels were detached from the surface of the wells by rimming the lattice with a sterile spatula and images of the floating lattices were captured at 0.5, 1, 2 and 4 h. To quantify lattice shrinking, FPCL surface area was measured with ImageJ software and values were normalized to the area of the lattices before being released. The experiment was repeated three times including three replicates per condition.

3.2.11 Western Blotting

Expression of alpha-smooth muscle actin (α-SMA) by fibroblasts incubated in the collagen lattices with different calcium concentrations was quantified by immunoblot analysis. Each gel used in the FPCL experiment was washed with PBS after the last picture acquisition and transferred into microcentrifuge tubes. Cell lysate was obtained by incubating the gels with RIPA supplemented with protease inhibitor cocktail (Santa Cruz Biotechnology) for 20 min in ice. To ensure complete cell lysis, gels were also sonicated (Ultrasonic Processor UP50H) 5 sec at 100% potency in ice twice. Finally, samples were centrifuged at 10,000 g for 10 min at 4 °C and supernatants were transferred into clean microcentrifuge tubes. DNA concentration of each sample was measured with the Picogreen ds DNA Assay Kit (Invitrogen) and equal DNA quantities were mixed with 6x Laemmli buffer and resolved in 10% (wt/v) acrylamide gels followed by transfer onto nitrocellulose membranes (0.45 μm,Bio-Rad). Membranes were blocked in 5% skim milk in Tris-buffered saline containing 0.1% Tween® 20 (TTBS) at room temperature for 1 h, and were sequentially probed with a goat anti-α-SMA polyclonal antibody (1:500 dilution, PA5-18292,Thermo Fisher Scientific) overnight at 4 °C and then glyceraldehyde-3-phosphate dehydrogenase (GAPDH) (1:500, G8795, Sigma) for 1 h at room temperature (RT). After washing 3 times with TTBS, the membranes were sequentially incubated with secondary antibodies conjugated with horseradish peroxidase mouse anti-goat (1:1,000 dilution, 2354, Santa Cruz Biotechnology) and donkey anti-mouse (1:3,000 dilution, SA1-100, Thermo Fisher Scientific) for 1 h in 5% milk-TTBS, and finally developed by Clarity™ Western ECL Substrate (Bio-Rad). The chemiluminescent signal was read with the densitograph LAS4000 Imaging System (GE Healthcare Life Sciences) and the intensities of the digitalized bands were measured with ImageJ

software. Density values were normalized to their correspondent GAPDH band.

3.2.12 Wound healing Real-Time PCR array

Differential gene expression of cells treated with 0.1 mM and 3.5 mM calcium concentration from $CaCl_2$ and from the release of the particles was assessed using the RT^2 Profiler^{TM} PCR Array Rat Wound Healing (PARN-121ZC-2, Qiagen). Cells (8 x 10^4) seeded on 6 well-plate were treated with conditioned media (10% FBS) for 24 h hours and RNA was extracted using the RNeasy PlusMinikit (Qiagen) following manufacturer's instructions. RNA (0.5 μg) of each condition were reversely transcribed with a RT2 First Strand Kit (Qiagen) and the cDNA was used with the RT2 SYBR Green Mastermix (Qiagen) in array plates containing a panel of 84 wound-healing-related genes, 5 housekeeping control genes, a rat genomic contamination control and RT-controls. Quantitative real-time PCR was performed with the StepOnePlus Real-time PCR system (Appleid Systems). Cycling parameters were 10 min at 95 °C (activation) followed by 40 cycles consisting of 15 s at 95 °C (denaturation) and 1 min at 60 °C (extension). The CT threshold for all the conditions was matched and mRNA expression for each gene was normalized to the housekeeping genes of the array. Relative amounts of RNA for each gene and fold increase were calculated by using the 2 -ΔCT method or the 2 -$\Delta\Delta$CT method. The genes selected were the ones with, at least, two-fold higher or lower than the control sample.

3.2.13 Statistics

Data are presented as means ± Standard Deviation. The results were subjected to one or two-way ANOVA and statistical differences between the

groups were analyzed using post hoc Tukey's test at a significance level of 5%. The statistical software used was GraphPad Prism 6.0 (San Diego, CA, USA).

3.3 Results

3.3.1 Characterization of SG5 particles and ion release

Particle size measured with DLS showed an average of 357.3 $\pm$ 38.6 nm (Fig. 3.1A), corroborated with SEM images of the particles (Fig. 3.1B). SEM images also showed that particles presented agglomeration, even if non-ionic detergent Tween® 20 (Sigma) was used, and also amorphous shape.

Assessment of ion release from SG5 (Fig. 3.1C) showed that, after 24h in aqueous media, all the Ca and P were released from the particles. The release behaviour for these ions was the same in CCM and in MQ. Nevertheless, Ti release was significantly different between both solutions and compared to the total Ti in SG5. More specifically, Ti release in cell media was higher than in MQ. Due to the high concentration of Na in cell media and the MQ solution, Na released from the particles could not be properly quantified.

Change in pH in both aqueous solutions by the degradation of SG5 was also measured after adjusting the Ca concentration to the levels used *in vitro* (Fig. 3.1D). While the ionic product degradation of SG5 slightly acidified MQ solution, no changes in pH were detected in CCM.

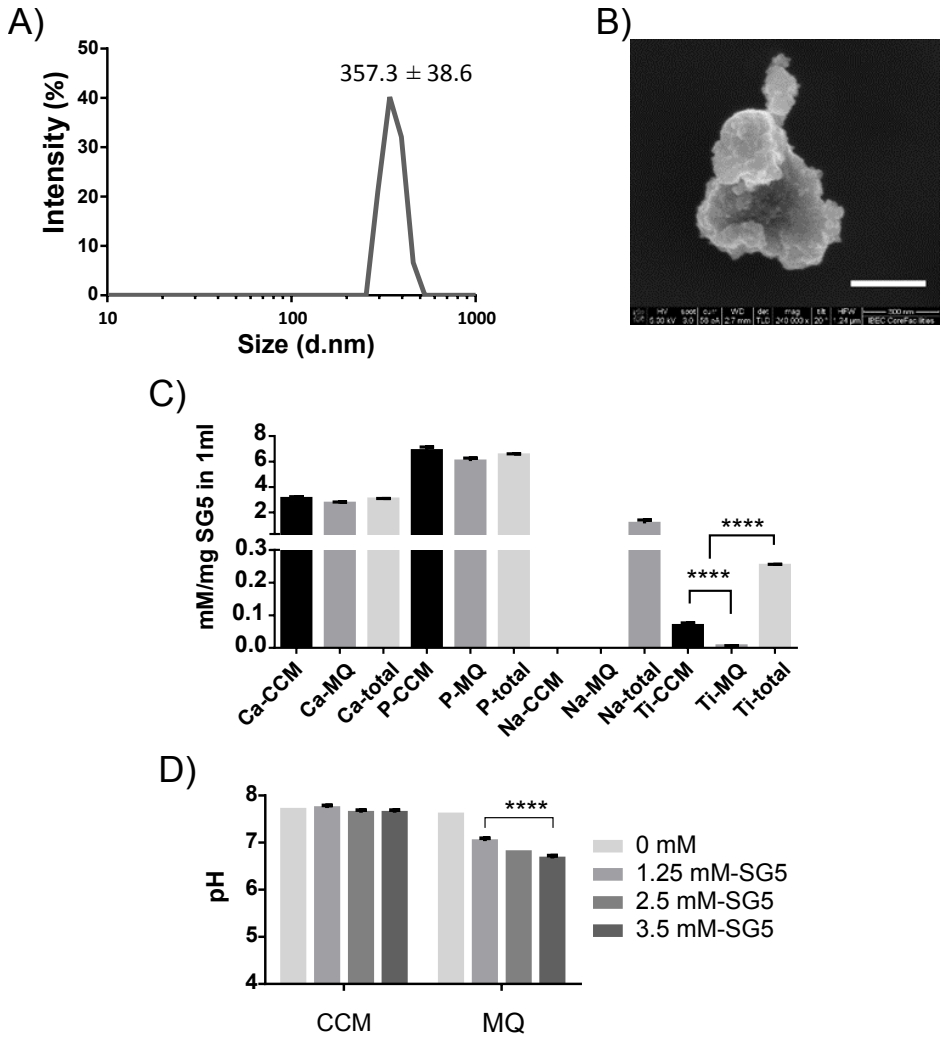

Figure 3.1: Characterization of SG5 particles. A) Particle size by DLS, B) morphology by SEM, C) ion release quantified with ICP-OES and D) pH change in CCM and MQ. Scale bar of 300 nm.****p<0.0001 .

3.3.2 Metabolic activity and proliferation of rat dermal fibroblasts

Different calcium concentrations, from 0.1 mM to 7.5 mM, were used to assess rat dermal fibroblast viability along 6 days. Concentration of 0.1

mM was the lowest tested because it is optimal for keratinocyte growth while does not promote fibroblast proliferation (Kulesz-Martin et al., 1984). At day 3, significant increase in metabolic activity was detected in the 2.5 and 3.5 mM Ca-$CaCl_2$ conditions, while concentrations of 5 mM or higher maintained static or even decreased viability (Fig. 3.2A). Ca-SG5 media stimulated a different behavior. The concentration of 3.5 mM Ca^{2+} Ca-SG5 increased metabolic activity of cells from day 1, but a significant decrease was observed at day 6.

The increase in metabolic activity did not correlate with an increased cell growth, as assessed by total DNA quantification. The assay showed that 2.5 mM and 3.5 mM Ca-$CaCl_2$ did not increase fibroblast number compared to the lowest concentration tested (0.1 mM) (Fig. 3.2B). In addition, 2.5 mM and 3.5 mM Ca-SG5 showed a slower growth rate compared to their Ca-$CaCl_2$ counterpart.

3.3.3 Effect on cell migration

To test whether the different Ca^{2+} treatments might have an effect on fibroblast migration, a scratch wound assay was performed (Fig. 3.3A). The area of the wound covered by the cells 24h after scratching is shown in Fig. 3.3B. All calcium concentrations significantly stimulated cell migration compared to the lowest concentration. In addition, the intensity of the effect seemed to be concentration-dependent and the maximum migration was achieved using 2.5 mM Ca^{2+}. Similar stimulation of cell migration was found when media with Ca-SG5 was used. Quantification of the increase in perimeter of the cell front also revealed that concentrations of 2.5 mM and above stimulated a more invasive migration behavior (Fig. 3.3C).

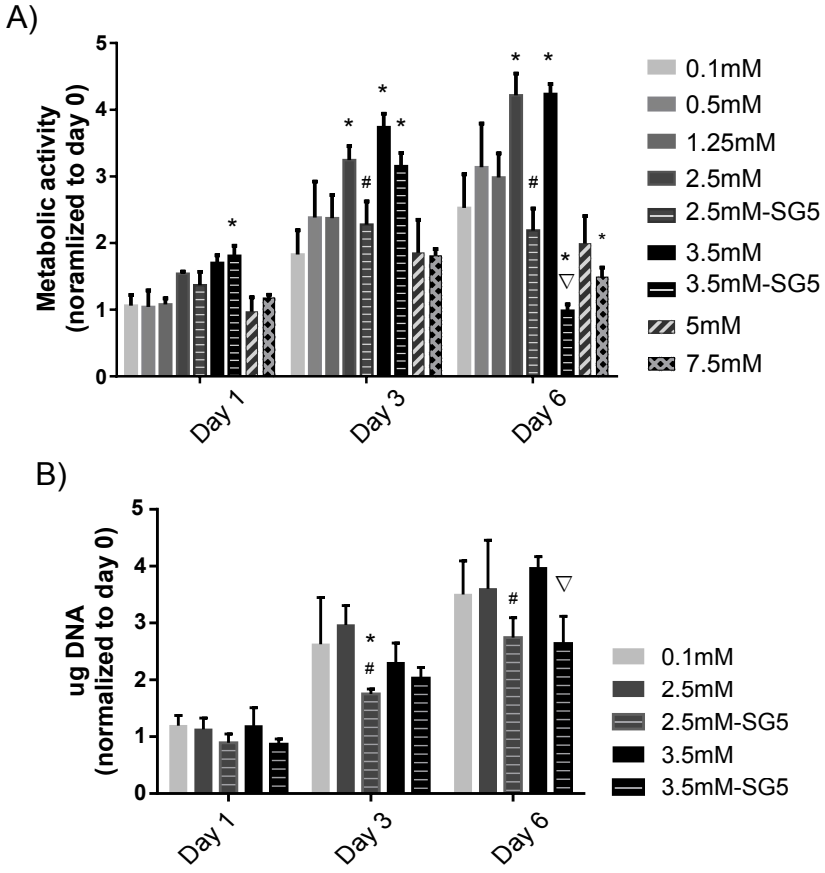

Figure 3.2: Growth of dermal fibroblast in media containing different Ca^{2+} concentrations from $CaCl_2$ and the ionic release of SG5. A) Metabolic activity and B) increase in cell number was quantified after 1, 3 and 6 days of incubating rat dermal fibroblasts in media (10% FBS) with different Ca^{2+} concentrations. Data is expressed as the mean of at least four replicates ± standard deviation (SD). *p<0.05 0.1 mM vs all, #p< 0.05 2.5 mM vs 2.5 mM-SG5, ∇ p<0.05 3.5 mM vs 3.5 mM-SG5.

3.3.4 MMP activity and collagen synthesis

Gelatin zymography was used to assess MMP2 and MMP9 activity, two key players in ECM degradation (Fig. 3.4A). The results show that 3.5

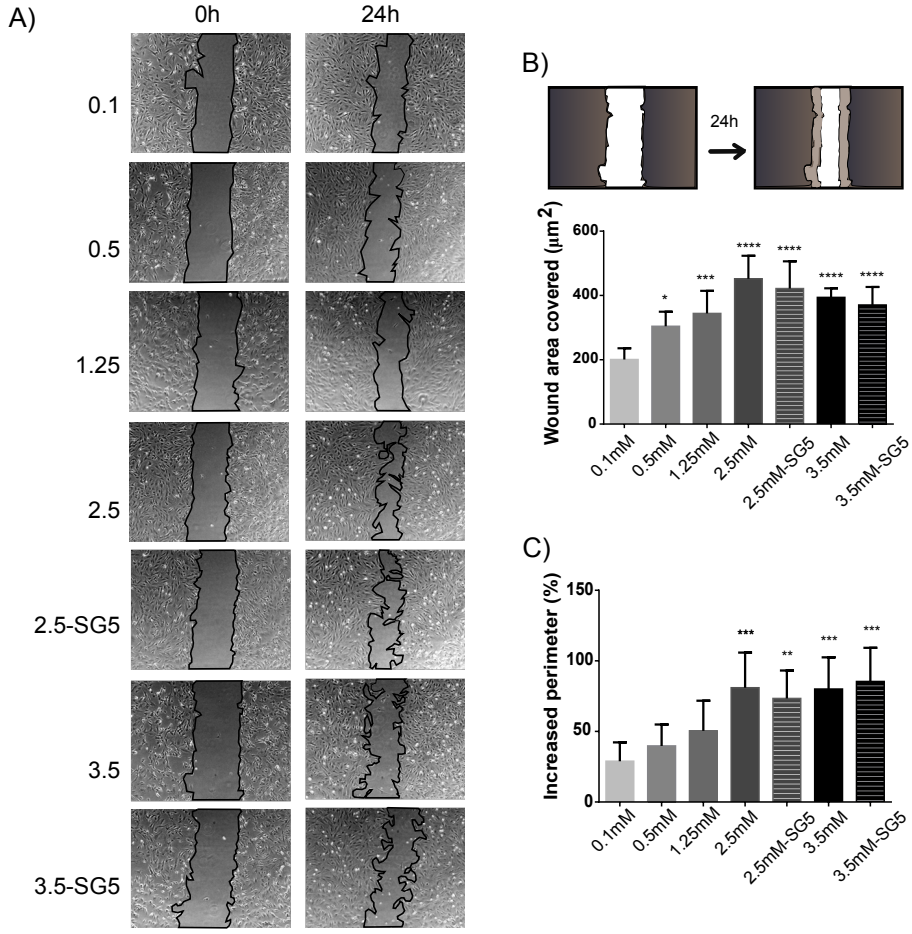

Figure 3.3: Dermal fibroblast migration in the scratch wound assay in media containing different Ca^{2+} concentrations from $CaCl_2$ and the ionic release of SG5. Cells were incubated in low serum conditioned media containing different Ca^{2+} concentrations. A) Images of the scratch were acquired at 0 h and 24 h and B) the area of the wound covered by the cells after 24 h and C) the perimeter of the front cells compared to time 0 h were quantified. Data shows the mean ± SD of at least four replicates. *p<0.05 Condition vs 0.1 mM¸**p<0.01 Condition vs 0.1 mM, ***p<0.001 Condition vs 0.1 mM; ****p<0.0001 Condition vs 0.1 mM.

mM Ca-$CaCl_2$ increased MMP9 activity compared to the other Ca^{2+}concentrations (Fig. 3.4B). An increase in the active forms of MMP2 were also observed by incubating cells with 3.5 mM Ca-$CaCl_2$ (Fig. 3.4C). In contrast, in the presence of 3.5 mM Ca-SG5 there was no increase of the gelatinases analyzed (Fig. 3.4B-C).

To study whether calcium might stimulate collagen production of fibroblast, total collagen secreted in the different test media was quantified. Ca^{2+}concentrations of 2.5 and 3.5 mM Ca-$CaCl_2$ significantly stimulated collagen synthesis, and a similar effect was observed in the Ca-SG5 condition (Fig. 3.4D).

3.3.5 VEGF synthesis

Release of VEGF from fibroblasts cultured in complete media containing different concentrations of Ca-$CaCl_2$ or Ca-SG5 was measured on day 1 and 3. For all conditions, VEGF synthesis was higher on day 1 than on day 3 (Fig. 3.5). On day 1 the condition 3.5 mM-SG5 presented significant differences compared to 0.1 mM and 3.5 mM of the same time point, showing a decreased synthesis (Fig. 3.5). On day 3, significant differences between samples were not detected.

3.3.6 Contractile capacity

The ADR-FPCL model was used to quantify the contractile capacity of fibroblast cultured with different Ca^{2+} concentrations. Fibroblasts cultured in lower Ca^{2+} concentrations (0.1 mM and 1.25 mM) were able to contract the collagen matrix faster and in greater extent than higher Ca^{2+} concentrations (2.5 mM and 3.5 mM) (Fig. 3.6A). Differences observed among conditions revealed a concentration-dependent behavior. Moreover, significant differences between Ca-$CaCl_2$ and their equivalent Ca-SG5 con-

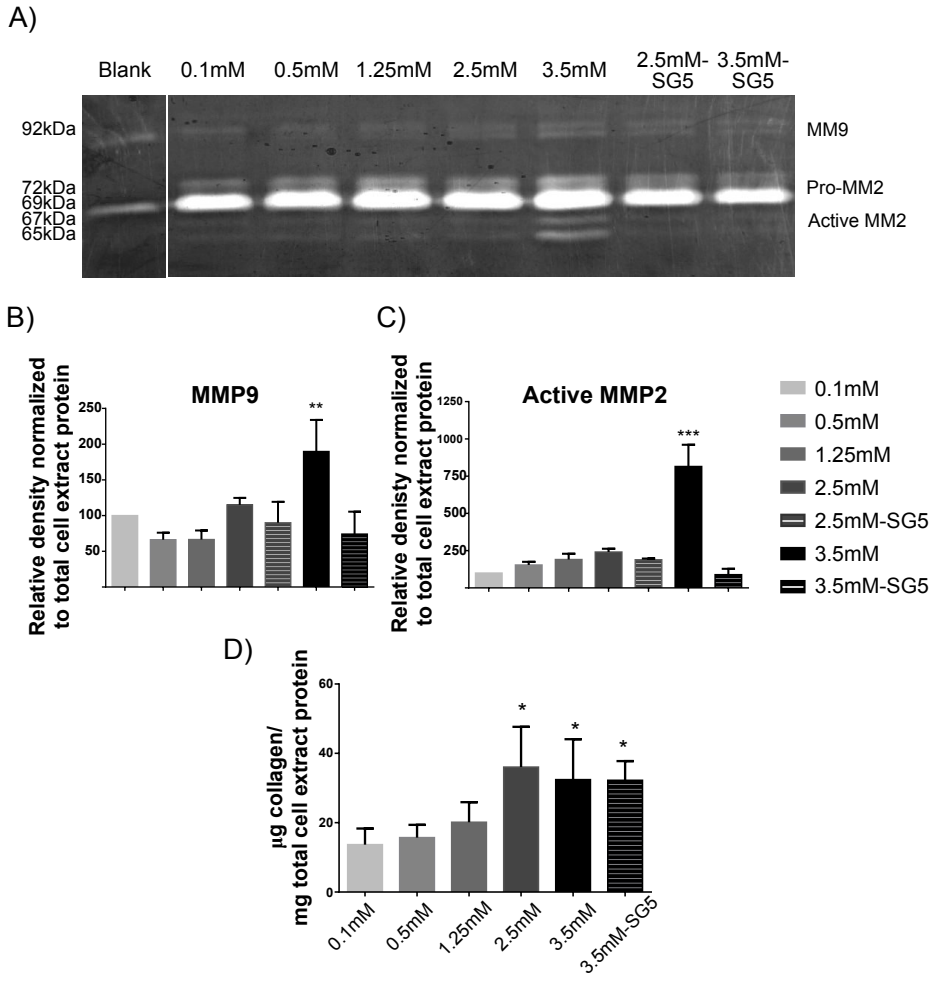

Figure 3.4: Dermal fibroblast remodeling stimulation studied by analyzing gelatinase activity and collagen synthesis in cell-conditioned media after treatment of cells with Ca-$CaCl_2$ and Ca-SG5. A) Cell-conditioned media was used in a zymography assay to detect total MMP9 and active MMP2 activity and D) to measure the collagen concentration produced. Densitometry of the zymography of B) MMP9 and C) active MMP2. Values were normalized to the 0.1 mM condition and then to the total protein from the cell extract of each sample. Data is expressed as the mean of at least four replicates ± SD. *p<0.05 Condition vs 0.1 mM;**p<0.01 Condition vs 0.1 mM¸***p<0.001 Condition vs 0.1 mM.

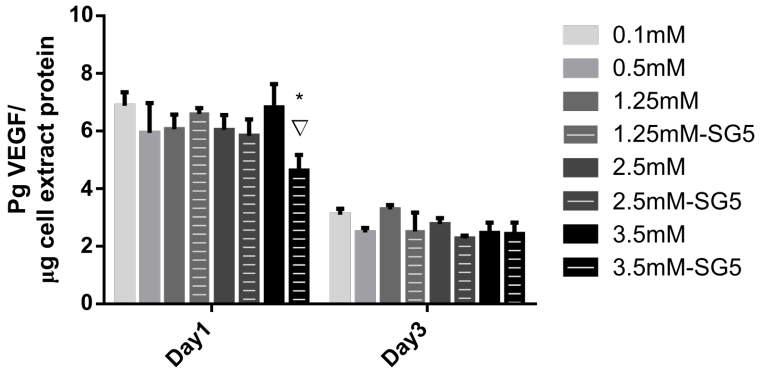

Figure 3.5: Dermal fibroblasts' synthesis of VEGF after incubation in media containing different Ca^{2+} concentrations from $CaCl_2$ or the ionic release of SG5. VEGF released in media was analyzed on day 1 and day 3. Media was conditioned for 24 hours. Data is expressed as the mean of at least three replicates ± SD. *p<0.05 Condition vs 0.1 mM; ▽ p<0.05 Condition vs 3.5mM.

centrations were detected only at the highest concentration, 3.5mM. More specifically, fibroblasts cultures in 3.5mM-SG5 showed reduced contractile capacity than their equivalent Ca-$CaCl_2$ (Fig. 3.6A).

Differences in fibroblasts' contractile capacity can be related to variations in expression of α-SMA (Hinz et al., 2001; Arora et al., 1999). To evaluate this hypothesis, we quantified levels of α-SMA expressed by cells in the FPCL cultured under the different conditions. The immunoblot analysis performed unveiled clear differences in expression among Ca^{2+} concentrations (Fig. 3.6B). At 0.1 mM and 1.25 mM the expression of α-SMA was the highest among the conditions tested, while at 2.5 and 3.5 mM the expression was significantly lower or even absent (Fig. 3.6B). Moreover, SG5 conditioned media stimulated similar levels of expression than their equivalent Ca-$CaCl_2$ concentration. Indeed, this test showed correlation between α-SMA levels of expression and fibroblast contractile capacity.

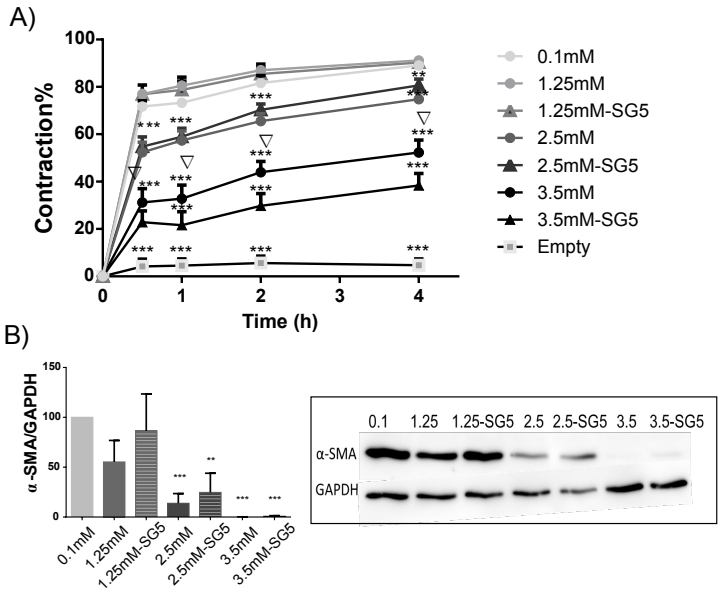

Figure 3.6: Fibroblast contractile capacity in different calcium concentrations studied in the ADR-FPCL model. Four days after casting, lattices were detached and images of the matrices were taken at different time points. A) The area of the lattices was quantified and is represented as the percentage contracted from the initial size. B) Cell lysates were subjected to immunoblotting and specific antibodies against α-SMA and GAPDH were used. Densitometry analysis of the bands was performed and intensity signal of α-SMA bands were normalized to the corresponding GAPDH signal. Data is expressed as a mean of four replicates ± SD. *p<0.05 Condition vs 0.1 mM;**p<0.01 Condition vs 0.1 mM¸***p<0.001 Condition vs 0.1 mM; ▽ p<0.05 3.5 mM vs 3.5 mM-SG5.

3.3.7 Expression of wound healing genes

In order to analyze whether extracellular Ca^{2+} is able to affect the expression of wound healing genes, a Real Time polymerase chain reaction (RT-PCR) for 84 key genes central to the wound healing response was used. Our results indicate that 38 genes including ECM components, remodeling enzymes, cellular adhesion, cytoskeleton, inflammatory chemokines and cytokines, growth factors, and signal transduction factors were upreg-

ulated at least 2-fold in fibroblasts cultured with 3.5 mM Ca-$CaCl_2$ compared to 0.1 mM (Fig. 3.7A). Gene expression correlated with the previously described biological effects. Signal transduction factors involved in cell proliferation, such as mitogen-activated protein kinase (MAPK) 3, were also detected. Several integrin subunits and the cytoskeleton regulator Rhoa, which is related to control the detachment of cell's rear (Alblas et al., 2001), presented increased expression. In addition, augmented expression of ECM components including different types of collagen as well as gelatinases MMP2 and MMP9 were detected. Similar results were observed in fibroblasts cultured with 3.5 mM Ca-SG5, for which the upregulated genes were 36 and only one gene was downregulated (Ccl12) (Fig. 3.7A). By comparing the expression between 3.5 mM Ca-$CaCl_2$ and Ca-SG5 we found downregulation in the expression of inflammatory cytokines and chemokines in cells stimulated with SG5 (Fig. 3.7B).

3.4 Discussion

This study shows that different concentrations of extracellular Ca^{2+} or the ionic dissolution of calcium-phosphate based particles can stimulate similar relevant wound healing responses of dermal fibroblasts. Extracellular Ca^{2+} concentrations of 2.5 mM and 3.5 mM had an impact in metabolic activity, migration, collagen synthesis, MMP activity, contractile capacity and wound-healing related gene expression and the wide range of concentrations tested allowed to detect a clear concentration-dependent behavior in cell migration and contractile capacity. The ionic dissolution of SG5 particles with Ca^{2+} concentrations adjusted to 3.5 mM elicited similar responses but decreased gelatinase activity, VEGF synthesis, and expression of inflammatory factors were observed. Overall, extracellular Ca^{2+} stimulates biological responses in dermal fibroblasts that might improve the

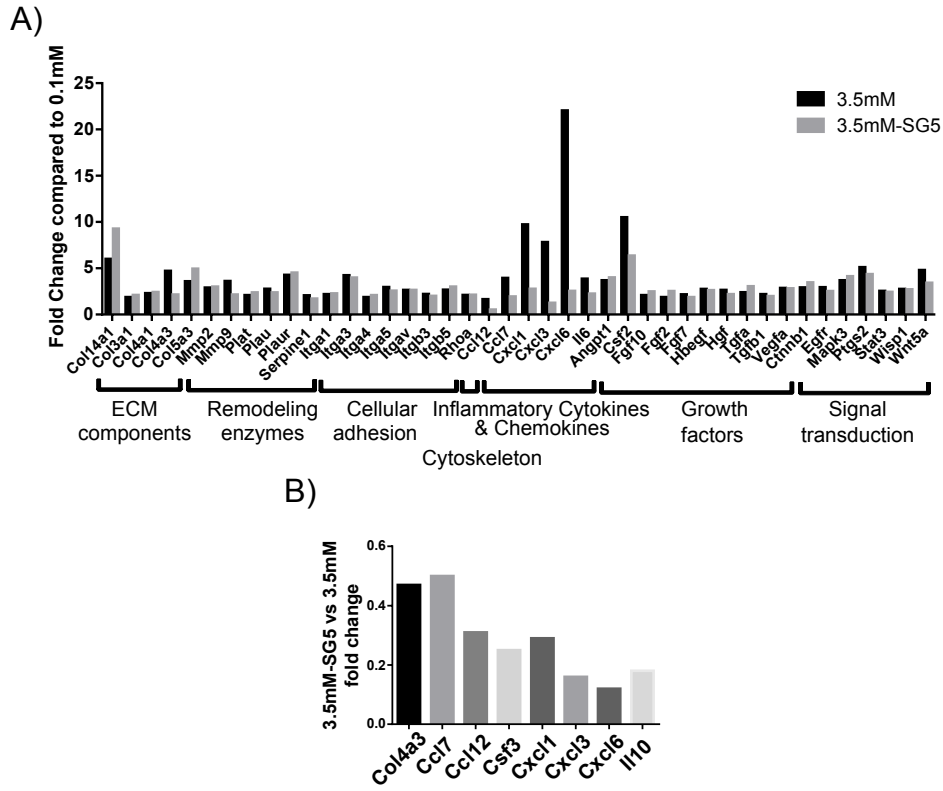

Figure 3.7: Gene expression comparison of an array of genes involved in wound healing of dermal fibroblast. Cells were incubated for 24 h in medium (10% FBS) conditioned with 0.1 mM, 3.5 mM and 3.5 mM-SG5 and cDNA from the samples was used in a RT-PCR array for wound healing. A) Genes from the samples 3.5 mM and 3.5 mM-SG5 that resulted in at least a 2 fold change expression compared to the calcium concentration 0.1 mM are shown. B) Fold expression of the sample 3.5 mM-SG5 compared to 3.5 mM. Abbreviations of the genes analyzed are defined in Appendix B.1.

healing of chronic wounds, and some of the responses that could be considered negative are countered when the ionic dissolution of the bioactive glass tested is used.

Our work shows that extracellular Ca^{2+} concentrations up to 1.25 mM did not affect fibroblast metabolic activity (Fig. 3.2A). Increased metabolic

activity was observed at concentrations starting from 2.5 mM up to 3.5 mM, being cytostatic or cytotoxic above 5 mM. Mitogenic activity of calcium has been known for many years, and proved by different studies (Dulbecco and Elkington, 1975; Epstein et al., 1992). However, the specific concentration seems to differ depending on species and cell type. For instance, murine fibroblast cell line 3T3 showed an optimal cell proliferation by addition of 10 mM $CaCl_2$ in DMEM containing 1.85 mM of Ca^{2+} (Epstein et al., 1992). Another study using mouse dermal fibroblasts found that the optimal concentration for proliferation was 1.4 mM Ca^{2+}, but this was the maximum concentration tested (Kulesz-Martin et al., 1984). In general, the mitogenic activity of calcium has been assessed through radioactive-thymide incorporation assays (Dulbecco and Elkington, 1975; Epstein et al., 1992; McNeil et al., 1998). In our study, different methodologies were employed and included metabolic activity assessment and dsDNA quantification. Even tough 24 h calcium stimulation increased metabolic activity and gene expression of the mitogenic protein MAPK3 (Fig. 3.7A), dsDNA quantification did not show increased cell number over time (Fig. 3.2B). This could be explained by the presence of growth factors contained in the FBS used in the media that could have masked the expected calcium-stimulated proliferative effect.

Here it is showed for the first time how calcium stimulates dermal fibroblasts migration in a concentration dependent manner (Fig. 3.3B). Other studies had shown migration stimulation with calcium on fibroblasts (Zhang et al., 2014) but, to our knowledge, the concentration-dependent behavior had not been reported. Fibroblast migration into the newly formed fibrin matrix at the wound site is an essential event for the progression of the wound healing. They move individually following a multistep cycle including protrution, adhesion formation thorugh integrin binding, stabilization of the leading edge, cell

body translocation and release of adhesions and detachment of cell's rear (Abercrombie et al., 1970; Heath and Dunn, 1978; Huttenlocher et al., 1995; Lauffenburger and Horwitz, 1996; Ridley, 2003). There is not a single proposed mechanism by which extracellular Ca^{2+} can affect cell migration due the plethora of events in which Ca^{2+} is implicated and the complexity of cell motility, but it can be linked to the activation of calcium-binding proteins. Studies have shown how increasing extracellular Ca^{2+} leads to increase in intracellular Ca^{2+} (McNeil et al., 1998) that results in the activation of calcium-dependent proteins involved in cell migration, such as calpains (Franco, 2005). Although it is out of the scope of this work, we hypotesize that the increase in gene expression of several integrins and of the rear dettachment regulator Rhoa (Alblas et al., 2001) triggered by extracellular calcium, as quantified by RT-PCR, could be partly responsible of this increased migration.

Our results also showed that high extracellular calcium concentrations stimulated fibroblast's ECM remodeling capacity by increasing the synthesis of MMP2, MMP9 and collagen (Fig. 3.4). During the remodeling and repair phase of the healing process, fibroblasts have an essential role in transforming the new matrix that is being created. Remodeling requires both degradation and synthesis of new extracellular matrix, but, as explained in Section 2.5.2, deposition of new tissue in chronic wounds is prevented or impaired by numerous factors (Medina et al., 2005). Increased collagenase activity was observed elsewhere in an *in vivo* study by administration of 5 mM Ca^{2+} (Sank et al., 1989), and increased expression of MMP2 and MMP9 by 2.5 mM Ca^{2+} had been previously described (Zhang et al., 2014). However, the clear increase in the active form of MMP2 by a specific calcium concentration (3.5 mM) (Fig. 3.4) had not been reported previously. Interestingly, when the same Ca^{2+} concentration was provided by the SG5 ionic release, MMP2 activation form was not in-

creased. This result might be beneficial in the context of chronic wound healing, since MMP2 and MMP9 seem to be abnormally expressed in these type of wounds (Wysocki et al., 1993) and are considered partly responsible for the chronic condition (Medina et al., 2005; Yager and Nwomeh, 1999). In fact, dressings with MMPs modulating properties have been designed as an approach to improve wound healing, but the inactivation is achieved by absorbing the protease-rich wound fluid and by providing a surrogate substrate to the proteases (Wiegand and Hipler, 2013; Cullen et al., 2002). In addition, the *de novo* deposition of collagen stimulated by both $CaCl_2$ and SG5 could also contribute to the improvement of the healing, since expression of the collagen gene in fibroblasts is suppressed in some types of chronic wounds (Hansen et al., 2003). Although the stimulating effect of calcium on collagen synthesis by fibroblasts has been suggested by others (Stefanovic et al., 2004; Wang et al., 2015), by testing a wide range of calcium concentrations we were able to identify an optimal calcium concentration to promote collagen production by dermal fibroblasts.

Differently to other bioactive glasses reported (Day et al., 2004; Keshaw et al., 2005; Day, 2005; Leu and Leach, 2008), the ionic dissolution of SG5 did not stimulate the release of VEGF. In fact, the concentration 3.5 mM-SG5 decreased the synthesis of this angiogenic protein (Fig. 3.5). Nevertheless, neovascularization is a complex process and even if the bioglass used decrease fibroblasts' synthesis of VEGF, blood formation in the wound site might not be impaired. The increased release of VEGF on day 1 compared to day 3 can be explained because at the beginning of the assay cells are in starving conditions, which render them more responsive to FBS and calcium concentrations of the media added.

After measuring fibroblasts contractile capacity in collagen lattices incubated with Ca-$CaCl_2$ and Ca-SG5 a clear effect was detected: the low

Ca^{2+}concentrations tested stimulated a high degree of contraction (Fig. 3.6A). Fibroblasts play a key role in the latest events of the healing process by providing the contractile forces that bring the wound edges together. As explained in Section 2.2.4, myofibroblasts are the main responsible of this contraction (Gabbiani et al., 1971). They arise mainly through differentiation of local fibroblasts and are characterized by the expression of α-SMA (Tomasek et al., 2002). Since expression of α-SMA is known to increase (myo)fibroblast contractile activity (Arora et al., 1999; Hinz et al., 2001), α-SMA expression levels were quantified and they were shown to correlate with the contractile capacity of fibroblasts (Fig. 3.6B). According to this result, extracellular Ca^{2+} would play a crucial role in fibroblasts differentiation to myofibroblasts. Differences in fibroblasts attachment to the collagen type I substrate in the presence of different Ca^{2+} concentrations is described elsewhere (Grzesiak et al., 1992) and might affect the mechanical tensions generated between the cells and the substrate having an impact on the α-SMA expression. Assuming that Ca^{2+} concentrations modulate the levels of expression of α-SMA and the contractile capacity of fibroblasts, the study of the influence and control of extracellular Ca^{2+} concentration in the latest stages of the healing process as an strategy to avoid scar formation would be a new concept to explore in the field.

The stimulating effects on metabolic activity, cell migration, MMP activity, collagen synthesis, and contractile capacity by the 3.5 mM concentration, both from the added $CaCl_2$ and from the ionic dissolution of SG5, were supported by the increased expression of genes involved in wound healing detected through the RT-PCR array (Fig. 3.7A). This result indicated an upregulation of genes of ECM components, remodeling enzymes, cellular adhesion, growth factors and signaling transduction in fibroblasts by calcium stimulation. In addition, increased expression of inflammatory

cues, especially neutrophil-recruiting CXC chemokines, were identified. Experimental studies have described a peak in the Ca^{2+} concentration of the wound site at the 5th day post-wound, coinciding with the period of maximal inflammatory activity within the wound (Lansdown et al., 1999). Although the role of extracellular Ca^{2+} in the inflammatory state of the wound is poorly defined, it seems to participate by activating the respiratory burst in neutrophils (Kim-Park et al., 1997) and by eliciting a chemotactic response from monocytes *in vitro* and *in vivo* (Olszak et al., 2000). According to our results, high extracellular Ca^{2+} could also contribute to the inflammatory state of the wound by increasing expression of inflammatory chemokines and cytokines of, at least, fibroblasts (Fig. 3.7B).

In general, the ionic dissolution of the calcium-releasing particles stimulated similar biological effects to their equivalent $CaCl_2$ concentration. However, relevant differences were detected in some biological responses. Even though short term incubation in particle-conditioned media stimulated cell metabolic activity, long term exposure of fibroblasts to this release provoked cytotoxicity *in vitro*. The method used for the production of SG5, based on sol-gel without posterior high temperature treatment, favors the presence of non-decomposed organic material in the structure of the particles that, when released, could induce some degree of cytotoxicity. However, it should be considered that in an open system such as in an *in vivo* situation, the cytotoxic effect should be attenuated, as previously observed (Castaño et al., 2014; Oliveira et al., 2016; Sachot et al., 2016).

In addition, Ca^{2+} concentrations of 3.5 mM from the ionic dissolution of the particles did not increase collagenase activity and expression of inflammatory factors as much as the $CaCl_2$ concentration. This is of particular interest, since increased collagenase activity and pro-inflammatory cytokines seem to be present in chronic wounds (Schultz and Mast, 1999; Wysocki et al., 1993) and stimulation of these responses should be avoided.

These differences in stimulation between the Ca-$CaCl_2$ and the Ca-SG5 can be explained due to the other products released by the particles, but not to changes in media pH (Fig. 3.1D). Together with calcium, phosphate is the most abundant ion released by these particles and it could be playing a role in the observed stimulation since it has been described to exert bioactive effects on proliferation or osteogenesis of osteoprogenitor cells and human mesenchymal stem cells (Chai et al., 2011; Danoux et al., 2015).

Hence, most of the biological effects stimulated by the ionic release of SG5 could be beneficial in the process of chronic wound healing. Nevertheless, repeating these experiments with human-derived dermal fibroblasts from ulcers might provide us with more trustworthy information of the effectiveness of these calcium-releasing particles. In addition, due to the complexity and plethora of players involved in the wound healing process, a deeper understanding of the effect of the release should be acquired on other cell types and processes, especially on keratinocytes, inflammatory cells, and angiogenesis. Last but not least, if the particles were to be used on chronic wounds, reliable measurements of the levels of calcium in the wound site during the healing process would be needed in order to design dressings that could deliver optimal doses at every stage.

3.5 Conclusions

In conclusion, extracellular calcium was able to stimulate relevant biological responses carried out by dermal fibroblasts in wound healing at specific concentrations including metabolic activity, MMP9 and MMP2 synthesis and activation respectively, collagen synthesis, contraction capacity, and expression of a myriad of genes involved in wound healing. Interesting biological effects were observed, such as the concentration-dependent stimulation of cell migration and matrix contraction. When equivalent calcium

concentrations were used adjusting the ionic dissolution of SG5 in the media, similar responses were obtained while undesired effects in chronic wounds such as increased gelatinase activity or expression of inflammatory factors were avoided or diminished. Thus, SG5 could improve the chronic wound outcome but the complexity of the healing process require its evaluation on other cell types and in an *in vivo* context.

4 Responses mediated by the calcium-sensing receptor

4.1 Introduction

In the previous chapter we showed how extracellular calcium stimulates different biological responses on dermal fibroblasts, including metabolic activity, migration, matrix metalloprotease (MMP)s activation, collagen synthesis, contraction capacity, and expression of inflammatory cues. This chapter aimed to gain insight into the signaling pathways mediating some of these effects. More specifically, we studied the implication of the calcium-sensing receptor (CaSR) in metabolic activity, migration, collagen synthesis, and MMPs activation through the use of different agonists and negative allosteric modulators of the receptor.

As commented in Section 2.4, intracellularly, calcium plays an essential role as secondary messenger in the transduction of numerous signaling pathways. Calcium signaling occurs with the sudden rise in cytoplasmic calcium through the opening and closing of different calcium channels present in the plasma membrane or intracellular reservoirs like the endoplasmic reticulum (Koolman and Roehm, 2005). Nevertheless, calcium can also act as an extracellular signal by binding to different receptors, the best studied of which is the CaSR (Hofer, 2005).

The CaSR belongs to the Family C of the G protein-coupled receptors (GPCR), which also includes the metabotropic glutamate receptors (mGluRs), $GABA_B$ receptors, and receptors for taste and pheromones, as well as an amino acid and divalent cation-sensing receptor called GPRC6A (Brauner-Osborne et al., 2007). Equally to the other members of the GPCR superfamily, CaSR is present in the plasma membrane in a dimeric configuration (Bai et al., 1998) and is structurally composed of three parts: seven transmembrane α-helices, an extracellular amino-terminal segment where ligands bind, and an intracellular carboxy-terminal tail (Fig. 4.1A).

The receptor is cooperatively activated by Ca^{2+} ions over a concentration range of 0.5-10 mM, and also by a plethora of other signals, such as divalent and trivalent cations -e.g. Sr^{2+}, Gd^{3+}-, organic polycations -e.g. spermine-, aminoacids, pH or ionic strength (Jensen and Brauner-Osborne, 2007). Upon activation, the CaSR can fire different intracellular signaling pathways as shown in Fig. 4.1B, such as the phospholipase C/inositol-1,4,5-trisphosphate (IP3)/Ca^{2+} signalling pathway, or mitogen-activated protein kinase (MAPK) cascades including the p42/44 MAPK, known as extracellular signal-regulated protein kinases 1 and 2 (ERK1/2) (Yamaguchi et al., 2000), the p38 MAPK (Maiti et al., 2008) and the c-Jun NH2-terminal kinase (JNK) (Arthur et al., 2000) pathways.

The CaSR is known to be essential to the parathyroid glands for the maintenance of the body calcium homeostasis, but it is expressed in other cell types and tissues, such as in kidney, stomach, bone, colon and the skin (Alfadda et al., 2014), where it has been linked to mediate many different functions. Study of the implication of the CaSR in the mediation of different biological processes has been mainly carried out with the use of calcimimetics and calcilytics, that selectively stimulate or inhibit the activation of the receptor (Alfadda et al., 2014). Calcimimetics are classified in type I or agonists, which bind to the orthosteric site of the receptor in the

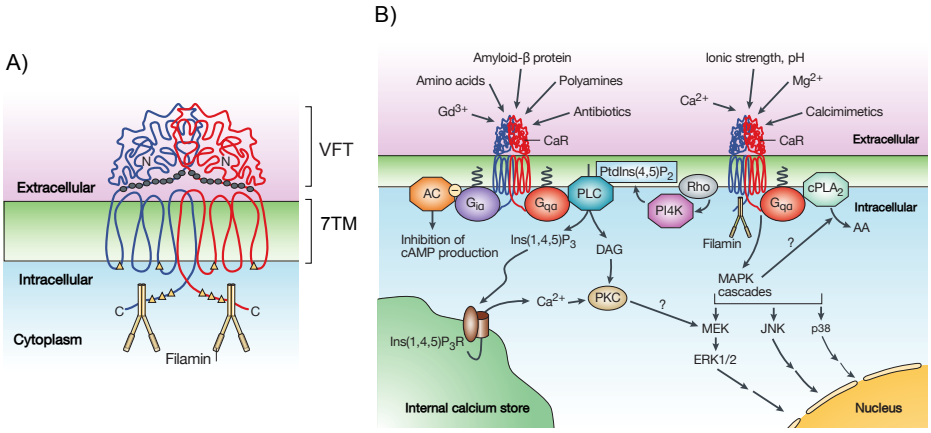

Figure 4.1: CaSR Structure and intracellular signaling activation A) A model of the dimeric form of the CaSR showing its three structural components: an extracellular domain (ECD), a seven transmembrane-spanning domain (7TM) and the intracellular domain (ICD). The extracellular matrix (ECM) contains the amino-terminal domain (N) and it is thought to be structured in a bi-lobed, venus-flytrap structure (VFT) that contains the ligand binding sites. The ICD contains the carboxyl-terminal group and is the binding site for G-proteins and the scaffolding protein filamin. B) Upon ligand binding, conformational changes of the receptor lead to activation of the G-proteins, which triggers a variety of intracellular signaling pathways. These include stimulation of phospholipase C (PLC)/IP3/Ca^{2+} signalling pathway, inhibition of adenylate cyclase (AC), activation of the Rho kinase, activation of MAPKs -e.g., ERK1/2, p38 MAPK, and JNK- and activation of cytosolic phospholipase A2 (cPLA2). Other proteins playing a role in these signaling pathways are arachidonic acid (AA), cyclic AMP (cAMP), diacylglycerol (DAG), inositol-1,4,5-trisphosphate receptor (Ins(1,4,5)P3R), MAPK kinase (MEK), phosphatidylinositol 4-kinase (PI4K), phoshatidylinositol-4,5-bisphosphate (PtdIns(4,5)P2). Adapated from Hofer and Brown (2003).

ECD, and type II or positive allosteric modulators, which bind to the 7TM leading to conformational changes of the receptor that increase sensitivity to physiological ligands (Alfadda et al., 2014). On the other hand, calcilytics are mainly composed by negative allosteric modulators, which, by binding to the 7TM, decrease sensitivity to physiological ligand (Alfadda

et al., 2014). Inhibition of the expression of the receptor through genetic manipulation has also been used in some studies (McNeil et al., 1998; Tu et al., 2004; Milara et al., 2010).

In the skin, the relevance of the CaSR has been mainly attributed to its role on keratinocytes. Indeed, *in vitro* studies showed that expression of the CaSR on keratinocytes is critical for their differentiation (Tu et al., 2001) and its absence in an *in vivo* model demonstrated perturbation in the calcium gradient of the epidermis and in the barrier permeability (Tu et al., 2012). On fibroblasts, the biological responses triggered by the CaSR have been less explored. *In vitro* studies have linked the activation of the CaSR by calcium, positive allosteric modulators, or agonists with activation of the ERK1/2 pathway (McNeil et al., 1998; Yu et al., 2006). In addition, fibroblasts exposed to calcimimetics show stimulation of cell proliferation (Bhagavathula et al., 2009; Jenkins et al., 2011; Zhang et al., 2014), migration (Zhang et al., 2014), MMPs expression (Bhagavathula et al., 2009; Jenkins et al., 2011; Zhang et al., 2014) and tissue inhibitor of metalloproteinase (TIMP) expression (Bhagavathula et al., 2009; Jenkins et al., 2011; Zhang et al., 2014).

In the present work, we exposed rat dermal fibroblasts to several agonists and negative allosteric modulators of the CaSR and study their effects on different biological responses stimulated by calcium. More precisely, we used Gd^{3+} to confirm activation of ERK1/2 and studied the effects of this agonist on metabolic activity, cell migration, collagen synthesis, and gelatinases activation. In addition, we used other agonists, including Sr^{2+}, Zn^{2+} and Mg^{2+}, to study their effect on metabolic activity and migration. Finally, the negative allosteric modulators NPS2143 and calhex231 were used to help elucidate the implication of the CaSR in the biological effects investigated.

4.2 Materials and Methods

4.2.1 Cell isolation and culture

Rat dermal fibroblasts were isolated and cultured as explained in Section 3.2.3. Cells were expanded in complete culture media (CCM) consisting of Dulbecco's Modified Eagle Medium (DMEM) (Gibco) supplemented with 10% fetal bovine serum (FBS) (Sigma-Aldrich), 2 mM L-Glut, and 100 U/mL penicillin/streptomycin (P/S), and were used between passage 4-6. During expansion, media was changed every three days. Media containing different Ca^{2+} concentrations were prepared by dissolving calcium chloride (>96%, Sigma-Aldrich) in calcium-free media with low (2%) or normal (10%) FBS concentration, 2 mM L-Glut, and 100 U/mL P/S. Solutions were sterilized through a filter (0.22 µm pore size) after preparation. Before treatment, cells were starved overnight in 2% FBS and 0.1 mM Ca^{2+}.

4.2.2 Immunofluorescence

Dermal fibroblasts were seeded on sterile 15 mm coverslips in 24-well plates in CCM. After overnight starvation, low-serum media with different calcium concentrations were added. Following a 24 h calcium treatment, cells were washed with Phosphate-Buffered Saline (PBS) and fixed with 4% paraformaldehyde solution (EM grade, Electron Microscopy Sciences) for 10 min. Then, cells were washed again with PBS and blocked with 3% bovine serum albumin (BSA) (Sigma-Aldrich) in PBS for 30 min. Afterwards, they were incubated overnight at 4 °C with anti-CaSR antibody (1:400 dilution, 5C10, Thermo Fisher Scientific) followed by incubation with secondary Alexa 488 goat-anti-mouse antibody (1:500 dilution, ab150113, Abcam) for 1 h at room temperature (RT). Antibody dilution

was made in 3% BSA-PBS and cells incubated with secondary antibody alone were used as negative controls. F-actin was stained incubating rhodamine phalloidin (1:400 dilution, Molecular Probes) for 10 min at RT, and cell nuclei were stained by incubating 4',6-diamidino-2-phenylindole, dilactate (DAPI) (1:200 dilution, Molecular Probes) for 2 min at RT. After thorough rinse with PBS, coverslips were mounted on mowiol 40-88 (Sigma-Aldrich) and allowed to dry protected from light. Images were obtained with a Nikon E600 microscope using a DP72 Olympus camera.

4.2.3 Agonists' treatment (Gd^{3+}, Zn^{2+}, Mg^{2+}, Sr^{2+})

Gadolinium (Gd^{3+}) chloride (99.99%, Sigma-Aldrich), zinc (Zn^{2+}) chloride (Bioreagent, Sigma-Aldrich), magnesium (Mg^{2+}) chloride anhydrous (>98%, Sigma-Aldrich) and strontium (Sr^{2+}) chloride hexahydrate (99.995%, Sigma-Aldrich) were used. For cell treatment, stock solutions of 10 mM in MilliQ were prepared for Gd^{3+} and Zn^{2+}. Sr^{2+} and Mg^{2+} dilutions were made from a freshly prepared 10 mM solution in calcium-free media. Solutions were sterilized through a filter (0.22 μm pore size) after preparation. Experimental media was prepared by diluting these solutions in low (2%) or normal serum (10%) containing calcium-free DMEM with 2 mM L-glutamine, 100 U/mL P/S.

4.2.4 Negative allosteric modulators treatment (NPS2143 and calhex231)

NPS2143 hydrochloride (Santa Cruz Biotecnhology) (Fig. 4.2A) and Calhex 231 hydrochloride (Axon Medchem) (Fig. 4.2B) were dissolved in Dimethyl sulfoxide (DMSO) (100 mM) and ethanol absolute (10 mM), respectively, and stored at -20 °C. Prior to use, stock solutions were diluted 1:100 in PBS. NPS2143 and calhex231 were used in a concentration of

2.5 μM and 1 μM respectively in calcium-free medium. Groups treated with these modulators were preincubated in the above-mentioned concentrations for one hour before calcium addition, and they were also added in the calcium solutions.

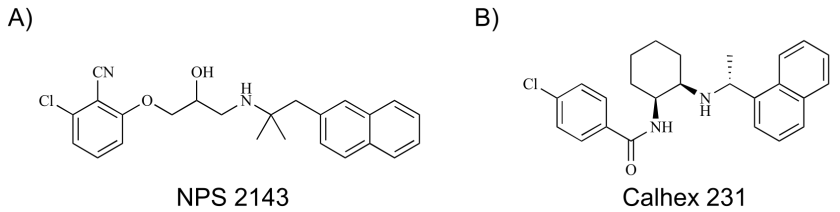

Figure 4.2: Chemical structures of synthetic negative allosteric modulators of CaSR. A) Structure of NPS2143 and B) calhex231. Adapted from Jensen and Brauner-Osborne (2007).

4.2.5 Western Blotting

Western blot analysis was used to detect CaSR protein (150–135 kD) and phospho-ERK1/2 (42, 44 kD) in dermal fibroblasts. Cells were seeded in 6-well plates (5 x 10^4 cells/well) and allowed to proliferate until 80% confluence. Then, cells were starved overnight and, after media treatment, cells were washed with PBS and lysed with RIPA supplemented with protease inhibitor cocktail (Santa Cruz Biotechnology) plus 50 mM phosphatase inhibitor sodium fluoride (Sigma-Aldrich) for 20 min in ice. Samples were transfered to microcentrifuge tubes and centrifuged at 10,000 g for 10 min at 4 °C. Finally, supernatants were transferred into clean microcentrifuge tubes and stored at -80 °C until needed. Western blotting was performed as explained in Section 3.2.11 with some changes. Protein concentration of each cell lysate was quantified with the bicinchoninic acid (BCA) protein assay (Thermo Fisher Scientific) following manufacturer's instructions, and a total of 15 μg of protein mixed with 3x Laemmli buffer was loaded per lane. For experiments detecting CaSR protein, sam-

ples were run in 8% (wt/v) acrylamide gels. Transference was performed at 40 mV overnight and, after blocking, membranes were incubated with anti-CaSR (1:500 dilution, 5C10, Thermofisher Scientific) overnight at 4 °C and then with β-tubulin (1:600, 2146, Cell Signaling Technology) for 1 h at RT. The secondary HRP-linked antibodies used were anti-mouse IgG (1:5,000 dilution, SA1-100, Thermofisher Scientific) and anti-rabbit IgG (1:3,000 dilution, 7074, Cell Signaling Technologies), which were incubated for 1 h at RT. Assays detecting ERK1/2 used 10% (wt/v) acrylamide gels and transference was carried out at a constant voltage of 100 mV for 1 h. In this case, antibodies used were the phospho-44/42 MAPK antibody (1:1000, 4376, Cell Signaling Technologies), incubated overnight at 4 °C, and the secondary anti-rabbit IgG antibody (1:3,000), incubated at RT for 1 h. For these membranes, Ponceau staining (Sigma-Aldrich) made after transference was used as loading control.

4.2.6 Metabolic activity

Cellular metabolic activity was measured after exposing cells to conditioned media containing 10% FBS for six days. Cells (2.5 x 10^3 cells/well) were seeded in 48 well plates. At the specified time point, Alamar Blue™ (Thermo Scientific) was added following manufacturer's instructions and fluorescence was read at Ex/Em wavelength of 530/590. Values were normalized to control condition containing 0.1 mM Ca^{2+}.

4.2.7 Scratch wound assay

Scratch wound assay was performed as explained in Section 3.2.7.

4.2.8 Collagen synthesis

Synthesized collagen present in the supernatant was quantified as described in Section 3.2.6.

4.2.9 Statistical analysis

Each experiment were performed in triplicate including, at least, three replicates. Data are presented as means ± Standard Deviation. The results were subjected to one or two-way ANOVA and statistical differences between the groups were analyzed using post hoc Tukey's test at a significance level of 5%. The statistical software used was GraphPad Prism 6.0 (San Diego, CA, USA).

4.3 Results

4.3.1 Analysis of expression of the CaSR in dermal fibroblasts

To investigate if the CaSR might be mediating some of the effects stimulated by extracellular Ca^{2+} in primary dermal fibroblasts reporter in Chapter 3, we first analyzed the expression of this receptor by Western blotting and immunofluorescence. For the analysis, cells were incubated for 24 h in low serum media containing different calcium concentrations: 0.1, 1.25, 2.5, and 3.5 mM.

Western blot showed similar expression of CaSR in all Ca^{2+} concentrations tested (Fig. 4.3A). Two major bands were identified in the Western blot: at ∼130 kD, corresponding to an incompletely processed, high mannose intracellular form, and at ∼150 kD, associated to the fully gly-

cosylated, cell surface-expressed form of the receptor (Fan et al., 1997) (Fig. 4.3A).

Immunofluorescence staining confirmed the presence of the protein in fibroblasts cultured under the different Ca^{2+} concentrations. Since no differences were observed in the amount and location of the signal among conditions, here we show only a representative image corresponding to the 1.25 mM Ca^{2+} condition (Fig. 4.3B-G). As observed in Fig. 4.3D-E, the signal was mainly localized at the membrane edge and, interestingly, in some areas CaSR signal seemed to be concentrated in clusters (Fig. 4.3F-G). The control used without anti-CaSR antibody showed presence of background signal (Fig. 4.3B) but, in samples incubated with the primary antibody, a different signal corresponding to the presence of CaSR was detected (Fig. 4.3D). All in all, these results demonstrate expression of the CaSR on rat dermal fibroblasts cultured under different calcium concentrations, and show that the receptor might me organized in clusters at the edge of the plasma membrane.

4.3.2 Effect of gadolinium on metabolic activity and cell migration

Two of the biological effects found to be stimulated by extracellular calcium on dermal fibroblasts in Chapter 3 were metabolic activity and cell migration. More specifically, we detected that concentrations of 2.5 and 3.5 mM Ca^{2+} stimulated these effects compared to a low Ca^{2+} concentration of 0.1 mM. To explore if metabolic activity and cell migration could be mediated through the CaSR, we compared fibroblasts' responses to calcium with fibroblasts' responses to a widely reported agonist of the receptor, Gd^{3+}.

Metabolic activity was quantified after exposing fibroblasts to Ca^{2+} or Gd^{3+} containing-media for six days. Gd^{3+} stimulated fibroblasts'

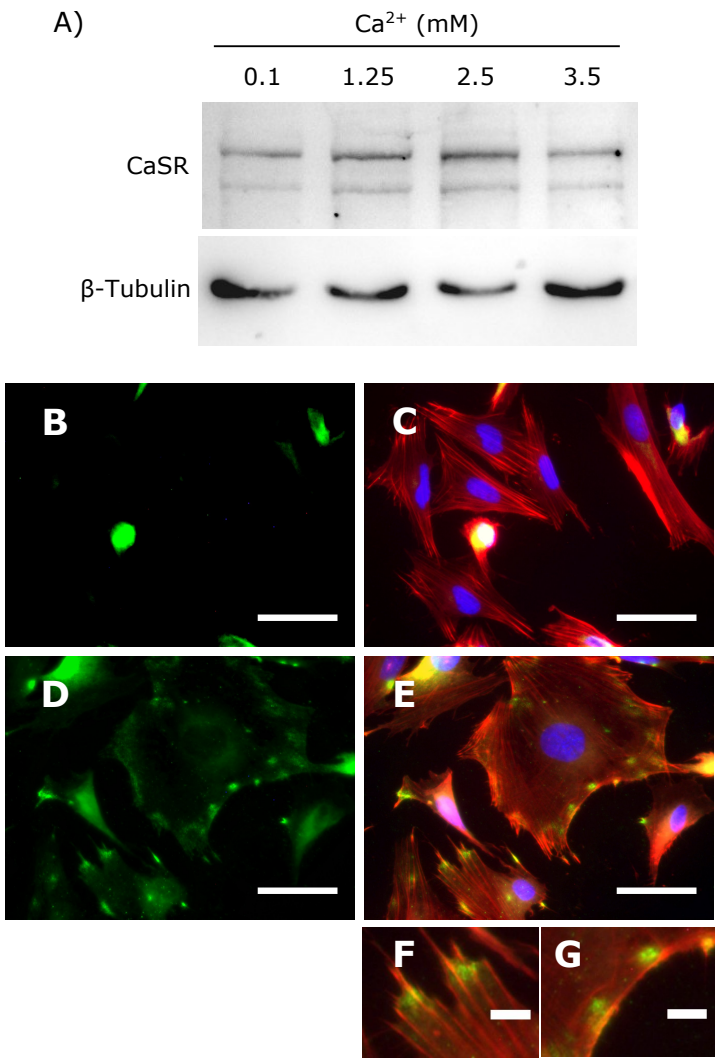

Figure 4.3: Expression of the CaSR in calcium-treated rat dermal fibroblasts. A) Cells were cultured for 24 h in low-serum media containing different calcium concentrations and cell lysate was analyzed by Western Blot. Anti-β-tubulin was used as loading control. B-G) Immunofluorescent staining was performed on cells cultured under the same conditions. Here we show a representative image corresponding to 1.25 mM Ca^{2+}. CaSR is stained in green, F-actin in red, and nuclei in blue. B) CaSR for the negative control and C) merge with F-actin and nuclei signal are shown. D) Positive signal for CaSR and E) merge are also shown. F-G) Magnified images of the clusters of CaSR observed at the edge of the cell membrane. Scale bar for B-E is 50 μm while for F-G is 10 μm.

metabolic activity in a concentration dependent fashion (Fig. 4.4A). Significant differences to 0.1 mM Ca^{2+} were detected from 10 μM Gd^{3+} and reached its maximum in the highest Gd^{3+} concentration tested: 50 μM (Fig. 4.4A). In addition, Gd^{3+} concentrations in the range 10-50 μM stimulated the same level of metabolic activity as 3.5 mM Ca^{2+} (Fig. 4.4A).

Media containing Gd^{3+} also increased cell migration, as shown by the scratch wound assay (Fig. 4.4B-C). A scratch was performed on a confluent layer of fibroblasts and cells were exposed to media containing calcium or gadolinium. Cell migration was quantified by analyzing the area of the scratch covered by cells before and 24 h after media addition. To avoid cell proliferation during the assay, cells were rendered quiescent overnight in low calcium and FBS media before the scratch, and, during the assay, they were cultured in low serum media. Results showed that 50 μM Gd^{3+} stimulated migration as 2.5 mM Ca^{2+} (Fig. 4.4C). Concentrations lower than 50 μM Gd^{3+} did not show significant increase in migration when compared to the low calcium concentration tested. However, a concentration dependent stimulation trend was observed among the different Gd^{3+} concentrations tested (Fig. 4.4C), as previously reported for calcium (Section 3.3.3).

4.3.3 Effect of gadolinium on gelatinase activation and collagen synthesis

Now we wanted to investigate the possible implication of the CaSR in mediating the remodeling capacity stimulated by calcium, as described in Section 3.3.4. In that section we detected increased MMP9 and the active form of MMP2, as well as stimulation of collagen synthesis by 2.5 and 3.5 mM Ca^{2+}. Here, we wanted to study if the CaSR agonist Gd^{3+} might be stimulating these same effects.

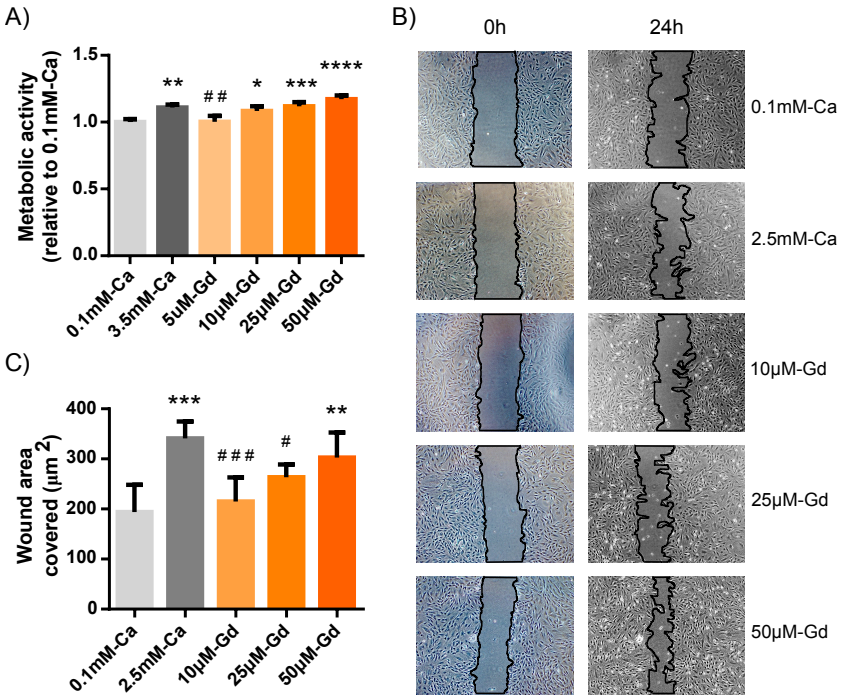

Figure 4.4: Gadolinium effect on metabolic activity and cell migration. A) Metabolic activity of cells cultured in 10% FBS with calcium or gadolinium for six days was determined by Alamar Blue^{TM} reduction. B) For migration assessment in the scratch wound assay, low serum media containing calcium or gadolinium were used and images of the scratch were acquired at 0 h and 24 h. C) The area of the wound covered by the cells after 24 h compared to time 0 h was quantified. Experiments were performed in triplicate and data shows the mean ± standard deviation (SD) of at least four replicates. *p<0.05 Condition vs 0.1 mM-Ca; **p<0.01 Condition vs 0.1 mM-Ca; *** p<0.001 Condition vs 0.1 mM-Ca; **** p<0.0001 Condition vs 0.1 mM-Ca; # p<0.05 Condition vs 2.5 mM-Ca; ## p<0.01 Condition vs 3.5 mM-Ca; ### p<0.001 Condition vs 2.5 mM-Ca.

Both gelatinase activation and collagen synthesis were analyzed from the supernatant of cells incubated for 24 h in low serum media with different Ca^{2+} and Gd^{3+} concentrations. As shown in the zymography in Fig. 4.5A, Gd^{3+} concentrations tested did not increase the active form of MMP2 or synthesis of MMP9 as the 3.5 mM Ca^{2+}. Nevertheless, increase in the inactive form of MMP2 was observed if compared to 0.1 mM Ca^{2+}, specially for the concentration of 50 μM. This concentration also stimulated collagen synthesis (Fig. 4.5B).

To ensure that the differences observed between conditions were not caused due to variations in cell density, quantification of total protein of the cell extract was performed. As shown in Fig. 4.5C, the amount of protein extracted from the cells cultured under the studied conditions was equal. Overall, from the concentrations tested, we can conclude that gadolinium did not stimulate gelatinase activation as calcium, but it increased collagen synthesis.

4.3.4 Activation of the ERK1/2 pathway with gadolinium

One of the signaling pathways that the CaSR can activate when stimulated by calcium or its agonists is the p44/42 MAPK pathway, also known as Erk1/2 pathway (Yamaguchi et al., 2000). When the signaling pathway of the CaSR leads to phosphorilation of the Erk1/2 complex, these protein kinases translocate into the cell nucleus and affect expression of genes that control important cell responses such as proliferation and apoptosis (Mebratu and Tesfaigzi, 2009). Therefore, ERK1/2 could be playing a role in the biological effects stimulated by calcium on dermal fibroblasts.

To study if this pathway was activated on dermal fibroblasts exposed to calcium or Gd^{3+} we analyzed phosphorilation of ERK1/2 by Western blot. Cells were serum-starved overnight in low calcium and exposed to 2.5 mM Ca^{2+} or 25 μM Gd^{3+} (Fig. 4.6). Finally, cell lysate was obtained

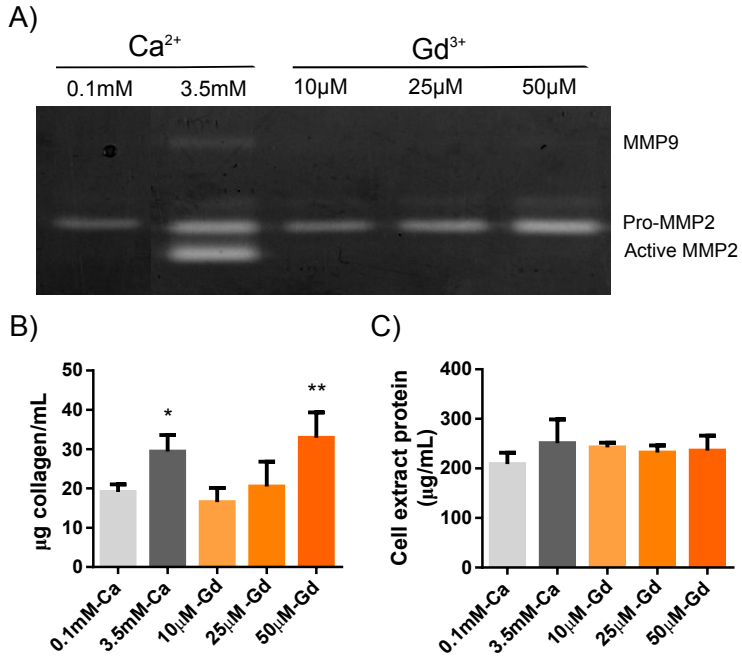

Figure 4.5: Gadolinium effect on gelatinase activation and collagen synthesis. Cells were incubated for 24 h in low serum media containing calcium or gadolinium and supernatant was analyzed using gelatin zymography and Sircol Collagen Assay ™. A) Representative zymogram showing MMP9 and MMP2 forms for the different conditions. B) Collagen quantification from the supernatant. C) Protein concentration quantified from the cell extract. Experiments were performed two times and data from the plot shows the mean ± SD of at least three replicates.*p<0.05 Condition vs 0.1 mM-Ca¸**p<0.01 Condition vs 0.1 mM-Ca.

at 0, 5, 15, 30 and 60 min post addition, and phosphorilation of ERK1/2 was assessed.

Results showed that both Ca^{2+} and Gd^{3+} triggered ERK1/2 phosphorilation (Fig. 4.6). The maximum phosphorilation was observed at 5 min post treatment, seeming higher for the Ca^{2+} concentration tested than for Gd^{3+}. After this time point, the signal decreased progressively in both treatments. Therefore, we showed that activation of the ERK1/2 cascade was taking place in a very similar fashion in dermal fibroblasts exposed

either to calcium or gadolinium, and this activation could be mediated through the CaSR.

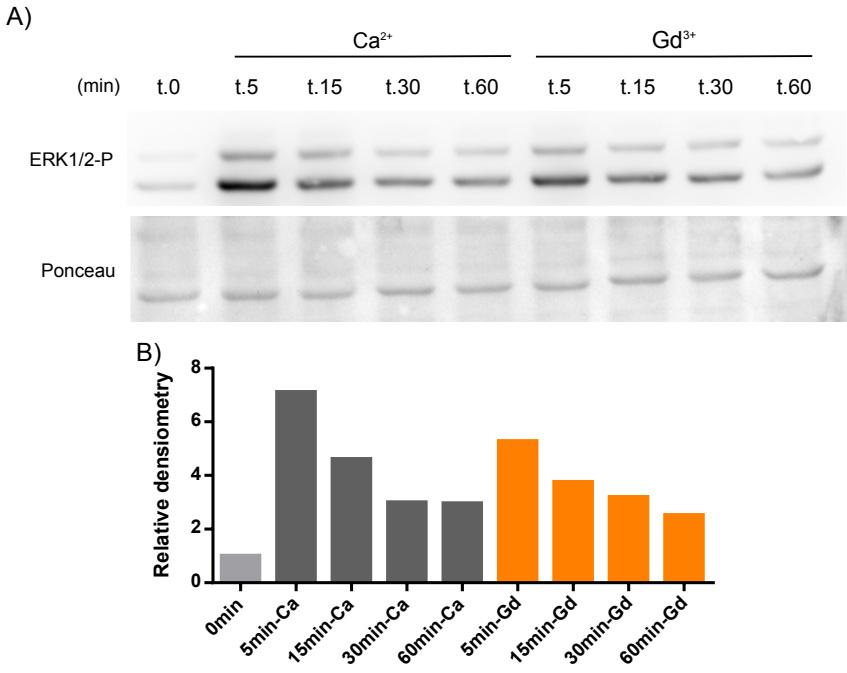

Figure 4.6: ERK1/2 phosphorilation after addition of calcium or gadolinium. A) Cells were rendered quiescent and were incubated in low serum media containing 2.5 mM calcium or 25 μM gadolinium for 5, 15, 30 and 60 min. Cell lysates were used for Western blotting and probed with antiphospho-ERK1/2 antibody. Ponceau staining was used as loading control. B) Densiometry analysis relative to the condition at time 0 min is shown.

4.3.5 Effect of other CaSR agonists on metabolic activity and cell migration

To increase evidence of the implication of the CaSR in mediating stimulation in metabolic activity and cell migration, other agonists were used.

Stimulation of metabolic activity was assessed with 10% FBS media containing different concentrations of Zn^{2+} and Mg^{2+} after six days of treatment. All Zn^{2+} concentrations tested, ranging from 5 to 60 μM, increased metabolic activity compared to 0.1 mM Ca^{2+} (Fig. 4.7A). As for Mg^{2+}, increased metabolic activity was found only for a concentration of 10 mM, while lower concentrations did not affect cell activity (Fig. 4.7B).

Cell migration in the scratch wound assay was studied with Zn^{2+}, Mg^{2+} and Sr^{2+} (Fig. 4.7C). Significant differences were detected for 3.5 mM Mg^{2+}, and for 1.25 and 3.5 mM Sr^{2+} (Fig. 4.7C). The concentration of 50 μM Zn^{2+} did not stimulate cell migration (Fig. 4.7C) and 100 μM was toxic in low-serum conditions (data not showed). From the agonists and concentrations used, 3.5 mM Sr^{2+} stimulated the highest level of migration, even though it did not reach the levels of migration promoted by 2.5 mM Ca^{2+} (Fig. 4.7C). To sum up we can conclude that, in general, these CaSR agonists tested stimulated metabolic activity and cell migration.

4.3.6 Effect of NPS2143 on ERK1/2 phosphorilation, gelatinase activation, cell migration, and metabolic activity

The specific negative allosteric modulator for CaSR, NPS2143, was used to further unravel the implication of this receptor in mediating increase of gelatinases, cell migration, and metabolic activity. NPS2143 did not alter MMP activation of cells exposed to 3.5mM Ca^{2+} (Fig. 4.8C) but it decreased cell migration in the wound scratch assay (Fig. 4.8D) and metabolic activity (Fig. 4.8E). Nonetheless, the vehicle alone also had an impact on cell behavior. Since these interferences due to the presence of

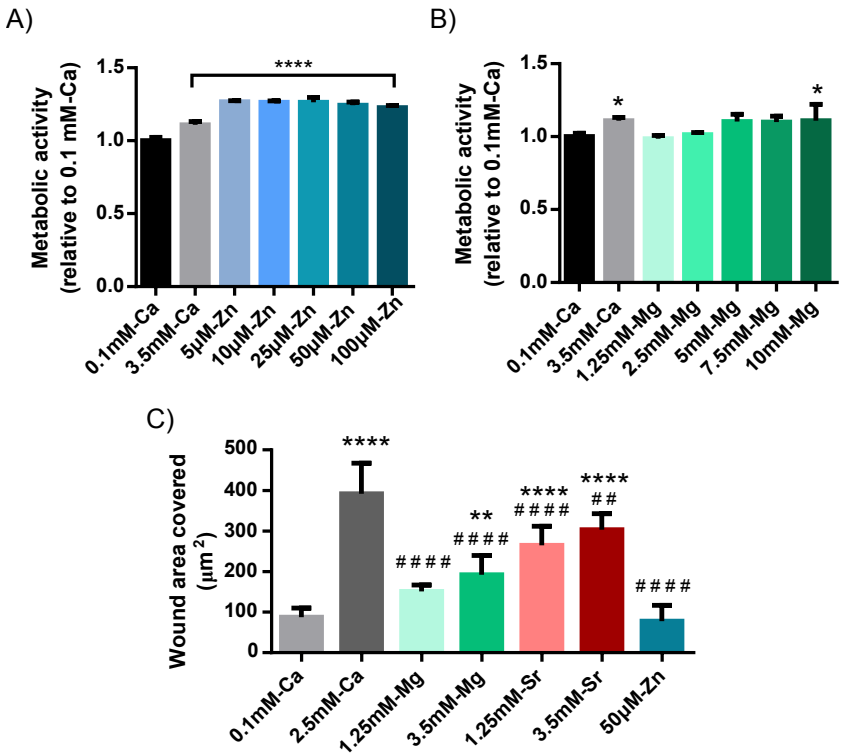

Figure 4.7: Effect of other CaSR agonists on metabolic activity and cell migration. Metabolic activity of cells after being incubated for six days in media containing 10% FBS and different concentrations of A) Zn^{2+} and B) Mg^{2+}, compared to Ca^{2+} stimulation. C) Comparison of the area covered by migrated cells after 24 h of being exposed to low-serum media containing Ca^{2+} versus different concentrations of Zn^{2+}, Mg^{2+}, and Sr^{2+}. Experiments were performed three times and data shows the mean ± SD of at least four replicates. **p<0.01 Condition vs 0.1 mM-Ca; ****p<0.0001 Condition vs 0.1 mM-Ca; #### p<0.0001 Condition vs 2.5 mM-Ca.

the vehicle were detected, we did not carry on with collagen quantification using NPS2143.

In addition, ERK1/2 phosphorilation was compared to calcium-treated cells in the absence or presence of the antagonist. A control containing the same dilution of the vehicle used to dissolve NPS2143, 0.0025% DMSO,

was included. As shown in Fig. 4.8A-B, the presence of 2.5 μM NPS2143 decreased phosphorilation after 5 min of treatment. However, the vehicle alone also modified the resulting phosphorilation.

4.3.7 Comparison of ERK1/2 phosphorilation with calcium and calhex231

Since DMSO used to dissolve NPS2143 seemed to affect cell behavior, we tried a different antagonist dissolved in a different vehicle. More precisely, we used calhex231 (1 μM) in ethanol absolute to analyze ERK1/2 phosphorilation of cells treated with calcium (Fig. 4.9A). Western blot analysis showed decreased signal at 5 min in samples treated with calhex231. Nevertheless, the same behavior was detected in samples treated with the vehicle only, even though the concentration of ethanol was as low as 0.01% (Fig. 4.9B). Thus, the vehicle used with calhex also affected ERK1/2 phosphorilation.

4.4 Discussion

Extracellular calcium stimulates relevant biological processes carried out by dermal fibroblasts during skin wound healing, as demonstrated in Chapter 3. Several membrane receptors and ion channels have been implicated with the biological responses that extracellular calcium promote on cells, among which the CaSR has been one of the most studied. In the skin, the role of this transmembrane receptor in keratinocytes has been widely investigated, but only a few studies have focused on dermal fibroblasts. By using different agonists and negative allosteric modulators of the receptor, the present work gained insight into the mediation of the CaSR on calcium-stimulated processes including metabolic activity, cell migration, gelatinases activity, and collagen synthesis.

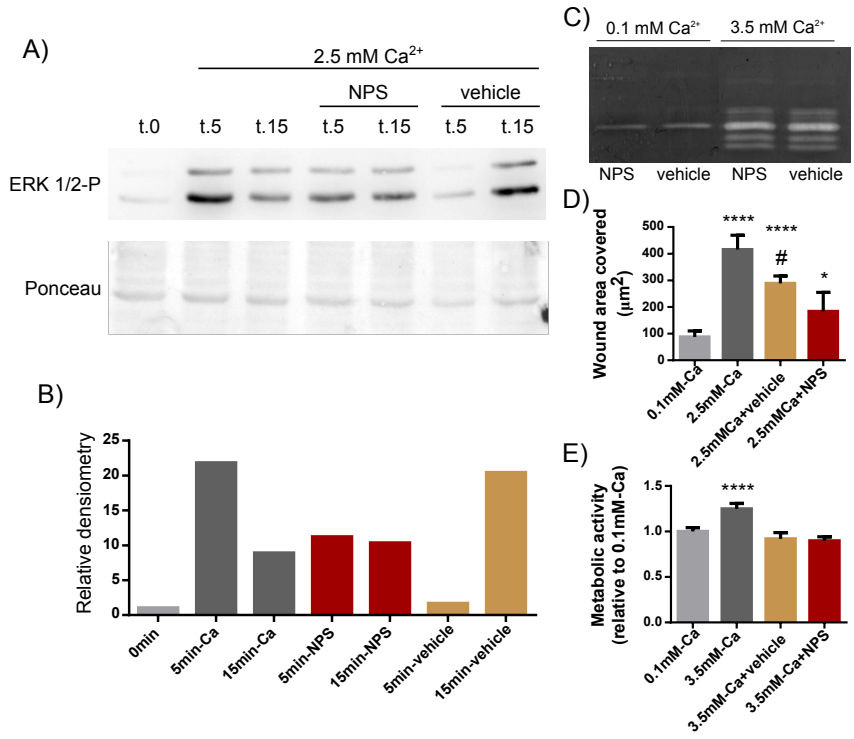

Figure 4.8: Effect of NPS2143 on ERK1/2 phosphorilation, gelatinase activation, cell migration and metabolic activity. A) ERK1/2 phosphorilation after addition of 2.5 mM Ca^{2+} alone, with 2.5 µM of the CaSR antagonists NPS2143 or with the same concentration of vehicle (0.0025% DMSO) contained in the sample with NPS2143, analyzed by Western Blot. Phosphorilation is shown after 5 and 15 min post treatment and B) densiometric analysis relative to time 0 min is represented in the plot. C) Gelatin zymography of the supernatant of cells incubated for 24h in low serum media containing calcium and 2.5 µM NPS2143 or its vehicle (0.0025% DMSO). D) Migration comparison in the scratch wound assay among cell exposed to 2.5 mM Ca^{2+} alone, with 2.5 µM NPS2143 or with the same concentration of vehicle (0.0025% DMSO) contained in the sample with NPS2143. E) Metabolic activity analyzed with Alamar Blue^{TM} of cells cultured in Ca^{2+} alone, 3.5 mM Ca^{2+} with 2.5 µM NPS2143 or 3.5 mM Ca^{2+} with the same concentration of vehicle (0.0025% DMSO) contained in the sample with NPS2143. Each experiment was repeated three times including at least three replicates. *p<0.05 Condition vs 0.1 mM-Ca; ****p<0.0001 Condition vs 0.1 mM-Ca; # p<0.01 Condition vs 2.5 mM-Ca.

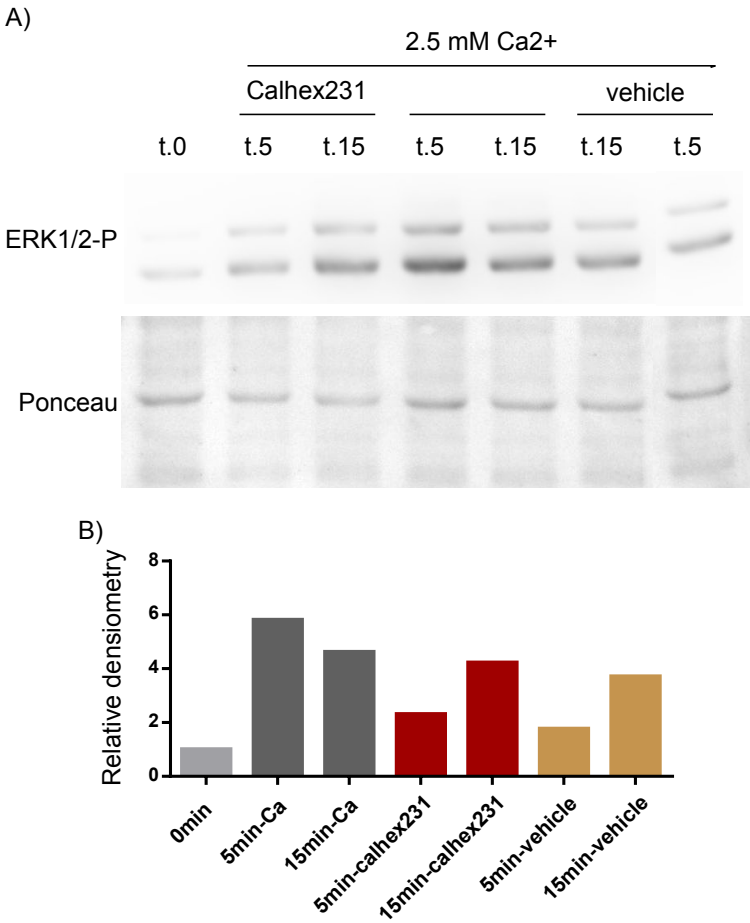

Figure 4.9: Phosphorilation of ERK1/2 after addition of calcium, calcium and calhex231, and calcium and calhex231 vehicle, ethanol. A) ERK1/2 phosphorilation of samples treated with 2.5 mM Ca^{2+} alone or with 1 µM calhex231 or its vehicle (0.01% ethanol absolute) was analyzed by Western blot. B) Densiometry of the membrane relative to time point prior to treatment is represented.

CaSR expression in primary rat dermal fibroblasts cultured under different extracellular calcium concentrations was detected by immunoblotting and immunofluorescence (Fig. 4.3). Two bands were detected in the Western blot against CaSR, as previously reported (Fan et al., 1997). Moreover, immunofluorescence of non-permeabilized cells allowed to localize

the receptor in the plasma membrane. Interestingly, clusters of the receptor were detected at specific points of the membrane edge (Fig. 4.3F-G). To our knowledge, these clusters of CaSR had not been observed before. However, a study by Tharmalingam et al. (2011) showed that CaSR is expressed in the plasma membrane with β-1 integrins in a macromolecular complex in rat thyroid carcinoma cells, and that stimulation of the CaSR promotes cell adhesion and migration via integrin activation. Since fibroblast's migration depends largely on the clustering of integrins in the so called focal adhesions (Huttenlocher and Horwitz, 2011), we hypothesize that the clusters of CaSR might co-localize with focal adhesions in the plasma membrane.

Stimulation of dermal fibroblast's metabolic activity by 3.5 mM Ca^{2+} was compared to a wide range of concentrations of different agonists for the CaSR, as well as to the negative allosteric modulator NPS2143. All agonists tested, including Gd^{3+}, Mg^{2+}, and Zn^{2+} stimulated responses as with Ca^{2+}. In addition, for the different ions, the concentrations that stimulated the response were in accordance to the range of concentrations reported to activate the receptor. Gd^{3+}, which is considered to have a high affinity to the receptor and has been reported to stimulate in the submicromolar to tens of micro-molar range (Breitwieser et al., 2004), promoted metabilic activity in the range of 10-50 μM (Fig. 4.4A). Zn^{2+} has been classified as a mid-stimulator of the CaSR with affinities in the micromolar to submillimolar range. In our study, we detected stimulation in the range from 5-100 μM (Fig. 4.7A). Mg^{2+} is considered a physiological agonist of the receptor, and to stimulate it in the millimolar range. As previously reported, the affinity of this ion was lower than for Ca^{2+} (Brown et al., 1993), since stimulation was detected only from 10 mM of Mg^{2+} (Fig. 4.7B).

Metabolic activity was impaired when we used the negative allosteric modulator NPS2143, but the same behavior was detected for the control

group containing the vehicle alone (Fig. 4.8E). Thus, the interference of the vehicle does not allow to ensure that inhibition of metabolic activity is taken place through the CaSR. Stimulation of metabolic activity through CaSR in fibroblasts had been shown before in the study made by Zhang et al. (2014), in which they used a positive and negative allosteric modulator of the receptor, calindol and calhex231 respectively, on neonatal rat cardiac fibroblasts. Nevertheless, the study failed to include a control group with the concentration of vehicle of these substances.

Cell migration was also studied with different agonists and NPS2143. Gd^{3+}, Mg^{2+}, and Sr^{2+} stimulated migration in a concentration-dependent fashion. However, we were unable to detect stimulation by Zn^{2+}. Of the two concentrations tested, 50 μM did not trigger migration, while 100 μM was toxic in low serum conditions. It is possible that an intermediate concentration might have stimulated migration, but it could also be that Zn^{2+} is not activating the CaSR. Differently to Gd^{3+}, Mg^{2+}, and Sr^{2+}, widely proved CaSR agonists (Coulombe et al., 2004; Jensen and Brauner-Osborne, 2007; Hurtel-Lemaire et al., 2009; Aguirre et al., 2010), no clear evidence exists of the activation of CaSR with Zn^{2+}. As a matter of fact, Zn^{2+} has been found to activate the ERK1/2 pathway through a G-protein coupled receptor (Oh et al., 2002) but, rather than the CaSR, the one mediating this signaling could be another receptor specific for zinc (Hershfinkel et al., 2007). On the other hand, NPS2143 decreased calcium-stimulated migration but, again, the vehicle alone also affected cell behaviour. The only study that we have found to show fibroblasts' stimulation of migration with activators or inhibitors of the CaSR is the abovementioned work by Zhang et al. (2014). Nonehtheless, this study lacks important information, such as the culture conditions during migration and a control that shows the possible effects of the vehicles alone. Thus, we show some evidence of

the mediation of cell migration thorugh the CaSR, but further experiments should be performed to prove it.

Mediation of the CaSR in fibroblasts' remodeling capacity was assessed with Gd^{3+} and NPS2143. Gd^{3+} did not stimulate MMP2 activation as high Ca^{2+} concentration (3.5 mM), and NPS2134 did not impair or reduce its activation. Previous studies had shown increased expression of some MMPs in fibroblasts with CaSR agonists (Bhagavathula et al., 2009; Jenkins et al., 2011; Zhang et al., 2014), but not of MMP2 activation (Jenkins et al., 2011). Thus, CaSR does not seem to mediate high calcium-stimulated gelatinase activation. In contrast, collagen synthesis was stimulated in the presence of Gd^{3+}. This result differs from previous studies, which did not find collagen synthesis stimulation by Gd^{3+} or other agonists (Bhagavathula et al., 2009; Jenkins et al., 2011). Therefore, more agonists and allosteric modulators of the receptor should be tested to better explore the implication of CaSR in collagen synthesis.

Another way to study the activation of the CaSR is by analyzing the intracellular pathways that get activated when it is exposed to agonists or inhibitors. Here, we focused on the detection of the phosphorilation of the MAP kinases ERK1/2 through Western blotting. Analysis of ERK1/2 phosphorilation as a signal of CaSR activation in fibroblasts was first reported by McNeil et al. (1998), which used different agonists, including Gd^{3+}. In our study, both extracellular Ca^{2+} and Gd^{3+} triggered ERK1/2 phosphorilation. The signal peaked at 5 min, being more intense for the Ca^{2+} concentration tested (2.5 mM) than the Gd^{3+} (25 μM), and continuously decreased afterwards (Fig. 4.6). The differences in intensities could be explained by the fact that ERK1/2 phosphorilation signal trough the CaSR is not only time-dependent but also dose-dependent (Kifor et al., 2001). Nevertheless, Gd^{3+} has been reported to activate other transmembrane receptors such as platelet derived growth factor (PDGF) receptor

(Bhagavathula et al., 2010) and the metabotropic glutamate receptor1α (mGluR1α) (Abe et al., 2003), which can lead to ERK1/2 phosphorilation. For this reason, CaSR activation of the ERK1/2 pathway was also studied by exposing calcium-treated fibroblasts to negative allosteric modulators. When we used NPS2143, we detected decreased phosphorilation on time 5 min but the vehicle employed to dissolve the drug alone, DMSO at 0.0025%, seemed to affect the firing of the signal (Fig. 4.8). Unfortunately, alteration of the phosphorilation was also observed when using a different vehicle (0.01% ethanol absolute) for another negative allosteric modulator, calhex231 (Fig. 4.9). Therefore, owing to the interferences observed by the vehicles used with the negative allosteric modulaors, we cannot conclude that the activation of the ERK1/2 pathway is being initiated by the CaSR.

To better unravel the implication of the CaSR in the biological responses analyzed in this study, more agonists, and positive and negative allosteric modulators should be used. In addition, activation of other signaling pathways, such as p38, JNK or the PLC/IP3/Ca^{2+}, when exposed to the different modulating substances should be analyzed. Specific blockers of these pathways can be used to study their implication in the different biological responses. Moreover, knocking-out the expresion of CaSR or inhibiting the receptor with siRNA would also clarify the role of the CaSR in the biological responses, as done in previous studies (McNeil et al., 1998; Maiti et al., 2008; Milara et al., 2010). Nevertheless, the results presented here show that CaSR agonists can stimulate beneficial biological responses carried out by dermal fibroblast in wound healing, including migration and collagen synthesis, while avoid gelatinases activation. Since calcium can affect cell behavior through other pathways, the use of these ions may allow a more specific and directed cellular stimulation. The controlled release of these ions by bioceramics could therefore contribute with improved healing of wounds.

4.5 Conclusions

This work showed expression of the CaSR in rat dermal fibroblasts in clusters at the edge of the plasma membrane that had not been reported before. CaSR agonists, including Gd^{3+}, Mg^{2+}, and Zn^{2+} stimulated metabolic activity and Gd^{3+}, Mg^{2+}, and Sr^{2+} promoted cell migration. In addition, Gd^{3+} also stimulated collagen synthesis, but not gelatinases activation. Since Gd^{3+} activated the MAP kinase pathway of ERK1/2 in a similar fashion as calcium, we hypothesized that this pathway might mediate some of the observed stimulations. To grow evidence of the implication of the CaSR in the mediation of the biological stimulations observed, we used negative allosteric modulators but encountered a difficulty. The vehicles alone employed to dissolve these substances were interfering with the cellular response. Therefore, when using these reagents, studies should always include a vehicle control, and in many cases they are missing. Thus, the role of CaSR in mediating the biological responses stimulated in fibroblasts should be further studied with other modulators and inhibitors of the receptor. Nonetheless, the observation that CaSR agonists stimulate useful responses for wound healing suggest the possibility of using materials that release these ions instead of calcium, since a more controlled cellular response might be achieved.

5 *In vivo evaluation of a calcium-releasing composite on a pressure ulcer diabetic model*

5.1 Introduction

In Chapter 3 we reported that the calcium-phosphate ormoglass SG5 promotes favorable responses on dermal fibroblasts for an improved healing, such as increased cell migration and collagen synthesis. Based on these results, we suggested that these particles could be incorporated in a biological-free novel dressing for the treatment of chronic wounds. This chapter was devoted to designing and testing such a dressing.

As mentioned in Section 2.5.3, novel therapies are needed for the treatment of chronic wounds. Conventional dressings, which improve healing by keeping a moist environment in the wound, are not effective enough for many chronic injuries (Margolis et al., 1999; Werdin et al., 2009). Over the last years, the development of biological based therapies, such as growth factor administration or the use of skin equivalents, have raised high expectations, but its translation into the clinics has been hampered due to regu-

latory, economic and safety issues (European Medicines Agency, 2017; FDA, 2008; Frykberg and Banks, 2015). Thus, new, off-the-shelf, cost effective, and secure treatments are in urgent need.

Recently, the use of bioceramics has been suggested for the treatment of wounds, as explained in Section 2.6.1. Indeed, some compositions have shown improved wound closure when applied topically (Jebahi et al., 2013; Li et al., 2016; Sen et al., 2002) or intravenously (Kawai et al., 2011) in different animal models, mostly in full-thickness wounds of rat and mice. In general, these studies report increased number of vessels or expression of angiogenic factors when bioceramics are applied, so the accelerated healing has been explained by increased vascularization (Sen et al., 2002; Lin et al., 2012; Jebahi et al., 2013; Li et al., 2016).

Based on our previous experience in the use of the electrospinning technique and the use of poly(lactic acid) (PLA) for the generation of biomaterials, we synthesized a novel composite material made of electrospun PLA fiber-based membranes containing SG5. This material showed gradual calcium release and pro-angiogenic properties *in vitro* and *in vivo* (Oliveira et al., 2016). More specifically, human progenitor-derived endothelial cells (HDECs) cultured on this material proliferated well and increased vascular endothelial growth factor (VEGF) expression (Oliveira et al., 2016). When implanted subcutaneously in mice, the ormoglass-containing composite increased the expression of pro-angiogenic factors, such as VEGF, Insulin growth factor 2 (IGF-2), Interleukin 1 beta (IL-1 β) and interleukin 6 (IL-6), as well as the number of vessels (Oliveira et al., 2016).

Our results obtained *in vitro* exposing dermal fibroblasts to the ion release of SG5, together with the angiogenic effect observed subcutaneously *in vivo* with the composite material, prompted us to test this material on skin wounds. The dressing was synthesized and characterized, and evaluation of cell viability was performed in media conditioned by the material.

To achieve a better understanding of the current needs in the treatment of chronic wounds and improve the design of the *in vivo* model, we carried out a survey addressed to medical professionals specialized in the treatment of chronic wounds. Then, the dressing was applied on pressure ulcer wounds generated in diabetic mice. Its effect on wound closure, collagen deposition, blood vessel generation, and granulation tissue formation was compared to a particle-free PLA membrane and to a commercial dressing frequently used in the treatment of chronic wounds. In addition, the overall performance of the dressing was compared to the unmet needs of current treatments for chronic wounds, according to our survey.

5.2 Materials and methods

5.2.1 Calcium-phosphate particle synthesis

Calcium-phosphate ormoglass particles referred as SG5 with a composition of $CaO{:}P_2O_5{:}Na_2O{:}TiO_2$ (44.5:44.5:6:5) were produced by the sol-gel method as described in Section 3.2.1.

5.2.2 Synthesis of electrospun PLA/calcium-phosphate composite

PLA nanofibers loaded with 25% (w/w) SG5 were generated with the electrospinning technique as explained elsewhere (Oliveira et al., 2016; Sachot et al., 2016). The process of electrospinning is a widely used method to produce biomaterials and allows to generate mats of polymer nanofibers by subjecting a polymer solution to electrostatic forces (Kamudzandu et al., 2015).

The main components needed for electrospinning are a syringe, a spinneret -e.g. needle-, a pump, a high voltage power source, and a fiber col-

lector device placed as in Fig. 5.1A (Kamudzandu et al., 2015). A polymer is dissolved in a highly volatile solvent, loaded in a syringe with a needle at the end, and placed in a pump that forces the solution through the needle (Sill and von Recum, 2008; Mouthuy and Ye, 2011). The needle is connected to a high voltage power supply, which injects charge of a certain polarity into the polymer solution (Sill and von Recum, 2008; Mouthuy and Ye, 2011). If the electrostatic force created by the repulsion of similar charges is sufficient to balance out the surface tension of the polymer solution, a protuberance know as the Taylor cone is formed at the tip of the needle and a jet is emitted from its apex (Fig. 5.1B) (Sill and von Recum, 2008; Mouthuy and Ye, 2011). While the fiber jet is traveling towards the grounded collector it undergoes a chaotic whipping instability, which increases the transit time and the path length to the collector and aids in the fiber thinning and solvent evaporation processes (Sill and von Recum, 2008). The fiber jet is then deposited on the collector the configuration of which will determine if the fibers of the generated mat are aligned or randomly oriented.

To generate the PLA fiber mat loaded with SG5 particles, we electrospun a solution of 4% w/w PLA (70/30 L-lactide/DL-lactide copolymer, Purasorb PLDL 7038) in 2,2,2-trifluoroethanol (TFE) (99.8%, Panreac) with 25% w/w SG5 particles to PLA. First, SG5 particles were homogeneously dispersed in TFE within a glass container with ultrasounds (Branson Ultrasonic Sonifier, Model 102C) for 30 s at 30% amplitude with intermittent pulses of 1 s ON and 2 s OFF. Then, PLA pellets were added and stirred until completely dissolved at room temperature (RT), for about 3 h. The solution was transfered in a plastic syringe with a 23 GA tip (Precision tips, Nordson EFD) and the electrospinning process was performed under the following parameters: 10 kV applied voltage, 1 mL/h dispensing pump rate, and 15 cm tip-collector distance. Fibers were deposited on aluminum

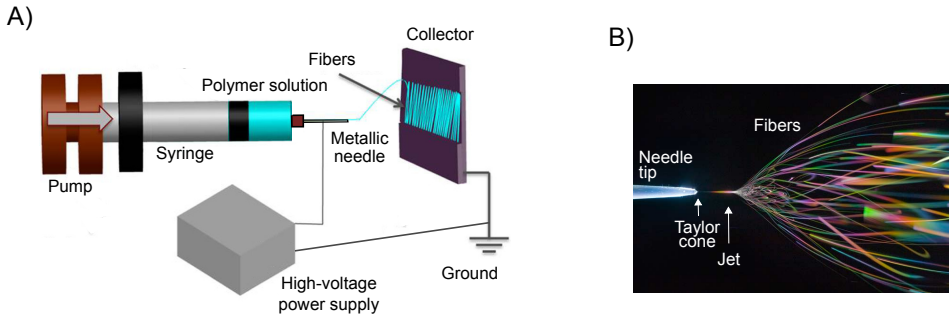

Figure 5.1: Schematic representation and functioning of the typical electrospinning system. A) The electrospinning technique is performed with a syringe loaded with a polymer solution placed on a pump which controls the speed of extrusion of the solution through a metallic needle. The needle is connected to a high voltage supply, which injects charge of a certain polarity into the polymer solution. When the charge of the solution reaches a critical value, the solution is accelerated towards a collector of opposite polarity. B) The electrospinning process takes place due to the effects of the forces generated by the electric field on the polymer solution. Under the electric field, the repulsive electrical forces generated in the solution change the rounded shape of the solution hold by surface tension forces at the exit of the needle into a cone shape, known as Taylor cone. At a critical value of the electric field applied to the solution, the repulsive electrical forces overcome the surface tension forces of the polymer solution and a jet is ejected from the tip of the Taylor cone. As the jet travels towards the collector, whipping instabilities draw out the fiber to nanoscale diameters as the solvent in which the polymer was dissolved evaporates. Adapted from Kamudzandu et al. (2015).

foil hold on a rotor turning at 1200 rpm. Thus, the final orientation of the fibers in the mat was aligned. To facilitate detachment of the deposited fibers from the aluminum foil, this was covered with a thin layer of glycerol (99%, Panreac) prior to the electrospinning. Control fibers consisting of PLA fibers alone were produced under comparable conditions but without particles. Once synthesized, fibers were kept in a desiccator to allow evaporation of TFE traces and improve fiber preservation.

5.2.3 Calcium release, pH and FE-scanning electron microscope (SEM) characterization

Measurement of calcium release from the fibers was performed in cell culture media at different time points. Fibers were cut in squares of 1.7 cm x 1.7 cm, sterilized under UV for 15 min on each site, and introduced separately in a 24-well plate. Then, 500 µL of media consisting of calcium-free Dulbecco's Modified Eagle Medium (DMEM) (Gibco), 2 mM L-Glut (Invitrogen), 100 U/mL penicillin/streptomycin (P/S) (Gibco), and 10% (v/v) fetal bovine serum (FBS) (Sigma-Aldrich) was added in the wells and samples were incubated at 37 °C in 5% (v/v) CO_2. At each time point (30 min, 60 min, 90 min, 120 min, 24 h, 48 h, 72 h) 100 µL were removed to be analyzed and replaced with fresh media. Calcium concentration was assessed with the colorimetric method 0-Cresolphtalein Complexone (Sigma) (Cohen and Sideman, 1979) reading absorbance at 570 nm on the Infinite M200pro microplate reader (Tecan). Cumulative calcium release was calculated taking into account the total calcium moles cumulated at each time point, including the ones removed over time and subtracting the background signal from media. pH was measured with a Laquatwin pH-meter (B-712, Horiba). Five replicates were used per condition.

Mats' thickness was measured with an electronic digital micrometer, and micro- and macro-morphology was observed using an Ultra-High Resolution Field Emission Scanning Electron Microscopy (Nova Nano SEM-230; FEI Co.) operating at 5.00 kV. Prior to imaging, samples were coated with an ultra-thin layer of carbon to render them conductive.

5.2.4 Fibroblast viability in conditioned media

Evaluation of viability of cells cultured for 24 h in media previously incubated with the fibers was assessed with the Alamar Blue™ (Thermo Sci-

entific) reagent following manufacturer's instructions. For this experiment, commercially available human dermal fibroblasts from healthy adults (Promocell) were used. These cells were expanded in complete culture media (CCM) consisting of DMEM with 1.8 mM calcium, 10% FBS, 2 mM L-Glut, and 100 U/mL P/S at 37 °C in 5% (v/v) CO_2 changing media every 3 days and used at passages 4-7.

Conditioned media was prepared by adding 500 µL of CCM on previously UV-sterilized fibers of 1.7 cm x 1.7 cm and incubating them for 24 h at 37 °C in a CO_2 incubator. Media incubated with mats from the same condition, either PLA or PLA-SG5 mats, was pooled before adding it to the cells.

Cells (15,000 cells/well) were seeded in 24-well plates in CCM and, after 24 h, conditioned media was added. At 1 and 4 days post-treatment, media of each well was replaced by 400 µL of CCM containing 10% Alamar Blue™ and incubated at 37 °C for 3 h. Then, 100 µL of each well was transferred to a 96 well plate in triplicates and fluorescence was measured at Ex/Em wavelength of 530/590 using a microplate reader (Infinite M200 Pro, Tecan). The remaining culture medium containing Alamar Blue™ was removed and cells were washed with Phosphate-Buffered Saline (PBS), 500 µL of fresh conditioned medium was added to each well and cells were cultured until the next time point. Eight replicates were used per condition, and the experiment was repeated three times. Background values from Alamar Blue™ containing media not incubated with cells were subtracted from all measured values and these final values were normalized to the average value corresponding to the control sample with non-conditioned media on day 1.

5.2.5 Survey

An on-line survey of 20 questions was addressed to medical professionals of the metropolitan area of Barcelona specialized in the treatment of chronic wounds. Details about the survey are given in Appendix A.2.

5.2.6 Animal model

Thirty-two obese and diabetic mice with a mutation in the leptin receptor, know as db/db, were obtained from Charles River Laboratory and used at 8-weeks old. To avoid hormone interference in the healing of wounds, male mice were used. Once received, all mice were housed in specific pathogen-free barrier facility and were acclimatized to their new environment for 7 days before the beginning of the study. Animals were fed on a pellet diet of LabDiet® 5K52 formulation (6% fat) and water ad libitum. For the experiment, mice were randomly divided in two groups: one group was treated with PLA and PLA-SG5 mats while others were treated with the commercial dressing Mepilex® (Mölnlycke Health Care) and PLA-SG5. During the experiment, mice were caged individually to prevent magnets of different animals from sticking together and to avoid mice interfering with dressings from other mice. All studies and procedures were performed with the approval of the animal care committee of the Government of Catalonia.

5.2.7 Generation of a pressure ulcer wound

To generate pressure ulcers on the dorsal side of mice a previously reported model was used that consisted in performing cycles of ischemia-reperfusion (IR) with the external application of two magnets (Stadler et al., 2004; Saito et al., 2008; Wassermann et al., 2009).

On the first day of the experiment, mice were anesthetized in a chamber with 5% isoflurane and maintained at 2% isoflurane during the procedure. Mice backs were shaved with an electric razor and cleaned with 70% ethanol. Then, the skin was gently pulled and placed between two round ceramic magnetic plates (12 mm diam, 5 mm thickness, IMA) previously sterilized with ethanol, pinching the epidermis, dermis, hypodermis, and panniculus carnosus. An unpinched space of 0.5 to 1 cm was left between magnets (Fig. 5.2A) so that two separate injuries could be generated on each animal. Six IR cycles were performed in each mouse to generate pressure ulcers. A single IR cycle consisted of a 12-hour period of magnet placement, followed by a release or rest period of 12 h. Animals were anesthetized for magnet placement, but not for magnet removal, and magnets sterility was ensured by spraying them with 70% ethanol and exposing them under UV before each application. Mice tolerated the procedure well. After anesthesia, animals were monitored for a few minutes until they returned to normal activity. This process produced two circular ulcers covered by necrotic tissue separated by a bridge of healthy skin.

5.2.8 Dressing application

Dressings consisting of PLA mats, PLA-SG5 mats, or commercially available Mepilex® were applied on the ulcers generated on the back of the mice. PLA and PLA-SG5 were synthesized as explained in Section 5.2.2. Then, mats were cut in squares of 1.7 cm x 1.7 cm and weighed to ensure similar thickness and material content within each condition. Then, they were UV-sterilized for 15 min on each side and kept under sterile conditions. Mepilex® was also cut in squares of 1.7 cm x 1.7 cm under sterile conditions.

Prior to dressing application, mice were anesthetized and necrotic tissue was mechanically removed with scissors. Dressings were wettened in

a sterile solution of sodium chloride at 0.9% (w/v) in water and placed on each wound. The size of the dressings allowed a complete coverage of the wounds. To maintain dressings in site, they were covered with an adhesive plaster (Coverplast® Latex-free, BSN medical) and further secured with an elastic gauze (Genové Dermatologics), as illustrated in Fig. 5.2 B-D.

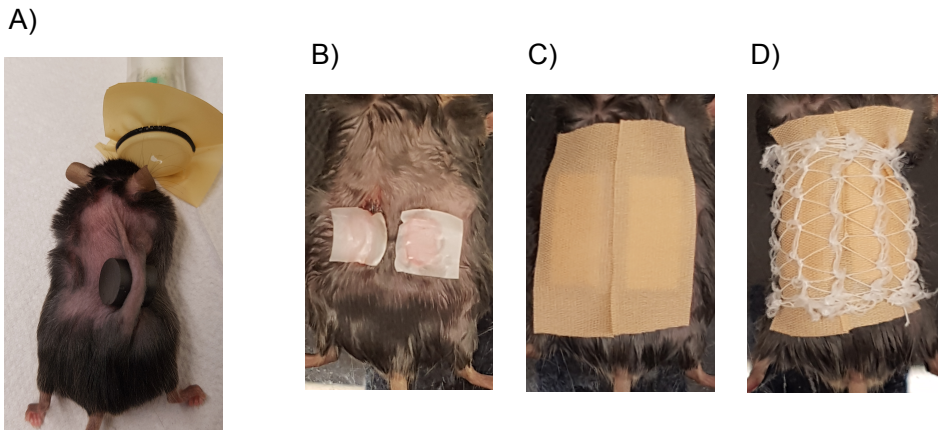

Figure 5.2: Magnet and dressing placement on the back of mice A) The skin of the back of diabetic mice was pinched with two magnets as shown. The wounds created were covered with B) the experimental dressings, which were secured with C) adhesive plasters and D) an elastic gauze.

Dressing change was performed every 24 h placing animals under anesthesia. At every change, a few drops of the saline solution were added on the dressings covering the wound to facilitate their detachment.

5.2.9 Measurement of wound size

Right before dressing application and at every dressing change, digital imaging of wounds was performed using a digital camera (Mavica FD91, Sony) and the ORCA-2BT Imaging System (Hamamatsu Photonics) provided with a C4742-98-LWG-MOD camera fitted with 512x512-pixel charge-couple device (CCD) cooled at -80 °C. Wound size was quantified

from images obtained with the abovementioned camera using the Wasabi image analysis software (Hamamatsu Photonics). The area measured at each time point was normalized to the size of the wound before dressing application (day 0).

In addition, wound images acquired were shared with highly experienced nurses in the treatment of chronic wounds so that they could evaluate the wound appearance.

5.2.10 Histological staining

On 3 and 8 days post-treatment, 8 animals from each group were anesthetized and sacrificed by cervical dislocation. Then, wounds were excised with margins of 2 mm, cut in half and fixed in 10% neutral buffered formalin solution (Sigma-Aldrich) for 24 h. Samples were dehydrated in alcohol and paraffin-embedded. Sections (8 μm) performed with microtome (RM2255, Leica) were stained against hematoxylin-eosin (H&E) and modified Masson's trichrome for examining re-epithelialization and collagen deposition, respectively. Prior to the staining, sections were deparaffinized with three baths of 3 min in xylene (Sigma-Aldrich), and hydrated through a graded ethanol series consisting of 2 baths of 20 s in 100% ethanol (Panreac), a 20 s bath in 95% ethanol, and a 3 min bath in 70% ethanol.

For the H&E staining, slides were washed in running tap water for 1 min and stained with previously filtered Harris hematoxylin modified solution (Sigma-Aldrich) for 3 min. Then, sections were washed again under running tap water until water was clear and treated for 1 min with 0.3% acid alcohol consisting of 0.3% HCl (37%, Sigma-Aldrich) in 70% ethanol. Samples were rinsed for 3 min in running water, added in 0.3% ammonia water for 1 min, and rinsed again for 3 min. Slides were submerged in eosin (0.5%, Casa Alvarez) for 1 min, and samples were re-dehydrated for 15 s in 95% ethanol, 30 s in 100% ethanol, 1 min in 100% and two

consecutive baths of 5 min in xylene. Finally, samples were mounted in xylene-based mounting medium (Eukitt, Panreac) and covered with glass coverslips.

Masson's trichrome (Trichrome stain kit, Sigma-Aldrich) staining was performed following the manufacturer's instructions by submerging the slides with sections in the different solutions provided by the commercial kit for the specified times. After re-dehydration, samples were mounted as explained above. Low magnification images of the stained tissue were acquired with an Olympus DP72 camera from an Olympus Macro Zoom flourescence microscope MVX10 (Olympus Life Science), and for high magnification images, a Nikon E600 microscope with an Olympus DP72 camera was used.

5.2.11 Immunohistochemistry

Deparaffinized sections were stained against CD31 and counterstained with hematoxylin. Briefly, antigen retrieval was performed by incubating the samples for 20 min at 95 °C in a sodium citrate buffer solution containing 10 mM sodium citrate tribasic dihydrate (Sigma-Aldrich) with 0.05% Tween® 20 (Sigma-Aldrich) (pH 6.0). Then, samples submerged in the citrate buffer were allowed to cool down for 30 min and were washed three times. A circle surrounding the sections was drawn on each slide with a Pap pen (Dako) and samples were blocked for 1 h with a solution made with Tris-buffered saline (TBS) containing 0.0025% (v/v) Triton ® X-100 (Sigma-Aldrich), 10% FBS and 1% (w/v) bovine serum albumin (BSA) (Sigma-Aldrich). Afterwards, sections were placed in a humidity chamber and incubated with rabbit polyclonal anti-CD31 antibody in a TBS-1% BSA solution (dilution 1:35, ab28364, Abcam) at 4 °C overnight. Following two washes of 5 min, samples were incubated in 3% H_2O_2 (33%, Panreac) in PBS (Invitrogen) for 15 min and washed

again three times with 10 min washes. Then, the biotinylated secondary antibody goat anti-rabbit (ab128978, Abcam) was added and incubated for 1 h at RT, and samples were washed again three times with 10 min washes. Samples were subsequently incubated with streptoavidin peroxidase (ab128985, Abcam) for 20 min, washed three times, and developed with DAB Chromogen (ab 64239, Abcam) for 4 min. Slides were submerged in distilled water for 10 min and weakly counterstained with a Harris hematoxylin modified solution diluted 1:10 in deionized water for 40 s. Finally, sections were re-dehydrated and mounted as reported in the previous section. All the abovementioned washes were performed with TBS-0.0025% Triton® solution. Images of the wound site were acquired with a a Nikon E600 microscope with an Olympus DP72 camera and vessel quantification was performed from three images of four different wounds per condition.

5.3 Results

5.3.1 Dressing characterization

Electrospun mats of PLA fibers containing or not sol-gel produced calcium-phosphate SG5 particles were synthesized and imaged by SEM. Both PLA and PLA-SG5 mats presented a similar dense fiber bundle with a fiber diameter between 0.5-1 μm (Fig. 5.3A-B). The thickness of the mats used for this study were between 200 to 260 μm. SG5 particles were observed embedded within the PLA fibers (Fig. 5.3B).

A gradual release of calcium was measured for the PLA-SG5 mats when incubated in CCM, reaching its maximum after 48 h with values between 3 and 4 mM (Fig. 5.3E). As expected, particle-free PLA fibers did not release any calcium (Fig. 5.3E). In addition, conditioned media did not present significant changes in pH (data not shown).

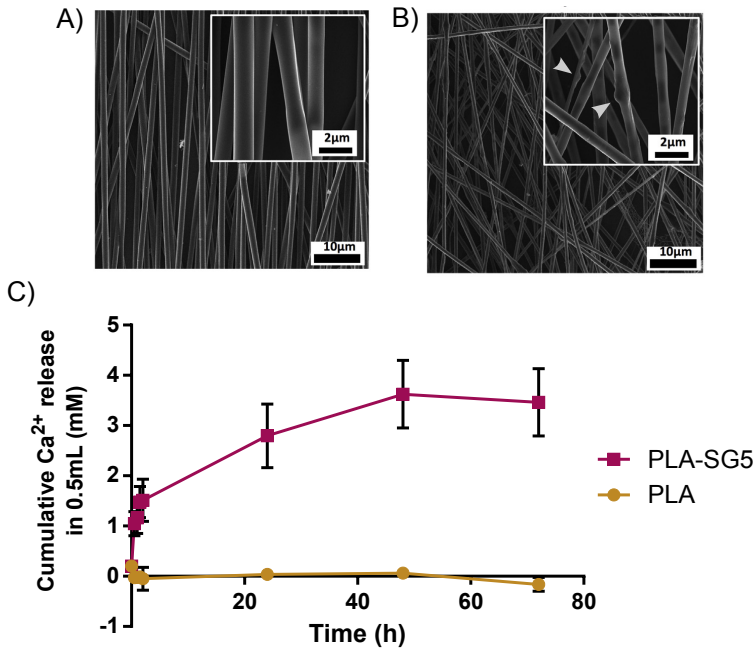

Figure 5.3: Characterization of electrospun PLA mats with and without SG5 particles. A-B) PLA (left) and PLA-SG5 (right) mats imaged with SEM. Arrowheads mark the presence of particles embedded in the fibers. C) Cumulative calcium release over time from 1.7 cm x 1.7 cm mats in complete culture medium (CCM). (n = 5, mean ± standard deviation (SD)).

5.3.2 Cell viability *in vitro*

An indirect viability test on cells exposed to media conditioned by the release of the PLA and PLA-SG5 mats was performed to detect possible material cytotoxicity. More specifically, adult human dermal fibroblasts were exposed to CCM conditioned for 24 h with the materials and metabolic activity was measured from Alamar Blue™ reduction after 1 and 4 days post-treatment. Results were compared to a control sample consisting of cells exposed to non-conditioned media. As shown in Fig. 5.4, no alter-

ations in metabolic activity were detected in dermal fibroblasts exposed to material-conditioned media.

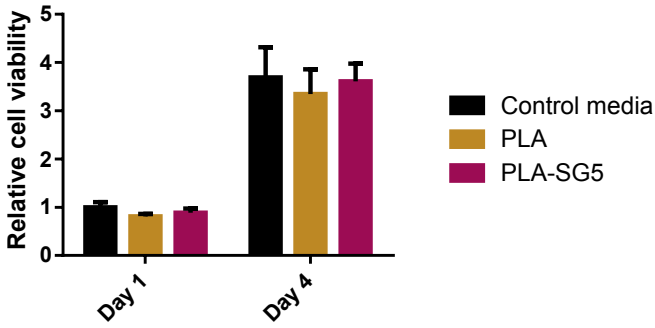

Figure 5.4: Assessment of human dermal fibroblasts viability in conditioned media. Adult human dermal fibroblast from healthy donors were exposed to CCM previously incubated with PLA or PLA-SG5 mats, and metabolic activity was quantified after 1 and 4 days post-treatment. Values were normalized to the average of the control sample exposed to non-conditioned media on day 1. (n = 8, mean ± SD).

5.3.3 Survey results

To obtain a better understanding of the way chronic wounds are treated and what is the perception of health professionals about the products currently available and their limitations, we decided to carry out a survey. The results obtained in the survey are extensively commented in Appendix A.3 but, for the sake of briefness, this section only focuses on the information relevant for this chapter.

Although only thirteen people participated in the survey, more than a half of them had at least 16 years of experience in the treatment of chronic injuries. The survey pointed out that nurses are the main health professionals responsible for the treatment of chronic wounds. When choosing a dressing, the factor that they prioritize is speed in wound closure.

In the case of pressure ulcers, diabetes is perceived within the top three risk factors for this type of wounds and the most common treatment they apply is debridement. When inquired about the aspects of wound healing that are not properly covered by current dressings, the most voted aspect was control of tissue maceration at the wound edge, followed by stimulation of granulation tissue.

5.3.4 Wound healing performance and gross examination of the healing process

Wound-healing efficacy of PLA-SG5 mats in the treatment of chronic wounds was evaluated *in vivo*. Two pressure ulcers were created on the back of obese and diabetic mice that allowed to compare the healing capability of PLA-SG5 against PLA mats and Mepilex®, a commercially available dressing frequently used in the treatment of chronic wounds. Wound area reduction was followed daily for 8 days (Fig. 5.5A-F) and values are shown in Fig. 5.5G. PLA-SG5 treatment presented the fastest healing rate compared to both PLA and Mepilex® controls at every time point analyzed. On the other hand, both controls showed a comparable percentage of wound closure, since differences were not significant between them (Fig. 5.5G).

Wound images were evaluated by nurses with wide experience in chronic wound treatment and they detected a wound complication known as slough in some wounds of all the experimental groups. Slough is a type of necrotic tissue with a yellowish appearance made up of white blood cells, bacteria and debris, which tends to form in chronic wounds (Brown, 2013). This dead tissue can be noticed in some wounds shown in Fig. 5.5, specially in image G, C, H, D, I, and J. Normally, this tissue is debrided through mechanical or chemical methods but this was not done in this study.

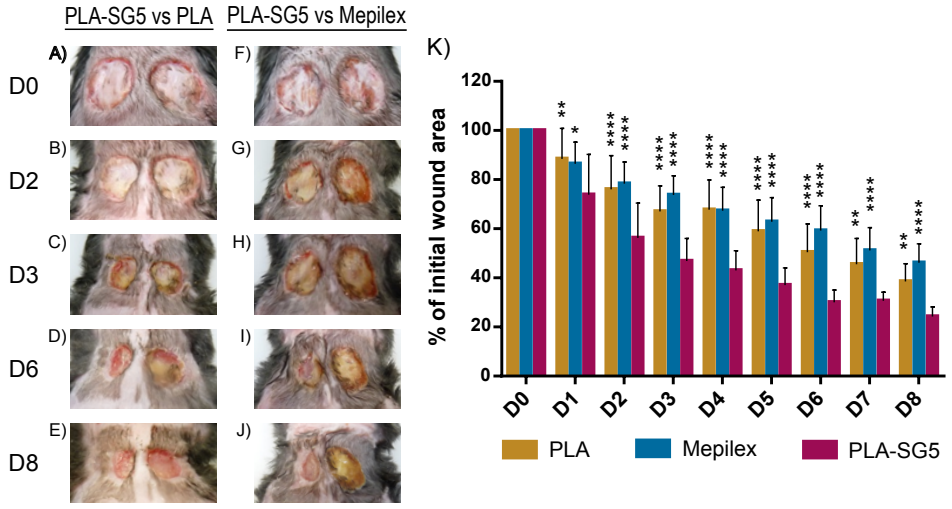

Figure 5.5: Assessment of wound healing size at different time points. A-E) Representative images of the group treated with PLA-SG5 (left) and PLA (right) on day 0, 3, and 8 post-treatment. F-J) Representative images of the group treated with PLA-SG5 (left) and Mepilex® (right) on day 0, 3, and 8 post-treatment. Scale bar = 1mm. K) Percentage of wound size relative to the initial size during the course of the experiment. Data is expressed as the mean ± SD (n=8). *p<0.05 (vs PLA-SG5),**p<0.01 (vs PLA-SG5),****p<0.0001 (vs PLA-SG5).

Histological analysis was performed on wounds excised on day 3 and 8 post-treatment. Sections were stained with H&E (Fig. 5.6A) and histomorphological analysis of the unepithelialized surface revealed a significant decrease in length for the PLA-G5 treated wounds compared to Mepilex® treated at both 3 and 8 days post application (Fig. 5.6B). On the other hand, even though the mean value measured for PLA-SG5 on day 3 was lower than for PLA, differences were not significant between these two treatments.

Gross examination of Masson's trichrome-stained sections was also performed (Fig. 5.7). Regarding the collagen distribution, differences in collagen structure were not detected among conditions. However, as it can be noticed in Fig. 5.7, by day 8 the structure of both PLA and PLA-SG5

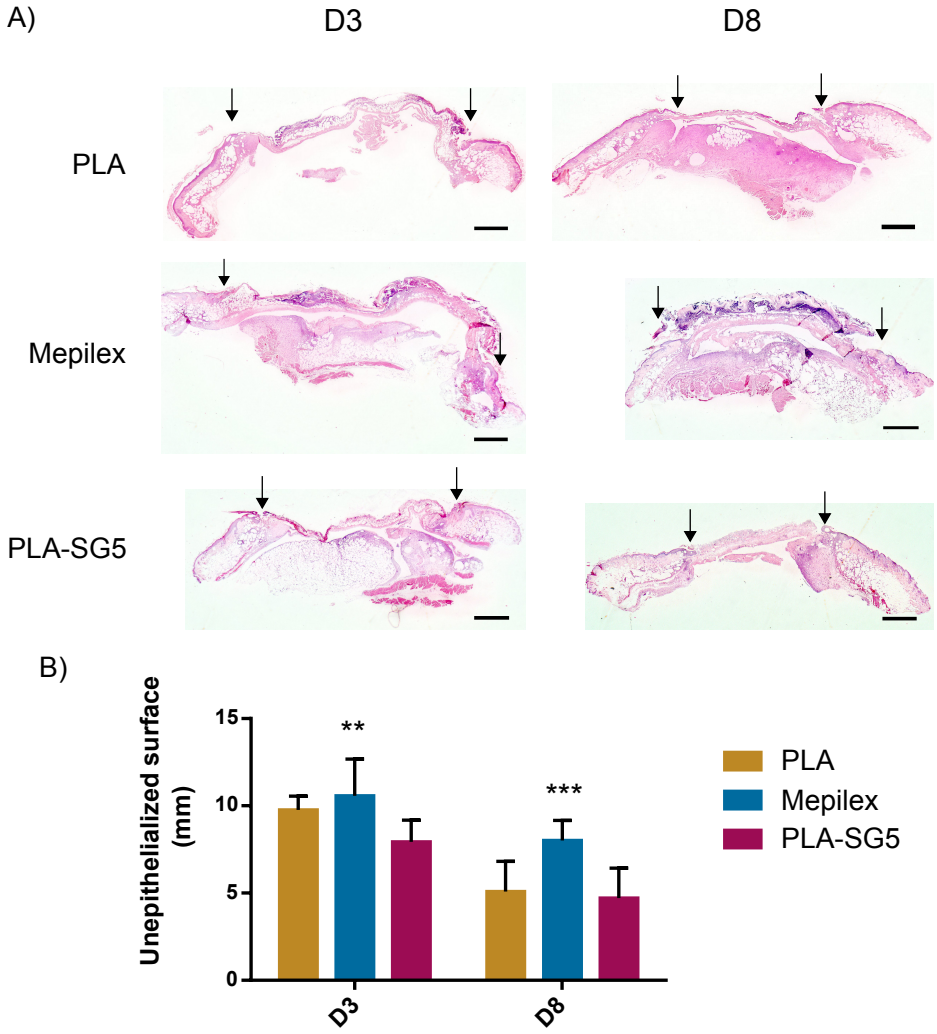

Figure 5.6: Analysis of wound structure from sections stained with H&E. A) Representative images of wound sections stained with H&E from day 3 and 8 post-treatment. Arrows delimit the unepithelialized surface of the wound. B) Quantification of the unepithelialized length from each experimental condition on day 3 and 8 post-treatment. Data is expressed as the mean ± SD of at least 5 wounds from different animals. **p<0.01 (vs PLA-SG5). ***p<0.001 (vs PLA-SG5).

conditions had a better resemblance to healthy skin than the Mepilex® condition.

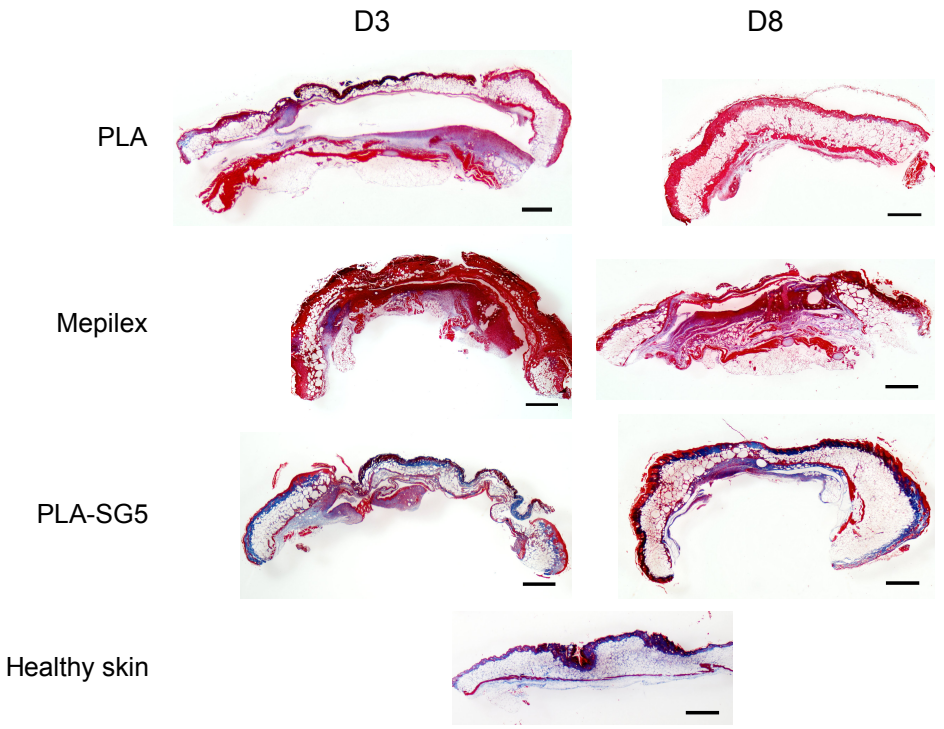

Figure 5.7: Masson's trichrome staining of sections Representative Masson's trichrome-stained sections of bisected wounds treated with PLA, Mepilex®, and PLA-SG5, after 3 and 8 days. Cell nuclei are stained in black, muscle and cytoplasma are in red, and collgen is stained blue. Scale bar = 1mm.

5.3.5 Vessel quantification

Neovascularization is a key process for the successful healing of wounds and, for this reason, vessel density was analyzed from sections immunolabelled against CD31, a marker for endothelial cells (Fig. 5.8A-D). Sections from wounds treated with PLA-SG5 for 3 days showed significantly higher vessel density than both treatment controls

and to healthy skin (Fig. 5.8F). On day 8 post-treatment, vessel density from the PLA-SG5 group regressed and reached similar values to the treatment controls (Fig. 5.8F). Wounds treated with PLA and PLA-SG5 mats presented lower vessel density than healthy skin at this final time point analyzed (Fig. 5.8F). Significant differences in vessel density were not detected between the PLA and Mepilex® treatments at any of the two time points analyzed.

5.3.6 Granulation tissue assessment

H&E and CD31 stained sections were also used to analyze granulation tissue formation at the wound bed. On the third day of treatment, PLA and PLA-SG5 treated wounds showed increased cellularity in the wound area compared to Mepilex® (Fig. 5.9A-C). As mentioned before, PLA-SG5 treated wounds also presented increased vessel density (Fig. 5.8F). The presence of this two features indicate that PLA-SG5 treated wounds have more granulation tissue at initial time points than the controls.

5.4 Discussion

Chronic wounds are a socioeconomic burden for first world countries and new therapies are needed in order to accelerate their healing. Biological based therapies have been developed over the last few years with promising results, but due to regulatory, economic and safety concerns their translation into the clinics has been very limited. Owing to the wound healing capability recently reported by bioceramics together with their lower cost of production and smaller safety risks, these materials arise like an interesting alternative to produce new translational off-the-shelf dressings. In this study, we tested the healing capability of electrospun PLA mats incorporating the calcium-phosphate ormoglass particles SG5 on a pressure

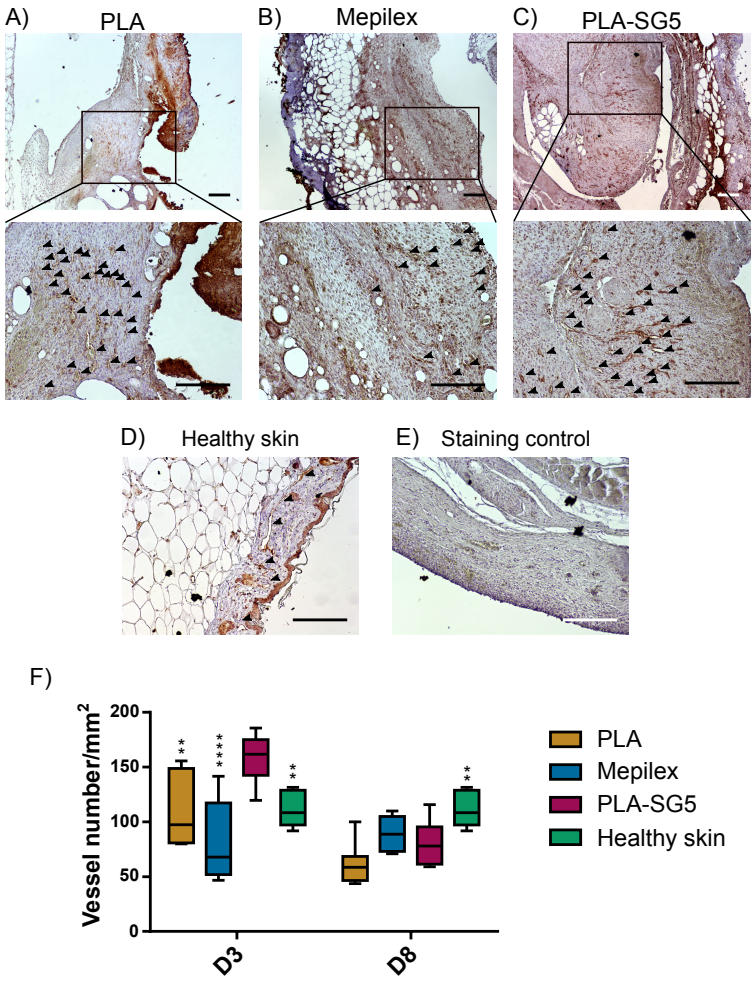

Figure 5.8: Imaging and quantification of blood vessels immunolabelled for CD31. A-C) Representative images of the immunostaining against CD31 of the sections of the wounds on day 3 of the PLA, Mepilex®, and PLA-SG5 condition. D) Representative image of non-wounded skin stained against CD31. E) Control section stained without primary antibody for CD31. F) Quantification of the number of vessels from the immunostained images. Data is represented in box-and-whisker plots in which the central line of each box is the median, the edges of the box are the first and third quartiles, and whiskers extend to 1.5 times the interquartile range or, if smaller, to the highest or lowest value measured. Three images from four different wounds per condition were analyzed. **p<0.01 (vs. PLA-SG5). ****p<0.0001 (vs. PLA-SG5).

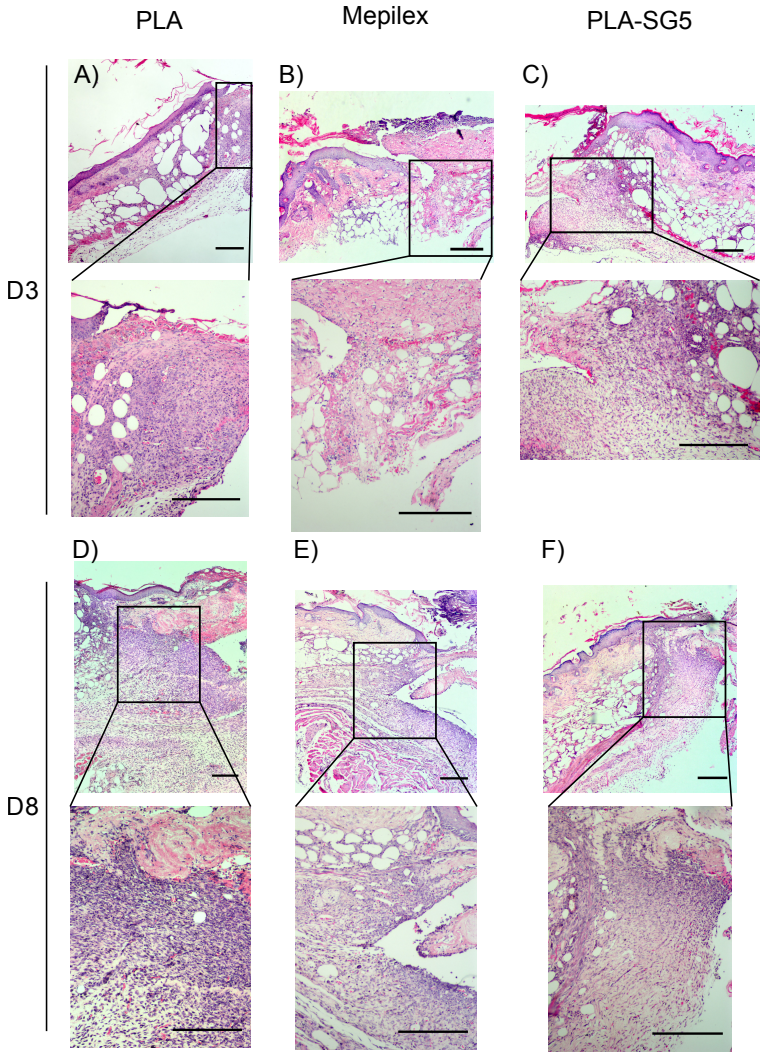

Figure 5.9: Analysis of granulation tissue from sections stained with H&E. Representative images of all conditions from wound sections stained H&E from day 3 (A-C) and 8 (D-F) post-treatment at two different magnifications showing the granulation tissue. Scale bar = 250 μm.

ulcer model in diabetic mice. The presence of the particles stimulated a faster wound area reduction, increased vascularization, and formation of granulation tissue. In addition, the wound generated presented increased

re-epithelialization and improved morphogenesis compared to a commercially available dressing frequently used in the clinics.

After generating the PLA-SG5 composite using electrospinning, its structure and biocompatibility was evaluated. The mats were composed by a dense network of aligned PLA fibers smaller than a micron, they were easy to manipulate, and they presented a gradual calcium release for up to 48 h, reaching values between 3 and 4 mM without significantly altering the pH of the media. Most of the released happened along the first 24 h. In addition, media conditioned by this material for 24 h did not alter metabolic activity of human dermal fibroblast over time when tested *in vitro*.

The choice of the animal wound healing model is of great relevance when testing a therapy because the healing response can vary significantly depending on the type of wound and the presence of complication factors - e.g. advanced age, obesity, diabetes, etc- (Lin et al., 2012). Studies that have evaluated the healing capability of bioceramics have generally used full-thickness wounds generated with scissors on healthy mice or rats (Sen et al., 2002; Jebahi et al., 2013; Zhao et al., 2015; Li et al., 2016), which does not model correctly the pathophysiology of chronic wounds. Only a few studies used diabetic animals (Lin et al., 2012; Mao et al., 2014), which present impaired wound healing capability, but, again, the type of wound generated was an acute full-thickness injury.

In our study, the *in vivo* model chosen to test the healing capability of the newly synthesized mats consisted of pressure ulcer wounds generated in mice. Moreover, the animals used presented common comorbidities associated with chronic wounds that complicate the healing process: advanced age, diabetes, and obesity. Both diabetes and advanced age are acknowledged pressure ulcers risk factors (Lyder and Ayello, 2008) and were also pointed out in our survey (Appendix A). In addition, obesity is

a comorbidity often present in diabetic patients that can further complicate the healing process (Anderson and Hamm, 2012). Mice were aged as much as possible considering that the life expectancy of the strain db/db is 10 months (The Jackson Laboratory, 2017). This strain presents a point mutation in the leptin receptor that induces severe hyperphagia, leading to obesity and manifestation of some Type-II diabetes mellitus characteristics (Wang et al., 2014). Although mice and human present different healing mechanisms (Dorsett-Martin and Wysocki, 2008), this model enabled us to test our developed dressing on a wound with a much more similar pathophysiology to human chronic wounds than previously reported models.

Low-exuding ulcerous wounds were generated after several ischemia-reperfusion cycles performed with external application of magnets. As previously reported, this process produced a full-thickness wound with necrotic damage down to the subcutaneous tissue and decreased blood flow to the injured area (Stadler et al., 2004). Before dressing application, wound debridement was performed, a procedure routinely carried out in the treatment of chronic wounds of human patients, as noted by our survey. PLA-SG5 mats were placed on one of the two wounds created on the back of each mouse, while a dressing control was applied on the other wound. Controls consisted of either particle-free PLA mats or a portion of Mepilex®, which is a frequently used dressing for the treatment low-exuding chronic wounds. While the PLA control enabled us to discern the specific healing contribution of the calcium-releasing particles, the Mepilex® control allowed to compare the efficacy of the novel treatment to a market product.

The wound size was monitored daily for a period of 8 days, and area quantification revealed a significant reduction in wounds treated with PLA-SG5 mats compared to both controls, from the first day of treatment to the end of the study. On the other hand, the epithelial gap measured in the

PLA-SG5 wound-treated sections only displayed differences against the Mepilex® control. This discrepancy between wound size and unepithelialized surface can be explained due to the error originated by the diagonal section performed on the wounds after excision. Once excised, wounds were cut in half and, since they are not perfectly rounded, the distance from side to side might be subjected to the spot were the cut was performed. Thus, the measurement of the length of the epithelium's gap might not be a complete trustworthy measurement.

Next, we hypothesized that the accelerated healing promoted by PLA-SG5 could be triggered by an increase in vascularization, since bioceramics have been reported to stimulate angiogenesis not only *in vitro* (Leu and Leach, 2008; Zeng et al., 2014) but also in wound healing studies *in vivo* (Lin et al., 2012; Xu et al., 2015b; Zhao et al., 2015; Zeng et al., 2015; Li et al., 2016). Indeed, as early as 3 days post-treatment, vessel density was significantly increased in the PLA-SG5 treated wounds compared to the controls, and also to healthy skin. In addition, these wound also presented increased cellularity at the wound bed. These two features seem to indicate the presence of more granulation tissue in PLA-SG5 treated wounds. On day 8, however, density levels for the PLA-SG5 condition decreased and were similar to the PLA and Mepilex® controls. At this time points, cell density in the injured site was also similar among conditions.

It is known that, in the progression of an acute wound, the density of blood vessels generated during the proliferative phase is higher than in uninjured skin, and, during the remodeling phase, the vascular network returns to levels close to healthy skin (Johnson and Wilgus, 2014). However, in chronic wounds, the formation of new blood vessels is limited by several factors, including diabetes and obesity. Despite the fact that these comorbidites were inherent in our *in vivo* model, the presence of SG5 was able to stimulate neovascularization, while the controls used were unable

to induce such an effect. To our knowledge, this is the first study showing stimulation of blood vessel formation by bioceramics in a pressure ulcer wound with impaired vascularization.

Based on the findings of the *in vivo* study presented here, and the conclusions that we reached with the on-line survey, our dressing seems a promising product to reach the market. The PLA-SG5 mat not only accelerated wound closure, which is the main factor prioritized by nurses when choosing a dressing, but also stimulated granulation tissue formation, one of the main uncovered wound aspects of current dressings.

Further analysis of the wounded skin is necessary to unravel whether SG5 stimulates fibroblast activities as reported in our *in vitro* study (Chapter 3). Since tissue biopsies were not kept after the experiment, future analysis should be performed on paraffin embedded tissue sections. Immunostaining against collagen I and III would allow to study differences in tissue quality generated during the healing process. Antibodies against matrix metalloproteases (MMPs) and their regulators, tissue inhibitor of metalloproteinases (TIMPs), could also be employed to detect differences in remodeling capability. Moreover, using specific markers for fibroblasts and myofibroblasts, such as the recently reported TE-7 (Goodpaster et al., 2008), might enable to detect changes in fibroblast density in the wound. Unfortunately, due to time constraints, these analysis could not be carried out during the course of this thesis project.

5.5 Conclusions

This study evaluated for the first time the healing capability of calcium-releasing bioceramic particles on a pressure ulcer model with impaired vascularization. The particles, which were embedded in a dressing composed of PLA nanofibers, accelerated wound closure and granulation tis-

sue formation, and produced a tissue structure similar to uninjured skin. In addition, they promoted increased vascularization at initial time points, which can be responsible for the improved healing. Further tissue characterization might provide us with more data to unravel other mechanisms that led to improved healing. The overall performance of the newly designed mat was remarkably better than a commercially available dressing frequently used for the treatment of low-exuding chronic wounds. Moreover, the effects stimulated by this dressing seem to be needed in clinical settings. As both PLA and calcium-phosphate materials are currently accepted for clinical application, these novel off-the-shelf dressing has great potential to reach the market within reasonable time.

6 *Vessel maturation promoted by a glass-ceramic/hydrogel composite with hMSC*

6.1 Introduction

This study was devoted to further explore the angiogenic properties of bioceramics, as reported in the previous chapter and by the literature (Section 2.6.2). More specifically, we designed and tested the vasculogenic properties of a new tissue-engineered composite that aimed to provide a sustained calcium-release overtime and to possess suitable mechanical and biodegradable properties to be implanted in soft tissue.

As explained, during the healing process, restoration of vasculature in the newly formed tissue must take place for its successful progression (Section 2.2.3). When blood supply to the tissue is restricted, it becomes ischemic and not only repair is impaired but also tissue degeneration is enhanced (Ouriel, 2001; Nunan et al., 2014). This process leads to the generation of chronic wounds, as described in Section 2.5.2, and also to other high incidence disorders such as peripheral artery disease (PAD) and myocardial infarction (Ouriel, 2001; Nunan et al., 2014).

In adults, blood vessel formation occurs through three different mechanisms: arteriogenesis, angiogenesis and vasculogenesis, described in Section 2.2.3. However, since these endogenous mechanisms are generally not enough to restore blood supply in ischemic tissues, different therapies are being investigated. These include administration of angiogenic proteins, delivery of cells, or use of non-biological biomaterials (Gorustovich et al., 2010; Chung and Shum-Tim, 2012).

Protein therapy through the administration of angiogenic growth factors, either individually or as a cocktail (Chung and Shum-Tim, 2012), has been one of the most explored strategies, including delivery of vascular endothelial growth factor (VEGF) and fibroblast growth factor (FGF) (Chung and Shum-Tim, 2012). Whereas this strategy has been successful in promoting new capillary formation, these vessels are often dysfunctional and regress upon loss of the vasculogenic stimulus (Benjamin et al., 1999). In addition, translation of vasculogenic proteins faces several challenges, including excessive costs of production, poor stability and short half-life of the protein, and difficulties in delivering safe and effective doses (Formiga et al., 2012). Protein administration in the diseased tissues through gene therapy has improved vascularization but safety and regulatory concerns remain in the treatment with genetic manipulations (Kalka and Baumgartner, 2008).

Cell therapy has emerged as a promising strategy to promote revascularization because cells can function as release systems of a complex mixture of signaling factors in a controlled and sustained manner (Compagna et al., 2015). Indeed, human mesenchymal stromal cells (hMSC) have attracted significant attention as they can promote neovascularization (Amin et al., 2010; Kuo et al., 2011). The angiogenic potential of hMSC arises mainly from the myriad of angiogenic proteins that they release, which can stimulate endothelial cells (ECs) (Kinnaird, 2004; Gruber

et al., 2005; Potapova et al., 2007; Duffy et al., 2009; Estrada et al., 2009; Boomsma and Geenen, 2012; Burlacu et al., 2013; Kwon et al., 2014). In addition, hMSC contribute to the maturation and stabilization of ECs of newly formed vessels by acting as mural cells (Au et al., 2008; Duffy et al., 2009). However, when administered either intravascularly (Horwitz et al., 2002; Hou et al., 2005) or directly into the tissue (Kang et al., 2006; Wu et al., 2007), MSC survival is very low.

To improve cell retention and function in the implanted site, biomaterials have been explored as delivery systems. Among them, hydrogels are particularly promising because they enable cell encapsulation and their mechanical properties can resemble native tissues (Rowley et al., 1999; Mann et al., 2001; Weber et al., 2007; Robinson et al., 2016). Hydrogels are cross-linked hydrophilic polymers of natural and/or synthetic sources. The main advantage of synthetic polymers, such as polyethylene glycol (PEG), over natural polymers is the greater control of the hydrogel's composition and properties (Zhu and Marchant, 2011). In addition, synthetic hydrogels can be functionalized to promote cell adhesion, migration and scaffold degradation (Zhu and Marchant, 2011).

Interestingly, recent studies have shown that the ionic release of bioglasses and glass-ceramic materials can trigger angiogenic effects both *in vivo* and *in vitro*, as explained in Section 2.6.2. Calcium is one of the ions reported to stimulate the formation of vessels (Aguirre et al., 2010; Castaño et al., 2014; Chen et al., 2015; Oliveira et al., 2016). Notably, extracellular calcium stimulates migration, tube formation, and activation of signaling pathways of endothelial progenitor cells (EPCs) (Aguirre et al., 2010). In addition, calcium-phosphate degradable ceramics that are silicon and titanium-free, such as β-tricalciumphosphate, promote angiogenesis by increasing proliferation and tube formation of human umbilical vein endothelial cells (HUVEC) (Chen et al., 2015). The dissolution product

of these materials consist of Ca^{2+} and P^{5+} ions and no evidence is found in the literature of the angiogenic properties of P^{5+}. Moreover, composite materials of calcium-releasing bioglasses and polymeric matrices such as poly(lactic acid) and poly(caprolactone) promote blood vessel formation *in vivo* (Castaño et al., 2014; Oliveira et al., 2016). Nevertheless, the combined vasculogenic effect of bioactive glasses/glass-ceramics with hMSC in a hydrogel system for soft tissue applications has not been examined.

In the present study, we analyzed the vasculogenic potential of a new composite biomaterial composed of a cell-adhesive biodegradable hydrogel containing bone marrow-derived hMSC and calcium-releasing glass-ceramic microparticles. In addition to assessing the vasculogenic potential of calcium-phosphate glass-ceramic particles, we studied whether the incorporation of the particles in the hydrogel alters the mechanical properties of the hydrogel, stimulates the release of vasculogenic factors by hMSC, and impacts cell survival and vascularization in an *in vivo* model.

6.2 Materials and Methods

6.2.1 Calcium-phosphate particles synthesis and characterization

Glass-ceramic particles with composition CaO:P2O5:Na2O:TiO2 in a 44.5:44.5:3:8 molar ratio (respectively), referred to as GC8, were prepared by controlled hydrolysis sol-gel method under an inert atmosphere. Chemicals utilized in the sol-gel fabrication process included phosphorous pentoxide (P2O5, 99.99+%, Sigma-Aldrich), metallic calcium (Ca^{2+}, 99%, Sigma-Aldrich), metallic sodium (Na^{+}, 99%, Panreac), titanium tetraisopropoxide (Ti(OCH(CH3)2)4, 97%, Alfa Aesar), absolute ethanol (EtOH, 99.99% Sigma-Aldrich), anhydrous

2-methoxyethanol (C3H8O2, 99.8%, Sigma-Aldrich), 2-propanol (99.7%, Sigma-Aldrich,), hydrochloric acid (HCl, 37%, Sigma-Aldrich) and MilliQ water.

Calcium and sodium 2-methoxyethoxides precursor solutions were prepared by refluxing metallic calcium and sodium respectively in anhydrous 2-methoxyethanol at 124 °C for 24 h. Phosphorus ethoxide precursor solution was prepared by refluxing phosphorous pentoxide in absolute ethanol at 78 °C for 24 h. Titanium alkoxides precursor solution was prepared by diluting titanium tetraisopropoxide in absolute ethanol.

The sol-gel gel process started with the addition of the calcium, sodium and titanium precursors in a balloon maintained under an inert and dry atmosphere in an ice bath. After 1 h of vigorous stirring to ensure solution homogeneity, the phosphorous solution was added at a controlled rate of 2.5 mL/h with an infusion pump. Acid catalyst with a molar ratio of 1:60:0.3:15 (Ti:H2O:HCl:2-propanol) was then added at a controlled flux of 1.0 mL/h. This mixture was transferred into a sealed vial and aged for 18 h at room temperature (RT) and 72 h at 80 °C. Vials were then opened, and samples were dried via heating from 80 °C to 120 °C through a slow ramp (2 h) and treated at 120 °C for 24 h in a Nabertherm® oven (LV 9/11/P330). The dry sample was heated to 540 °C by a slow ramp (3 °C/min) followed by treatment at said temperature for 5 h. Finally, the resulting powder was mashed in a planetary ball miller (PM 100, Retsch®) and manually filtered through a 40 μm porous filter to ensure the micro/nano-metric scale of the final material.

Scanning electron microscope (SEM) images were obtained from uncoated GC8 particles mounted on a silicon wafer (Nova Nano SEM-230; FEI Co.) at 20 kV, and material composition analysis was carried out on samples coated with an ultra-thin layer of carbon on a FESEM (J-7100F, Jeol) containing the Inca 250 energy dispersive spectroscopy (EDS) micro-

analysis system (Oxford Instruments) at 5 kV. Zeta potential (ζ) measurements were carried out on a Zetasizer Nano ZS (Malvern Instruments) and size measurement was performed in a LS Particle Size Analyzer through laser diffraction (LS 13 320, Beckman Coulter). For these analyses, the micrometric powder sample was dispersed in absolute ethanol to avoid particle dissolution and was sonicated in an ultrasonic bath (142-6044, VWR Collection) to avoid the presence of agglomerates.

6.2.2 Preparation of the PEG-MAL hydrogel / calcium-phosphate particle composite

Hydrogels were cast as previously described (Phelps et al., 2012, 2013). Briefly, polyethylene glycol-maleimide (PEG-MAL) four-arm macromers (20 kDa MW, Laysan Bio) were prefunctionalized with the peptide GRGDSPC containing the cell adhesive site RGD (Aaptec) for 15 min at 37 °C. At this point, cells and/or particles were added and mixed to disperse homogeneously. The mixture was crosslinked with the addition of the protease degradable peptide GCRDVPMMRGGDRCG (VPM) (Aaptec) at 1:2 molar ratio of VPM peptide to available MAL groups. The final concentration of PEG-MAL and RGD peptide was 5% (w/v) and 1.0 mM, respectively. Hydrogels were cast on plastic paraffin film (Parafilm M®, Bemis NA) under sterile conditions, with previously sterilized reagents, and were incubated for 15 min at 37 °C to ensure complete crosslinking before transferring them into media. Sterile-filtered Phosphate-Buffered Saline (PBS) supplemented with 20 mM HEPES with pH adjusted to 7.4 was used as buffering solution to dissolve the reagents.

6.2.3 Calcium release

Precast 30 μL hydrogels containing 1% (w/v) particles and 0.5 mg of particles without hydrogel were introduced in microtubes and incubated in 500 μL of either complete culture media (CCM) or MilliQ water with 10 mM HEPES (pH 7.4). The lid of the microtubes containing CCM was perforated with a needle to allow gas exchange and all samples were incubated at 37 °C in a humidified atmosphere containing 5% (v/v) CO_2. At different time points for a period of 13 days, 100 μL of media was replaced to measure pH and calcium concentration. pH was measured with a Laquatwin pHmeter (B-712, Horiba) while calcium released in the media was assessed using the quantitative colorimetric method 0-cresolphtalein complexone (Sigma-Aldrich) (Cohen and Sideman, 1979). Absorbance readings were determined at 570 nm on the Infinite M200pro microplate reader (Tecan). Cumulative release was quantified taking into account the calcium moles removed at each time point and values were normalized to the total weight of particles per sample.

6.2.4 Mass swelling ratio

Hydrogels were formed as previously described and were allowed to completely swell in di-H2O for 24 h at 37 °C. Gels were removed from solution and excess water was eliminated from the surface of hydrogels with filter paper prior to weighing. Then, swollen hydrogels were snap-frozen in liquid N_2 and lyophilized followed by dry mass measurement. Five replicates of 30 μL were used per condition. The mass swelling ratio is reported as the ratio of swollen mass to dry mass.

6.2.5 Rheological properties

Storage (G´) and loss (G") moduli of hydrogels were assessed by dynamic oscillatory strain and frequency sweeps on a Discovery HR-2 rheometer (TA Instruments) with a 8 mm diameter, flat geometry (Plate SST 8mm Smart-Swap, TA Instruments). Since hydrogel surfaces were required to be flat for the measurement, 25 μL hydrogels were casted in 4 mm diameter molds of polydimethylsiloxane (PDMS). Once crosslinked, hydrogels were allowed to swell in PBS for 24 h. For the measurement, hydrogels were loaded between the flat platen and the Peltier plate and the measuring system was lowered until the axial force detected was 0.02 N. To determine the viscoelastic range of the hydrogel, strain amplitude sweeps were performed at an angular frequency (ω) of 10 rad s-1. After determining that 1% was a suitable strain, oscillatory frequency sweeps were used to quantify the storage and loss moduli (ω= 0.25-10 rad s-1). Collagen hydrogels of 3.5 mg/mL (OptiCol™ Rat Type I Acid Soluble Collagen, Cell Guidance Systems) were used as an inter-experimental control. Five replicates were used per condition.

6.2.6 Cell culture and encapsulation

Human bone marrow-derived MSC provided by the Texas A&M Health Science Center College of Medicine Institute for Regenerative Medicine at Scott & White (NIH Grant P40RR017447) were used without further characterization. Following the provider's protocol, cells were expanded at low seeding densities (150 cells/cm^2) in CCM composed of Minimum Essential Medium Alpha (α-MEM) (Invitrogen) supplemented with 2 mM L-Glut(Invitrogen), 100 U/mL penicillin/streptomycin (P/S) (Invitrogen), and 16% Hyclone fetal bovine serum (FBS) (GE Healthcare). Cells were maintained at 37 °C in an atmosphere of 5% CO_2 and were used up to pas-

sage 5. During expansion, media was refreshed every 3 days. After 5 or 6 days of expansion, hMSC were detached with TrypLE™ Express (Thermo Fisher Scientific), centrifuged at 300 g for 5 min and they were encapsulated as previously described at a concentration of 3.5 x 10^6 cells/mL of gel, in 20 µL hydrogels. Free-floating cell-containing hydrogels were cultured in 1 mL CCM in 24 well plates and media was replaced every 3 days.

HUVEC were kindly provided by Dr. Joëlle Amédée's laboratory from the University of Bordeaux. These cells were expanded at 2.5 x 10^3 viable cells/cm^2 on fibronectin (Sigma-Aldrich) coated flasks in M199 media (Sigma-Aldrich) containing 10% FBS, 2 mM L-Glut, 100 U/mL P/S, 1% sodium pyruvate (Invitrogen), 20 ng/mL VEGF (Peprotech), 20 ng/mL R3-IGF 1 (Sigma-Aldrich), 5 ng/mL epidermal growth factor (Sigma-Aldrich), 5 ng/mL bfibroblast growth factor (Peprotech), 0.1 ng/mL ascorbic acid (Sigma-Aldrich) and 22 µg/mL heparin (Sigma-Aldrich). Media was changed every two days and they were used up to passage 5. At 80% confluence, they were carefully tripsinized with TrypLE™ Express (Thermo Fisher Scientific), centrifuged at 200 g for 7 min and used in the experiment.

6.2.7 *In vitro* cell survival within hydrogels

A Calcein assay was used to stain live hMSC and observe them within hydrogels after 24 h and 72 h of cell encapsulation. To avoid particle autofluorescence in the green and red fluorescent channels Calcein Deep Red acetate-TM (ATT Biorequest) was used following the manufacturer's instructions. Briefly, after being washed with Dulbecco's phosphate-buffered saline (DPBS) (Invitrogen), cell-containing hydrogels were incubated for 1 h at 37 °C in 5% (v/v) CO_2 with 1 mL of non-supplemented α-MEM containing 7.5 µM calcein reagent and 2.5 mM probenecid (Sigma-Aldrich).

After 30 min of incubation, two drops of a solution of Hoechst 33342 (NucBlue® Live ReadyProbes® Reagent, Life Technologies) were added to stain the nuclei of all cells. Following incubation, hydrogels were washed with DPBS and cells were observed in media containing serum-free α-MEM and 2.5 mM probenecid. Three replicates were used per condition and a z-stack of 400 μm was acquired with a Leica TCS SP5 confocal laser scanning microscope (Leica Micro-systems) at three random spots per replicate. Images were processed with the ImageJ 1.51h software to obtain z-stack projections of the outer 200 μm thick section and a more inner section of 200 μm thick.

6.2.8 Cell number within hydrogels

Cell number was assessed at 1, 3 and 7 days of cell encapsulation through the detection of lactate dehydrogenase (LDH) activity of the cell lysate contained in the hydrogels. Briefly, hydrogels were washed with DPBS Ca^{2+} Mg^{2+} (Invitrogen) and incubated at 37 °C for 1 h in Eppendorf microtubes containing 50 μL of 3 mg/mL of collagenase type II (Invitrogen) for complete gel degradation. Thereafter, cells were lysed by adding 400 μL Mammalian Protein Extraction Reagent (M-PER) (Thermo Fisher) followed by incubation for 30 min in ice. Samples were sonicated with an ultrasonic processor (UP50H, Hielscher) in cold to ensure complete cell lysis and centrifuged at 10,000 rpm for 10 min at 4 °C. Supernatant was used with the LDH quantification kit (Roche) following the manufacturer's instructions and cell concentration was calculated through a calibration curve made with cell lysates of known cell concentration. Absorbance was read at 490 nm with an Infinite M200 PRO multimode plate reader instrument (Tecan). The experiment was carried out three times using triplicates per condition.

6.2.9 Chick chorioallantoic membrane model

An *ex ovo* chorioallantoic membrane (CAM) assay was performed as previously described (Deryugina and Quigley, 2008; Buschmann et al., 2012). Briefly, fertilized chicken eggs (Granjas Gibert SA) were incubated for 3 days in a humidified incubator at 37 °C. The entire egg content was then carefully transferred into a Petri dish (430167, Corning) and incubated for another 6 days. On embryonic day E9, sterile methylcellulose disks containing or without GC8 particles were carefully placed on the CAM. For each experimental condition, six specimens were used and 4 disks were placed on each membrane. The disks were prepared previously to the implantation day by drying 50 μL drops of a solution containing 1.5% (w/v) (hydroxypropyl)methyl cellulose (Sigma-Aldrich) in MilliQ water with or without homogeneously distributed GC8 particles on a Teflon surface (Yang and Moses, 1990). After 3 more days of incubation (E12), embryos were humanely sacrificed by decapitation and CAM was immediately fixed with a neutral buffered 10% formalin solution (Sigma-Aldrich) for 30 min. Finally, the membranes containing the disks were excised and images were acquired with an Olympus MVX10 Macroscope. Angiogenesis stimulation was quantitatively measured by counting the vessels converging towards the disks using ImageJ. A minimum of 10 samples were analyzed per condition.

6.2.10 Expression of vasculogenic proteins *in vitro*

CCM conditioned for 3 days by cells encapsulated in the hydrogels was used to detect release of angiogenic proteins using a commercial array for proteins (C-Series Human Angiogenesis Antibody Array C1, Tebu-bio) following manufacturer's instructions. For this assay, low serum (5%) media was used to avoid background interference of FBS proteins.

Several commercial Enzyme-Linked ImmunoSorbent Assay (ELISA) kits (R&D systems) were used to quantify VEGF, interleukin 6 (IL-6), interferon-gamma (IFN-γ), transforming growth factor-beta (TGF-β)1 and insulin-like growth factor 1 (IGF-1) in normal serum media, following manufacturer's instructions.

In both the array and ELISA assays, conditioned media was centrifuged at 10,000 rpm at 4 °C for 10 min and the supernatant was stored at -80 °C until needed. For all experiments, a blank sample was included to subtract the protein background present in non-conditioned media.

For the array, membranes provided in the array were incubated with the hMSC conditioned media pooled from 4 replicates and were developed with the Clarity™ Western ECL Substrate (Bio-Rad). The chemiluminescent signal was read with a densitograph (LAS4000 Imaging System) and the intensities of the digitalized bands were measured with ImageJ software.

ELISA absorbance was determined at 455 nm with a multimode microplate reader (Infinite M200 PRO, Tecan) setting wavelength correction to 540 nm. The results were normalized to the cell number concentration in the hydrogel quantified with the LDH detection kit as previously described. Six replicates were used per condition.

6.2.11 Matrigel tube formation assay

To investigate the tubule formation activity of HUVECs under conditioned media, the formation of capillary-like structures on a growth-factor reduced Matrigel™ matrix (Corning) was assessed. Experimental media used in this assay contained 1:1 M199/α-MEM without added growth factors and with 5% or 16% of Hyclone FBS. For the pre-starved condition, HUVEC were incubated for 3 h in the factor-free experimental media containing 5% FBS prior being seeded on Matrigel™. Positive control media

was obtained by adding 20 ng/mL VEGF in the experimental media. Matrigel was thawed at 4 °C overnight, transfered into 48-well plate (120 µL/well) with a cold tip and allowed to polymerize at 37 °C for 30 min. During Marigel™ incubation, HUVEC were tripsinized, resuspended in 5% FBS experimental media, counted and a suspension of 3 x 10^6 cells/mL was prepared. Following Matrigel™ polymerization, 280 µL/well of pre-warmed experimental media was added, as well as 20 µL/well of the cell suspension, to achieve a final cell concentration of 60,000 cells/well. After gently shaking the plate to uniformly distribute cells within the wells, plates were introduced in the CO_2 incubator and imaged after 4 h and 8 h with the inverted phase-contrast microscope Nikon TE200 using a DP72 Olympus camera. From the triplicates used for each condition, three pictures at random sites were taken. Finally, image analysis was performed with the "Angiogenesis Analyzer" plugin developed by Gilles Carpentier for the open-source software Image J.

6.2.12 Immunostaining of *in vitro* cultured hMSC in hydrogels

hMSC incubated in the hydrogels for 7 days were immunostained against CD31. Briefly, cells were encapsulated as explained before and cultured in CCM for 7 days, changing media every 3 days. Then, hydrogels were washed with PBS and cells were fixed with 4% paraformaldehyde solution (EM grade, Electron Microscopy Sciences) for 20 min and permeabilized in 0.1% Triton® X-100 (Sigma-Aldrich) for 20 min. Afterwards, cells were washed again with PBS, blocked with 3% bovine serum albumin (BSA) (Sigma-Aldrich) in PBS for 1 h and incubated overnight at 4 °C with anti-CD31 antibody (1:20 dilution, ab28364, Abcam). The secondary antibody anti-rabbit CF 647 (1:800 dilution, SAB4600184, Sigma-Aldrich) was incubated for 1 h at RT, followed by 1 h incubation of green phalloidin to

stain F-actin (1:200 dilution, Cytoskeleton) and 15 min of 4',6-diamidino-2-phenylindole, dilactate (DAPI) (1:200, Molecular Probes) to stain nuclei.

For the control of cells seeded in 2D, hMSC were seeded on sterile 15 mm coverslips in 24-well plates in CCM. The staining procedure was the same as for cells in hydrogels, except for the incubation times, which were increased in the conditions with hydrogel to allow a proper diffusion of the compounds within the hydrogels. Samples with cells seeded on coverslips were fixed for 10 min and permeabilized for 5 min. Green phalloidin and DAPI were incubated for 30 min and 5 min, respectively. Finally, coverslips were mounted on mowiol 40-88 (Sigma-Aldrich) and allowed to dry protected from light.

Stained samples were imaged under a SP5 spectral confocal microscope (Leica) using the 405 nm diode laser, Argon lasers, and the 633 nm HeNe laser. For the hydrogel samples, images were acquired in z-stack at random spots. More specifically, a stack of 15 images separated by 3 μm was acquired per site and projected with Image J.

6.2.13 hMSC transduction with luciferase lentivirus

hMSC were cultured up to 60-70% confluence and they were transduced with lentivirus encoding for luciferase/tdtomato (pLenti-UbC-RFLuc-tdtomato, Targeting Systems, MOI 5-20) in complete media containing 100 μg/mL protamine sulfate [45]. 24 hours after initial infection, media was replaced with fresh complete media. Six days after initial infection, transduction efficiency was measured by tdtomato expression by flow cytometry.

6.2.14 Implantation into mice and cell tracking

All animal experiments were performed with the approval of the Georgia Tech Animal Care and Use Committee (IACUC) under the supervision of a research veterinarian and within the guidelines of the Guide for the Care and Use of Laboratory Animals. Precast hydrogels containing luciferase-expressing hMSC were implanted in the epididymal fat pad (EFP) of 8-12 week old immunocompromised B6.129S7-Rag1tm1Mom/J male mice (Jackson Laboratory). Three conditions were examined: hydrogels without particles, hydrogels with 0.5% (w/v) GC8 particles and a positive control hydrogel containing 10 μg/mL VEGF. Six animals were used per condition. Animals were anesthetized in a chamber with 5% isoflurane and maintained at 2% isoflurane during surgery. A midline incision in the abdominal wall was performed, and each EFP was exposed on sterile gauze pre-wet with sterile saline for hydrogel implantation. One hydrogel (30 μL) was implanted in each EFP by wrapping the EFP tissue around it. To ensure hydrogel retention in site, a small suture of non-degradable thread (Ethicon) was applied to the proximal site of the tissue. The interior abdominal layer was closed with degradable suture while the exterior layer was sealed with wound clips. During surgical preparation, one dose of sustained-release buprenorphine (1 mg/kg) was administered intraperitoneally (IP) during surgical preparation to provide 72 continuous hours of pain relief.

At selected time points following implantation (0, 2, 4, 7, 13 days), anesthetized mice were IP injected with 150 mg/kg body weight of beetle luciferin (Promega) diluted in PBS and bioluminescence was acquired 15 min post-injection on an IVIS SpectrumCT imaging system. The signal detected was quantified by gating a region of interest (ROI) around the periphery of the implant and subtracting the average background counts in the surrounding tissue from the average total counts in the implant, as

background intensity varied between animals. The final averaged count was normalized by the signal on day 0 of each animal.

6.2.15 Vessel labeling and quantification

Prior to euthanasia, animals were injected intravenously with Dylight 488-labeled tomato lectin (Vector Laboratories) to label functional vasculature (Phelps et al., 2013). After lectin was allowed to circulate for 15 min, animals were humanely euthanized with carbon dioxide and were perfused intracardially with 10 mL of saline through a 23-gauge cannula inserted into the left atrium. Blood and saline exited through the cut vena cava. EFPs were removed and fixed in 10% buffered formalin for 24 h at RT. Z-stack images were acquired of the fluorescent vasculature with a Nikon C2-Confocal Module connected to a Nikon Eclipse Ti inverted microscope with a 488 nm laser (Melles-Griot) and 525/50 filter. Images were processed with ImageJ for vasculature quantification. From each image, three different sites were analyzed and at least six fat pads of each condition were used for the quantification.

6.2.16 Immunostaining of histological sections

For immunostaining analyses, fixed EFPs were dehydrated, embedded in paraffin and cut into 8-µm thick sections. These sections were deparaffinized in xylene and ethanol, subjected to antigen retrieval by heating the samples at 95 °C for 20 min in sodium citrate buffer (10 mM sodium citrate, 0.05% Tween 20, pH 6.0) and permeabilized with 0.1% Triton X-100 (Sigma-Aldrich) in Tris-buffered saline (TBS) for 30 min. After blocking the tissue samples with 1% BSA and 0.025% Triton X-100 for 2 h, sections were stained with primary antibodies against alpha-smooth muscle actin (α-SMA) (dilution 1:500), A5228,Sigma-Aldrich) at 4 °C overnight.

Sections were then incubated with biotinylated secondary antibody goat anti-mouse (dilution 1:500, ab64255, Abcam) for 1 h at RT. Following a 10 min incubation of streptavidin-peroxidase (Abcam), samples were exposed to DAB solution (Abcam) for 3 min and rinsed thoroughly with water. Specimens were counterstained with a 1/10 hematoxylin dilution for 1 min and mounted for imaging with a Nikon Eclipse E600 microscope (Nikon Instruments Inc.). The tissue area surrounding the hydrogel was used to quantify positively stained vessels, lumen area and thickness of vessels. Sections of five different fat pads of each condition were analyzed.

6.2.17 Statistics

Data are expressed as mean ± standard deviation (SD). Statistical analyses were performed using one-way ANOVA with Tukey's test for post hoc comparisons using GraphPad Prism software. A p-value of 0.05 was considered significant.

6.3 Results

6.3.1 GC8 particle characterization

GC8 particles were synthesized and characterized. SEM images showed high polydispersion of particle size (Fig. 6.1A) confirmed by size quantification through laser diffraction (Fig. 6.1C). Although average particle size was ∼9 μm (Fig. 6.1C), SEM images showed that micrometric GC8 particles were structured in subunits of approximately 200 nm (Fig. 6.1B). Nanoparticle sintering might have occurred during the thermal treatment applied in the synthesis process. Atomic composition analysis by EDS showed that the GC8 particles had equivalent composition as the theorical value (Fig. 6.1D), an indication that the particle composition is properly

controlled in the synthesis. Finally, Z-potential analysis indicated a value of -15.75 mV (Fig. 6.1D). This low value might indicate the tendency of the particles to agglomerate.

Since extracellular calcium can stimulate biological responses on cells, calcium released from the particles was measured in two different solutions (Fig. 6.1B). Calcium release was sustained for 13 days in both media, although release in CCM was significantly lower than in buffered MilliQ water. In addition, pH was measured from the samples and no changes were detected compared to the media without particles (data not shown). Thus, GC8 degradation does not contribute to changes in pH in the media.

6.3.2 Calcium release and mechanical properties of hydrogels with GC8

GC8 particles were embedded within PEG-MAL hydrogels as explained in Fig. 6.2A. The PEG-MAL hydrogel has been used in previous studies (Phelps et al., 2012; Salimath et al., 2012; Phelps et al., 2013) and contains the cell adhesive peptide RGD and the protease-degradable VPM crossliker, which serves as substrate of many proteases including matrix matrix metalloprotease (MMP)2 and MMP9. Gel crosslinking occurred in less than 10 min, allowing for uniform particle distribution within the hydrogel.

Calcium release from GC8 encapusalted in PEG-MAL hydrogels was quantified as before, and release was again higher in MilliQ water compared to CCM (Fig. 6.2B). In addition, calcium release was also higher for GC8 particles embedded in the hydrogels compared to free particles (Fig. 6.2B).

We next measured the equilibrium mass swelling ratio and viscoelastic properties of hydrogels without particles or with 0.5% or 1% (w/v) GC8 content. Fig. 6.2C shows that the equilibrium mass swelling ratio is sig-

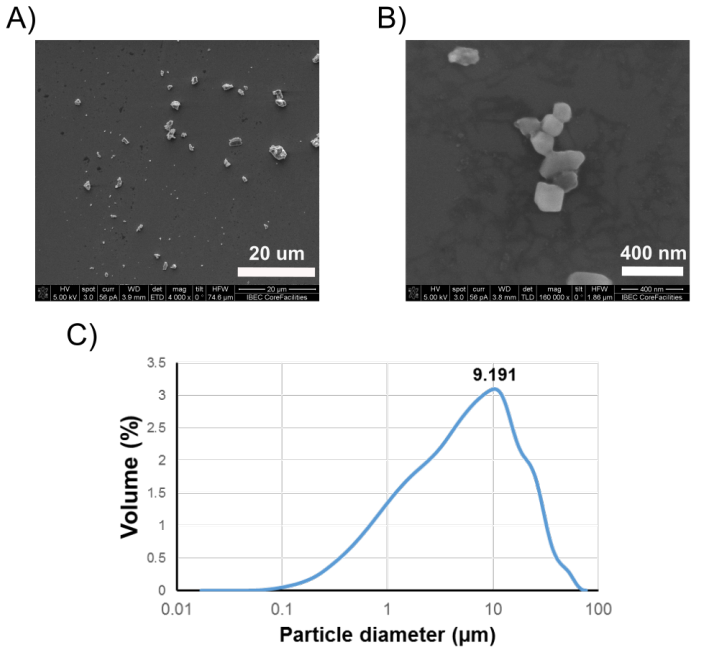

D)

Composition (mol %)				Z-potential (mV)
P_2O_5	CaO	TiO_2	Na_2O	
44.1 ± 2.42	45.3 ± 2.85	7.3 ± 1.77	3.3 ± 1.65	-15.75 ± 0.15

Figure 6.1: GC8 particles characterization. A) GC8 imaged with SEM, B) magnified image of GC8, in which nanoparticle sintering can be observed. C) Distribution of particle size measured with laser diffraction. D) Table showing atomic composition of GC8 measured with EDS and z-potential value.

nificantly higher in empty hydrogels than in hydrogels with particles, indicating that the particles decrease the hydrogel capacity to absorb water. The viscoelastic properties of the hydrogel were modified in the presence of 1% (w/v) GC8 particles but there were no differences between the 0.5% GC8 formulation and the control (Fig. 6.2D). The storage modulus for the 1% GC8 formulation was approximately 50% lower than that for empty gels.

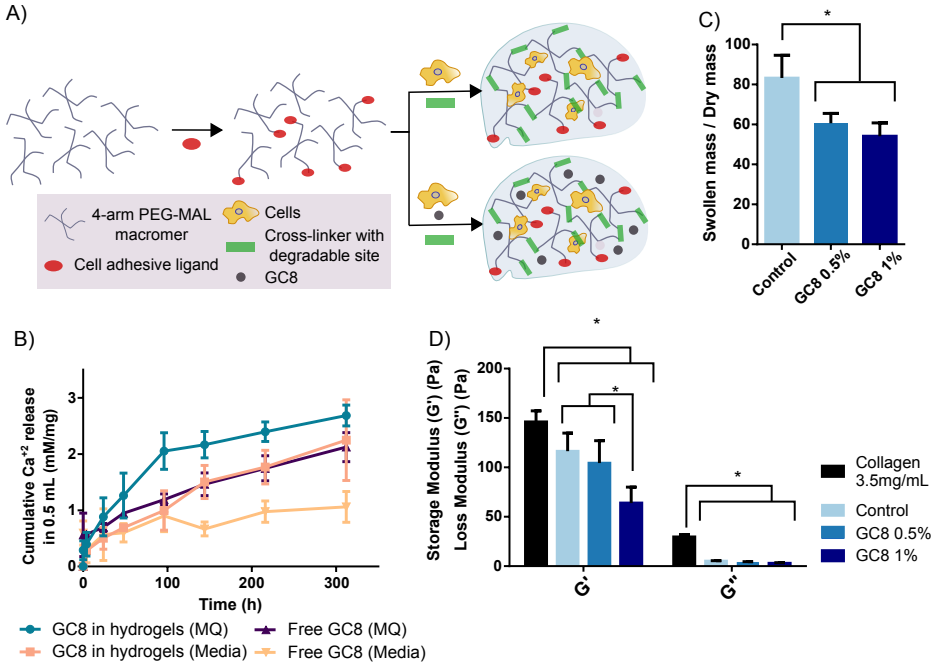

Figure 6.2: Synthesis and characetrization PEG-MAL hydrogels containing GC8 particles. A) 4-arm PEG-MAL macromer is functionalized with the cell adhesive peptide RGD. Cells and GC8 particles are added and the hydrogel is crosslinked via reaction with VPM peptide. B) Cumulative calcium release in two different solutions (buffered MilliQ water or CCM) for free GC8 or GC8 particles encapsulated in hydrogels. C) Effect of GC8 particle concentration (w/v) on the equilibrium swelling ratio. D) Storage (G') or loss (G") moduli for PEG-MAL hydrogels with or without different GC8 concentrations. A crosslinked type I collagen hydrogel is shown for reference.*p<0.05.

6.3.3 hMSC survival and growth within PEG-MAL hydrogels *in vitro*

hMSC survival and morphology within the hydrogels was studied by calcein staining of live cells on day 1 and 3 post-encapsulation (Fig. 6.3A). A far red calcein molecule was used to avoid GC8 autofluorescence in the red and green channel. Cell nuclei were stained in blue with Hoechst® 33342.

Cell behavior was similar for all the conditions tested, with hMSC forming networks and showing high viability and spreading in the outer zones ($\sim$ 200 μm), but lower survival and spreading in the interior of the gel. On day 1, hMSC showed a spread morphology and on day 3 most of the cells were organized in a complex network structure. In general, calcein signal was much lower in the interior. However, nuclei distribution changed from a homogeneous dispersion on day 1 to a more clustered organization on day 3, which implies that cell reorganization is also taking place in the interior of the hydrogel.

Cell number within the hydrogels was determined on day 1, 3 and 7 (Fig. 6.3B). The initial cell number seeded per hydrogel was 80,000 cells, and 24 h after encapsulation cell survival was 80-100% for all conditions tested. Cell number remained constant throughout the 7 days in culture, except for the 1% GC8 formulation for which cell number decreased significantly by day 7.

6.3.4 Proangiogenic effect of GC8 particles on CAM model

The proangiogenic effect of GC8 particles was tested on the CAM model. This extra-embryonic vascularized membrane that facilitates gas exchange during chick embryogenesis is a widely used system to test the pro- and antiangiogenic properties of substances and materials (Baiguera et al., 2012), including bioglasses (Handel et al., 2013; Haro Durand et al., 2015). The experiment was performed *ex ovo* to avoid possible interferences of calcium from the egg shell and to test more replicates per embryo. Methylcellulose disks were used as support materials for the particles in the assay as previously reported (Yang and Moses, 1990; Ribatti et al., 1995; Struman et al., 1999; Hagedorn et al., 2004; Das et al., 2012). Disks were placed on the CAM on E9 (Fig. 6.4A) and fixed, excised and imaged on

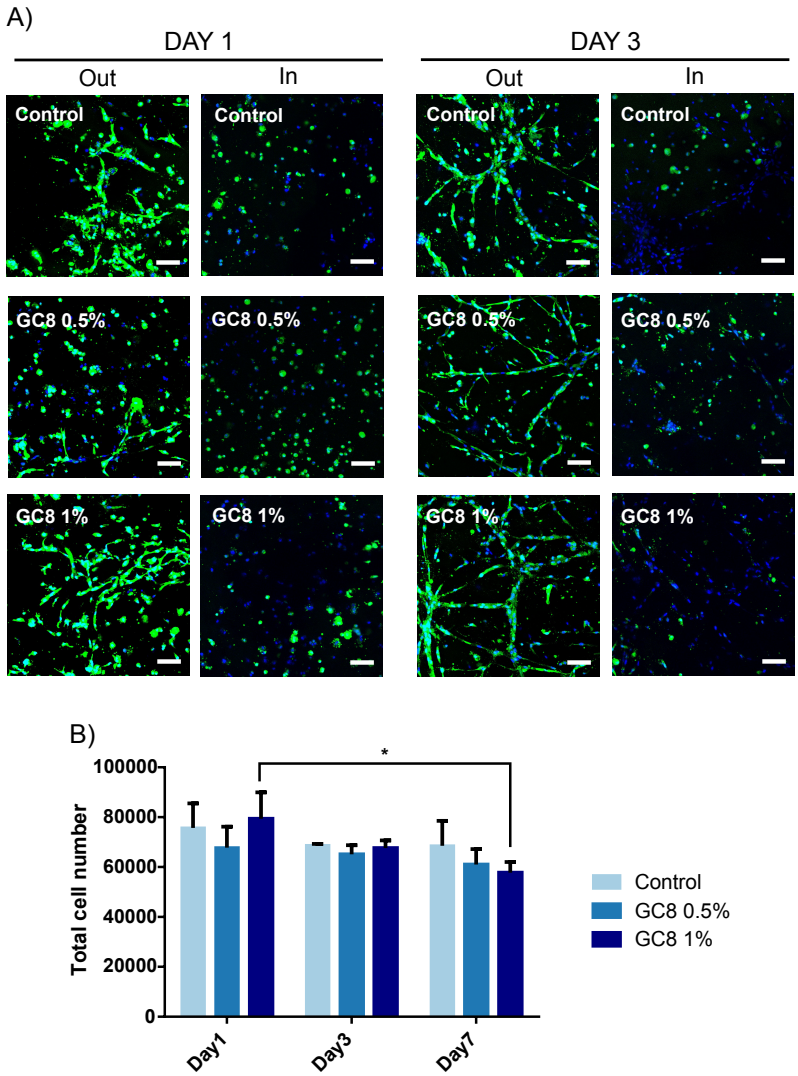

Figure 6.3: ***In vitro*** **hMSC viability and spreading within hydrogels.** A) Fluorescent image stacks of 200 μm of the outer and inner part of the hydrogels showing staining of the cytoplasm of live cells with calcein (green) and cell nuclei with Hoechst (blue) on day 1 and 3 after cell encapsulation. Scale bar: 100 μm. B) Quantification of cell number within the hydrogels on day 1, 3 and 7 post-encapsulation. Data represent the mean of three experiments with the S.D. *p<0.05.

E12 (Fig. 6.4B). Analysis of angiogenic stimulation found increased vascularization in the conditions with GC8 (Fig. 6.4C). No differences were detected between 0.5% and 1% GC8 content. This result suggests that the GC8 particles can stimulate angiogenesis in an *in vivo* context.

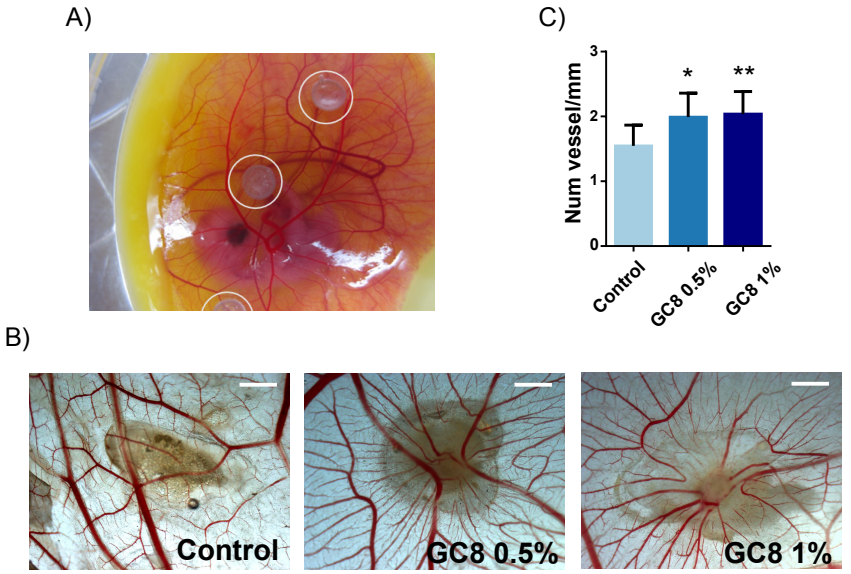

Figure 6.4: Angiogenic effects of the GC8 particles on the CAM of chick embryos. A) Methyl cellulose disks containing GC8 particles were applied on the CAM on E9. B) Representatives images of the disks on the CAM after fixation and excision on E12. Scale bar 2 mm. C) Quantification of the number of vessels converging towards the material normalized by the perimeter of the area selected performed through image processing. A minimum of 10 samples were used per condition and data is expressed as mean ± S.D. *p<0.05 (vs. control). **p<0.01 (vs. control).

6.3.5 Release of angiogenic factors by hMSC encapsulated in GC8-containing hydrogels

We examined whether the presence of GC8 particles within the hydrogels stimulates encapsulated hMSC to release angiogenic factors. Because we

did not see any effects in the CAM assay between 0.5% and 1% GC8 particles and there are no differences in viscoelastic properties between 0.5% GC8 and empty gels, we compared 0.5% GC8-containing gels to empty hydrogels. A protein array was performed to screen for differences in expressed proteins (Fig. 6.5A) from which we selected VEGF, IL-6, IFN-γ, TGF-β1 and IGF-1 to be quantitatively evaluated by ELISA. As shown in Fig. 6.5B, hMSC released VEGF, IL-6, TGF-β1 and IGF-1, but IFN-γ was not detected in any of the conditions. Furthermore, a significant increase in IGF-1 secretion was detected in the hydrogels containing GC8 particles compared to empty hydrogels.

6.3.6 Optimization of the tube formation assay

To asses the angiogenic capacity of media conditioned by hMSC encapsulated in the hydrogels, the tube formation assay was considered. Before testing this media, the assay was performed with different conditions to find the optimal experimental conditions. Media used contained either 5% or 16% FBS without additional growth factors, except for the positive control conditions, in which 20 ng/mL VEGF was added (Bussolati et al., 2001; Hwang et al., 2016). In some groups, HUVEC were pre-starved by incubating them for 3 h in 5% FBS experimental media to adapt them to low-factor media and make them more responsive to media with angiogenic factors. Starving HUVEC overnight or for longer periods highly decreased cell viability (data not shown). By using these conditions, we wanted to ensure that significant differences would be obtained between media without and with additional angiogenic factor added.

Images were acquired at 4 (Fig. 6.6A-D) and 8 h (Fig. 6.6E-H), and different parameters were quantified, including number of junctions, number of loops, number of branches, total length of network, and loop mean size. As Fig. 6.6I shows, there were not statistical differences for the dif-

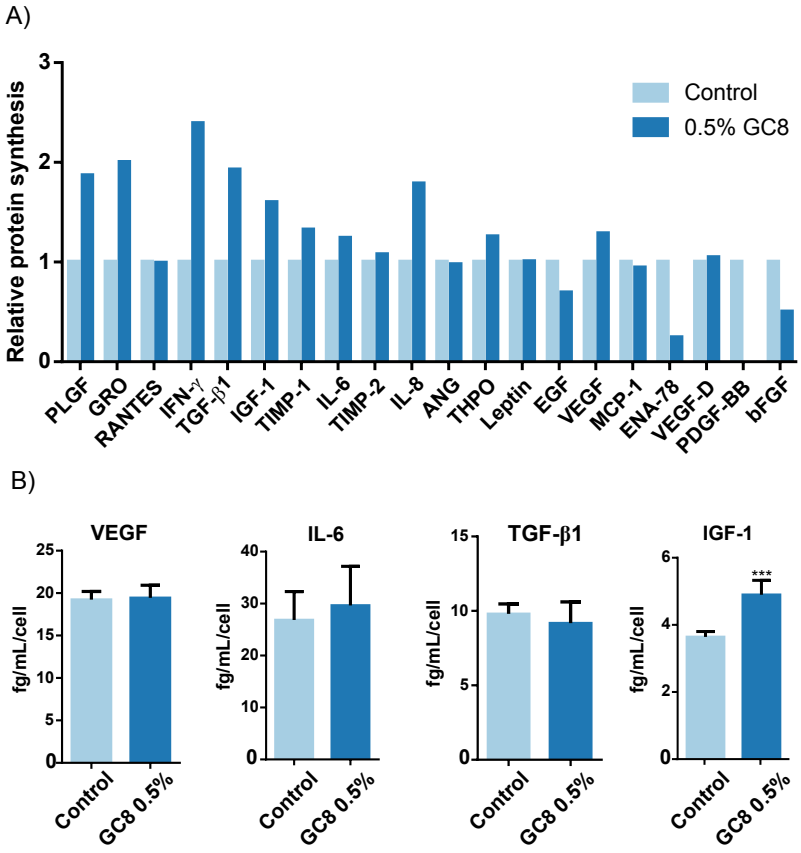

Figure 6.5: Synthesis of angiogenic proteins by hMSC embedded in the hydrogels. A) Protein array of angiogenic proteins. Cell media (5% FBS) incubated for 3 days with the hydrogels containing hMSC was used on a protein array to detect differences in secretion of angiogenic proteins. Values of each protein were normalized to the value measured for the control. Abbreviations of the proteins analyzed are defined in Appendix B.2. B) ELISA quantification of angiogenic factors VEGF, IL-6, TGF-β1 and IGF-1 secreted by hMSC in PEG-MAL hydrogels without particles or with 0.5% (w/v) GC8 particles. Blank values were subtracted and concentrations were normalized to the total number of cells contained in the hydrogel. Data represent the mean of six replicates ± S.D. ***p<0.001.

ferent parameters analyzed between any of the conditions tested and their respective positive control. Since media with lower FBS concentrations than the ones tested greatly decrease hMSC viability when cultured for three days (data not shown), this assay could not be performed with the hMSC-conditioned media.

6.3.7 hMSC differentiation into endothelial cells

By day three after encapsulation, hMSC presented capillary-like morphology stable over time in both the hydrogel without particles or with 0.5%-GC8 (Fig. 6.7A-B). Observation of the rapid network that hMSC formed once encapsulated in the hydrogels together with the detection of a stable cell number overtime prompted us to analyze whether these cells might be differentiating towards endothelial cells. Because CD31 is a marker for endothelial cells, cells were stained for CD31 after 7 days post-encapsulation. As shown in Fig. 6.7G-J, both hydrogels with or without 0.5%-GC8 were positively stained for CD31. However, control cells seeded on glass were also positive for CD31 (Fig. 6.7C), meaning that the pre-encapsulated hMSC already expressed CD31.

6.3.8 Enhanced hMSC survival in GC8-hydrogels implanted in the EFP

The vasculogenic properties of the PEG-MAL-GC8 system containing hMSC were next tested following implantation in the EFP of immunocompromised mice, in which hydrogels containing 0.5% GC8 particles were compared to empty hydrogels and hydrogel delivering VEGF. Avoiding or decreasing cell death associated with *in vivo* implantation is a major issue in tissue engineering (Koç and Gerson, 2003). To track cell survival post-transplantation, hMSC were transduced

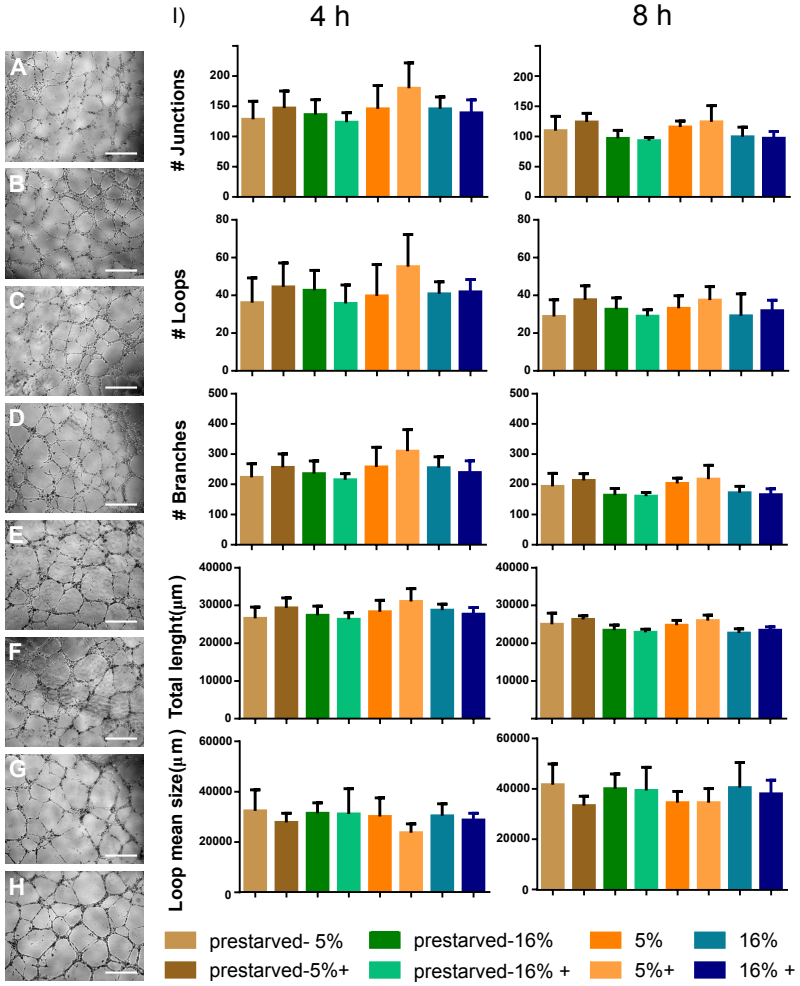

Figure 6.6: Optimization of the tube formation assay. HUVEC were seeded on matrigel either pre-starved for 3 h in 5% FBS media or without starving. Media used during the assay had 5% or 16% FBS, and for positive controls (+) 20 ng/mL VEGF was added. Images were acquired after 4 h (A-D) and 8 h (E-H). A) 5% FBS media at 4 h; B) 5% FBS media, positive control, at 4 h; C) 16% FBS media at 4 h; D)16% FBS media, positive control, at 4 h; E) 5% FBS media at 8 h; F) 5% FBS media, positive control, at 8 h; G) 16% FBS media at 8 h; H) 16% FBS media, positive control, at 8 h. I) Images were processed to analyze number of junctions, number of loops, number of branches, total length of branches and mean size of loops. Each group was seeded in triplicates and three random images were taken per well. Data shows mean ± SD from images acquired per condition. Scale bar: 500 µm.

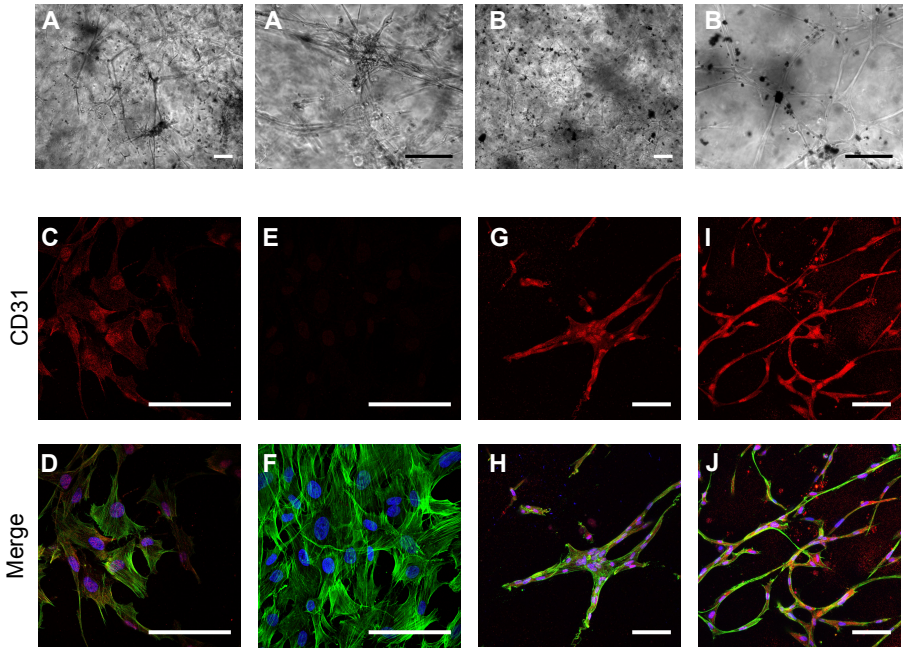

Figure 6.7: Expression of CD31 by hMSC cultured in the hydrogels. A-B) Bright field images showing networks formed by hMSC on day 3 in the A) hydrogel without particles and B) 0.5%-GC8 hydrogel. C-J) Immunostaining of hMSC cultured for 7 days in vitro, stained for CD31 in red, F-actin in green, and nuclei in blue. C-D) Control seeded on glass; E-F) Control without primary antibody seeded on glass; G-H) Hydrogel without particles; I-J) Hydrogel with 0.5%-GC8. Scale bar: 200 μm.

to constitutively express luciferase and transplanted cells were monitored longitudinally by bioluminescence imaging (Fig. 6.8A-B). Bioluminescence signal decreased over time to background levels for all groups. However, higher signal was detected for hMSC implanted in hydrogels containing GC8 particles compared to hMSC in control hydrogels (Fig. 6.8B). This result indicates that GC8-containing hydrogel supported enhanced hMSC survival at early time points compared to control gels.

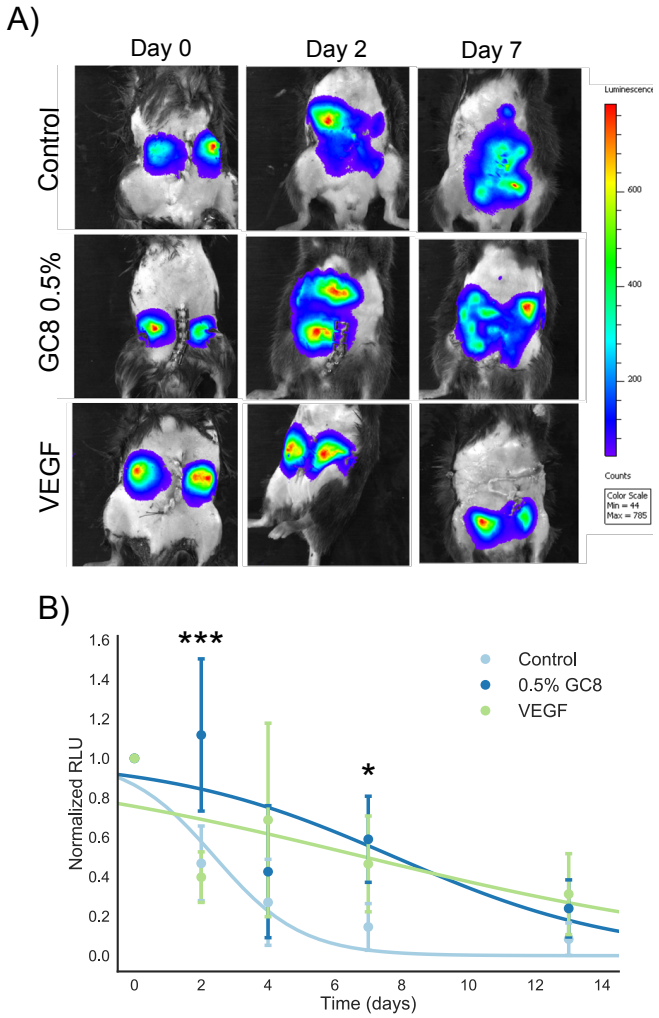

Figure 6.8: ***In vivo*** **survival tracking of transplanted hMSC.** A) Representative images from IVIS scanning of the bioluminescence signal of hMSC in the hydrogels implanted in the EFP after luciferin injection on day 0, 2 and 7 post-implantation. The conditions used included a control without particles, a hydrogel with 0.5% (w/v) content and a positive control containing 10 µg/mL VEGF. B) Bioluminescence signal was determined by quantifying the average counts per unit area within a ROI and values were normalizing to day 0. The plot shows the mean of the six animals used for each condition at every time point (dot). The error bars are the S.D. Lines are sigmoid curves fitted to all the samples per condition. ***p<0.001 (vs. control and VEGF). *p<0.05 (vs. control).

6.3.9 Analysis of vascularization at the implantation site

We evaulated vascularization in the implant site at 2 weeks post-implantation. Prior to euthanasia, functional vasculature in the mice was labeled by an intravenous injection of fluorescent lectin. Microscopic imaging of the excised fat pads (Fig. 6.9A) made possible the quantification of branch and junction density, average branch length and vessel diameter (Fig. 6.9B-E). Significant differences were detected only in vessel diameter, suggesting the development of a more mature vasculature in the EFP with the GC8 hydrogel compared to the empty hydrogel control (Fig. 6.9E).

Sections of the tissue were immunostained for α-SMA and positively stained vessels surrounding the area of implantation of the hydrogel were counted (Fig. 6.10A). Hydrogels delivering VEGF and hydrogels containing GC8 particles showed significantly higher vessel density and thicker wall vessels than the control empty hydrogel (Fig. 6.10B). In addition, the condition with 0.5% GC8 contained a greater number of vessels with bigger lumen area (Fig. 6.10C) and significantly thicker wall vessels than the VEGF condition (Fig. 6.10D). Taken together, these results indicate the presence of a denser and more mature vasculature for GC8-containing hydrogels with hMSC compared to control hydrogels containing hMSC.

6.4 Discussion

Cell therapy using hMSC for the treatment of pathologies with poor vascularization has received considerable interest, as demonstrated by recent clinical trials (Lu et al., 2011; Powell et al., 2012; Hare et al., 2013; Gupta et al., 2013). However, several issues need to be improved to achieve clinical success, such as sustained cell survival that allows a controlled and sustained release of signaling factors in the implanted site (Shen et al.,

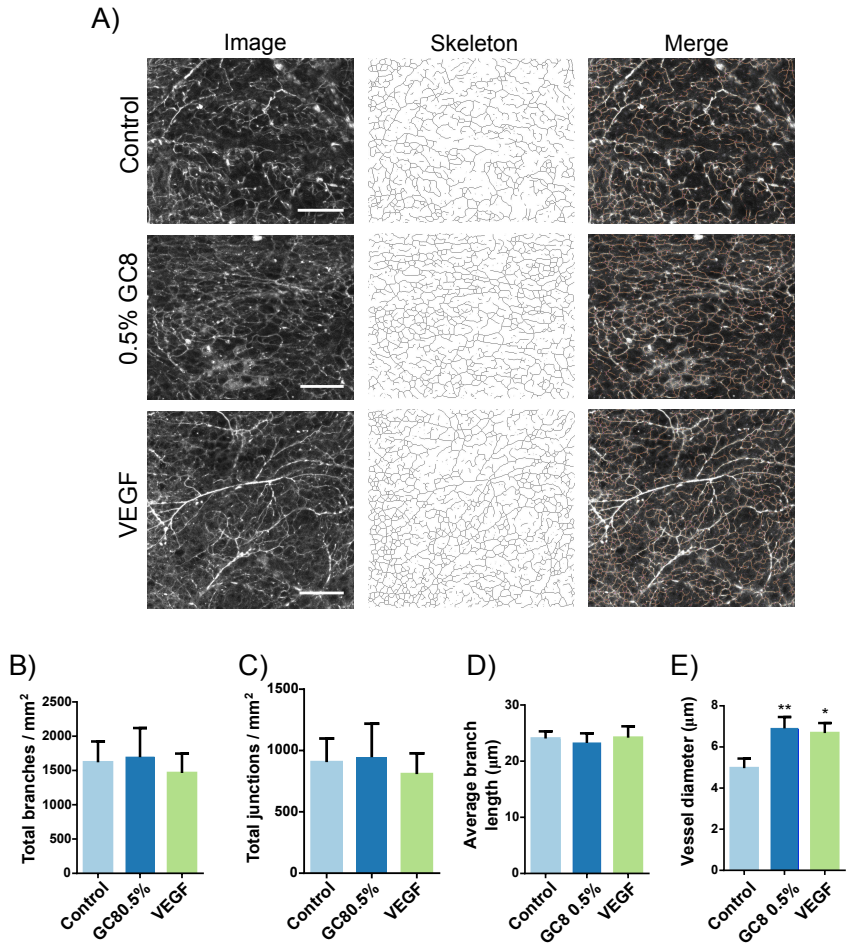

Figure 6.9: Analysis of the lectin-stained vasculature of excised EFP. A) Fluorescent images of the EFP were acquired and processed for quantification of B) total number of branches per area, C) total number of junctions per area, D) average branch length, and E) measurement of vessel width for each condition. Data is expressed as the mean ± S.D of at least six fat pads per condition, from which three random areas were processed. *p<0.05 (vs. control). **p<0.01 (vs. control). Scale bar: 200 µm.

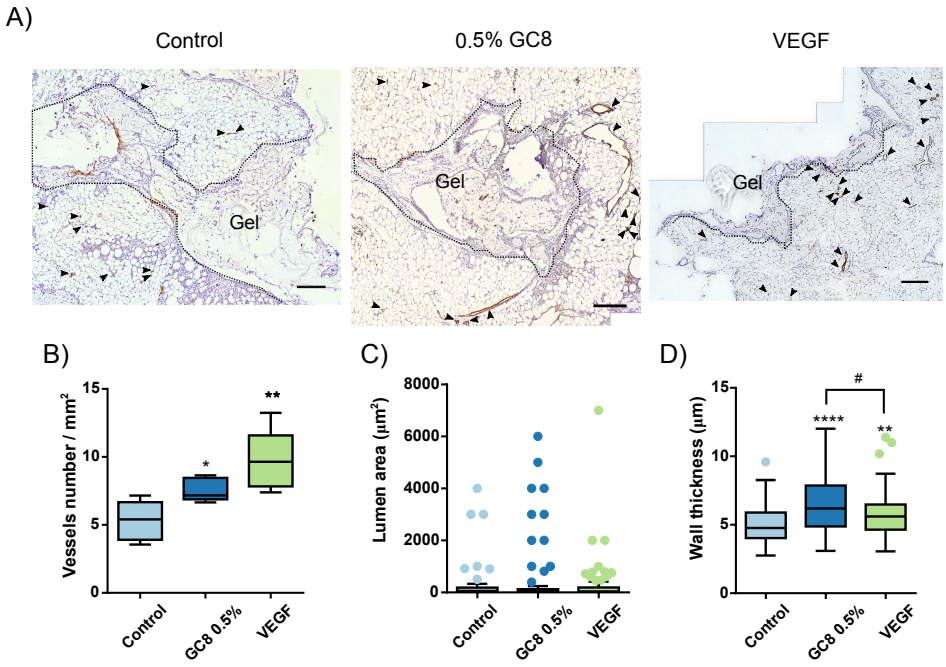

Figure 6.10: Blood vessel analysis from histological sections stained with anti-α-SMA and hematoxylin. A) Representative image of the hydrogel and the surrounding tissue. Positively stained vessels are indicated with an arrowhead (▲) and hydrogel area is delimited by a dotted line (·····). Scale bar: 250 µm. B) Vessel density, C) lumen size and D) wall thickness of vessels stained for α-SMA in the area surrounding the hydrogel. Data is represented in box-and-whisker plots in which the central line of each box is the median, the edges of the box are the first and third quartiles, and whiskers extend to 1.5 times the interquartile range or, if smaller, to the highest or lowest value measured. The outliers are plotted as individual points (dots). Sections from five different fat pads were analyzed per condition. *p<0.05 (vs. control). **p<0.01 (vs. control). ****p<0.0001 (vs. control). # p<0.05.

2012) and stabilization of the newly formed vessels (Carmeliet and Conway, 2001). Regarding their angiogenic properties, the use of bioglasses and glass-ceramics for soft tissue regeneration has also been suggested recently (Gorustovich et al., 2010; Rahaman et al., 2011; Ivanova et al., 2014; Miguez-pacheco et al., 2015), but further research needs to be performed

to show their angiogenic effects *in vivo* and on hMSC. In this study, we explored the vasculogenic potential of calcium-releasing glass-ceramic particles and their combination in a degradable hydrogel containing hMSC for soft tissue regeneration. The particles alone fostered angiogenesis in the CAM model, showing enhanced angiogenesis at the site of implantation. When particles were encapsulated in the hydrogel containing hMSC, cell number remained stable *in vitro*, and improved survival was observed for acute time points *in vivo* when compared to empty hydrogels. In addition, the calcium-releasing particles increased hMSC secretion of IGF-1, an important vasculogenic factor. Finally, hydrogels containing GC8 particles and hMSC stimulated increased and more mature vascularization compared to hydrogels containing hMSC.

Many studies have attributed the angiogenic potential of bioglasses and glass-ceramics to the bioactive ions they liberate (Keshaw et al., 2005; Gorustovich et al., 2008; Vargas et al., 2009), but normally fail in reporting their release profile over time. The ion degradation profile of a material with the same atomic composition as the GC8 particles was described in a previous report from our group (Navarro et al., 2003). This study showed that, in contact with aqueous solutions, the material degrades slowly releasing Ca^{2+}, P^{5+}, Na^{+}, and Ti^{4+} ions. Ca^{2+} and P^{5+} are released in similar fashion and levels (mM range), and Na+ is released in the sub-mM range. In addition, Ti^{4+} is the ion released slower and in lower concentration, within the μM range.

Here, we measured the release of Ca^{2+} because previous studies support a major role for calcium as the main stimulating agent in our material (Aguirre et al., 2010; Vila et al., 2013; Castaño et al., 2014; Chen et al., 2015; Oliveira et al., 2016, 2017). While no evidence is found in the literature of the angiogenic potential of P^{5+}, Na^{+}, and Ti^{4+} ions, reports attributing these properties to titanium-containing surfaces exist (Saghiri

et al., 2016). Nevertheless, because the concentration of particles incorporated in the hydrogels used for the biological studies is relatively low (0.5% w/v), the surface of particles available for the attachment of the encapsulated cells is also small. Therefore, we posit that the biologic stimulation that we observe arises mainly from the calcium ions released, not by the contact with titanium-containing surfaces.

Since the type of media can influence degradation rate of bioglasses/glass-ceramics, we used CCM and buffered MilliQ water (Theodorou et al., 2011; Miller et al., 2012; Rohanová et al., 2014). Despite achieving a sustained release for several days, calcium release was slower in CCM. This slower release could be explained by Le Chatelier's principle, owing to the different calcium concentrations between both solutions. Alternatively or simultaneously, the differences in release could have been caused by the organic content of CCM, which has been reported to interfere in the degradation of bioglasses (Theodorou et al., 2011). These differences in calcium release highlight the importance in the selection of media to study bioglass/glass-ceramic degradation.

The glass-ceramic particles used in this study stimulated angiogenesis in the CAM model, and we attribute this effect to calcium released from the particles. Extracellular calcium concentrations of 10 mM were reported to stimulate migration and tube formation of EFPs (Aguirre et al., 2010). Although our material did not reach this concentration in bulk solution, it is possible that the concentration sensed locally by the cells is higher than the one measured. Other studies have shown that the ionic release of calcium-phosphate ceramics can stimulate the release of angiogenic factors from fibroblasts (Chen et al., 2015), HUVEC (Chen et al., 2015), and EFPs (Aguirre et al., 2012) *in vitro*, so we speculate that the observed angiogenic

effect in the CAM model might have been stimulated by the release of angiogenic factors from the cells present in the membrane.

Addition of glass-ceramic particles in hydrogels alters several physical properties that can modify the biological performance of the material. The degradation profile of the particles, as illustrated by the measurement of the calcium release, was improved by increasing the release rate and becoming more sustained, specially in CCM. We posit that particle degradation is faster within hydrogels as these are separated from each other whereas free particles aggregate likely influencing local release rates. Both particle concentrations tested reduced the swelling capacity of the hydrogel. Also, the condition with higher particle concentration tested (1%) reduced the storage modulus of the material. We attribute the reductions in swelling capacity and storage modulus to the high content of micrometric particles in this hydrogel that disrupts the hydrogel network reducing the ability of the hydrogel to absorb water and support a load.

Incorporation of GC8 particles within hydrogels also increased the secretion of vasculogenic factors by encapsulated hMSC, supporting the conception that the degradation product of these biomaterials can stimulate cells to release factors (Leu and Leach, 2008; Chen et al., 2015). More specifically, increased levels of IGF-1 were detected in media conditioned by hMSC encapsulated in hydrogels with glass-ceramic particles compared to media from hMSC encapsulated in control gels. IGF-1 stimulates angiogenesis *in vitro* and *in vivo* (Su et al., 2003; Dobrucki et al., 2010; Jacobo and Kazlauskas, 2015). Su et al. (2003) showed induced ECs migration and capillary formation in an aorta ring assay, and Jacobo and Kazlauskas (2015) recently demonstrated a role of this factor in stabilizing neovessels. In addition, sustained IGF-1 expression through gene delivery improved cardiac function in a myocardial infarction model (Dobrucki et al., 2010). Extracellular calcium had been shown to increase IGF-1 expression

in other cell types, such as EFPs and osteoblasts (Sugimoto et al., 1994; Aguirre et al., 2010), contributing to EPCs maturation (Aguirre et al., 2010, 2012). Although it is possible that the control and 0.5% GC8 gels present some structural differences that could affect cell behavior, the CAM assay indicates that the particles *per se* trigger a biological response. Therefore, we posit that it is the effect of the calcium released by the particles, and not the structural properties of the hydrogel, the main factor responsible of stimulating the cellular response.

To provide more evidence of the angiogenic potential of the factors released by encapsulated hMSC with GC8, we wanted to use the conditioned media in the tube formation assay. However, while optimizing the assay, we found that non-conditioned media containing as few as 5% FBS stimulated capillary-like formation as the positive control. Other studies performing the tube formation assay seem to use FBS at a concentration of 1% or less (Gruber et al., 2005; Ko and Lung, 2012; Hwang et al., 2016; McQuilling et al., 2017). Considering that hMSC survival in media with less than 5% for three days was impaired, this assay was discarded.

On the other hand, based on the observation of the capillary-like structures that hMSC were forming within the hydrogels, we explored the possibility that these cells might be differentiating towards endothelial cells, as reported by other studies (Oswald et al., 2004; Janeczek Portalska et al., 2012; Wang et al., 2012). More specifically, we analyzed the expression of the endothelial cell surface marker CD31 by immunostaining. To our surprise, embedded hMSC were strongly stained by CD31. Nevertheless, hMSC seeded on glass also presented CD31, meaning that the starting population already expressed CD31, although the signal was weaker than for cells embedded in the hydrogels. Even though hMSC are not normally reported as CD31 positive cells, it had been shown elsewhere (Sheng et al., 2016). Expression of CD31 should have been confirmed with flow-

cytometry, and real-time quantitative PCR could have been used to determine differences in expression. However, the capability of hMSC to differentiate towards bona fide endothelial cells is a controversial topic within the scientific community. *In vitro*, not only upregulation of markers such as CD31, CD34, VEGF receptors (VEGF-R1, VEGF-R2) and vonWillebrand factor must be shown, but also functional test such as tube formation and uptake of acetylated-low density lipoproteins should be performed (Pacini and Petrini, 2014). In addition, differentiation should be proven *in vivo* by showing their involvement in blood vessels formation, but considering the role of hMSC as pericyte cells it is difficult to determine. Unfortunately, due to time constrictions, we could not further explore the differentiation of the embedded hMSC towards an endothelial linage.

Cell survival within the hydrogel is of great relevance for their application into clinics. We used hMSC expressing luciferase to track cell survival following cell transplantation within different hydrogel formulations in the murine EFP. Bioluminescence signal decreased over time to background levels for all groups. However, higher signal was detected for hMSC implanted in hydrogels containing GC8 particles compared to hMSC in control hydrogels. This result indicates that GC8-containing hydrogel supported enhanced hMSC survival at early time points compared to control gels.

We evaluated the effect of GC8 glass-ceramic particles on vascularization using two models: an ex ovo CAM assay and an *in vivo* study in the murine EFP. Both models agreed in finding increased vascularization in hydrogels containing glass-ceramic particles compared to control gels. In addition, the murine EFP where hMSC-containing hydrogels were implanted showed enhanced vessel maturation in hydrogels containing the particles compared to empty and VEGF-releasing hydrogels. Other studies had reported angiogenic properties for bioglasses and glass-ceramics

(Day et al., 2004; Castaño et al., 2014; Chen et al., 2015; Oliveira et al., 2016), but to our knowledge, this is the first report demonstrating that these materials stimulate functional vasculature in mammalian soft tissues. In the EFP model, the number of vessels present around the implanted material containing particles was lower than for the positive control releasing VEGF. This angiogenic factor has been widely reported to stimulate increase in vessel number, but it is also known that vessel regression may occur upon loss of the vasculogenic stimuli (Benjamin et al., 1999). Therefore, since both increased vessel number and maturation are detected for the condition with particles, the results obtained for this material have an enhanced effect compared to the positive control containing VEGF at early time points.

Due to the complexity of the signaling pathways involved in the formation of stable vasculature, it is challenging to hypothesize what specific factor(s) might have promoted these effects. Increased release of IGF-1, as observed in our *in vitro* study, could have contributed to vessel stabilization (Jacobo and Kazlauskas, 2015). In addition, because cell survival is improved in the condition with particles, the release of other factors associated with vessel stabilization, such as TGF-β (Murakami, 2012), might have been higher than for the other conditions tested. Another possibility is that implanted hMSC may have contributed as mural cells (Au et al., 2008). Nevertheless, the contributing role of the glass-ceramic particles should be further studied in order to unravel the specific pathway by which they can stimulate vessel maturation. Overall, the material here presented made by the combination of a functionalized degradable PEG hydrogel, hMSC and calcium-phospate glass-ceramic microparticles shows high vasculogenic potential in an *in vivo* context, as it permitted a more sustained cellular survival and stimulated increased vessel formation and maturation in the tissue.

6.5 Conclusions

Novel strategies are needed to improve vascularization of ischemic tissues with cell therapy, especially regarding cell survival and vessel stabilization. Here, we present a composite construct consisting of hMSC and calcium-releasing microparticles within a functionalized synthetic hydrogel system that enhances blood vessel formation and maturation in vivo. The presence of the glass-ceramic particles seems to stimulate these effects by improving implanted cell survival and angiogenic factor release. This study provides further evidence on the vasculogenic effect of bioglasses/glass-ceramics observed in hard tissue and sheds light into the potential use of these materials in the improvement of cell therapy for soft tissue regeneration and vessel stabilization.

7 Conclusions and future perspectives

This thesis project was devoted to gaining insight into the application of bioceramics in soft tissue repair, particularly chronic wounds. More specifically, we focused on the role of calcium and evaluated the capability of calcium-releasing bioceramics to accelerate healing of skin ulcers and to stimulate the formation of new blood vessels. Below, the main conclusions reached throughout the different chapters included in this thesis are summarized:

Chapter 3: Effects of extracellular calcium and calcium-phosphate bioglass on dermal fibroblast

- Extracellular calcium, in the range of 2.5 and 3.5 mM, affects the biological behavior of rat dermal fibroblasts. More specifically, calcium stimulates metabolic activity, MMP9 and MMP2 synthesis and activation respectively, collagen synthesis, and expression of myriad genes involved in wound healing. In addition, it decreases the contraction capacity of fibroblasts.
- Both cell migration and contraction capacity are stimulated in a concentration-dependent manner.

- The ionic dissolution of the fast calcium-releasing ormoglass SG5 with adjusted calcium concentrations also stimulates metabolic activity, cell migration, collagen synthesis, and reduces contractile capacity. Moreover, some unwanted responses for chronic wound healing are avoided or diminished, such as increased gelatinase activity and expression of inflammatory factors. Nevertheless, it triggers other undesired effects, such as reduction of proliferation rate and VEGF synthesis.

Chapter 4: Responses mediated by the calcium-sensing receptor

- Dermal fibroblasts show expression of the calcium-sensing receptor (CaSR) organized in clusters at the edge of their plasma membrane.
- CaSR agonists, including Gd^{3+}, Mg^{2+}, and Zn^{2+} stimulate metabolic activity, and Gd^{3+}, Mg^{2+}, and Sr^{2+} promote cell migration. In addition, Gd^{3+} also stimulates collagen synthesis, but not gelatinase activation.
- CaSR agonist-releasing bioceramics could be considered over calcium-releasing bioceramics to stimulate more specific responses on wound healing.
- The extracellular signal-regulated protein kinases 1 and 2 (ERK1/2) pathway is similarly activated with Ca^{2+} and Gd^{3+}, so this pathway could be involved with some of the biological responses stimulated on fibroblasts.
- The vehicles used to dissolve the CaSR negative allosteric modulators NPS2143 and calhex231 interfere with the biological responses studied.

Chapter 5: *In vivo* evaluation of a calcium-releasing composite on a pressure ulcer diabetic model

- A novel dressing generated with the electrospinning technique composed of poly(lactic acid) (PLA) fibers containing SG5 particles accelerated the healing of pressure ulcers on diabetic and obese mice.
- The dressing promoted increased vessel density at initial time points. This effect can explain, at least in part, the faster healing rate detected for this material.
- The overall biological performance of the designed material surpassed a dressing frequently used in the treatment of chronic wounds.
- Considering that both PLA and bioceramics are currently accepted for clinical application, that these materials and the production technique are relatively inexpensive, and that the final dressing has good stability, this product has great translational potential.

Chapter 6: Vessel maturation promoted by a glass-ceramic / hydrogel composite with hMSC

- Glass-ceramic microparticles coded as GC8 present a sustained calcium-release and stimulate vessel formation in the CAM model.
- These particles are successfully incorporated into a degradable and cell-adhesive synthetic hydrogel.
- This composite material allows a sustained survival of encapsulated hMSC and stimulates the release of the angiogenic factor IGF-1 from these cells *in vitro*.
- The composite material promotes an improved survival of the encapsulated hMSC when implanted in soft tissue of mice, as well as increases vessel maturation at the site of implantation.

- Overall, this novel composite shows great potential to improve cell therapy for soft tissue regeneration.

Future perspectives

The work developed during this thesis has contributed to expand the knowledge of the potential of bioceramics to improve of wound healing and soft tissue regeneration. Novel products have been designed and tested *in vitro* and *in vivo* showing promising results. However, research must continue to better understand the interactions of calcium and other products released by bioceramics with soft tissue, specially to unravel the mechanisms involved in the stimulated effects, and to find the optimal release to improve the healing of a human wound. The continuation of the studies presented in this thesis could provide interesting answers. Below, some suggestions of what could be done are given.

One of the reasons why biomedical treatments fail when reaching clinical trials is the inaccuracy of the models used along the preclinical studies to mimic the real situation. In the case of chronic wound healing research, there is significant room for improvement regarding designing and executing more reliable models. In the *in vitro* studies presented in Chapter 3, we used primary rat dermal fibroblasts because they were the ones available in the lab. However, considering that fibroblasts from chronic wound patients present a senescent state (Hasan et al., 1997; Ågren et al., 1999; Wall et al., 2008; Brem et al., 2007), it would be interesting to repeat the experiments using human dermal fibroblasts from diabetic and/or aged patients. In addition, regarding the relevance of ECM-cells and cell-cell interactions in wound healing, the study of the effect of calcium and bioceramics on bilayered 3D skin equivalent models would be highly informative.

The idea of using CaSR analog-releasing bioceramics is very appealing, because considering the wide contribution of calcium in different biological processes, they may allow a more specific stimulation of the heal-

ing response. Our study presented in Chapter 4 provides insight into this matter, but further experiments should be performed. For instance, other CaSR analogs could be tested, and not only on dermal fibroblasts but also on keratinocytes and immune cells. Moreover, to overcome the difficulties found in the use of the negative allosteric modulators, the expression of the CaSR receptor could be reduced or knocked down with specific siRNA or CRISP/Cas9 technology.

The results obtained in Chapter 5 from the *in vivo* pressure ulcer model are very promising and a more extensive characterization of the tissue should be performed in order to unravel the mechanisms that have favored an accelerated healing. Specific tissue stainings could be carried out to quantify the density of fibroblasts and myofibroblast at the injured site, analyze expression of MMPs and tissue inhibitor of metalloproteinases (TIMPs), and detect keratinocyte proliferation. Analysis of the immune cell population present in the tissue, such as macrophages, might also provide useful information. In view of the positive results attained, the novel designed dressing could be a suitable candidate to be evaluated on swine, the skin of which is considered to be structurally more similar to human than mouse.

Finally, more experiments are needed to understand the vasculogenic capability of the composite material presented in Chapter 6. More *in vitro* tests could be performed to analyze the angiogenic potential of the media conditioned with the release of hMSC in the material. Also, tissue sections from the *in vivo* experiment could be proved against human-specific antibodies to detect hMSC incorporation into the blood vessels surrounding the site of implantation. Furthermore, evaluation of the material in a different *in vivo* model, such as the murine hind limb ischemia model, would allow the identification of real functional gain in vascularization.

Even though the focus of this study was on the role of calcium, the effect of the other ions released by bioceramics should not be underestimated. Phosphate is released in similar concentrations to calcium in the bioceramics tested in this project, and experiments assessing its effect on fibroblasts and other cell types as well as the combination of both calcium and phosphate ions should be undertaken. Moreover, although we did not detect it in our *in vivo* studies, the risk of tissue calcification should be noted when using bioceramics due to their release of calcium and phosphate (Bueno et al., 2016; Habibovic et al., 2010). Thus, specific assays should be performed to detect tissue calcification, specially for long-term implantation of the particles in soft tissues.

A Survey

A.1 Aim

The development of novel biomedical therapies require of a deep understanding of the patophysiology of the disease that aims to be treated, as well as of the situation and shortcomings of current treatments. Bibliographic review is obviously an essential step to gain this knowledge but first hand opinion of medical professionals is also very valuable and informative. To attain a better understanding of the way chronic wounds are treated and what is the perception of medical professionals about the products currently available and their limitations, we decided to carry out a survey.

A.2 Methodology

The survey consisted of 20 questions (Q) to be responded on-line. Questions 1 to 5 (Q1-Q5) were devoted to learn about the profile and experience of the survey respondents. Q8-Q11 consisted of general questions about chronic wounds and the dressings used to treat them. Q12-Q14 and Q15-Q17 were specific questions about pressure ulcers and vascular wounds, respectively. Finally, Q18-Q20 were questions to learn about the knowl-

edge of participants in skin substitutes and the impact of this therapy in the clinics.

In most of the questions, participants were asked to choose a single answer from different proposed options. These questions were Q1, Q2, Q3, Q4, Q5, Q6, Q8, Q9, Q10, Q11, Q18, Q19, and Q20. In some questions, survey responders could comment or justify their answer: Q8, Q11, Q14, Q17, Q19, and Q20. In other questions, they were asked to mark from 1 (very high) to 5 (very low) the relevance or frequency of the wounds: Q7, Q12, Q13, Q15, and Q16.

Several professionals from primary care centers and hospitals of the metropolitan area of Barcelona were contacted and were kindly asked to anonymously participate in the on-line survey and to share the survey with their co-workers. A total of thirteen people accepted to participate and answered all the questions.

A.3 Results

A.3.1 General questions about the survey respondents

All participants were women (Q1) with a nursing degree (Q3), eight of which worked in primary care centers while the remaining five worked in hospitals (Q2). More than 50% were specialized in treating chronic wounds (Q4) and had more than 16 years of experience on it (Q5). The majority of the patients treated by these professionals, 90%, are older than 61 years old (Q6), pointing out that advanced age is a key risk factor in chronic wounds. Moreover, the type of chronic wounds that they most commonly treat are vascular, diabetic food, and pressure ulcers, in this order of frequency (Q7).

A.3.2 General questions about chronic wounds and dressings

Some general questions about the use of dressings in chronic wounds were asked. They answered that dressings were always changed by nurses (Q9). Also, 70% responded that dressings are normally changed every 2 to 4 days, while the rest answered that the frequency of dressing change depends on the requirements of each particular wound (Q8). Some commented that wounds must be monitored frequently to detect infection or change the type of products needed as the wound evolves, but it was best to keep it covered if possible.

By far, the main factor that they prioritize when choosing a dressing is the speed of wound closure (Q10). While most of the nurses that work in primary care centers answered that they can easily choose a dressing that provides the factor they prioritize, in hospitals, nurses are more limited (Q11). Nurses in hospitals commented that they have less power of decision because it is the hospital and not themselves who can choose the dressings that are available to use. On the other hand, nurses in primary care centers have much more influence on this choice.

A.3.3 Questions about pressure ulcers and vascular ulcers

When inquired about pressure ulcers, all the risk factors proposed in the survey were chosen as relevant. Nevertheless, the ones considered more important were immobility and diabetes, followed by infection, circulation problems, advanced age, malnutrition, and obesity (Q12). In this type of wounds, products that promote wound debridement are very often applied. Antimicrobials and dressings that control exudate are also commonly used. On the other hand, products that actively stimulate wound closure, such as

growth factor therapy, are less common, and skin substitutes and grafts are very rare or not used. Survey respondents were also asked to choose what aspects involved in the healing of pressure ulcers are not well covered by current dressings. 35% responded *control of tissue maceration at the wound edge*, 22% chose *stimulation of granulation tissue*, and 17% answered *debridement* and *infection control*. Only 4% considered that *stimulation of re-epithelialization* is not well covered.

All the risk factors for vascular ulcers that were proposed in the question were considered relevant in this order: infection, immobility, diabetes, hipertension, malnutrition, obesity, advanced age, and smoking (Q15). For these ulcers, antimicrobial products were chosen as the most commonly used treatment (Q16). Debridement was not so relevant as for pressure ulcer, but was still one of the most common treatments applied, followed by exudate control (Q16). Products that stimulate an active healing are a bit less commonly used, and, again, skin substitutes and grafts are very rare or not used (Q16). The aspects of these wounds that they considered not to be properly covered by current products were: 30% *control of tissue maceration at the wound edge*, 20% *infection control* and *stimulation of granulation tissue*, 10% debridement and exudate control, and only 5% chose *stimulation of re-epithelialization* (Q17).

A.3.4 Questions about skin substitutes

Finally, respondents were inquired about skin substitutes. First, a brief definition of skin substitutes was provided, explaining that these products involve the use of human cells embedded in 3D-scaffolds. Most of the nurses working in primary care centers did not know about this products, while hospital nurses were more acquainted with their existence (Q18). Moreover, the majority of the participants answered that they had never used these products or met anyone using them. Nevertheless, nurses were quite

optimistic about the future perspectives of skin substitutes, since many of them considered that they might be regularly used in 5 to 10 years. On the other hand, others commented that this is not likely to happen due to restrictions in healthcare budget.

A.4 Conclusions

The survey points out the key role that nurses play in the treatment of chronic wounds in both primary care centers and hospitals. They are the medical professionals who take direct care of these wounds and decide the type of dressing to be used on each patient.

Dressings are most commonly changed every 2 to 4 days, and, generally, different products are used as wound healing progresses because wound requirements evolve. Moreover, their first choice is to use dressings that accelerate the healing process.

The main risk factors shared by both pressure and vascular ulcers perceived by nurses that answered the survey are immobility, diabetes and infection. While pressure ulcers require more debridement, vascular ulcers are more sensitive to infection. According to the nurses that we interviewed, the most important aspect not covered by current dressings for the treatment of these chronic wounds is control of tissue maceration at the wound edge. In pressure ulcers, the second aspect not well covered is stimulation of granulation tissue, followed very closely by infection and debridement. Similarly, in vascular wound ulcers, both stimulation of granulation tissue and infection control are considered the second most important aspects to improve, followed by debridement and exudate control.

This survey also highlight that skin substitutes are not yet a current treatment in our local hospitals and primary care centers.

General questions about the survey respondents

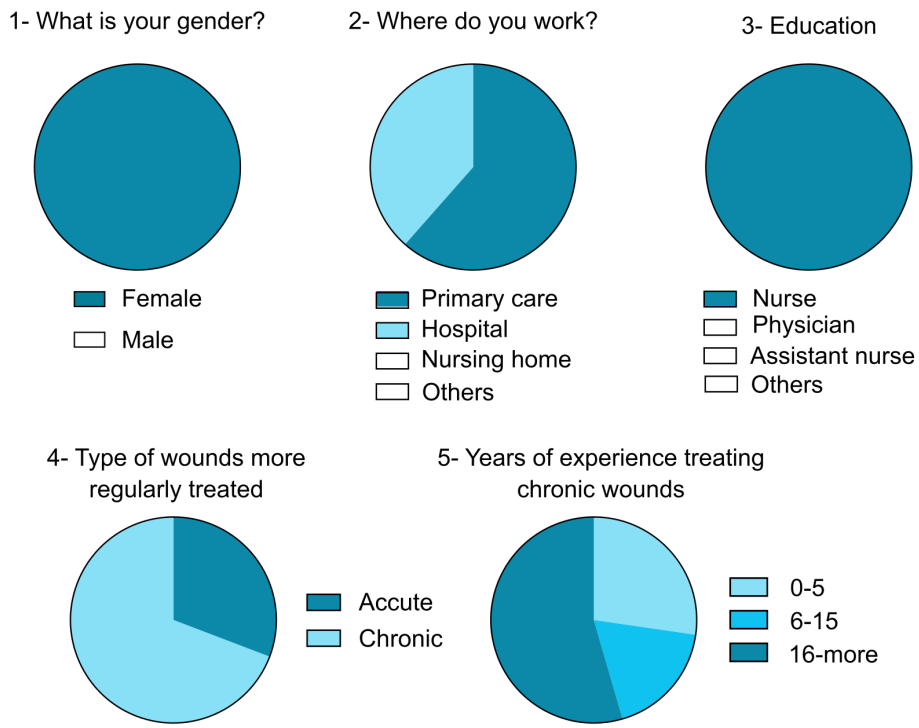

General questions about chronic wounds and dressings

6- Patients age range

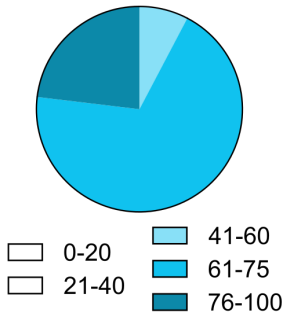

7- Most often treated chronic wounds

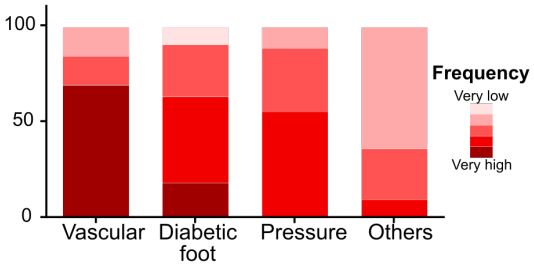

8- Frequency of dressing change

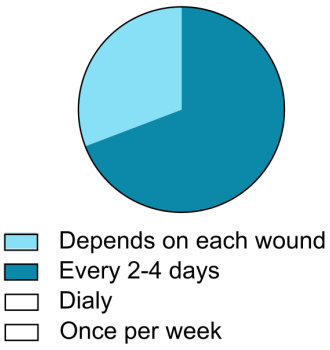

9- Who changes the dressing?

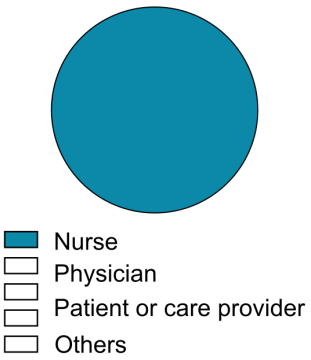

10- Prioritized factor when choosing a dressing

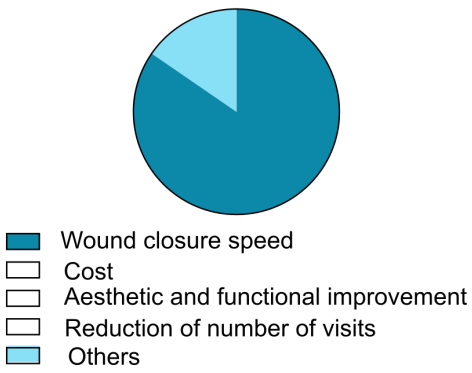

11- Is it easy at your workplace to apply the factor you prioritize?

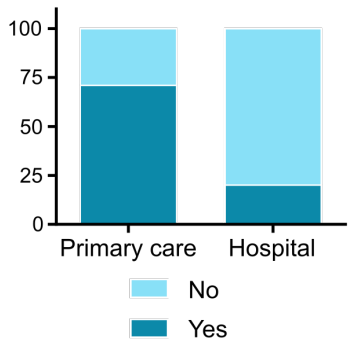

Questions about pressure ulcers

12- Relevance of risk factors to hamper healing

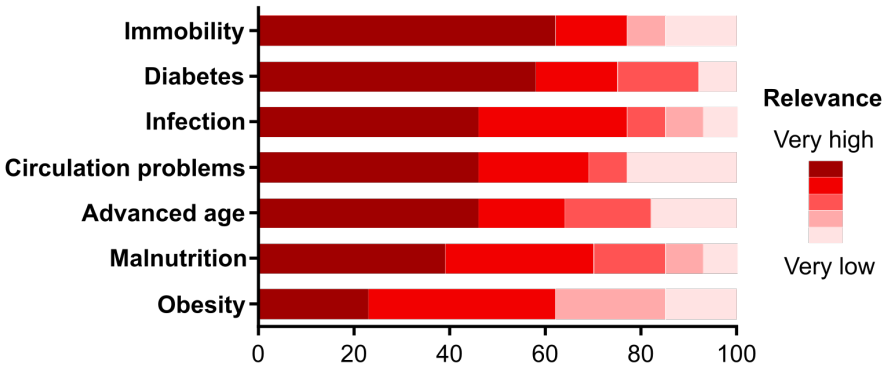

13- How often do you use these treatments?

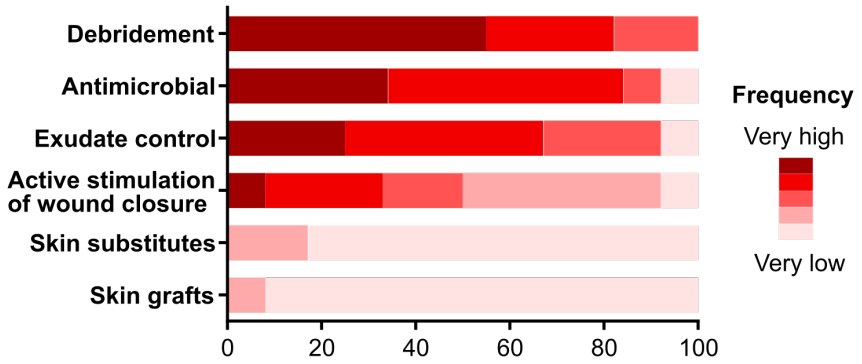

14- Aspects of wounds not well covered by current dressings

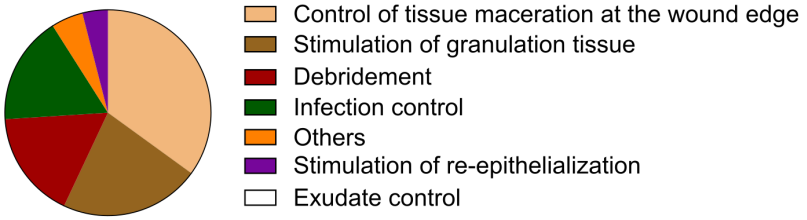

Questions about vascular ulcers

15- Relevance of risk factors to hamper healing

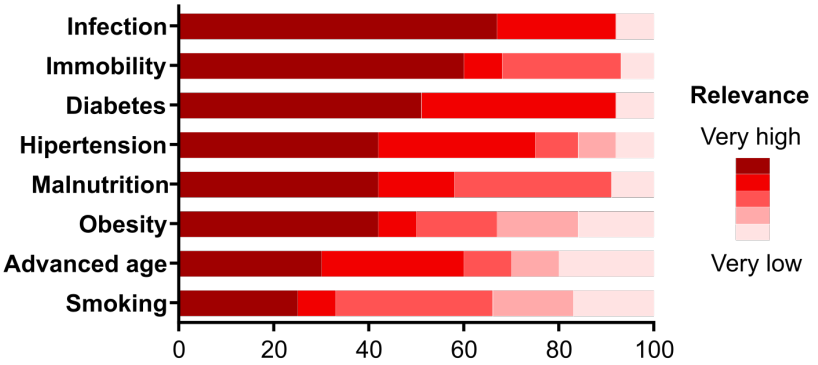

16- How often do you use these treatments?

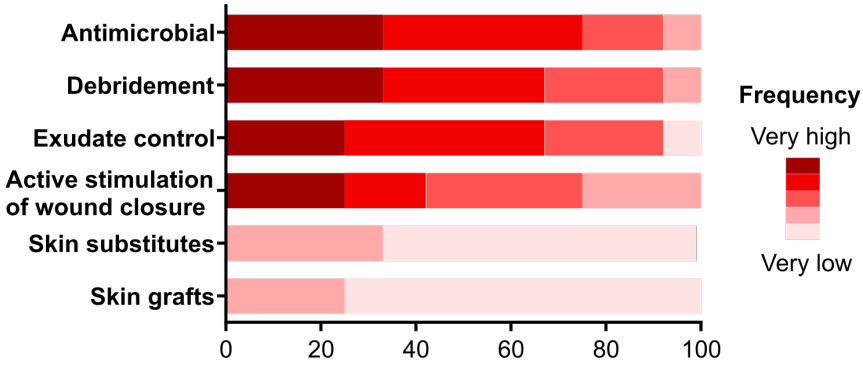

17- Aspects of wounds not well covered by current dressings

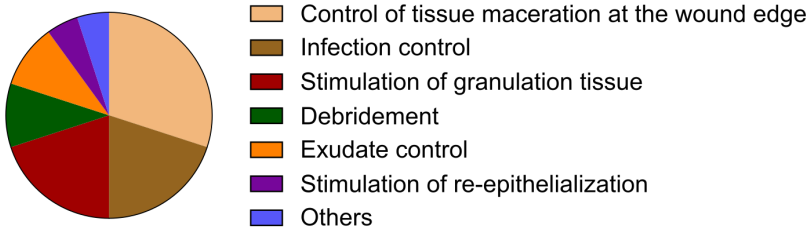

Questions about skin substitutes

18- Do you know what skin substitutes are?

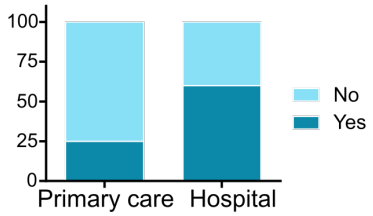

19- Have you or someone you know used these products?

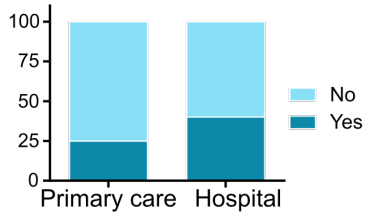

20- Do you think these products will be regularly used in the near future (5-10 years)?

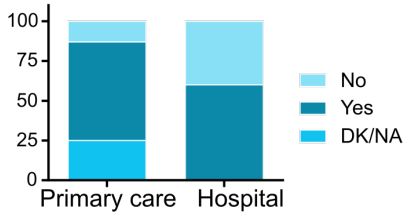

B Abbreviation lists for arrays

B.1 Wound healing RT-PCR array

Abb	Name	Abb	Name
Angpt1	Angiopoietin 1	Itga1	Integrin subunit alpha 1
Ccl12	Chemokine (C-C motif) ligand 12	Itga3	Integrin subunit alpha 3
Ccl7	Chemokine (C-C motif) ligand 7	Itga4	Integrin subunit alpha 4
Col3a1	Collagen type IV alpha 1	Itga5	Integrin subunit alpha 5
Col4a1	Collagen type IV alpha 1	Itgav	Integrin subunit alpha V
Col4a3	Collagen type IV alpha 3	Itgb3	Integrin subunit beta 3
Col5a3	Collagen type V alpha 3	Itgb5	Integrin subunit beta 5
Col14a 1	Collagen type XIV alpha 1 Chain	Mapk3	Mitogen activated protein kinase 3
Csf2	Colony stimulating factor 2	Plat	Plasminogen activator, tissue type
Ctnnb1	Catenin beta 1	Plau	Plasminogen activator, urokinase
Cxcl1	Chemokine (C-X-C motif) ligand 1	Plaur	Plasminogen activator, urokinase receptor
Cxcl3	Chemokine (C-X-C motif) ligand 3	Ptgs2	Prostaglandin-endoperoxide synthase 2
Cxcl6	Chemokine (C-X-C motif) ligand 6	Rhoa	Rashomolog family member A
Egfr	Epidermal growth factor receptor	Serpine 1	Serpin peptidase inhibitor, clade E
Fgf10	Fibroblast growth factor 10	Stat3	Signal transducer and activator of transcription 3
Fgf2	Fibroblast growth factor 2	Tgfa	Transforming growth factor alpha
Fgf7	Fibroblast growth factor 7	Tgfb1	Transforming growth factor, beta 1
Hbegf	Heparin-binding EGF-like growth factor	Vegfa	Vascular endothelial growth factor A
Hgf	Hepatocyte growth factor	Wisp1	WNT1 inducible signaling pathway protein 1
Il6	Interleukin 6	Wnt5a	Wingless-type MMTV integration site family, member 5A.

B.2 Angiogenesis protein array

Abbreviation	Name
ANG	Angiogenin
EGF	Endothelial growth factor
ENA-78	Neutrophil-activating peptide 78
GRO	Growth-regulated protein
Hbegf	Heparin-binding EGF-like growth factor
Hgf	Hepatocyte growth factor
IFN gamma	Interferon-gamma
IGF-1	Insulin-like growth factor I
IL-6	Interleukin 6
IL-8	Interleukin 8
Leptin	Leptin
MCP-1	Monocyte chemotactic protein 1A
PDGF-BB	Platelet-derived growth factor
PLGF	Placenta growth factor
RANTES	C-C motif chemokine 5 (Small-inducible cytokine A5)
TGF beta 1	Transforming growth factor-beta 1
THPO	Thrombopoietin
TIMP-1	TIMP metallopeptidase inhibitor 1
TIMP-2	TIMP metallopeptidase inhibitor 2
VEGF	Vascular endothelial growth factor

C Scientific contributions and awards

C.1 Publications

- Claudia Navarro-Requena, Jessica D. Weaver, Amy Y. Clark, Douglas A. Clift, Soledad Perez-Amodio, Óscar Castaño, Dennis W. Zhou, Andrés J. García, Elisabeth Engel. PEG Hydrogel Containing Calcium-Releasing Particles and Mesenchymal Stromal Cells Promote Vessel Maturation. Acta Biomaterialia. 2017. *Under review*.

- Claudia Navarro-Requena, Soledad Perez-Amodio, Oscar Castaño, Elisabeth Engel. Wound Healing-Promoting Effects Stimulated by Extracellular Calcium and Calcium-Releasing Nanoparticles on Dermal Fibroblasts. Journal of Materials Chemistry B. 2017. *Submitted*.

- Soledad Perez-Amodio, Nuria Rubio, Olaia F. Vila, Claudia Navarro-Requena, Oscar Castaño, Aitor Sanchez Ferrero, Joan Marti-Munoz, Jeronimo Blanco, Elisabeth Engel. Accelerated Wound Healing by Novel Polymeric Composite Dressings. Journal of Tissue en Regenerative Medicine. 2017. *To be submitted*.

C.2 Posters and oral presentations in conferences

- Claudia Navarro-Requena, Soledad Pérez-Amodio, Óscar Castaño and Elisabeth Engel. "Pursuing a Novel Bioactive Dressing: Stimulation of Dermal Fibroblasts With Calcium-Phosphate Nanoparticles". Poster presented at the IBEC's 9th annual Symposium: Bioengineering for Active Ageing. Barcelona, Spain. 29th June 2016.

- Claudia Navarro-Requena, Soledad Pérez-Amodio, Óscar Castaño and Elisabeth Engel. "Pursuing a Novel Bioactive Dressing: Stimulation of Dermal Fibroblasts with Calcium-Phosphate Nanoparticles". Poster presented at the 10th World Biomaterials Congress. Montreal, Canada. 17th-22nd May 2016

- Claudia Navarro-Requena, Jessica Weaver, Óscar Castaño, Amy Clark, Jose García, Soledad Pérez-Amodio, Dennis Zhou, Douglas Clift, Andrés J. García, Elisabeth Engel. "Vasculogenesis by a Maleimide Cross-Linked PEG Hydrogel Containing Calcium Phosphate Glass Particles". Oral presented at the 27th European Congress for Biomaterials- European Society for Biomaterials, Krakow, Polony, 30th August- 3rd September 2015.

- Claudia Navarro-Requena, Jessica Weaver, Óscar Castaño, Amy Clark, Jose García, Soledad Pérez-Amodio, Dennis Zhou, Douglas Clift, Andrés J. García, Elisabeth Engel."Vasculogenic Effect of Calcium Phosphate Glass Particles in a Maleimide Cross-Linked PEG Hydrogel". Poster presented at the 5th Advanced Summer School: Interrogations at the Biointerface, Oporto, Portugal, 29th June-3rd July 2015.

- Claudia Navarro-Requena, Jessica Weaver, Óscar Castaño, Amy Clark, Jose García, Soledad Pérez-Amodio, Dennis Zhou, Douglas Clift, Andrés J. García, Elisabeth Engel. "Angiogenic Stimulation by Calcium Phosphate Glass-Ceramic Particles in a Maleimide Cross-Linked PEG Hydrogel". Poster and oral presented at the IBEC's 7th annual Symposium: Bioengineering for Future Medicine. Barcelona, Spain. 29th September 2014.

- Claudia Navarro, Soledad Pérez-Amodio, Óscar Castaño, J.A. Planell and Elisabeth Engel. "The Effect of Extracellular Calcium on Dermal Fibroblasts with Potential Applications in Skin Wound Healing". Oral presented at the European Wound Management Association -Grupo Nacional para el Estudio y Asesoramiento en Úlceras por Presión y Heridas Crónicas (EWMA-GNEAUPP) 2014 congress. Madrid, Spain. 14th-16th May 2014.

- Claudia Navarro, Soledad Pérez-Amodio, Óscar Castaño, J.A. Planell and Elisabeth Engel. "The Effect of Extracellular Calcium on Dermal Fibroblasts with Potential Applications in Skin Wound Healing". Poster presented at the Advanced Summer School: Inflammation/Repair Interface. Porto, Portugal. 25th-28th June 2013.

- Claudia Navarro, Soledad Pérez-Amodio, Óscar Castaño, J.A. Planell and Elisabeth Engel. "The Effect of Extracellular Calcium on Dermal Fibroblasts with Potential Applications in Skin Wound Healing". Poster presented at the IBEC's 6th annual Symposium on Bioengineering and Nanomedicine. Barcelona, Spain. 8th May 2013.

C.3 Awards

- “Best Oral Presentation” Award in the 27 th European Congress for Biomaterials- European Society for Biomaterials. 2015.
- "EWMA First Time Presenter Award 2014" in the congress EWMA-GNEAUPP, 2014.

Bibliography

Abe, H., Tateyama, M., and Kubo, Y. (2003). Functional identification of Gd3+ binding site of metabotropic glutamate receptor 1alpha. *FEBS letters*, 545(2-3):233–8.

Abercrombie, M., Heaysman, J. E., and Pegrum, S. M. (1970). The locomotion of fibroblasts in culture I. Movements of the leading edge. *Experimental Cell Research*, 59(3):393–398.

Ågren, M. S., Steenfos, H. H., Dabelsteen, S., Hansen, J. B., and Dabelsteen, E. (1999). Proliferation and Mitogenic Response to PDGF-BB of Fibroblasts Isolated from Chronic Venous Leg Ulcers is Ulcer-Age Dependent11Presented in part at the Gordon Research Conference on Wound Repair July 2–7 1995 and at an IBC meeting on Fibrosis in Washingto. *Journal of Investigative Dermatology*, 112(4):463–469.

Aguirre, A., González, A., Navarro, M., Castaño, Ó., Planell, J. a., and Engel, E. (2012). Control of microenvironmental cues with a smart biomaterial composite promotes endothelial progenitor cell angiogenesis. *European cells & materials*, 24:90–106.

Aguirre, A., González, A., Planell, J., and Engel, E. (2010). Extracellular calcium modulates in vitro bone marrow-derived Flk-1+ CD34+ progenitor cell chemotaxis and differentiation through a calcium-sensing receptor. *Biochemical and Biophysical Research Communications*, 393(1):156–161.

Ahn, S. T. and Mustoe, T. A. (1990). Effects of ischemia on ulcer wound healing: a new model in the rabbit ear. *Annals of Plastic Surgery*, 24(1):17–23.

Alblas, J., Ulfman, L., Hordijk, P., and Koenderman, L. (2001). Activation of RhoA and ROCK Are Essential for Detachment of Migrating Leukocytes. *Molecular Biology of the Cell*, 12(7):2137–2145.

Aleksandrowicz, E. (2015). Ethical euthanasia and short-term anesthesia of the chick embryo. *ALTEX*, 32(2):143–147.

Alfadda, T. I., Saleh, A. M. A., Houillier, P., and Geibel, J. P. (2014). Calcium-sensing receptor 20 years later. *AJP: Cell Physiology*, 307(3):C221–C231.

Allen-Hoffmann, B. L. and Rooney, P. J. (2016). Current Innovations for the Treatment of Chronic Wounds. In *Skin Tissue Engineering and Regenerative Medicine*, chapter 13, pages 265–287. Elsevier.

Amin, A. H., Abd Elmageed, Z. Y., Nair, D., Partyka, M. I., Kadowitz, P. J., Belmadani, S., and Matrougui, K. (2010). Modified multipotent stromal cells with epidermal growth factor restore vasculogenesis and blood flow in ischemic hind-limb of type II diabetic mice. *Laboratory Investigation*, 90(7):985–996.

Anderson, K. and Hamm, R. L. (2012). Factors That Impair Wound Healing. *The journal of the American College of Clinical Wound Specialists*, 4(4):84–91.

Arora, P. D., Narani, N., and McCulloch, C. A. (1999). The compliance of collagen gels regulates transforming growth factor-beta induction of alpha-smooth muscle actin in fibroblasts. *The American journal of pathology*, 154(3):871–82.

Arthur, J. M., Lawrence, M. S., Payne, C. R., Rane, M. J., and McLeish, K. R. (2000). The calcium-sensing receptor stimulates JNK in MDCK cells. *Biochem Biophys Res Commun*, 275(2):538–541.

Asahara, T. (1997). Isolation of Putative Progenitor Endothelial Cells for Angiogenesis. *Science*, 275(5302):964–966.

Au, P., Tam, J., Fukumura, D., and Jain, R. K. (2008). Bone marrow-derived mesenchymal stem cells facilitate engineering of long-lasting functional vasculature. *Blood*, 111(9):4551–4558.

Bai, M., Trivedi, S., and Brown, E. M. (1998). Dimerization of the extracellular calcium-sensing receptor (CaR) on the cell surface of CaR-transfected HEK293 cells. *Journal of Biological Chemistry*, 273(36):23605–23610.

Baiguera, S., Macchiarini, P., and Ribatti, D. (2012). Chorioallantoic membrane for in vivo investigation of tissue-engineered construct biocompatibility. *Journal of Biomedical Materials Research Part B: Applied Biomaterials*, 100B(5):1425–1434.

Bainbridge, P. (2013). Wound healing and the role of fibroblasts. *Journal of Wound Care*, 22(8):407–412.

Barralet, J., Gbureck, U., Habibovic, P., Vorndran, E., Gerard, C., Doillon, C. J., Ph, D., Gbureck, U., Ph, D., Habibovic, P., Ph, D., Vorndran, E., Sc, M., Gerard, C., Ph, D., Doillon, C. J., and Ph, D. (2009). Angiogenesis in calcium phosphate scaffolds by inorganic copper ion release. *Tissue engineering. Part A*, 15(7):1601–1609.

Bartholomew, J. R. and Olin, J. W. (2006). Pathophysiology of peripheral arterial disease and risk factors for its development. *Cleveland Clinic Journal of Medicine*, 73(SUPPL.4):8–14.

B.E.C.Nordin (1988). *Calcium in Human Biology*. Springer London.

Bell, E., Ivarsson, B., and Merrill, C. (1979). Production of a tissue-like structure by contraction of collagen lattices by human fibroblasts of different proliferative potential in vitro. *Proceedings of the National Academy of Sciences of the United States of America*, 76(3):1274–8.

Benjamin, L. E., Golijanin, D., Itin, A., Pode, D., and Keshet, E. (1999). Selective ablation of immature blood vessels in established human tumors follows vascular endothelial growth factor withdrawal. *Journal of Clinical Investigation*, 103(2):159–165.

Bergmann, C. and Stumpf, A. (2013). Biomaterials. In *Dental Ceramics*, volume 61 of *Topics in Mining, Metallurgy and Materials Engineering*, chapter 2, pages 502–5. Springer Berlin Heidelberg, Berlin, Heidelberg.

Bhagavathula, N., Dame, M. K., DaSilva, M., Jenkins, W., Aslam, M. N., Perone, P., and Varani, J. (2010). Fibroblast response to gadolinium: role for platelet-derived growth factor receptor. *Investigative radiology*, 45(12):769–77.

Bhagavathula, N., DaSilva, M., Aslam, M. N., Dame, M. K., Warner, R. L., Xu, Y., Fisher, G. J., Johnson, K. J., Swartz, R., and Varani, J. (2009). Regulation of collagen turnover in human skin fibroblasts exposed to a gadolinium-based contrast agent. *Invest Radiol*, 44(8):433–439.

Bhattacharya, S. and Mishra, R. K. (2015). Pressure ulcers: Current understanding and newer modalities of treatment. *Indian journal of plastic surgery : official publication of the Association of Plastic Surgeons of India*, 48(1):4–16.

Binder, K. and Skardal, A. (2016). Human Skin Bioprinting. In *Skin Tissue Engineering and Regenerative Medicine*, volume 30, chapter 20, pages 401–420. Elsevier Inc.

Biswas, S., Roy, S., Banerjee, J., Hussain, S.-R. A., Khanna, S., Meenakshisundaram, G., Kuppusamy, P., Friedman, A., and Sen, C. K. (2010). Hypoxia inducible microRNA 210 attenuates keratinocyte proliferation and impairs closure in a murine model of ischemic wounds. *Proceedings of the National Academy of Sciences of the United States of America*, 107(15):6976–81.

Blakytny, R. and Jude, E. B. (2009). Altered Molecular Mechanisms of Diabetic Foot Ulcers. *The International Journal of Lower Extremity Wounds*, 8(2):95–104.

Boateng, J. S., Matthews, K. H., Stevens, H. N., and Eccleston, G. M. (2008). Wound Healing Dressings and Drug Delivery Systems: A Review. *Journal of Pharmaceutical Sciences*, 97(8):2892–2923.

Bonjour, J.-P. (2011). Calcium and phosphate: a duet of ions playing for bone health. *Journal of the American College of Nutrition*, 30(5 Suppl 1):438S–48S.

Boomsma, R. A. and Geenen, D. L. (2012). Mesenchymal Stem Cells Secrete Multiple Cytokines That Promote Angiogenesis and Have Contrasting Effects on Chemotaxis and Apoptosis. *PLoS ONE*, 7(4):1–8.

Bott, K., Upton, Z., Schrobback, K., Ehrbar, M., Hubbell, J. a., Lutolf, M. P., and Rizzi, S. C. (2010). The effect of matrix characteristics on fibroblast proliferation in 3D gels. *Biomaterials*, 31(32):8454–8464.

Boulton, A. J., Vileikyte, L., Ragnarson-Tennvall, G., and Apelqvist, J. (2005). The global burden of diabetic foot disease. *The Lancet*, 366(9498):1719–1724.

Brauner-Osborne, H., Wellendorph, P., and Jensen, A. (2007). Structure, Pharmacology and Therapeutic Prospects of Family C G-Protein Coupled Receptors. *Current Drug Targets*, 8(1):169–184.

Breitwieser, G. E. (2008). Extracellular calcium as an integrator of tissue function. *The International Journal of Biochemistry & Cell Biology*, 40(8):1467–1480.

Breitwieser, G. E., Miedlich, S. U., and Zhang, M. (2004). Calcium sensing receptors as integrators of multiple metabolic signals. *Cell Calcium*, 35(3):209–216.

Brem, H., Stojadinovic, O., Diegelmann, R. F., Entero, H., Lee, B., Pastar, I., Golinko, M., Rosenberg, H., and Tomic-Canic, M. (2007). Molecular markers in patients with chronic wounds to guide surgical debridement. *Molecular medicine (Cambridge, Mass.)*, 13(1-2):30–9.

Brennan, E. P., Tang, X. H., Stewart-Akers, A. M., Gudas, L. J., and Badylak, S. F. (2008). Chemoattractant activity of degradation products of fetal and adult skin extracellular matrix for keratinocyte progenitor cells. *Journal of Tissue Engineering and Regenerative Medicine*, 2(8):491–498.

Brigido, S. A. (2006). The use of an acellular dermal regenerative tissue matrix in the treatment of lower extremity wounds: A prospective 16-week pilot study. *International Wound Journal*, 3(3):181–187.

Brown, A. (2013). The role of debridement in the healing process. *Nursing times*, 109(40):16–9.

Brown, E. M., Gamba, G., Riccardi, D., Lombardi, M., Butters, R., Kifor, O., Sun, A., Hediger, M. A., Lytton, J., and Hebert, S. C. (1993). Cloning and characterization of an extracellular Ca2+-sensing receptor from bovine parathyroid. *Nature*, 366(6455):575–580.

Bueno, C. R. E., Valentim, D., Marques, V. A. S., Gomes-Filho, J. E., Cintra, L. T. A., Jacinto, R. C., and Dezan-Junior, E. (2016). Biocompatibility and biomineralization assessment of bioceramic-, epoxy-, and calcium hydroxide-based sealers. *Brazilian oral research*, 30(1).

Burlacu, A., Grigorescu, G., Rosca, A.-M., Preda, M. B., and Simionescu, M. (2013). Factors Secreted by Mesenchymal Stem Cells and Endothelial Progenitor Cells Have Complementary Effects on Angiogenesis In Vitro. *Stem Cells and Development*, 22(4):643–653.

Buschmann, J., Härter, L., Gao, S., Hemmi, S., Welti, M., Hild, N., Schneider, O. D., Stark, W. J., Lindenblatt, N., Werner, C. M., Wanner, G. a., and Calcagni, M. (2012). Tissue engineered bone grafts based on biomimetic nanocomposite PLGA/amorphous calcium phosphate scaffold and human adipose-derived stem cells. *Injury*, 43(10):1689–1697.

Bussolati, B., Dunk, C., Grohman, M., Kontos, C. D., Mason, J., and Ahmed, A. (2001). Vascular endothelial growth factor receptor-1 modulates vascular endothelial growth factor-mediated angiogenesis via nitric oxide. *The American journal of pathology*, 159(3):993–1008.

Caley, M. P., Martins, V. L., and O'Toole, E. A. (2015). Metalloproteinases and Wound Healing. *Advances in Wound Care*, 4(4):225–234.

Cardinal, M., Eisenbud, D. E., Armstrong, D. G., Zelen, C., Driver, V., Attinger, C., Phillips, T., and Harding, K. (2009). Serial surgical debridement: a retrospective study

on clinical outcomes in chronic lower extremity wounds. *Wound repair and regeneration*, 17(3):306–311.

Carlson, M. a. and Longaker, M. T. (2004). The fibroblast-populated collagen matrix as a model of wound healing: a review of the evidence. *Wound Repair and Regeneration*, 12(2):134–147.

Carmeliet, P. and Conway, E. M. (2001). Growing better blood vessels. *Nature biotechnology*, 19(11):1019–20.

Carmeliet, P. and Jain, R. K. (2011). Molecular mechanisms and clinical applications of angiogenesis. *Nature*, 473(7347):298–307.

Castaño, O., Sachot, N., Xuriguera, E., Engel, E., Planell, J. a., Park, J.-H., Jin, G.-Z., Kim, T.-H., Kim, J.-H., and Kim, H.-W. (2014). Angiogenesis in Bone Regeneration: Tailored Calcium Release in Hybrid Fibrous Scaffolds. *ACS Applied Materials & Interfaces*, 6(10):7512–7522.

Catalano, E., Cochis, A., Varoni, E., Rimondini, L., and Azzimonti, B. (2013). Tissue-engineered skin substitutes: an overview. *Journal of Artificial Organs*, 16(4):397–403.

Chai, Y. C., Roberts, S. J., Schrooten, J., and Luyten, F. P. (2011). Probing the osteoinductive effect of calcium phosphate by using an in vitro biomimetic model. *Tissue engineering. Part A*, 17(7-8):1083–97.

Chen, C., Schultz, G. S., Bloch, M., Edwards, P. D., Tebes, S., and Mast, B. A. (1999). Molecular and mechanistic validation of delayed healing rat wounds as a model for human chronic wounds. *Wound Repair and Regeneration*, 7(6):486–494.

Chen, W. Y. J., Rogers, A. A., and Lydon, M. J. (1992). Characterization of Biologic Properties of Wound Fluid Collected During Early Stages of Wound Healing. *Journal of Investigative Dermatology*, 99(5):559–564.

Chen, Y., Wang, J., Zhu, X., Tang, Z., Yang, X., Tan, Y., Fan, Y., and Zhang, X. (2015). Enhanced effect of β-tricalcium phosphate phase on neovascularization of porous calcium phosphate ceramics: In vitro and in vivo evidence. *Acta Biomaterialia*, 11(1):435–448.

Chung, J. and Shum-Tim, D. (2012). Neovascularization in Tissue Engineering. *Cells*, 1(4):1246–1260.

Clapham, D. E. (2007). Calcium Signaling. *Cell*, 131(6):1047–1058.

Cohen, S. A. and Sideman, L. (1979). Modification of the o-cresolphthalein complexone method for determining calcium. *Clinical chemistry*, 25(8):1519–20.

Compagna, R., Amato, B., Massa, S., Amato, M., Grande, R., Butrico, L., de Franciscis, S., and Serra, R. (2015). Cell Therapy in Patients with Critical Limb Ischemia. *Stem Cells International*, 2015:1–13.

Coulombe, J., Faure, H., Robin, B., and Ruat, M. (2004). In vitro effects of strontium ranelate on the extracellular calcium-sensing receptor. *Biochemical and Biophysical Research Communications*, 323(4):1184–1190.

Crosby, J. R., Kaminski, W. E., Schatteman, G., Martin, P. J., Raines, E. W., Seifert, R. A., and Bowen-Pope, D. F. (2000). Endothelial cells of hematopoietic origin make a significant contribution to adult blood vessel formation. *Circulation research*, 87(9):728–30.

Cullen, B., Smith, R., Mcculloch, E., Silcock, D., and Morrison, L. (2002). Mechanism of action of PROMOGRAN, a protease modulating matrix, for the treatment of diabetic foot ulcers. *Wound Repair and Regeneration*, 10(1):16–25.

Dai, C., Yuan, Y., Liu, C., Wei, J., Hong, H., Li, X., and Pan, X. (2009). Degradable, antibacterial silver exchanged mesoporous silica spheres for hemorrhage control. *Biomaterials*, 30(29):5364–5375.

Danoux, C. B., Bassett, D. C., Othman, Z., Rodrigues, A. I., Reis, R. L., Barralet, J. E., van Blitterswijk, C. a., and Habibovic, P. (2015). Elucidating the individual effects of calcium and phosphate ions on hMSCs by using composite materials. *Acta Biomaterialia*, 17:1–15.

Das, S., Singh, S., Dowding, J. M., Oommen, S., Kumar, A., Sayle, T. X., Saraf, S., Patra, C. R., Vlahakis, N. E., Sayle, D. C., Self, W. T., and Seal, S. (2012). The induction of angiogenesis by cerium oxide nanoparticles through the modulation of oxygen in intracellular environments. *Biomaterials*, 33(31):7746–7755.

Day, R. M. (2005). Bioactive Glass Stimulates the Secretion of Angiogenic Growth Factors and Angiogenesis in Vitro. *Tissue Engineering*, 11(5-6):768–777.

Day, R. M., Boccaccini, A. R., Shurey, S., Roether, J. a., Forbes, A., Hench, L. L., and Gabe, S. M. (2004). Assessment of polyglycolic acid mesh and bioactive glass for soft-tissue engineering scaffolds. *Biomaterials*, 25(27):5857–5866.

Dead Sea Source (2016). Skin structure.

Demidova-Rice, T. N., Hamblin, M. R., and Herman, I. M. (2012). Acute and impaired wound healing: pathophysiology and current methods for drug delivery, part 1: normal and chronic wounds: biology, causes, and approaches to care. *Advances in skin & wound care*, 25(7):304–14.

Deryugina, E. I. and Quigley, J. P. (2008). Chick Embryo Chorioallantoic Membrane Models to Quantify Angiogenesis Induced by Inflammatory and Tumor Cells or Purified Effector Molecules. In *Methods Enzymol*, volume 444, chapter 2, pages 21–41.

Dobrucki, L. W., Tsutsumi, Y., Kalinowski, L., Dean, J., Gavin, M., Sen, S., Mendizabal, M., Sinusas, A. J., and Aikawa, R. (2010). Analysis of angiogenesis induced by local IGF-1 expression after myocardial infarction using microSPECT-CT imaging. *Journal of Molecular and Cellular Cardiology*, 48(6):1071–1079.

Dorsett-Martin, W. a. and Wysocki, A. B. (2008). Rat Models of Skin Wound Healing. In *Sourcebook of Models for Biomedical Research*, chapter 65, pages 631–638.

Driver, V. R., Lavery, L. A., Reyzelman, A. M., Dutra, T. G., Dove, C. R., Kotsis, S. V., Kim, H. M., and Chung, K. C. (2015). A clinical trial of Integra Template for diabetic foot ulcer treatment. *Wound Repair and Regeneration*, 23(6):891–900.

Duffy, G. P., Ahsan, T., O'Brien, T., Barry, F., and Nerem, R. M. (2009). Bone Marrow–Derived Mesenchymal Stem Cells Promote Angiogenic Processes in a Time- and Dose-Dependent Manner In Vitro. *Tissue Engineering Part A*, 15(9):2459–2470.

Dulbecco, R. and Elkington, J. (1975). Induction of growth in resting fibroblastic cell cultures by Ca++. *Proceedings of the National Academy of Sciences of the United States of America*, 72(4):1584–8.

Dvir, T., Timko, B. P., Kohane, D. S., and Langer, R. (2011). Nanotechnological strategies for engineering complex tissues. *Nature Nanotechnology*, 6(1):13–22.

Eady, R. A. (1988). The basement membrane. Interface between the epithelium and the dermis: structural features. *Archives of dermatology*, 124(5):709–12.

Eaglstein, W. H. (2001). Moist Wound Healing with Occlusive Dressings: A Clinical Focus. *Dermatologic Surgery*, 27(2):175–182.

Eccles, S. A., Court, W., Patterson, L., and Sanderson, S. (2009). In Vitro Assays for Endothelial Cell Functions Related to Angiogenesis: Proliferation, Motility, Tubular Differentiation, and Proteolysis. In Murray, C. and Martin, S., editors, *Angiogenesis Protocols*, volume 467 of *Methods in Molecular Biology*, chapter 9, pages 159–181. Humana Press, Totowa, NJ.

El Ghalbzouri, A., Hensbergen, P., Gibbs, S., Kempenaar, J., van der Schors, R., and Ponec, M. (2004). Fibroblasts facilitate re-epithelialization in wounded human skin equivalents. *Laboratory Investigation*, 84(1):102–112.

Elias, P. M., Ahn, S. K., Denda, M., Brown, B. E., Crumrine, D., Kimutai, L. K., Kömüves, L., Lee, S. H., and Feingold, K. R. (2002). Modulations in Epidermal Calcium Regulate the Expression of Differentiation-Specific Markers. *Journal of Investigative Dermatology*, 119(5):1128–1136.

Engler, A. J., Sen, S., Sweeney, H. L., and Discher, D. E. (2006). Matrix Elasticity Directs Stem Cell Lineage Specification. *Cell*, 126(4):677–689.

Epstein, R. J., Druker, B. J., Irminger, J. C., Jones, S. D., Roberts, T. M., and Stiles, C. D. (1992). Extracellular calcium mimics the actions of platelet-derived growth factor on mouse fibroblasts. *Cell growth & differentiation : the molecular biology journal of the American Association for Cancer Research*, 3(3):157–64.

Estrada, R., Li, N., Sarojini, H., AN, J., Lee, M.-J., and Wang, E. (2009). Secretome from mesenchymal stem cells induces angiogenesis via Cyr61. *Journal of Cellular Physiology*, 219(3):563–571.

European Medicines Agency (2017). Product information: Regranex.

Falanga, V., Isaacs, C., Paquette, D., Downing, G., Kouttab, N., Butmarc, J., Badiavas, E., and Hardin-Young, J. (2002). Wounding of bioengineered skin: Cellular and molecular aspects after injury. *Journal of Investigative Dermatology*, 119(3):653–660.

Fan, G., Goldsmith, P. K., Collins, R., Dunn, C. K., Krapcho, K. J., Rogers, K. V., and Spiegel, A. M. (1997). N-linked glycosylation of the human Ca2+ receptor is essential for its expression at the cell surface. *Endocrinology*, 138(5):1916–1922.

FDA (2008). Warning for Regranex.

Feng, W., Ye, F., Xue, W., Zhou, Z., and Kang, Y. J. (2009). Copper regulation of hypoxia-inducible factor-1 activity. *Molecular pharmacology*, 75(1):174–82.

Fenner, J. and Clark, R. A. (2016). Anatomy, Physiology, Histology, and Immunohistochemistry of Human Skin. In *Skin Tissue Engineering and Regenerative Medicine*, chapter 1, pages 1–17. Elsevier.

Fleck, C. A. and Simman, R. (2010). Modern Collagen Wound Dressings: Function and Purpose. *The Journal of the American College of Certified Wound Specialists*, 2(3):50–54.

Follonier Castella, L., Gabbiani, G., McCulloch, C. a., and Hinz, B. (2010). Regulation of myofibroblast activities: Calcium pulls some strings behind the scene. *Experimental Cell Research*, 316(15):2390–2401.

Formiga, F. R., Tamayo, E., Simón-Yarza, T., Pelacho, B., Prósper, F., and Blanco-Prieto, M. J. (2012). Angiogenic therapy for cardiac repair based on protein delivery systems. *Heart Failure Reviews*, 17(3):449–473.

Franco, S. J. (2005). Regulating cell migration: calpains make the cut. *Journal of Cell Science*, 118(17):3829–3838.

Frykberg, R. G. and Banks, J. (2015). Challenges in the Treatment of Chronic Wounds. *Advances in Wound Care*, 4(9):560–582.

Furth, M. E. (2016). Translational Research of Skin Substitutes and Wound Healing Products. In *Skin Tissue Engineering and Regenerative Medicine*, pages 421–429. Elsevier.

Gabbiani, G., Ryan, G. B., and Majne, G. (1971). Presence of modified fibroblasts in granulation tissue and their possible role in wound contraction. *Experientia*, 27(5):549–50.

Gerhardt, H., Golding, M., Fruttiger, M., Ruhrberg, C., Lundkvist, A., Abramsson, A., Jeltsch, M., Mitchell, C., Alitalo, K., Shima, D., and Betsholtz, C. (2003). VEGF guides angiogenic sprouting utilizing endothelial tip cell filopodia. *Journal of Cell Biology*, 161(6):1163–1177.

Gerhardt, L. C., Widdows, K. L., Erol, M. M., Burch, C. W., Sanz-Herrera, J. A., Ochoa, I., Stämpfli, R., Roqan, I. S., Gabe, S., Ansari, T., and Boccaccini, A. R. (2011). The pro-angiogenic properties of multi-functional bioactive glass composite scaffolds. *Biomaterials*, 32(17):4096–4108.

Gilaberte, Y., Prieto-Torres, L., Pastushenko, I., and Juarranz, Á. (2016). Anatomy and Function of the Skin. In *Nanoscience in Dermatology*, chapter 1, pages 1–14. Elsevier Inc.

Gillette, R. L., Swaim, S. F., Sartin, E. A., Bradley, D. M., and Coolman, S. L. (2001). Effects of a bioactive glass on healing of closed skin wounds in dogs. *American Journal of Veterinary Research*, 62(7):1149–1153.

Goh, E., Kirby, G., Jayakumar, R., Liang, X.-J., and Tan, A. (2016). Accelerated Wound Healing Using Nanoparticles. In *Nanoscience in Dermatology*, chapter 23, pages 287–306. Elsevier.

Goodpaster, T., Legesse-Miller, A., Hameed, M. R., Aisner, S. C., Randolph-Habecker, J., and Coller, H. A. (2008). An Immunohistochemical Method for Identifying Fibroblasts in Formalin-fixed, Paraffin-embedded Tissue. *Journal of Histochemistry & Cytochemistry*, 56(4):347–358.

Gorustovich, A. A., Roether, J. A., and Boccaccini, A. R. (2010). Effect of Bioactive Glasses on Angiogenesis: A Review of In Vitro and In Vivo Evidences. *Tissue Engineering Part B: Reviews*, 16(2):199–207.

Gorustovich, A. A., Vargas, G. E., Bretcanu, O., Vera Mesones, R., Porto López, J. M., and Boccaccini, A. R. (2008). Novel bioassay to evaluate biocompatibility of bioactive glass scaffolds for tissue engineering. *Advances in Applied Ceramics*, 107(5):274–276.

Gottrup, F. (2004). A specialized wound-healing center concept: importance of a multidisciplinary department structure and surgical treatment facilities in the treatment of chronic wounds. *The American Journal of Surgery*, 187(5):S38–S43.

Green, H., Kehinde, O., and Thomas, J. (1979). Growth of cultured human epidermal cells into multiple epithelia suitable for grafting. *Proceedings of the National Academy of Sciences*, 76(11):5665–5668.

Grinnell, F. (2003). Fibroblast biology in three-dimensional collagen matrices. *Trends in Cell Biology*, 13(5):264–269.

Groeber, F., Holeiter, M., Hampel, M., Hinderer, S., and Schenke-Layland, K. (2011). Skin tissue engineering - In vivo and in vitro applications. *Advanced Drug Delivery Reviews*, 63(4-5):352–366.

Groves, A. and Clawrence, J. (1986). Alginate dressing site haemostat. *Annals of the Royal College of Surgeons of England*, 68:1–2.

Gruber, R., Kandler, B., Holzmann, P., Vögele-Kadletz, M., Losert, U., Fischer, M. B., and Watzek, G. (2005). Bone Marrow Stromal Cells Can Provide a Local Environment That Favors Migration and Formation of Tubular Structures of Endothelial Cells. *Tissue Engineering*, 11(5-6):896–903.

Grzesiak, J. J., Davis, G. E., Kirchhofer, D., and Pierschbacher, M. D. (1992). Regulation of alpha 2 beta 1-mediated fibroblast migration on type I collagen by shifts in the concentrations of extracellular Mg2+ and Ca2+. *The Journal of cell biology*, 117(5):1109–17.

Grzesiak, J. J. and Pierschbacher, M. D. (1995). Shifts in the concentrations of magnesium and calcium in early porcine and rat wound fluids activate the cell migratory response. *Journal of Clinical Investigation*, 95(1):227–233.

Günter, C. and Machens, H.-G. (2012). New Strategies in Clinical Care of Skin Wound Healing. *European Surgical Research*, 49(1):16–23.

Guo, S. and DiPietro, L. A. (2010). Factors Affecting Wound Healing. *Journal of Dental Research*, 89(3):219–229.

Gupta, P. K., Chullikana, A., Parakh, R., Desai, S., Das, A., Gottipamula, S., Krishnamurthy, S., Anthony, N., Pherwani, A., and Majumdar, A. S. (2013). A double blind randomized placebo controlled phase I/II study assessing the safety and efficacy of allogeneic bone marrow derived mesenchymal stem cell in critical limb ischemia. *Journal of translational medicine*, 11(72):143.

Habibovic, P., Bassett, D. C., Doillon, C. J., Gerard, C., McKee, M. D., and Barralet, J. E. (2010). Collagen Biomineralization In Vivo by Sustained Release of Inorganic Phosphate Ions. *Advanced Materials*, 22(16):1858–1862.

Hagedorn, M., Balke, M., Schmidt, A., Bloch, W., Kurz, H., Javerzat, S., Rousseau, B., Wilting, J., and Bikfalvi, A. (2004). VEGF Coordinates Interaction of Pericytes and Endothelial Cells During Vasculogenesis and Experimental Angiogenesis. *Developmental Dynamics*, 230(1):23–33.

Han, S. K. (2015). Basics of Wound Healing. In *Innovations and Advances in Wound Healing*, chapter 1, pages 1–287.

Han, S.-K. (2016). *Innovations and Advances in Wound Healing*. Springer Berlin Heidelberg, Berlin, Heidelberg.

Handel, M., Hammer, T. R., Nooeaid, P., Boccaccini, A. R., and Hoefer, D. (2013). 45S5-Bioglass ® -Based 3D-Scaffolds Seeded with Human Adipose Tissue-Derived Stem Cells Induce In Vivo Vascularization in the CAM Angiogenesis Assay. *Tissue Engineering Part A*, 19(23-24):2703–2712.

Hansen, S. L., Young, D. M., and Boudreau, N. J. (2003). HoxD3 expression and collagen synthesis in diabetic fibroblasts. *Wound Repair and Regeneration*, 11(6):474–480.

Harding, K., Sumner, M., and Cardinal, M. (2013). A prospective, multicentre, randomised controlled study of human fibroblast-derived dermal substitute (Dermagraft) in patients with venous leg ulcers. *International Wound Journal*, 10(2):132–137.

Harding, K. G. (2002). Science, medicine, and the future: Healing chronic wounds. *BMJ*, 324(7330):160–163.

Hare, J. M., Traverse, J. H., Henry, T. D., Dib, N., Strumpf, R. K., Schulman, S. P., Gerstenblith, G., DeMaria, A. N., Denktas, A. E., Gammon, R. S., Hermiller, J. B. J., Reisman, M. A., Schaer, G. L., and Sherman, W. (2013). A randomized, double-blind, placebo-controlled, dose-escalation study of intravenous adult human mesenchymal stem cells (Prochymal) after acute myocardial infarction. *Journal*, 54(24):2277–2286.

Haro Durand, L. A., Vargas, G. E., Romero, N. M., Vera-Mesones, R., Porto-López, J. M., Boccaccini, A. R., Zago, M. P., Baldi, A., and Gorustovich, A. (2015). Angiogenic effects of ionic dissolution products released from a boron-doped 45S5 bioactive glass. *J. Mater. Chem. B*, 3(6):1142–1148.

Harris, I. R., Yee, K. C., Walters, C. E., Cunliffe, W. J., Kearney, J. N., Wood, E. J., and Ingham, E. (1995). Cytokine and protease levels in healing and non-healing chronic venous leg ulcers. *Experimental Dermatology*, 4(6):342–349.

Hasan, A., Murata, H., Falabella, A., Ochoa, S., Zhou, L., Badiavas, E., and Falanga, V. (1997). Dermal fibroblasts from venous ulcers are unresponsive to the action of transforming growth factor-beta 1. *Journal of dermatological science*, 16(1):59–66.

Hastings, G. (1989). Definitions in Biomaterials. *Biomaterials*, 10(3):216.

Heath, J. P. and Dunn, G. A. (1978). Cell to substratum contacts of chick fibroblasts and their relation to the microfilament system. A correlated interference-reflexion and high-voltage electron-microscope study. *Journal of cell science*, 29(1):197–212.

Helisch, A. and Schaper, W. (2003). Arteriogenesis: the development and growth of collateral arteries. *Microcirculation (New York, N.Y. : 1994)*, 10(1):83–97.

Hench, L. L., Splinter, R. J., Allen, W. C., and Greenlee, T. K. (1971). Bonding mechanisms at the interface of ceramic prosthetic materials. *Journal of Biomedical Materials Research*, 5(6):117–141.

Hench, L. L. and Wilson, J. (1984). Surface-active biomaterials. *Science*, 226(4675):630–6.

Hennings, H., Michael, D., Cheng, C., Steinert, P., Holbrook, K., and Yuspa, S. H. (1980). Calcium regulation of growth and differentiation of mouse epidermal cells in culture. *Cell*, 19(1):245–54.

Herber, O. R., Schnepp, W., and Rieger, M. A. (2007). A systematic review on the impact of leg ulceration on patients' quality of life. *Health and Quality of Life Outcomes*, 5(1):44.

Hershfinkel, M., Silverman, W. F., and Sekler, I. (2007). The zinc sensing receptor, a link between zinc and cell signaling. *Molecular medicine (Cambridge, Mass.)*, 13(7-8):331–6.

Hinz, B., Celetta, G., Tomasek, J. J., Gabbiani, G., and Chaponnier, C. (2001). Alpha-Smooth Muscle Actin Expression Upregulates Fibroblast Contractile Activity. *Molecular Biology of the Cell*, 12(9):2730–2741.

Hofer, A. M. (2005). Another dimension to calcium signaling: a look at extracellular calcium. *Journal of Cell Science*, 118(5):855–862.

Hofer, A. M. and Brown, E. M. (2003). Calcium: Extracellular calcium sensing and signalling. *Nature Reviews Molecular Cell Biology*, 4(7):530–538.

Hoppe, A., Güldal, N. S., and Boccaccini, A. R. (2011). A review of the biological response to ionic dissolution products from bioactive glasses and glass-ceramics. *Biomaterials*, 32(11):2757–2774.

Horwitz, E. M., Gordon, P. L., Koo, W. K. K., Marx, J. C., Neel, M. D., McNall, R. Y., Muul, L., and Hofmann, T. (2002). Isolated allogeneic bone marrow-derived mesenchymal cells engraft and stimulate growth in children with osteogenesis imperfecta:

Implications for cell therapy of bone. *Proceedings of the National Academy of Sciences*, 99(13):8932–8937.

Hou, D., Youssef, E. A.-S., Brinton, T. J., Zhang, P., Rogers, P., Price, E. T., Yeung, A. C., Johnstone, B. H., Yock, P. G., and March, K. L. (2005). Radiolabeled cell distribution after intramyocardial, intracoronary, and interstitial retrograde coronary venous delivery: implications for current clinical trials. *Circulation*, 112(9 Suppl):I150–I156.

Hu, X. and Beeton, C. (2010). Detection of Functional Matrix Metalloproteinases by Zymography. *Journal of Visualized Experiments*, (45):1–4.

Hughes, O. B., Rakosi, A., Macquhae, F., Herskovitz, I., Fox, J. D., and Kirsner, R. S. (2016). A Review of Cellular and Acellular Matrix Products. *Plastic and Reconstructive Surgery*, 138(3 Suppl):138S–147S.

Hurtel-Lemaire, A. S., Mentaverri, R., Caudrillier, A., Cournarie, F., Wattel, A., Kamel, S., Terwilliger, E. F., Brown, E. M., and Brazier, M. (2009). The calcium-sensing receptor is involved in Strontium ranelate-induced osteoclast apoptosis new insights into the associated signaling pathways. *Journal of Biological Chemistry*, 284(1):575–584.

Huttenlocher, A. and Horwitz, A. R. (2011). Integrins in cell migration. *Cold Spring Harbor Perspectives in Biology*, 3(9):1–16.

Huttenlocher, A., Sandborg, R. R., and Horwitz, A. F. (1995). Adhesion in cell migration. *Current opinion in cell biology*, 7(5):697–706.

Hwang, S. H., Lee, B. H., Choi, S. H., Kim, H. J., Won, K. J., Lee, H. M., Rhim, H., Kim, H. C., and Nah, S. Y. (2016). Effects of gintonin on the proliferation, migration, and tube formation of human umbilical-vein endothelial cells: Involvement of lysophosphatidic-acid receptors and vascular-endothelial-growth-factor signaling. *Journal of Ginseng Research*, 40(4):325–333.

Ignacio, G., El-Amin, I., and Mendenhall, V. (2016). Animal Models for Wound Healing. In *Skin Tissue Engineering and Regenerative Medicine*, chapter 19, pages 387–400. Elsevier Inc.

International Consensus (2010). Acellular Matrices for the Treatment of Wounds. An expert working group review. *Wounds International*.

International Diabetes Federation (2017). Diabetes: facts and figures.

Ito, M., Liu, Y., Yang, Z., Nguyen, J., Liang, F., Morris, R. J., and Cotsarelis, G. (2005). Stem cells in the hair follicle bulge contribute to wound repair but not to homeostasis of the epidermis. *Nature medicine*, 11(12):1351–1354.

Ivanova, E. P., Bazaka, K., and Crawford, R. J. (2014). *New Functional Biomaterials for Medicine and Healthcare*.

Jacobo, S. M. P. and Kazlauskas, A. (2015). Insulin-like Growth Factor 1 (IGF-1) Stabilizes Nascent Blood Vessels. *Journal of Biological Chemistry*, 290(10):6349–6360.

Jain, R. K., Au, P., Tam, J., Duda, D. G., and Fukumura, D. (2005). Engineering vascularized tissue. *Nature Biotechnology*, 23(7):821–823.

Janeczek Portalska, K., Leferink, A., Groen, N., Fernandes, H., Moroni, L., van Blitterswijk, C., and de Boer, J. (2012). Endothelial Differentiation of Mesenchymal Stromal Cells. *PLoS ONE*, 7(10):e46842.

Jankunas, V., Bagdonas, R., Samsanavicius, D., and Rimdeika, R. (2007). An analysis of the effectiveness of skin grafting to treat chronic venous leg ulcers. *Wounds: A Compendium of Clinical Research & Practice*, 19(5):128–137.

Järbrink, K., Ni, G., Sönnergren, H., Schmidtchen, A., Pang, C., Bajpai, R., and Car, J. (2016). Prevalence and incidence of chronic wounds and related complications: a protocol for a systematic review. *Systematic Reviews*, 5(1):152.

Jebahi, S., Oudadesse, H., Jardak, N., Khayat, I., Keskes, H., Khabir, A., Rebai, T., El Feki, H., and El Feki, A. (2013). Biological therapy of strontium-substituted bioglass for soft tissue wound-healing: Responses to oxidative stress in ovariectomised rats. *Annales Pharmaceutiques Françaises*, 71(4):234–242.

Jenkins, W., Perone, P., Walker, K., Bhagavathula, N., Aslam, M. N., DaSilva, M., Dame, M. K., and Varani, J. (2011). Fibroblast Response to Lanthanoid Metal Ion Stimulation: Potential Contribution to Fibrotic Tissue Injury. *Biological Trace Element Research*, 144(1-3):621–635.

Jensen, A. and Brauner-Osborne, H. (2007). Allosteric Modulation of the Calcium-Sensing Receptor. *Current Neuropharmacology*, 5(3):180–186.

Johnson, K. E. and Wilgus, T. A. (2014). Vascular Endothelial Growth Factor and Angiogenesis in the Regulation of Cutaneous Wound Repair. *Advances in wound care*, 3(10):647–661.

Jones, J. R. (2013). Review of bioactive glass: From Hench to hybrids. *Acta Biomaterialia*, 9(1):4457–4486.

Jones, V. (2006). Wound dressings. *BMJ*, 332(7544):777–780.

Kalka, C. and Baumgartner, I. (2008). Gene and stem cell therapy in peripheral arterial occlusive disease. *Vascular Medicine*, 13(2):157–172.

Kamudzandu, M., Roach, P., Fricker, R. A., and Yang, Y. (2015). Nanofibrous scaffolds supporting optimal central nervous system regeneration : an evidence-based review. *Journal of Neurorestoratology*, 3:123–131.

Kang, W. J., Kang, H.-J., Kim, H.-S., Chung, J.-K., Lee, M. C., and Lee, D. S. (2006). Tissue distribution of 18F-FDG-labeled peripheral hematopoietic stem cells after intracoronary administration in patients with myocardial infarction. *Journal of nuclear medicine : official publication, Society of Nuclear Medicine*, 47(8):1295–301.

Kawai, K., Larson, B. J., Ishise, H., Carre, A. L., Nishimoto, S., Longaker, M., and Lorenz, H. P. (2011). Calcium-Based Nanoparticles Accelerate Skin Wound Healing. *PLoS ONE*, 6(11):e27106.

Keshaw, H., Forbes, A., and Day, R. M. (2005). Release of angiogenic growth factors from cells encapsulated in alginate beads with bioactive glass. *Biomaterials*, 26(19):4171–4179.

Kifor, O., MacLeod, R. J., Diaz, R., Bai, M., Yamaguchi, T., Yao, T., Kifor, I., and Brown, E. M. (2001). Regulation of MAP kinase by calcium-sensing receptor in bovine parathyroid and CaR-transfected HEK293 cells. *American journal of physiology. Renal physiology*, 280(2):F291–302.

Kim-Park, W. K., Moore, M. A., Hakki, Z. W., and Kowolik, M. J. (1997). Activation of the neutrophil respiratory burst requires both intracellular and extracellular calcium. *Annals of the New York Academy of Sciences*, 832:394–404.

Kinnaird, T. (2004). Local Delivery of Marrow-Derived Stromal Cells Augments Collateral Perfusion Through Paracrine Mechanisms. *Circulation*, 109(12):1543–1549.

Kirsner, R. S., Sabolinski, M. L., Parsons, N. B., Skornicki, M., and Marston, W. A. (2015). Comparative effectiveness of a bioengineered living cellular construct vs. a dehydrated human amniotic membrane allograft for the treatment of diabetic foot ulcers in a real world setting. *Wound Repair and Regeneration*, 23(5):737–744.

Ko, H., Cho, C.-H., and Roberts, M. S. (2005). Internet uses and gratifications: A structural equation model of interactive advertising. *Journal of Advertising*, 34(2):57–70.

Ko, J. and Lung, M. (2012). In vitro Human Umbilical Vein Endothelial Cells (HUVEC) Tube-formation Assay. *BIO-PROTOCOL*, 2(18):2–7.

Kobilka, B. K. (2007). G protein coupled receptor structure and activation. *Biochimica et Biophysica Acta (BBA) - Biomembranes*, 1768(4):794–807.

Koç, O. N. and Gerson, S. L. (2003). Akt helps stem cells heal the heart. *Nature Medicine*, 9(9):1109–1110.

Koolman, J. and Roehm, K. H. (2005). *Color atlas of biochemistry*.

Kulesz-Martin, M. F., Fabian, D., and Bertram, J. S. (1984). Differential calcium requirements for growth of mouse skin epithelial and fibroblast cells. *Cell and tissue kinetics*, 17(5):525–33.

Kumar, P., Kumar, S., Udupa, E. P., Kumar, U., Rao, P., and Honnegowda, T. (2015). Role of angiogenesis and angiogenic factors in acute and chronic wound healing. *Plastic and Aesthetic Research*, 2(5):243.

Kuo, Y.-R., Wang, C.-T., Cheng, J.-t., Wang, F.-S., Chiang, Y.-C., and Wang, C.-J. (2011). Bone Marrow–Derived Mesenchymal Stem Cells Enhanced Diabetic Wound Healing through Recruitment of Tissue Regeneration in a Rat Model of Streptozotocin-Induced Diabetes. *Plastic and Reconstructive Surgery*, 128(4):872–880.

Kwon, H. M., Hur, S.-M., Park, K.-Y., Kim, C.-K., Kim, Y.-M., Kim, H.-S., Shin, H.-C., Won, M.-H., Ha, K.-S., Kwon, Y.-G., Lee, D. H., and Kim, Y.-M. (2014). Multiple paracrine factors secreted by mesenchymal stem cells contribute to angiogenesis. *Vascular Pharmacology*, 63(1):19–28.

Ladwig, G. P., Robson, M. C., Liu, R., Kuhn, M. A., Muir, D. F., and Schultz, G. S. (2002). Ratios of activated matrix metalloproteinase-9 to tissue inhibitor of matrix metalloproteinase-1 in wound fluids are inversely correlated with healing of pressure ulcers. *Wound Repair and Regeneration*, 10(1):26–37.

Lali, F. V., Martin, Y. H., and Metcalfe, A. D. (2016). Advances in Biopharmaceutical Agents and Growth Factors for Wound Healing and Scarring. In *Skin Tissue Engineering and Regenerative Medicine*, chapter 17, pages 337–355. Elsevier.

Lansdown, A. B., Sampson, B., and Rowe, A. (1999). Sequential changes in trace metal, metallothionein and calmodulin concentrations in healing skin wounds. *Journal of anatomy*, 195:375–86.

Lansdown, A. B. G. (2002a). Calcium: a potential central regulator in wound healing in the skin. *Wound repair and regeneration : official publication of the Wound Healing Society [and] the European Tissue Repair Society*, 10(5):271–85.

Lansdown, a. B. G. (2002b). Silver. 2: Toxicity in mammals and how its products aid wound repair. *Journal of wound care*, 11(5):173–177.

Lauffenburger, D. A. and Horwitz, A. F. (1996). Cell migration: a physically integrated molecular process. *Cell*, 84(3):359–69.

Leblebici, B., Turhan, N., Adam, M., and Akman, M. N. (2007). Clinical and epidemiologic evaluation of pressure ulcers in patients at a university hospital in Turkey. *Journal of wound, ostomy, and continence nursing : official publication of The Wound, Ostomy and Continence Nurses Society / WOCN*, 34(4):407–11.

Lee, K. C. and Jung, D.-I. (2016). An Outline of the Integumentary System. In *Integumentary Physical Therapy*, chapter 1, pages 1–42.

Leu, A. and Leach, J. K. (2008). Proangiogenic Potential of a Collagen/Bioactive Glass Substrate. *Pharmaceutical Research*, 25(5):1222–1229.

Li, F., Li, W., Johnson, S., Ingram, D., Yoder, M., and Badylak, S. (2004). Low-molecular-weight peptides derived from extracellular matrix as chemoattractants for primary endothelial cells. *Endothelium : journal of endothelial cell research*, 11(3-4):199–206.

Li, H., He, J., Yu, H., Green, C. R., and Chang, J. (2016). Bioglass promotes wound healing by affecting gap junction connexin 43 mediated endothelial cell behavior. *Biomaterials*, 84:64–75.

Lin, C., Mao, C., Zhang, J., Li, Y., and Chen, X. (2012). Healing effect of bioactive glass ointment on full-thickness skin wounds. *Biomedical Materials*, 7(4):045017.

Lin, Y., Brown, R. F., Jung, S. B., and Day, D. E. (2014). Angiogenic effects of borate glass microfibers in a rodent model. *Journal of Biomedical Materials Research - Part A*, 102(12):4491–4499.

Liu, Y. C., Margolis, D. J., and Rivkah Isseroff, R. (2011). Does Inflammation Have a Role in the Pathogenesis of Venous Ulcers?: A Critical Review of the Evidence. *Journal of Investigative Dermatology*, 131(4):818–827.

Lovas, K. (2002). *Apligraf(R) the role of economic evaluations in the reimbursement strategy in a case of tissue-engineered product*. PhD thesis, Semmelweis University.

Lu, D., Chen, B., Liang, Z., Deng, W., Jiang, Y., Li, S., Xu, J., Wu, Q., Zhang, Z., Xie, B., and Chen, S. (2011). Comparison of bone marrow mesenchymal stem cells with bone marrow-derived mononuclear cells for treatment of diabetic critical limb ischemia and foot ulcer: A double-blind, randomized, controlled trial. *Diabetes Research and Clinical Practice*, 92(1):26–36.

Lugović, L., Lipozenocić, J., and Jakić-Razumović, J. (2001). Atopic dermatitis: immunophenotyping of inflammatory cells in skin lesions. *International journal of dermatology*, 40(8):489–94.

Lyder, C. H. and Ayello, E. A. (2008). Pressure Ulcers: A Patient Safety Issue. In *Patient Safety and Quality: An Evidence-Based Handbook for Nurses*, chapter 12, pages 268–299. Agency for Healthcare Research and Quality (US).

Ma, W., Yang, X., Ma, L., Wang, X., Zhang, L., Yang, G., Han, C., and Gou, Z. (2014). Fabrication of bioactive glass-introduced nanofibrous membranes with multifunctions for potential wound dressing. *RSC Adv.*, 4(104):60114–60122.

Magee, A. I., Lytton, N. A., and Watt, F. M. (1987). Calcium-induced changes in cytoskeleton and motility of cultured human keratinocytes. *Experimental Cell Research*, 172(1):43–53.

Maione, A. G., Brudno, Y., Stojadinovic, O., Park, L. K., Smith, A., Tellechea, A., Leal, E. C., Kearney, C. J., Veves, A., Tomic-Canic, M., Mooney, D. J., and Garlick, J. a. (2015). Three-dimensional human tissue models that incorporate diabetic foot ulcer-derived fibroblasts mimic in vivo features of chronic wounds. *Tissue engineering. Part C, Methods*, 21(5):499–508.

Maiti, A., Hait, N. C., and Beckman, M. J. (2008). Extracellular Calcium-sensing Receptor Activation Induces Vitamin D Receptor Levels in Proximal Kidney HK-2G Cells by a Mechanism That Requires Phosphorylation of p38 MAPK. *Journal of Biological Chemistry*, 283(1):175–183.

Majeed, A. A. and Naimi, R. A. A. (2012). Role of Hydroxyapatite in Healing of Experimentally Induced Cutaneous Wound in Rabbits. *Al-Anbar J. Vet. Sci.*, 5(1):74–81.

Mann, B. K., Gobin, A. S., Tsai, A. T., Schmedlen, R. H., and West, J. L. (2001). Smooth muscle cell growth in photopolymerized hydrogels with cell adhesive and proteolytically degradable domains: synthetic ECM analogs for tissue engineering. *Biomaterials*, 22(22):3045–3051.

Mao, C., Lin, C., and Chen, X. (2014). Enhanced healing of full-thickness diabetic wounds using bioactive glass and Yunnan baiyao ointments. *Journal of Wuhan University of Technology-Mater. Sci. Ed.*, 29(5):1063–1070.

Maragoudakis, M. E. (2000). Angiogenesis in health and disease. *General Pharmacology: The Vascular System*, 35(5):225–226.

Margolis, D. J., Kantor, J., and Berlin, J. A. (1999). Healing of diabetic neuropathic foot ulcers receiving standard treatment: A meta-analysis. *Diabetes Care*, 22(5):692–695.

Marquardt, Y., Amann, P. M., Heise, R., Czaja, K., Steiner, T., Merk, H. F., Skazik-Voogt, C., and Baron, J. M. (2015). Characterization of a novel standardized human three-dimensional skin wound healing model using non-sequential fractional ultrapulsed CO2 laser treatments. *Lasers in Surgery and Medicine*, 47(3):257–265.

Marston, W. A., Hanft, J., Norwood, P., and Pollak, R. (2003). The Efficacy and Safety of Dermagraft in Improving the Healing of Chronic Diabetic Foot Ulcers: Results of a prospective randomized trial. *Diabetes Care*, 26(6):1701–1705.

Mast, B. A. and Schultz, G. S. (1996). Interactions of cytokines, growth factors, and proteases in acute and chronic wounds. *Wound repair and regeneration*, 4(4):411–420.

McGrath, J., Eady, R., and Pope, F. (2010). Anatomy and Organization of Human Skin. In *Rook's Textbook of Dermatology*, number April, chapter 3, pages 3.1–3.84. 8th edition.

McGrath, J. A., Eady, R. A. J., and Pope, F. M. (2004). Anatomy and Organization of Human Skin. In Burns, T., Breathnach, S., Cox, N., and Griffiths, C., editors, *Rook's Textbook of Dermatology*, pages 45–128. Blackwell Publishing, Inc., Malden, Massachusetts, USA, 7th edition.

McNeil, S. E., Hobson, S. a., Nipper, V., and Rodland, K. D. (1998). Functional calcium-sensing receptors in rat fibroblasts are required for activation of SRC kinase and mitogen-activated protein kinase in response to extracellular calcium. *The Journal of biological chemistry*, 273(2):1114–20.

McQuilling, J. P., Vines, J. B., and Mowry, K. C. (2017). In vitro assessment of a novel, hypothermically stored amniotic membrane for use in a chronic wound environment. *International wound journal*, (7):1–13.

Mebratu, Y. and Tesfaigzi, Y. (2009). How ERK1/2 Activation Controls Cell Proliferation and Cell Death Is Subcellular Localization the Answer? *Cell cycle (Georgetown, Tex.)*, 8(8):1168–1175.

Medina, A., Scott, P. G., Ghahary, A., and Tredget, E. E. (2005). Pathophysiology of Chronic Nonhealing Wounds. *Journal of Burn Care & Rehabilitation*, 26(4):306–319.

Menon, G. K., Grayson, S., and Elias, P. M. (1985). Ionic Calcium Reservoirs in Mammalian Epidermis: Ultrastructural Localization by Ion-Capture Cytochemistry. *Journal of Investigative Dermatology*, 84(6):508–512.

Metcalfe, A. D. and Ferguson, M. W. (2007). Tissue engineering of replacement skin: the crossroads of biomaterials, wound healing, embryonic development, stem cells and regeneration. *Journal of The Royal Society Interface*, 4(14):413–437.

Michaels, J., Churgin, S. S., Blechman, K. M., Greives, M. R., Aarabi, S., Galiano, R. D., and Gurtner, G. C. (2007). db/db mice exhibit severe wound-healing impairments compared with other murine diabetic strains in a silicone-splinted excisional wound model. *Wound Repair and Regeneration*, 15(5):665–670.

Miguez-pacheco, V., Greenspan, D., Hench, L. L., and Boccaccini, A. R. (2015). Bioactive glasses in soft tissue repair. *American Ceramic Society Bulletin*, 94(6):27–31.

Mikaelsson, M. E. (1991). The Role of Calcium in Coagulation and Anticoagulation. In *Coagulation and Blood Transfusion*, pages 29–37. Springer US, Boston, MA.

Milara, J., Mata, M., Serrano, A., Peiró, T., Morcillo, E. J., and Cortijo, J. (2010). Extracellular calcium-sensing receptor mediates human bronchial epithelial wound repair. *Biochemical Pharmacology*, 80(2):236–246.

Miller, M. A., Kendall, M. R., Jain, M. K., Larson, P. R., Madden, A. S., and Tas, A. C. (2012). Testing of Brushite (CaHPO 4 ·2H 2 O) in Synthetic Biomineralization Solutions and In Situ Crystallization of Brushite Micro-Granules. *Journal of the American Ceramic Society*, 95(7):2178–2188.

Mizumoto, T. (1987). Effects of the calcium ion on the wound healing process. *[Hokkaido igaku zasshi] The Hokkaido journal of medical science*, 62(2):332–45.

Montfrans, C. V., Stok, M., and Geerkens, M. (2014). Biology of chronic wounds and new treatment strategies. *Phlebology*, 29(1_suppl):165–167.

Mostow, E. N., Haraway, G. D., Dalsing, M., Hodde, J. P., and King, D. (2005). Effectiveness of an extracellular matrix graft (OASIS Wound Matrix) in the treatment of chronic leg ulcers: A randomized clinical trial. *Journal of Vascular Surgery*, 41(5):837–843.

Mouthuy, P.-A. and Ye, H. (2011). Biomaterials: Electrospinning. In Moo-Young, M., editor, *Comprehensive Biotechnology*, number December, chapter 5, pages 23–36. MA: Academic Press.

Murakami, M. (2012). Signaling Required for Blood Vessel Maintenance: Molecular Basis and Pathological Manifestations. *International Journal of Vascular Medicine*, 2012:1–15.

Mustoe, T. A., O??Shaughnessy, K., and Kloeters, O. (2006). Chronic Wound Pathogenesis and Current Treatment Strategies: A Unifying Hypothesis. *Plastic and Reconstructive Surgery*, 117(SUPPLEMENT):35S–41S.

Navarro, M., Ginebra, M.-p., Clément, J., Salvador, M., Gloria, A., and Planell, J. A. (2003). Physicochemical Degradation of Titania-Stabilized Soluble Phosphate Glasses for Medical Applications. *Journal of the American Ceramic Society*, 86(8):1345–1352.

Nejati, R., Kovacic, D., and Slominski, A. (2013). Neuro-immune-endocrine functions of the skin: an overview. *Expert Review of Dermatology*, 8(6):581–583.

Nerem, R. M. (1992). Tissue engineering in the USA. *Medical & biological engineering & computing*, 30(4):CE8–12.

Nestle, F. O. and Nickoloff, B. J. (1995). A fresh morphological and functional look at dermal dendritic cells. *Journal of cutaneous pathology*, 22(5):385–93.

Nunan, R., Harding, K. G., and Martin, P. (2014). Clinical challenges of chronic wounds: searching for an optimal animal model to recapitulate their complexity. *Disease Models & Mechanisms*, 7(11):1205–1213.

Oh, S.-Y., Park, K.-S., Kim, J.-A., and Choi, K.-Y. (2002). Differential modulation of zinc-stimulated p21(Cip/WAF1) and cyclin D1 induction by inhibition of PI3 kinase in HT-29 colorectal cancer cells. *Experimental & molecular medicine*, 34(1):27–31.

Oliveira, H., Catros, S., Boiziau, C., Siadous, R., Marti-Munoz, J., Bareille, R., Rey, S., Castano, O., Planell, J., Amédée, J., and Engel, E. (2016). The proangiogenic potential of a novel calcium releasing biomaterial: Impact on cell recruitment. *Acta Biomaterialia*, 29:435–445.

Oliveira, H., Catros, S., Castano, O., Rey, S., Siadous, R., Clift, D., Marti-Munoz, J., Batista, M., Bareille, R., Planell, J., Engel, E., and Amédée, J. (2017). The proangiogenic potential of a novel calcium releasing composite biomaterial: Orthotopic in vivo evaluation. *Acta Biomaterialia*, 54:377–385.

Olszak, I. T., Poznansky, M. C., Evans, R. H., Olson, D., Kos, C., Pollak, M. R., Brown, E. M., and Scadden, D. T. (2000). Extracellular calcium elicits a chemokinetic response from monocytes in vitro and in vivo. *Journal of Clinical Investigation*, 105(9):1299–1305.

Organogenesis (2010). Apligraf : What is Apligraf?

Ostomel, T. A., Shi, Q., Tsung, C. K., Liang, H., and Stucky, G. D. (2006a). Spherical bioactive glass with enhanced rates of hydroxyapatite deposition and hemostatic activity. *Small*, 2(11):1261–1265.

Ostomel, T. A., Shi, Q., Tsung, C.-K., Liang, H., and Stucky, G. D. (2006b). Spherical Bioactive Glass with Enhanced Rates of Hydroxyapatite Deposition and Hemostatic Activity. *Small*, 2(11):1261–1265.

Oswald, J., Boxberger, S., Jorgensen, B., Feldmann, S., Ehninger, G., Bornhauser, M., and Werner, C. (2004). Mesenchymal stem cells can be differentiated into endothelial cells in vitro. *Stem Cells*, 22:377–384.

Ouriel, K. (2001). Peripheral arterial disease. *The Lancet*, 358(9289):1257–1264.

Ovalle, W. K. and Nahirney, P. C. (2007). *Netter's Essential Histology*. Elsevier/Saunders.

Pacini, S. and Petrini, I. (2014). Are MSCs angiogenic cells ? New insights on human nestin-positive bone marrow-derived multipotent cells. *Cell and Developmental Biology*, 2(May):1–11.

Palta, S., Saroa, R., and Palta, A. (2014). Overview of the coagulation system. *Indian journal of anaesthesia*, 58(5):515–23.

Pang, C., Ibrahim, A., Bulstrode, N. W., and Ferretti, P. (2017). An overview of the therapeutic potential of regenerative medicine in cutaneous wound healing. *International Wound Journal*, pages 1–10.

Pannier, F. and Rabe, E. (2013). Differential diagnosis of leg ulcers. *Phlebology*, 28(1_suppl):55–60.

Peirce, S. M., Skalak, T. C., and Rodeheaver, G. T. (2000). Ischemia-reperfusion injury in chronic pressure ulcer formation: a skin model in the rat. *Wound repair and regen-*

eration : official publication of the Wound Healing Society [and] the European Tissue Repair Society, 8(1):68–76.

Percival, N. J. (2002). Classification of Wounds and their Management. *Surgery (Oxford)*, 20(5):114–117.

Phelps, E. A., Enemchukwu, N. O., Fiore, V. F., Sy, J. C., Murthy, N., Sulchek, T. A., Barker, T. H., and García, A. J. (2012). Maleimide Cross-Linked Bioactive PEG Hydrogel Exhibits Improved Reaction Kinetics and Cross-Linking for Cell Encapsulation and In Situ Delivery. *Advanced Materials*, 24(1):64–70.

Phelps, E. A., Headen, D. M., Taylor, W. R., Thulé, P. M., and García, A. J. (2013). Vasculogenic bio-synthetic hydrogel for enhancement of pancreatic islet engraftment and function in type 1 diabetes. *Biomaterials*, 34(19):4602–4611.

Posnett, J., Gottrup, F., Lundgren, H., and Saal, G. (2009). The resource impact of wounds on health-care providers in Europe. *Journal of Wound Care*, 18(4):154–161.

Potapova, I. A., Gaudette, G. R., Brink, P. R., Robinson, R. B., Rosen, M. R., Cohen, I. S., and Doronin, S. V. (2007). Mesenchymal Stem Cells Support Migration, Extracellular Matrix Invasion, Proliferation, and Survival of Endothelial Cells In Vitro. *Stem Cells*, 25(7):1761–1768.

Powell, R. J., Marston, W. a., Berceli, S. a., Guzman, R., Henry, T. D., Longcore, A. T., Stern, T. P., Watling, S., and Bartel, R. L. (2012). Cellular Therapy With Ixmyelocel-T to Treat Critical Limb Ischemia: The Randomized, Double-blind, Placebo-controlled RESTORE-CLI Trial. *Molecular Therapy*, 20(6):1280–1286.

Rahaman, M. (2014). Bioactive ceramics and glasses for tissue engineering. In *Tissue Engineering Using Ceramics and Polymers*, chapter 3, pages 67–114. Elsevier.

Rahaman, M. N., Day, D. E., Sonny Bal, B., Fu, Q., Jung, S. B., Bonewald, L. F., and Tomsia, A. P. (2011). Bioactive glass in tissue engineering. *Acta Biomaterialia*, 7(6):2355–2373.

Rath, S. N., Brandl, A., Hiller, D., Hoppe, A., Gbureck, U., Horch, R. E., Boccaccini, A. R., and Kneser, U. (2014). Bioactive Copper-Doped Glass Scaffolds Can Stimulate Endothelial Cells in Co-Culture in Combination with Mesenchymal Stem Cells. *PLoS ONE*, 9(12):e113319.

Reilly, G. C. and Engler, A. J. (2010). Intrinsic extracellular matrix properties regulate stem cell differentiation. *Journal of Biomechanics*, 43(1):55–62.

Reinke, J. and Sorg, H. (2012). Wound Repair and Regeneration. *European Surgical Research*, 49(1):35–43.

Rep, B. L. (1998). FDA okays artificial skin for treatment of venous leg ulcers. Technical Report 4, FDA.

Rhee, S. and Grinnell, F. (2007). Fibroblast mechanics in 3D collagen matrices. *Advanced Drug Delivery Reviews*, 59(13):1299–1305.

Rheinwald, J. G. and Green, H. (1975). Serial Cultivation of Strains of Human Epidermal Keratinocytes: the Formation of Keratinizing Colonies from Single Cells. *Cell*, 6(3):331–344.

Ribatti, D., Nico, B., Vacca, A., and Presta, M. (2006). The gelatin sponge-chorioallantoic membrane assay. *Nature Protocols*, 1(1):85–91.

Ribatti, D., Urbinati, C., Nico, B., Rusnati, M., Roncali, L., and Presta, M. (1995). Endogenous basic fibroblast growth factor is implicated in the vascularization of the chick embryo chorioallantoic membrane. *Developmental biology*, 170(1):39–49.

Ridley, A. J. (2003). Cell Migration: Integrating Signals from Front to Back. *Science*, 302(5651):1704–1709.

Robinson, S. T., Douglas, A. M., Chadid, T., Kuo, K., Rajabalan, A., Li, H., Copland, I. B., Barker, T. H., Galipeau, J., and Brewster, L. P. (2016). A novel platelet lysate hydrogel for endothelial cell and mesenchymal stem cell-directed neovascularization. *Acta Biomaterialia*, 36:86–98.

Rodemann, H. P. and Rennekampff, H.-O. (2011). *Tumor-Associated Fibroblasts and their Matrix*. Springer Netherlands, Dordrecht.

Rohanová, D., Boccaccini, A. R., Horkavcová, D., Bozděchová, P., Bezdička, P., and Častorálová, M. (2014). Is non-buffered DMEM solution a suitable medium for in vitro bioactivity tests? *J. Mater. Chem. B*, 2(31):5068–5076.

Rokosova, B. and Bentley, J. P. (1986). Effect of calcium on cell proliferation and extracellular matrix synthesis in arterial smooth muscle cells and dermal fibroblasts. *Experimental and molecular pathology*, 44(3):307–17.

Romanoff, A. L. (1960). *The Avian Embryo. Structural and functional development*, volume 131. American Association for the Advancement of Science.

Rowley, J. A., Madlambayan, G., and Mooney, D. J. (1999). Alginate hydrogels as synthetic extracellular matrix materials. *Biomaterials*, 20(1):45–53.

Roy, S., Biswas, S., Khanna, S., Gordillo, G., Bergdall, V., Green, J., Marsh, C. B., Gould, L. J., and Sen, C. K. (2009). Characterization of a preclinical model of chronic ischemic wound. *Physiological Genomics*, 37(3):211–24.

Ruffner, H., Graf-Hausner, U., and Mathes, S. (2016). Skin Models for Drug Development and Biopharmaceutical Industry. In *Skin Tissue Engineering and Regenerative Medicine*, chapter 18, pages 357–386. Elsevier.

Sachot, N., Castano, O., Mateos-Timoneda, M. A., Engel, E., and Planell, J. A. (2013). Hierarchically engineered fibrous scaffolds for bone regeneration. *Journal of The Royal Society Interface*, 10(88):20130684–20130684.

Sachot, N., Castaño, O., Oliveira, H., Martí-Muñoz, J., Roguska, A., Amedee, J., Lewandowska, M., Planell, J. A., and Engel, E. (2016). A novel hybrid nanofibrous strategy to target progenitor cells for cost-effective in situ angiogenesis. *J. Mater. Chem. B*, 4(43):6967–6978.

Sachot, N., Mateos-Timoneda, M. A., Planell, J. A., Velders, A. H., Lewandowska, M., Engel, E., and Castaño, O. (2015). Towards 4th generation biomaterials: a covalent hybrid polymer–ormoglass architecture. *Nanoscale*, 7(37):15349–15361.

Saghiri, M., Asatourian, A., Garcia-Godoy, F., and Sheibani, N. (2016). The role of angiogenesis in implant dentistry part I: Review of titanium alloys, surface characteristics and treatments. *Medicina Oral Patología Oral y Cirugia Bucal*, 21(4):514–525.

Saito, Y., Hasegawa, M., Fujimoto, M., Matsushita, T., Horikawa, M., Takenaka, M., Ogawa, F., Sugama, J., Steeber, D. A., Sato, S., and Takehara, K. (2008). The loss of MCP-1 attenuates cutaneous ischemia-reperfusion injury in a mouse model of pressure ulcer. *The Journal of investigative dermatology*, 128(7):1838–51.

Salimath, A. S., Phelps, E. a., Boopathy, A. V., Che, P.-l., Brown, M., García, A. J., and Davis, M. E. (2012). Dual Delivery of Hepatocyte and Vascular Endothelial Growth Factors via a Protease-Degradable Hydrogel Improves Cardiac Function in Rats. *PLoS ONE*, 7(11):e50980.

Sank, A., Chi, M., Shima, T., Reich, R., and Martin, G. R. (1989). Increased calcium levels alter cellular and molecular events in wound healing. *Surgery*, 106(6):1141–7; discussion 1147–8.

Sanon, S., Hart, D. A., and Tredget, E. E. (2016). Molecular and Cellular Biology of Wound Healing and Skin Regeneration. In *Skin Tissue Engineering and Regenerative Medicine*, chapter 2, pages 19–47. Elsevier.

Sanz-Nogués, C. and O'Brien, T. (2016). In vitro models for assessing therapeutic angiogenesis. *Drug Discovery Today*, 21(9):1495–1503.

Sasanka, C. (2012). Venous ulcers of the lower limb: Where do we stand? *Indian Journal of Plastic Surgery*, 45(2):266.

Schultz, G. S. and Mast, B. A. (1999). Molecular Analysis of the Environments of Healing and Chronic Wounds: Cytokines, Proteases and Growth Factors. *Primary Intention*, 2:7–14.

Sen, C. K., Gordillo, G. M., Roy, S., Kirsner, R., Lambert, L., Hunt, T. K., Gottrup, F., Gurtner, G. C., and Longaker, M. T. (2009). Human skin wounds: A major and snowballing threat to public health and the economy. *Wound Repair and Regeneration*, 17(6):763–771.

Sen, C. K., Khanna, S., Venojarvi, M., Trikha, P., Ellison, E. C., Hunt, T. K., and Roy, S. (2002). Copper-induced vascular endothelial growth factor expression and wound healing. *American Journal of Physiology - Heart and Circulatory Physiology*, 282(5):H1821–H1827.

Shen, D., Cheng, K., and Marbán, E. (2012). Dose-dependent functional benefit of human cardiosphere transplantation in mice with acute myocardial infarction. *Journal of Cellular and Molecular Medicine*, 16(9):2112–2116.

Sheng, L., Mao, X., Yu, Q., and Yu, D. (2016). Effect of the PI3K/AKT signaling pathway on hypoxia-induced proliferation and differentiation of bone marrow-derived mesenchymal stem cells. *Experimental and Therapeutic Medicine*, 13(1):55–62.

Sill, T. J. and von Recum, H. A. (2008). Electrospinning: Applications in drug delivery and tissue engineering. *Biomaterials*, 29(13):1989–2006.

Singh, M. R., Saraf, S., Vyas, A., Jain, V., and Singh, D. (2013). Innovative approaches in wound healing: trajectory and advances. *Artificial Cells, Nanomedicine, and Biotechnology*, 41:1–11.

Slachta, P. A. (2012). Caring for chronic wounds : A knowledge update. *Wound Care Advisor*, 1(1):24–31.

Slomianka, L. (2000). Blue Histology - Integumentary System.

Soldevilla Agreda, J. J., Torra i Bou, J.-E., Posnett, J., Verdú Soriano, J., San Miguel, L., and Mayan Santos, J. M. (2007). An approach to the economic impact of the treatment of pressure ulcers in Spain. *Gerokomos*, 18(4):43–52.

Spentzouris, G. and Labropoulos, N. (2009). The evaluation of lower-extremity ulcers. *Seminars in Interventional Radiology*, 26(4):286–295.

Stadler, I., Zhang, R.-Y., Oskoui, P., Whittaker, M. S., and Lanzafame, R. J. (2004). Development of a Simple, Noninvasive, Clinically Relevant Model of Pressure Ulcers in the Mouse. *Journal of Investigative Surgery*, 17(August):221–227.

Stamm, A., Reimers, K., Strauß, S., Vogt, P., Scheper, T., and Pepelanova, I. (2016). In vitro wound healing assays – state of the art. *BioNanoMaterials*, 17(1-2):79–87.

Standards, I. (2009). ISO/EN10993-5. In *Biological evaluation of medical devices- Part 5: Tests for in vitro cytotoxicity*, page 42. 3rd edition.

Staton, C. A., Stribbling, S. M., Tazzyman, S., Hughes, R., Brown, N. J., and Lewis, C. E. (2004). Current methods for assaying angiogenesis in vitro and in vivo. *International Journal of Experimental Pathology*, 85(5):233–248.

Stavrou, D. (2008). Neovascularisation in wound healing. *Journal of wound care*, 17(7):298–300, 302.

Steed, D. L., Donohoe, D., Webster, M. W., and Lindsley, L. (1996). Effect of extensive debridement and treatment on the healing of diabetic foot ulcers. *Journal of the American College of Surgeons*, 183(1):61–64.

Stefanovic, B., Stefanovic, L., Schnabl, B., Bataller, R., and Brenner, D. A. (2004). TRAM2 protein interacts with endoplasmic reticulum Ca2+ pump Serca2b and is necessary for collagen type I synthesis. *Molecular and cellular biology*, 24(4):1758–68.

Struman, I., Bentzien, F., Lee, H., Mainfroid, V., D'Angelo, G., Goffin, V., Weiner, R. I., and Martial, J. a. (1999). Opposing actions of intact and N-terminal fragments of the human prolactin/growth hormone family members on angiogenesis: An efficient mechanism for the regulation of angiogenesis. *Proceedings of the National Academy of Sciences*, 96(4):1246–1251.

Su, E. J., Cioffi, C. L., Stefansson, S., Mittereder, N., Garay, M., Hreniuk, D., and Liau, G. (2003). Gene therapy vector-mediated expression of insulin-like growth factors protects cardiomyocytes from apoptosis and enhances neovascularization. *American Journal of Physiology - Heart and Circulatory Physiology*, 284(4):H1429–H1440.

Sugimoto, T., Kanatani, M., Kano, J., Kobayashi, T., Yamaguchi, T., Fukase, M., and Chihara, K. (1994). IGF-I mediates the stimulatory effect of high calcium concentration on osteoblastic cell proliferation. *The American journal of physiology*, 266(5 Pt 1):E709–16.

Sundin, B. M., Hussein, M. A., Glasofer, S., El-Falaky, M. H., Abdel-Aleem, S. M., Sachse, R. E., and Klitzman, B. (2000). The role of allopurinol and deferoxamine in preventing pressure ulcers in pigs. *Plastic and Reconstructive Surgery*, 105(4):1408–1421.

Tahergorabi, Z. and Khazaei, M. (2012). A review on angiogenesis and its assays. *Iranian journal of basic medical sciences*, 15(6):1110–26.

Takahashi, T., Kalka, C., Masuda, H., Chen, D., Silver, M., Kearney, M., Magner, M., Isner, J. M., and Asahara, T. (1999). Ischemia- and cytokine-induced mobilization of bone marrow-derived endothelial progenitor cells for neovascularization. *Nature medicine*, 5(4):434–8.

Tanaka, T., Kojima, I., Ohse, T., Ingelfinger, J. R., Adler, S., Fujita, T., and Nangaku, M. (2005). Cobalt promotes angiogenesis via hypoxia-inducible factor and protects tubulointerstitium in the remnant kidney model. *Laboratory Investigation*, 85(10):1292–1307.

Tebu-bio (2017). Extracellular matrix components detection.

Tharmalingam, S., Daulat, A. M., Antflick, J. E., Ahmed, S. M., Nemeth, E. F., Angers, S., Conigrave, A. D., and Hampson, D. R. (2011). Calcium-sensing Receptor Modulates Cell Adhesion and Migration via Integrins. *Journal of Biological Chemistry*, 286(47):40922–40933.

The Jackson Laboratory (2017). Mouse Strain Datasheet - 000642.

The Wound Healing Society (2006). Chronic wound care guidelines.

Theodorou, G., Goudouri, O. M., Kontonasaki, E., Chatzistavrou, X., Papadopoulou, L., Kantiranis, N., and Paraskevopoulos, K. M. (2011). Comparative Bioactivity Study of 45S5 and 58S Bioglasses in Organic and Inorganic Environment. *Bioceramics Development and Applications*, 1:1–4.

Thomas, S. (2000). Alginate dressings in surgery and wound management–Part 1. *Journal of wound care*, 9(2):56–60.

Tomasek, J. J., Gabbiani, G., Hinz, B., Chaponnier, C., and Brown, R. a. (2002). Myofibroblasts and mechano-regulation of connective tissue remodelling. *Nature Reviews Molecular Cell Biology*, 3(5):349–363.

Tomasek, J. J., Haaksma, C. J., Eddy, R. J., and Vaughan, M. B. (1992). Fibroblast contraction occurs on release of tension in attached collagen lattices: Dependency on an organized actin cytoskeleton and serum. *The Anatomical Record*, 232(3):359–368.

Trebaul, A., Chan, E., and Midwood, K. (2007). Regulation of fibroblast migration by tenascin-C. *Biochemical Society Transactions*, 35(4):695–697.

Tu, C.-L., Chang, W., and Bikle, D. D. (2001). The Extracellular Calcium-sensing Receptor Is Required for Calcium-induced Differentiation in Human Keratinocytes. *Journal of Biological Chemistry*, 276(44):41079–41085.

Tu, C.-L., Crumrine, D. A., Man, M.-Q., Chang, W., Elalieh, H., You, M., Elias, P. M., and Bikle, D. D. (2012). Ablation of the Calcium-Sensing Receptor in Keratinocytes Impairs Epidermal Differentiation and Barrier Function. *Journal of Investigative Dermatology*, 132(10):2350–2359.

Tu, C.-L., Oda, Y., Komuves, L., and Bikle, D. D. (2004). The role of the calcium-sensing receptor in epidermal differentiation. *Cell Calcium*, 35(3):265–273.

Ulrich, D., Smeets, R., Unglaub, F., Wöltje, M., and Pallua, N. (2011). Effect of Oxidized Regenerated Cellulose/Collagen Matrix on Proteases in Wound Exudate of Patients With Diabetic Foot Ulcers. *Journal of Wound, Ostomy and Continence Nursing*, 38(5):522–528.

Vallet-Regi, M. (2014). Bioceramics. In Maria Vallet-Regi, editor, *Bio-Ceramics with Clinical Applications*, chapter 1, pages 1–16. John Wiley & Sons, Ltd.

Vandooren, J., Geurts, N., Martens, E., Van den Steen, P. E., and Opdenakker, G. (2013). Zymography methods for visualizing hydrolytic enzymes. *Nature Methods*, 10(3):211–220.

Vargas, G. E., Mesones, R. V., Bretcanu, O., López, J. M. P., Boccaccini, A. R., and Gorustovich, A. (2009). Biocompatibility and bone mineralization potential of 45S5 Bioglass-derived glass-ceramic scaffolds in chick embryos. *Acta biomaterialia*, 5(1):374–80.

Varkey, M., Ding, J., and Tredget, E. (2015). Advances in Skin Substitutes—Potential of Tissue Engineered Skin for Facilitating Anti-Fibrotic Healing. *Journal of Functional Biomaterials*, 6(3):547–563.

Vezzoli, G., Soldati, L., and Mora, S. (2017). Calcium-Sensing Receptor Polymorphisms and Human Disease. In *Molecular, Genetic, and Nutritional Aspects of Major and Trace Minerals*, chapter 1, pages 3–13. Elsevier Inc.

Vila, O. F., Bagó, J. R., Navarro, M., Alieva, M., Aguilar, E., Engel, E., Planell, J., Rubio, N., and Blanco, J. (2013). Calcium phosphate glass improves angiogenesis capacity of poly(lactic acid) scaffolds and stimulates differentiation of adipose tissue-derived mesenchymal stromal cells to the endothelial lineage. *Journal of Biomedical Materials Research Part A*, 101A(4):932–941.

Vileikyte, L. (2001). Diabetic foot ulcers: A quality of life issue.

Visiongain-Ltd (2017). Global Bioactive Wound Care Market Forecasts 2017-2027.

Vowden, K., Vowden, K., and Carville, K. (2011). Antimicrobials made easy. *Wounds International*, 2(1):1–6.

Vu, T. H. (2000). Matrix metalloproteinases: effectors of development and normal physiology. *Genes & Development*, 14(17):2123–2133.

Wall, I. B., Moseley, R., Baird, D. M., Kipling, D., Giles, P., Laffafian, I., Price, P. E., Thomas, D. W., and Stephens, P. (2008). Fibroblast Dysfunction Is a Key Factor in the Non-Healing of Chronic Venous Leg Ulcers. *Journal of Investigative Dermatology*, 128(10):2526–2540.

Wang, B., Chandrasekera, P. C., and Pippin, J. J. (2014). Leptin- and leptin receptor-deficient rodent models: relevance for human type 2 diabetes. *Current diabetes reviews*, 10(2):131–45.

Wang, J., Najjar, A., Zhang, S., Rabinovich, B., Willerson, J. T., Gelovani, J. G., and Yeh, E. T. H. (2012). Molecular Imaging of Mesenchymal Stem Cell: Mechanistic Insight Into Cardiac Repair After Experimental Myocardial Infarction. *Circulation: Cardiovascular Imaging*, 5(1):94–101.

Wang, J. H., Thampatty, B. P., Lin, J.-S., and Im, H.-J. (2007). Mechanoregulation of gene expression in fibroblasts. *Gene*, 391(1-2):1–15.

Wang, T., Gu, Q., Zhao, J., Mei, J., Shao, M., Pan, Y., Zhang, J., and Wu, H. (2015). Calcium alginate enhances wound healing by up-regulating the ratio of collagen types I / III in diabetic rats. *Int J Clin Exp Pathol*, 8(6):6636–6645.

Warburg, F. E., Danielsen, L., Madsen, S. M., Raaschou, H. O., Munkvad, S., Jensen, R., and Siersen, H. E. (1994). Vein surgery with or without skin grafting versus conservative treatment for leg ulcers. A randomized prospective study. *Acta dermato-venereologica*, 74(4):307–309.

Wassermann, E., Van Griensven, M., Gstaltner, K., Oehlinger, W., Schrei, K., and Redl, H. (2009). A chronic pressure ulcer model in the nude mouse. *Wound Repair and Regeneration*, 17(4):480–484.

Weber, L. M., Hayda, K. N., Haskins, K., and Anseth, K. S. (2007). The effects of cell–matrix interactions on encapsulated β-cell function within hydrogels functionalized with matrix-derived adhesive peptides. *Biomaterials*, 28(19):3004–3011.

Werdin, F., Tennenhaus, M., Schaller, H.-E., and Rennekampff, H.-O. (2009). Evidence-based management strategies for treatment of chronic wounds. *Eplasty*, 9:e19.

Wiegand, C. and Hipler, U.-C. (2013). A superabsorbent polymer-containing wound dressing efficiently sequesters MMPs and inhibits collagenase activity in vitro. *Journal of Materials Science: Materials in Medicine*, 24(10):2473–2478.

Williams, D. F. (2009). On the nature of biomaterials. *Biomaterials*, 30(30):5897–5909.

Winter, G. D. (1995). Formation of the scab and the rate of epithelisation of superficial wounds in the skin of the young domestic pig. *Journal of wound care*, 4(8):366–71.

Wong, V. W., Sorkin, M., Glotzbach, J. P., Longaker, M. T., and Gurtner, G. C. (2011). Surgical Approaches to Create Murine Models of Human Wound Healing. *Journal of Biomedicine and Biotechnology*, 2011:1–8.

Wray, P. (2011). 'Cotton candy' that heals? *American Ceramic Society Bulletin*, 90(4):25–29.

Wu, C., Zhou, Y., Fan, W., Han, P., Chang, J., Yuen, J., Zhang, M., and Xiao, Y. (2012). Hypoxia-mimicking mesoporous bioactive glass scaffolds with controllable cobalt ion release for bone tissue engineering. *Biomaterials*, 33(7):2076–2085.

Wu, Y., Chen, L., Scott, P. G., and Tredget, E. E. (2007). Mesenchymal Stem Cells Enhance Wound Healing Through Differentiation and Angiogenesis. *Stem Cells*, 25(10):2648–2659.

Wysocki, a. B., Staiano-Coico, L., and Grinnell, F. (1993). Wound fluid from chronic leg ulcers contains elevated levels of metalloproteinases MMP-2 and MMP-9. *The Journal of investigative dermatology*, 101(1):64–8.

Xie, Y., Rizzi, S. C., Dawson, R., Lynam, E., Richards, S., Leavesley, D. I., and Upton, Z. (2010). Development of a Three-Dimensional Human Skin Equivalent Wound Model for Investigating Novel Wound Healing Therapies. *Tissue Engineering Part C: Methods*, 16(5):1111–1123.

Xu, H., Lv, F., Zhang, Y., Yi, Z., Ke, Q., Wu, C., Liu, M., and Chang, J. (2015a). Hierarchically micro-patterned nanofibrous scaffolds with a nanosized bio-glass surface for accelerating wound healing. *Nanoscale*, 7(44):18446–18452.

Xu, H., Lv, F., Zhang, Y., Yi, Z., Ke, Q., Wu, C., Liu, M., and Chang, J. (2015b). Hierarchically micro-patterned nanofibrous scaffolds with a nanosized bio-glass surface for accelerating wound healing. *Nanoscale*, 7(44):18446–18452.

Yager, D. R. and Nwomeh, B. C. (1999). The proteolytic environment of chronic wounds. *Wound Repair and Regeneration*, 7(6):433–441.

Yamaguchi, T., Chattopadhyay, N., Kifor, O., Sanders, J. L., and Brown, E. M. (2000). Activation of p42/44 and p38 Mitogen-Activated Protein Kinases by Extracellular Calcium-Sensing Receptor Agonists Induces Mitogenic Responses in the Mouse Osteoblastic MC3T3-E1 Cell Line. *Biochemical and Biophysical Research Communications*, 279(2):363–368.

Yang, E. Y. and Moses, H. L. (1990). Transforming growth factor beta 1-induced changes in cell migration, proliferation, and angiogenesis in the chicken chorioallantoic membrane. *The Journal of cell biology*, 111(2):731–41.

Yu, H., Peng, J., Xu, Y., Chang, J., and Li, H. (2016). Bioglass Activated Skin Tissue Engineering Constructs for Wound Healing. *ACS Applied Materials & Interfaces*, 8(1):703–715.

Yu, S., Hu, J., Yang, X., Wang, K., and Qian, Z. M. (2006). La3+-induced extracellular signal-regulated kinase (ERK) signaling via a metal-sensing mechanism linking proliferation and apoptosis in NIH 3T3 cells. *Biochemistry*, 45(37):11217–11225.

Zeng, Q., Han, Y., Li, H., and Chang, J. (2014). Bioglass/alginate composite hydrogel beads as cell carriers for bone regeneration. *Journal of Biomedical Materials Research Part B: Applied Biomaterials*, 102(1):42–51.

Zeng, Q., Han, Y., Li, H., and Chang, J. (2015). Design of a thermosensitive bioglass/agarose–alginate composite hydrogel for chronic wound healing. *J. Mater. Chem. B*, 3(45):8856–8864.

Zhang, X., Zhang, T., Wu, J., Yu, X., Zheng, D., Yang, F., Li, T., Wang, L., Zhao, Y., Dong, S., Zhong, X., Fu, S., Xu, C.-q., Lu, F., and Zhang, W.-h. (2014). Calcium Sensing Receptor Promotes Cardiac Fibroblast Proliferation and Extracellular Matrix Secretion. *Cellular Physiology and Biochemistry*, 33(3):557–568.

Zhao, S., Li, L., Wang, H., Zhang, Y., Cheng, X., Zhou, N., Rahaman, M. N., Liu, Z., Huang, W., and Zhang, C. (2015). Wound dressings composed of copper-doped borate bioactive glass microfibers stimulate angiogenesis and heal full-thickness skin defects in a rodent model. *Biomaterials*, 53:379–391.

Zhu, J. and Marchant, R. E. (2011). Design properties of hydrogel tissue-engineering scaffolds. *Expert Review of Medical Devices*, 8(5):607–626.

Abbreviations

α-MEM Minimum Essential Medium Alpha.

α-SMA alpha-smooth muscle actin.

7TM seven transmembrane-spanning domain.

BCA bicinchoninic acid.

BSA bovine serum albumin.

CAM chorioallantoic membrane.

CaSR calcium-sensing receptor.

CCM complete culture media.

DAPI 4',6-diamidino-2-phenylindole, dilactate.

DLS dynamic light scattering.

DMEM Dulbecco's Modified Eagle Medium.

DMSO Dimethyl sulfoxide.

DPBS Dulbecco's phosphate-buffered saline.

dsDNA double-stranded DNA.

ECD extracellular domain.

ECM extracellular matrix.

ECs endothelial cells.

EDS energy dispersive spectroscopy.

EFP epididymal fat pad.

ELISA Enzyme-Linked ImmunoSorbent Assay.

EPCs endothelial progenitor cells.

ERK1/2 extracellular signal-regulated protein kinases 1 and 2.

FBS fetal bovine serum.

FDA Food and Drug Administration.

FGF fibroblast growth factor.

FPCL fibroblast-populated collagen lattice.

GAPDH glyceraldehyde-3-phosphate dehydrogenase.

H&E hematoxylin-eosin.

hMSC human mesenchymal stromal cells.

HUVEC human umbilical vein endothelial cells.

ICP-OES inductively coupled plasma optical emission spectrometry.

IFN-γ interferon-gamma.

IGF-1 insulin-like growth factor 1.

IL-6 interleukin 6.

IP intraperitoneally.

IP3 inositol-1,4,5-trisphosphate.

IR ischemia-reperfusion.

JNK c-Jun NH2-terminal kinase.

LDH lactate dehydrogenase.

M-PER Mammalian Protein Extraction Reagent.

MAPK mitogen-activated protein kinase.

MMP matrix metalloprotease.

P/S penicillin/streptomycin.

PAD peripheral artery disease.

PBS Phosphate-Buffered Saline.

PDGF platelet derived growth factor.

PDMS polydimethylsiloxane.

PEG polyethylene glycol.

PEG-MAL polyethylene glycol-maleimide.

PLA poly(lactic acid).

PLC phospholipase C.

ROS reactive oxygen species.

RT room temperature.

RT-PCR Real Time polymerase chain reaction.

SD standard deviation.

SDS sodium dodecyl sulfate.

SEM scanning electron microscope.

TBS Tris-buffered saline.

TFE 2,2,2-trifluoroethanol.

TGF-β transforming growth factor-beta.

TIMP tissue inhibitor of metalloproteinase.

TNF-α tumor necrosis factor-alpha.

TTBS Tris-buffered saline containing 0.1% Tween® 20.

VEGF vascular endothelial growth factor.